Optimisation of radiation dose and image quality for AP pelvis radiographic examination

Hussien Abid Ali Bakir Mraity

(Medical physics)

School of Health Sciences,

College of Health and Social Care

University of Salford, Salford, UK

Submitted in Partial Fulfilment of the Requirements of the Degree of Doctor of Philosophy, November 2015

Table of contents

List of figures

List of tables

List of publications

No.	Title	Status
1	*Developing and validating a psychometric scale for image quality assessment*; H Mraity, A England, P Hogg - Radiography, Volume 20, Issue 4, P: 306–311 (2014)	Published
2	*Development and validation of a psychometric scale for assessing PA chest image quality*: A pilot study; H Mraity, A. England, I. Akhtar, A. Aslam, R. De Lange, H. Momoniat, S. Nicoulaz, A. Ribeiro, S. Mazhir, P. Hogg- Radiography, Volume 20, Issue 4, Pages 312–317,(2014)	Published
3	*A Novel approach for the development and validation of visual grading scales*; H Mraity; A England; S Cassidy; P Eachus; A Dominguez; P Hogg,(2015)	Under review in the BJR
4	*Observer studies in mammography*; P Hogg, S Millington, D Manning, and H Mraity- Book chapter in 'digital mammography : A holistic approach'; P Hogg, J Kelly, C Merver, (2015)	Published Book

Note: Publications No 3 and 4 are listed within the publications list as a supportive evidence for applicability of the method developed in sections I of this thesis.

List of presentations

No	Title	Note
1	*Developing and validating a psychometric scale for AP pelvis image quality assessment*; Mraity H, England A , Cassidy S, Eachus P, Dominguez A , Hogg P; poster presented in the UKRC 2015 in Liverpool.	Phantom and cadaver data
2	*Developing and validating a psychometric sale for AP pelvis image quality qssessment*; Mraity H, England A , Cassidy S, Eachus P, Dominguez A , Hogg P; presented as a paper in the ECR 2015 in Vienna.	Phantom and cadver data
3	*Developing and validating a psychometric scale for AP pelvis image quality assessment*; Mraity H, England A, Hogg P; presented in the UKRC 2014 in Manchester.	Phantom data only
4	*Development and validation of a psychometric scale for assessing PA chest image quality: A pilot study*; Mraity H, England A, Akhtar I, Aslam A, Lange R, Momoniat H, Nicoulaz S, Ribeiro A, Mazhir S, Hogg P; presented in the UKRC 2014 in Manchester.	Poster
5	*Development and validation of a psychometric scale for assessing PA chest image quality*; Mraity H, Akhtar I, Aslam A, England A, Lange R, Momoniat H, Nicoulaz S, Ribeiro A, Hogg P; presented in the Congresso Nacional ATARP 2013 in Lisbon	Paper
6	*Lateral hip X-ray imaging – which technique produces lowest gonad dose combined with acceptable visual image quality?;* Khalid S, Mraity H, Hogg P; presented in the UKRC 2013 in Liverpool.	Poster

List of developed skills

No.	Type of Skill
1	How to operate the X-ray Equipment (both CR & DR).
2	How to use MUSICA Software to manipulate the post-processing parameters (e.g. latitude).
3	How to use Monte Carlo software (PCXMC) for simulation.
4	How to use TLD system for the direct measurement of dose.
5	How to conduct different QC protocols for X-ray equipment, CR reader, AEC chambers, display monitors, TLD system and dosimeters.
6	How to operate and set-up the bespoke software for 2-AFC assessment.
7	How to use SPSS software for different and advanced statistics.
8	How to use Minitab statistical software for different factorial design statistics.
9	How to use Excel, Word, PowerPoint and publisher at an advanced level.
10	How to use ImageJ software for advanced image processing and manipulation.
11	How to critically analyse literature.
12	How to write journal papers (review & empirical), and design poster for conference presentation.
13	A variety of reading skills.
14	How to use Endnote software for references coding.
15	How to operate the Unfors dosimeter for dose measurements and QC protocols.
16	A variety of teaching skills (lecturing in Erasmus and undergraduates education course).

Training sessions attended and passed

Session No.	Title of training session	Date
Session 1	Introduction to the Module. The Nature, Role and Context of Research in Health and Social Care.	27th September 2012
Session 2	Developing Research Questions and Hypotheses & Approaches to Research. • Seminar 1: Lab-Based Research • Seminar 2: Qualitative Research • Seminar 3: Mixed Method Research	4th October 2012
Session 3	Searching for Evidence and Information. Critical Review of Existing Research.	11th October 2012

Session 4	Quantitative Designs
	
	• Methods of data collection
	  • Measurement
	    • Sampling
		18th October 2012

Session 5	Qualitative Designs
	
	• Methods of data collection
	  • Measurement
	    • Sampling
		25th October 2012

Session 4	Analysis, Presentation, Interpretation, and Rigour in Qualitative Research.	1st November 2012
Session 5	Analysis, Presentation, and Interpretation of Quantitative Research.	8th November 2012
Session 6	Software Packages for Data Analysis: • SPSS for quantitative data analysis • NVivo for qualitative data analysis	15th November 2012
Session 9	Ethical issues in research.	22nd November 2012

Session 10	Critiquing Research Papers. • Quantitative issues • Qualitative issues	29th November 2012
Session 11	Dissemination and Publication of Research.	6th December 2012
Session 12	Research in the Real World. • Presentations of research projects from PhD completions, staff and others.	13th December 2012
Session 13	PGR Welcome Event and workshop 'Getting Started with your PhD'.	22nd September 2012
Session 14	Electronic Resources for Researchers.	26th September 2012
Session 15	How to Complete a Learning Agreement.	2nd October 2012
Session 16	Doing a Literature Review.	10th October 2012
Session 17	Introduction to Endnote X5.	17th October 2012
Session 18	Supporting and Motivating your Research.	31st October 2012
Session 19	Critical Thinking at Postgraduate Level.	1st November 2012
Session 20	Designing a Research Project and Successful Project Application.	7th November 2012
Session 21	Intellectual Property Rights.	7th November
Session 22	Research Ethics.	13th November 2012

Session 23	SPSS – **5 hour session.**	14th November
Session 24	PhD Progression Points.	15th November 2012
Session 25	Scopus Writing.	10 Sessions 2012
Session 26	Research ideas, Questions and Theoretical Frameworks.	5th November 2012
Session 27	Literature Searching and Literary Review Skills.	5th November 2012
Session 28	Quantitative Research	6th November 2012
Session 29	Abstract Writing	15th Jan 2013
Session 30	Structuring your Research Findings	31st Jan 2013
Session 31	SPSS course; 5 sessions.	January - March 2013
Session 32	Thinking and Writing Critically.	22nd May 2013

Acknowledgement

Abbreviation

2AFC	2-Alternative Force Choice
AAPM	American Association of Physicists in Medicine
AEC	Automatic Exposure Control
Al	Aluminium
ALARA	As Low as Reasonably Achievable
ALARP	As Low as Reasonably Practicable
ANOVA	Analysis of Variance
AP	Anterio Posterior
APPS	Anterio Posterior Pelvis scale
C-d	Contrast details
CINAHL	Cumulative Index to Nursing and Allied Health Literature
cm	Centimetre
CNR	Contrast to Noise Ratio
CR	Computer Radiography
Cu	Copper
DAP	Dose Area Product
DDI	Dose Detector Index
df	Degree Of Freedom
DICOM	Digital Imaging and Communications in Medicine
DQE	Detective Quantum Efficiency
DRL	Diagnostic reference levels
DR	Digital Radiography
DROC	Differential Receiver Operating Characteristic
E	Effective Dose
EC	European Commission
EI	Exposure Index
ESD	Entrance Surface Dose
ESE	Entrance Skin Exposure
EU	European Union
FFE	Free-Response Forced Error
FOM	Figure Of Merit
FOM_{IQ}	Figure Of Merit Based On Image Quality Score
FOM_{SNR}	Figure Of Merit Based On Signal To Noise ratio
FROC	Free-Response Receiver Operating Characteristic
GSDF	Gray Scale Standard Display Function
HVL	Half Value Layer
IAEA	International Atomic Energy Agency
ICC	Intra-Class Correlation
ICRP	International Commission on Radiological Protection
ILO	International Labour Office
IQ	Image Quality
IQS	Image Quality Score
KMO	Kaiser–Meyer–Olkin
kVp	Kilovoltaget Peak
LCD	Liquid Crystal-Display
LGM	Logarithm Of Mean
LROC	Localisation Receiver Operating Characteristic

mAs	milliampere-second
mGy	milligray
mm	millimetre
mSv	millisievert
MTF	Modulation Transfer Function
nC	Nano-Coulomb
NCRP	National Council on Radiation Protection & Measurements
NPS	Noise Power Spectrum
PSL	Photo Stimulated Luminescence
QA	Quality Assurance
ROC	Receiver Operating Characteristic
ROI	Region Of Interest
RSNA	Radiological Society of North America
s	Second
SD	Standard Deviation
SID	Source To Image Detector Distance
SNR	Signal To Noise Ratio
TLD	Thermoluminescent Dosimeter
UNSCEAR	United Nations Scientific Committee on the Effects of Atomic Radiation
UOS	University Of Salford
VGA	Visual Grading Analysis
$VGAS_{abs}$	Visual Grading Analysis Score (absolute)
$VGAS_{rel}$	Visual Grading Analysis Score (relative)

Abstract

Background and rationale:

Optimising radiation dose and image quality in medical imaging is essential in minimising radiation risk and ensuring images are fit for purpose. This thesis uses novel methods for image quality assessment and radiation dose/image quality optimisation. The antero-posterior (AP) pelvis projection was used as a focus for optimisation.

Methods:

In the first part of this thesis a visual grading image quality assessment scale is developed and validated in order to assess radiographic image quality. The scale validation is conducted in two phases; the initial phase uses phantom images and is further tested in phase two with cadaveric images. The scale development and validation is guided by psychometric theory and in particular Bandura's guidelines. In the second part of this thesis a framework is developed to systematically optimise the radiation dose and image quality for AP pelvis radiographic examinations. The methodology development for this section is guided by the factorial based experimental design. The optimisation includes manual and automatic exposure control modes. The image quality is visually assessed using the previously developed (novel) image quality scale and physically using a signal to noise ratio. The optimisation work is conducted with the aim of achieving two objectives: 1) identifying the optimum practice that would produce images with suitable quality and low radiation dose; 2) conducting a systematic investigation into the main effect of the primary acquisition factors on the response variables (e.g. image quality (IQ) and effective dose (E)).

Results:

A scale of 24 items was produced. These scale items had good inter-item correlation (≥ 0.2) and high factor loadings (≥ 0.32). Cronbach's alpha (reliability) revealed that the scale has acceptable levels of internal reliability for both phantom and cadaver ($\alpha = 0.8$ and 0.9, respectively). The factor analysis suggested that the scale is multidimensional (assessing multiple quality themes). Accordingly, it is likely that this scale will be applicable in both clinical and research practices. The optimum practice was identified, resulting in suitable quality images with a lower dose (i.e. 88 to 94 % less than the UK average adult AP pelvis dose of 0.7 mSv) for both manual and AEC modes. Furthermore, it was identified that kVp had the biggest effect on radiation dose, image quality and figure of merit ($P<0.05$) when compared with mAs and SID. The factorial design proved to be an efficient approach in optimising the radiation dose and image quality, and also for exploring the main effect of acquisition factors on radiation dose and image quality.

Conclusion:

This novel method for developing and validating image quality assessment scale shows promise. As such it is a recommended model for developing scales for other radiographic projections. The factorial design should be considered for use in future work due to its efficiency in optimising the radiation dose and image quality systematically. Finally, the AP pelvis scale, in its current form, could be used in future assessments of AP pelvis image quality.

Section I

AP Pelvis Visual Image Quality Assessment Scale Development and Validation

(Secondary focus of the thesis)

Chapter 1: Introduction and background

1. 1. Introduction

The history of medical imaging began after the German scientist Dr. Wilhelm Röentgen discovered X-rays on the 8th of November, 1895. This revolutionary finding gave rise to the production of the first medical image in the world, when Roentgen radiographed his wife's hand (Goodman, Wilson, & Foley, 1988). This discovery gave the health care sector an incredible opportunity to improve health service which administered to the patients. To illustrate this, the human eye cannot use visible light to see internal organs as a part of a medical investigation because visible light is absorbed and/or reflected rather than penetrating the human body. In contrast, X-rays, as an electromagnetic radiation, has the power to penetrate through the body and display the required information about the organ/body part in question (Graham and Cloke, 2003). Medical imaging practice has undergone many stages of development with the aim of improving the way by which a patient's disease can be managed. For example, the early X-ray equipment started with a simple X-ray tube producing analogue images, whereas nowadays the current imaging systems are computer-based which have wider dynamic ranges and the ability to process images atomically (IAEA, 2007).

On the other hand, it should be remembered that ionising radiation has a potentially harmful effect on health (Hendee and O'Connor, 2012). This is because X-rays are high energy ionising photons and are capable of producing somatic and genetic effects (Kumar, Kumar, & Malleswararao, 2011; Compagnone, 2008). X-rays have the ability to ionise or excite the atomic structure which can result in marked changes in the molecular, or even cellular, level (Guy and Ffytche, 2005). As a result, ionising radiation used in medical applications significantly contributes to the amount of radiation the general public is exposed to (Ramanandraibe *et al.*, 2009). In this sense all radiographic examinations involving ionising radiation lead to radiation energy deposition within the body ($d\varepsilon/dm$), where $d\varepsilon$ represents the imparted energy by inoising radiation to a material of mass dm.This is also termed as radiation absorbed dose (Compagnone, 2008).

A few decades after Roentgen's discovery, it was felt that excessive exposure to ionising radiation for medical purposes could lead to serious biological and pathological consequences. From 1928 radiation protection emerged as a field of science and focused on the investigation of radiation and its biological effects on humans (Jones, 2005). The role of this discipline is to deal with radiation limitation/protection and to formulate guidelines which aim to reduce radiation exposure (Niroomand-Rad, 2003). It has been estimated, by the United Nations Scientific Committee on the Effects of Atomic Radiation (UNSCEAR) that around 95% of man-made radiation exposure to the population is caused by medical X-ray examinations (EC, 2009). The radiation risk is proportionate to the radiation dose received by humans. Accordingly, there

should be organisational measures to control and quantify the amount of radiation received by a population (ICRP, 2001a; UNSCEAR, 2000).

It is important to note that radiation monitoring in diagnostic radiology is essential for two main reasons: to estimate the amount of potential detriment a patient undergoing radiological examination is subjected to; and for use as an indicator for the purpose of quality assurance. One aim of a quality assurance programme is to keep radiation doses as low as possible without compromising the image quality (EC, 1997; Noel, 2007). To do so, a systematic approach to dose reduction should be taken; this involves considering the radiation reaching the imaging detector, as this relates to image quality (Motz & Danos, 1978). As a result, the quality and the quantity of radiation received by the detector vary with the amount of radiation delivered. Achieving a balance between administered radiation and image quality is of paramount importance. The process used in achieveing this balance is often referred to as 'dose and image quality optimisation' (ICRP, 1991). Optimisation of radiation dose and image quality has been conducted for many years across a wide range of imaging procedures. Nevertheless, variability in the obtained results (e.g. dose) is a common problem and different optimisation methods have been used (Johnston and Brennan, 2000). A wide range of approaches have been described to assess image quality, all of which were important in the construction of this thesis. This suggests there is a lack of standards for optimising dose and image quality, and this is especially true for the visual quality image assessments (Seeram, Davidson, Bushong, & Swan, 2013; Li, Poulos, McLean, & Rickard, 2010).

Optimisation of the dose and image quality *is the primary* focus of this thesis. To achieve this, an anterior-posterior (AP) pelvis radiograph was selected. Justification for choosing this projection relates to radiation dose and examination frequency (further information can be seen in page 19 and 123). The optimisation procedure of the AP pelvis projection was conducted via an experimental approach. This included dose estimation using a Monte Carlo model, organs doses directly measured using thermoluminescence dosimeters (TLD) and image quality assessments using both visual and mathematical techniques. The thesis consists of two sections; the first is dedicated to the creation and validation of a visual grading scale for assessing image quality with the purpose of optimisation. The reason for this is due to there being no image quality scales available, as the only criteria previously available (e.g. CEC quality criteria) can be considered outdated since they were established in the film screen era (1996) and could be deemed unsuitable for digital imaging. This assertion can be evidenced by the variation seen within the literature when using the CEC European Guidelines on Quality Criteria (CEC, 1996) for assessing the image quality of AP pelvis radiographs. The second section focuses on optimising the image quality and radiation dose of the AP pelvis projection systematically. This includes creating and conducting a framework which considers the primary and secondary acquisition factors when optimising the examination. Therefore, this thesis seeks to fill a gap in the literature wherein the majority of the optimisation attempts have considered one acquisition factor at time

and have ignored the *combined effects* of acquisition factors when seeking to optimise radiation dose alongside image quality using either human anthropomorphic phantom or cadavers/patients.

The structure of this thesis comprises of nine chapters, four chapters for each section and one chapter (9th) for an overall conclusion. Figure 1 summarises the entire PhD thesis layout.

PhD thesis layout

Chapter 1 (Background)

1. Image quality assessment approaches.
2. Critical analysis of CEC image quality criteria (1996).
3. Variation in using AP pelvis quality criteria.
4. Identify the appropriate approach to create a visual grading scale for assessing image quality.

Chapter 2 (Methodology)

1. Create a method to develop and validate an image quality visual grading scale; this is guided by the psychometric theory and Bandura guidelines for scale creation.

2. Using the method, to develop a scale to assess AP pelvis image quality.

3. Scale validations includes two phases, one phase with using phantom images and then using cadaveric images.

Chapter 3 (Results)

1. Presents data from different analyses for both phases; this includes :

A. Overall aggregated image quality scores (phantom & cadevric images).
B. Items analysis (descriptive statistics & inter-item correlation)
C. Scale reliability coefficients as indicated by Cronbach Alpha.
D. Scale validity testing as indicated by factor analysis.

Chapter 4 (Discussion)

1. This includes discussing the obtained results in light of the psychometric properties it had (reliability and validity); and for the both validation phases.
2. Explaining the utility of created scale for assessing the image quality and how it contributes to the current knowledge.
3. Finally, validated image quality assessment scale produced.

Section I

Section II

Chapter 5 (Background)
1. Optimisation of the protection in radiography.
2. Aspects of optimisation in CR and DR.
3. Strategies for optimising the radiographic examination .
4. Previous attempts for optimising the AP pelvis radiographic examinations .

Chapter 6 (Methodology)
1. Develop a framework to optimise the image quality and radiation dose systematically. Optimisation includes manual and AEC modes.
2. Estimating and measuring the radiation dose using a Monte Carlo simulation approach and thermoluminescence dosimeter (TLD).
3. Assessment of image quality visually using our novel scale and physically using signal to noise ratio (SNR).

Chapter 7 (Results)
1. Presents data from different optimisation experiments (manual & AEC modes); this includes two main themes:
A. Identify the optimum technique that produces suitable quality image and lowest radiation dose.
B. Study the main effect (strength) of the primary acquisition factors (e.g. kVp,

Chapter 8 (Discussion)
1. Results from different optimisation experiments were discussed. Discussion includes two main themes:
A. The optimum technique that produces suitable quality image and lowest radiation dose.
B. The main effect (strength) of the primary acquisition factors (e.g. kVp, mAs & SID).

Chapter 9 (Conclusion)
1. Conclusion regarding the utility of the created methodology to develop and validate another image quality assessment scale, and value of validated AP pelvis scale for clinical and research work.

2. Conclusion regarding the utility of the framework to optimise the image quality and radiation dose.

3. Identify the optimum technique that produced image with suitable quality and lowest radiation dose, for both manual and AEC modes.

4. Identify the acquisition factor that had the biggest effect on different response variables (e.g. E).

Figure 1-1. Schematic diagram illustrating the main layout of this PhD thesis.

In chapter one background information will be provided on the issue of image quality within medical imaging. Following this, the main options for assessing radiographic image quality will be explained with special attention given to visual approaches. Key issues associated with the use of CEC European Guidelines for image quality criteria will be discussed, with particular reference to intra- and inter-observer variability. The latter of which can be regarded as one of the main reasons for creating a new visual grading scale. An analysis of literature which includes the assessment of the quality of AP pelvis radiographs has also been conducted. The reason for this analysis is to see which quality criteria have been used by researchers for their image quality assessments. Additionally, identification of the appropriate theoretical framework that can be adopted to create and validate an image quality scale has been noted. **In chapter two**, details on the methodology used in creating and validating a visual grading scale will be described. Said methodology was conducted in two phases: one phase used images taken from a phantom, and was then further validated using images acquired from cadavers; and the second was to study the effect of anatomical variation and positioning problems on the scale utility. **In chapter three**, the results from both validation phases will be presented. This includes aggregating the overall scores from all participants in relation to each scale item. Following this, item analysis for each scale item will be conducted (descriptive and inter-item correlation). Finally, data on the reliability and validity will be presented using Cronbach's alpha coefficient and detailed factorial analysis. **In the fourth chapter**, the results will be discussed. This will include a discussion of the results of each validation phase independently. Then, the utility of the created methodology will be explained in light of the obtained psychometric properties of the current validated scale (reliability and validity).

In chapter five, after the visual grading scale creation and validation procedure has begun, a literature review will be conducted, serving as the main focus of this PhD thesis (optimisation). Chapter five will then include details of the philosophy of optimising radiation protection in medical imaging. Different aspects of optimisation conducted for different radiographic projections will then be described. Strategies established for optimising digital radiography are then discussed with associated advantages and disadvantages on image quality and radiation dose. Throughout this thesis the phrase 'digital radiography' refers to both direct digital radiography (DR) and computed radiography (CR). Lastly, previous optimisation attempts for AP pelvis are critically analysed in regards to their approaches, reported dose reductions and their current clinical practice utility (e.g. space required). **In chapter six,** details of the created framework for systematically optimising the AP pelvis projection will be described. This includes detailing the methodology for each of the manual and AEC modes using computed radiography (CR) and an anthropomorphic pelvis phantom. This is preceded by an explanation of the experimental design adopted to create a framework which considers the combined effect of the primary and secondary acquisition factors on radiation dose and image quality. **In chapter seven**, the results from different optimisation experiments will be presented. This includes the results from optimising the manual and AEC modes individually. Due to excessive amount of results obtained, the focus will be on the optimum technique identified to produce an image of

suitable quality whilst keeping a low dose of radiation, and the main effect the primary acquisition factor has on different response variables (e.g. dose). **In chapter eight,** the results from optimisation experiments were discussed. This discussion will also include both the manual and AEC modes separately. Similar to chapter seven, the results and discussion are done in two themes, namely the optimum technique and the main effect of acquisitions on radiation dose and image quality.

Finally, **chapter nine** presents the final conclusions in relation to utility of the created methodology to develop a visual grading scale and the value of the current validated scale in research and clinical work. The final optimum techniques will be then identified in relation to the manual and AEC modes which produced the lowest radiation dose image with a suitable image quality. The main effect of acquisition factors on response variables was identified. Finally, the value of the factorial design used to optimise the practice will be mentioned.

1.2. Literature review (A background)

1.2.1. Overview
This literature review focuses on the importance of assessing image quality in the major medical imaging applications. Following this, the main approaches for assessing the image quality are explained. In this context, the focus will be on the visual/clinical approaches, in regards to their relevance in the clinical environment. Variability in the results of image quality assessment which arise from the latter clinical approaches are discussed, as is how this issue has been addressed by the establishment of the EU Guidelines for quality criteria. After this, the previous attempts to upgrade or create criteria are described. Finally, a gap in the literature is discussed, as is how it will be addressed by this PhD thesis.

1.2.2. Image quality
The assessment of image quality is essential for a wide range of medical imaging applications. In general, image quality measures (metrics) provide three types of applications (Wang, Bovik, & Lu, 2002). Firstly, they can be used as a quality assurance/control indicator of imaging system performance. Secondly, to optimise patient radiation dose during X-ray practice because dose reduction percentage is limited by the quality of information provided (Jessen, 2004). Lastly, they can be used as a benchmark for choosing the appropriate image processing/post processing algorithm by which one can obtain relevant radiographic information. Dose optimisation and image post-processing measures are essential for imaging systems which use ionising radiation, as they minimise the need to repeat radiographic procedures, and expose the patient to unnecessary radiation (Sezdi, 2011).

1.2.2.1. Image quality versus optimisation
Image quality plays an essential role in radiographic dose optimisation. Optimisation involves producing an image with acceptable image quality and low patient radiation dose (ALARP principle) (Department of Health, 2007; ICRP, 2006). Estimates of the radiation dose received by patients are relatively easy to make; by contrast, image quality assessments can be difficult and

time consuming (Martin, Sutton, & Sharp, 1999). It is well known that establishing an accurate and reliable diagnosis from radiographic images requires a certain level of image quality. In this context, image optimisation generally concerns itself with creating an image which is fit for purpose (Tingberg *et al.*, 2000). The term, *fit for purpose* is rarely defined adequately within clinical journal papers. Consequently, the *quality of an image* refers to the subjective analysis of the visual data contained within it (Jessen, 2004). This would confirm that any image quality measure other than those based on the eyes of an observer could be regarded as a supportive or predictive measure (i.e. physical measure).This is because image perception is almost always based on the visualisation of anatomical features within an image, whereas the physical measure relates to a measure of detectability of relevant features but does not directly measure the fidelity of features.When defining the quality of an image, the purpose of the image should also be considered (Lemoigne, Caner, & Rahal, 2007). It is widely agreed that image quality can be defined in terms of its acceptability for answering the primary clinical questions (Sharp, 1990, Kundel, 1979; Shet, Chen, & Siegel, 2011).

1.2.2.2 Image quality versus quality control/assurance

Having identified the important link between image quality and radiation dose in diagnostic radiography, it is now necessary that image quality is employed as a form of quality control, and also as a quality assurance measure of imaging system performance (Carmichael, 1989; BIR, 1989a). A variety of quality control frameworks that assess image quality have been described in the literature. For instance, in 2001, Kotre and Marshall considered the quality control protocol for image quality in digital fluorography, and Karoussou (2005) reviewed the measurement standards of image quality in digital X-ray systems. The parameters that have been used within both studies are noise, sharpness and the level of image distortion (mostly physical). These measures (i.e. quality control protocols) are intended to reduce the amount of error that can be associated with the imaging process and how it could potentially affect the radiographic image quality (Zoetelief, Soldt, Suliman, Jansen, & Bosmans, 2005). As a result, an image with poor quality, caused by poor imaging system performance, could have an impact on the accuracy of the subsequent medical decisions and therefore influence patient health problem management.

The term 'image' refers to the visual communication of information produced by a given imaging system. By contrast, the word 'quality' can be defined as 'a set of factors or perceptions by which a given image can be judged'. For instance, the quality in diagnostic radiography is closely related to the diagnostic capability of an image, in which there are specified protocols for making this assessment (Engeldrum, 1999). Aside from the physical and technical factors, it is important to take into account human perception and cognition when assessing radiogarpgic images. Image perception refers to the unified realisation of the content of the image (image signal), whereas human cognition can be defined as the ability to determine the meaning of the image in the context of the medical problem. Accordingly, this may affect the process of image quality evaluation (Krupinski, 2011; Kundel, 2006).

1.2.3. Image quality evaluation

Both the utility of radiographic images and the precision of image interpretation are highly dependent upon image quality and observer competency. There are several approaches that can be used to measure the quality of an image (Alsleem & Davidson, 2012), and a review of the literature revealed even more methods for image quality evalutation in diagnostic imaging. These methods can be classified according to the type of information required (i.e. *Level of ambition*) into lowest and highest order tasks. To illustrate, those of low order task would measure exposure factors, equipment characteristics and test radiographic technique; by contrast, those of high order task would investigate the images taken of the patients (Seeram, Bushong, Davidson, & Swan, 2014). Both of these approaches include the appraisal of physical, psychophysical and diagnostic performance (figure 1-2). Details on these methods will be described in the next sub-section and the applications and the drawbacks of each will be taken into consideration, as will the appropriate solutions which have been established to counteract their limitations.
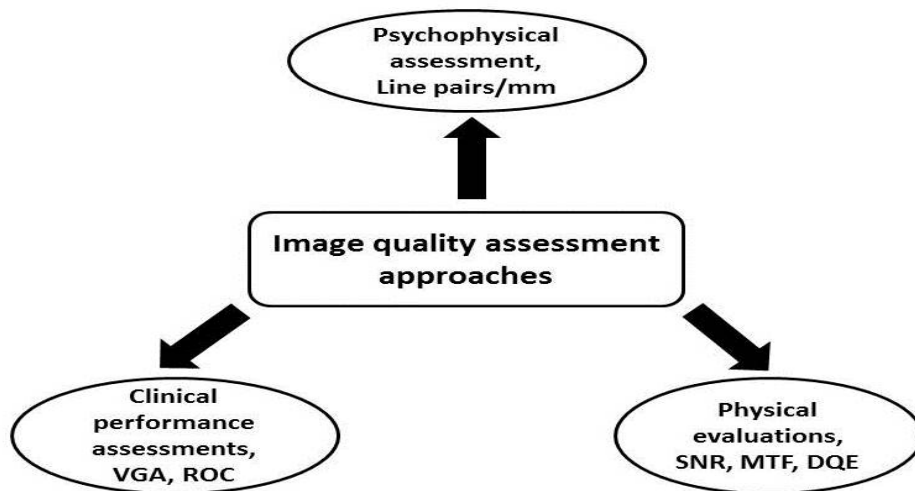
Figure 1-2. Different methods for image quality evaluation (adapted from Alsleem & Davidson, 2012).

1.2.3.1. Physical measures (Objective)

The term, *objective measurements* refer to the description of the physical characteristics within the digital radiographic system. They have the ability to describe the performance of the whole imaging system by referring to the image quality. These physical measures include a signal to noise ratio (SNR), contrast to noise ratio (CNR), a modulation transfer function (MTF), a noise power spectrum (NPS) and a detective quantum efficiency (DQE) (Månsson, 2000, & Seeram, Bushong, Davidson, & Swan, 2014). This sub-section will consider the most commonly adopted measures, namely DQE, CNR and specifically the SNR which was used in this thesis and information of their validity and clinical relevance will be discussed.

1.2.3.1.1. DQE

DQE is a physical tool used to describe the image quality in regards to how efficient the imaging system was in transferring the information from the patient to the imaging detector (Månsson, 2000).This approach is quite useful, especially when a novel detector is installed. The performance of DQE was reviewed and improved by incorporating additional descriptors such MTF and NPS. This was done with the aim to make the estimation of imaging detector performance more comprehensive (Båth, 2010). By doing so, DQE became a good descriptor for detector sensitivity and resolution. Despite its effectiveness in characterising the properties of a given detector, it should also be noted that it is a descriptor for a single component of imaging chain (Alsleem & Davidson, 2012) and does not take the effect of image processing and anatomical variation on the image quality into consideration. Overall, the validity of DQE in estimating the detector's efficiency is high, whereas its validity in being a clinical indicator in relation to the impression of an observer is much lower than would be expected (Båth, Sund, & Månsson, 2002).

1.2.3.1.2. SNR

SNR measurement explains the relationship between contrast and noise levels in an image for an object with a large scale. In this context, SNR is a simplistic method commonly used to describe the visibility of an object in the image (Lança & Silva, 2008). It can be determined by a ratio of mean signal value in the studied object (i.e. the mean signal difference between object and its background) to the standard deviation of the signal value of the background (Båth, 2010). SNR is widely used to assess the image quality of digital radiographic images. This is because, in digital radiography, the main determinant factor of image quality is the noise level. SNR's relationship to human observer detectability was first studied by Albert Rose in 1948 (Rose, 1973). He attempted to discover the minimal noise level required for an image to be viewed by the human eye. He found that a ratio value of ≥5 is required as a threshold for detectability. As such, SNR calculation provides a figure for image quality measurements based on connecting the mathematically calculated SNR to the findings of detection examinations (Alsleem & Davidson, 2012; Dobbins, 2000, Borasi, Samei, Bertolini, Nitrosi, & Tassoni, 2006).

On the other hand, there are a number of issues associated with this metric which may influence the reliability and validity of image quality measurements (Alsleem & Davidson, 2012). Firstly, the SNR measurement does not take the size of an object under study into account, thus its correlation with observer performance is low. Secondly, the noise description (i.e. standard deviation of pixel value) employed by this method is too simplistic for an observer who is sensitive to the noise texture (characteristics). To illustrate this, the SNR model is almost based on quantum noise which is related to the photon density at the detector, whereas the human observer is familiar with background texture of an image which may be affected by other noise types such as anatomical noise, detector noise and system noise (Bochud, Valley, & Verdun, 1999; Bath, 2010). Thirdly, to obtain similar imaging characteristics (a similar SNR), systems with smaller pixel size require a larger number of photons compared to those with a larger pixel

size. In fact, an observer is often not concerned with single pixel values; they instead integrate information over an area in the image and are not influenced by pixel-to-pixel variations (Båth, 2010). Lastly, in relation to the region of interest (ROI) location in estimating the noise level, placing it in a non-homogenous area of the image would lead to variability in the pixels values due to anatomical variations, and would therefore heavily affect SNR measurements. Previous studies (Bochud, Valley, & Verdun, 1999; Håkansson *et al*., 2005) have found that anatomical (background) noise rarely affects the observer.

To reflect on all this, SNR is an efficient and reliable measure of image quality for the purpose of being a constancy and quality assurance measurement of the imaging system. However, its utility in obtaining a measurement which is related to the observer perception is yet to be proven (Båth, 2010). This is because the SNR may not capture all the features that are clinically relevant in obtaining an accurate medical diagnosis. Therefore, SNR measurement should be accompanied by observer perceptions to improve its validity and reliability (McCollough, Bruesewitz, & Kofler, 2006). It is widely accepted that the SNR can be used as a good predictor of image quality, especially for optimisiation purposes (Kundel, 1979; Burgess, 1995; Månsson, 2000).

1.2.3.1.3. CNR
The CNR is another physical measure used to describe the image quality of medical images. It is likely be used to characterise the object of interest from its surrounding background. The CNR therefore provide a good metric regarding the capability of imaging system to visualise the anatomical structures, pathological lesions and/or abnormities with a given image (Dhawan, 2011). In this context, it has argued that, at certain conditions, that CNR provides good information about the effect of noise on contrast detectability when compared with SNR measure. This is because that an image with a high SNR does not necessarily have a good contrast unless it has a high CNR especially when an adequate differentiation between the pathology and health tissue is required (Smith & Webb, 2011). In practice, the CNR computed from the difference between the signal inside the region of interest and the background signal divided by the noise value of background ROI, $CNR = S_1 - S_2/\sigma$, where S_1 is the ROI signal value, S_2 is the background signal value and σ (standard deviation) is the noise value of the background ROI. Since this measure is based on the signals difference between the two ROIs, it is most likely that the CNR is used with a test object that generates homogenous signals unlike SNR which is not requiring such a homogenous object (Bushberg, Seibert, Leidholdt JR, & Boone, 2012). Finally, CNR utilities in medical imaging include optimising the kVp to imorpve bone contrast but at constat dose, and to identify at which dose a given level of CNR for a given object could be obtained.

1.2.3.2. Psychophysical measurement
This measurement requires an observer to give a subjective response in relation to a physical stimulus' influence on a test object being imaged. Test objects used in these measurements are usually simple, such as line pair (used to determine the spatial resolution), and discs made with holes of different contrasts and diameters, used to identify contrast details (C-d) diagrams (Zarb, Rainford, & McEntee, 2010). To obtain results with high reliability using this approach, the variation between observers should be considered, and an average of the findings from different readers should be taken. Although observers are involved in these measurements, correlation between the results obtained from clinical image quality and C-d analysis studies are not highly

impressive (Månsson, 2000). This therefore confirms the value of this approach for system performance over its clinical value, required for medical diagnoses.

1.2.3.3. Diagnostic performance (Receiver Operating Characteristic-ROC)

The primary task for an observer in medical imaging is to decide whether a given patient image shows evidence of pathology, or not. This therefore demands an approach which can identify the observer performance in relation to the diagnostic quality (Båth, 2010). ROC analysis is widely used in radiology to subjectively assess the diagnostic images and observer performance. This analysis originated from the Signal Detection Theory, in which an observer attempts to detect a low contrast signal in a noisy background. The clinical counterpart for this is for one to distinguish the abnormal case from a set of normal background cases (Månsson, 2000). For this, an observer is asked to rate images with suspected diseases, thus diagnostic performance can then be determined by the number of correct responses. However, ROC measures have a major drawback in that they are highly dependent upon disease prevalence. Furthermore, the images have to be divided into normal and abnormal, meaning a large number of images are required. ROC methodology does not work well for multiple lesions on one image, and the localisation of said lesion is not taken into account and therefore a case may be diagnosed as abnormal whilst still missing the true lesion (Båth, 2010; Zarb, Rainford, & McEntee, 2010). In order to overcome the above limitations in ROC analysis, measures have been taken to improve its performance and fill the existing gaps. These measures included the development of ROC related methods to increase its statistical power while using a low number of images (Månsson, 2000). For example, in LROC, the lesion has to be pointed out by an observer together with its location. Then, the latter method improved into FROC, in which the observer is required to detect several lesions together with their location. Also an observer has to rate his confidence level toward this lesion is malignant or not. This method allows for good statistical power with few cases and readers (Zarb, Rainford, & McEntee, 2010). Another ROC related improvement was free-response forced error (FFE), in which if the observer detect a high percentage of abnormality before any false positive error happens for one modality, then this modality is considered as better. Finally, DROC was developed to compare between different systems. The statistical power of DROC is found to be higher than that of ROC. All the above methods have been proven to be closely related to the clinical situations and addressed the above limitations (Båth, 2010).

1.2.3.4. Observer performance (Visual Grading Analysis-VGA)

This approach is highly relevant to the current thesis objectives: to create and validate a visual image quality assessment scale and use to use it for subsequent optimisation work. Advantages and disadvantages of the VGA will be described, showing the motivation for this scale's being developed. The visual grading of the visibility/reproduction of normal anatomy or pathology is a valid and commonly used approach to subjectively quantifying the quality of an image in medical imaging (Seeram, Bushong, Davidson, & Swan, 2014). Its application is based on how clearly the anatomical structures are visualised by an observer, such as by asking an observer to

rate the visibility and reproduction of details in the clinical images. A human-based approach like this makes it a clinically relevant and preferred way to assess the image quality (Smedby & Fredrikson, 2010). Also, the relevance of the VGA for detectability of pathology has been investigated, and ultimately has assessed there to be a strong correlation between the visibility of normal anatomy and the detectability of pathological structures (Sund, M., Kheddache, & Månsson, 2004; Sund, Båth, Kheddache, Tylén', & Månsson, 2000; Morán *et al.*, 2004).

1.2.3.4.1. Justification for VGA

In his article, Båth (2010) provides a number of reasons for using a visual grading approach: 1) that the validity of VGA studies can be regarded to be high, providing the anatomical structures are chosen based on their clinical relevance; 2) in certain cases visual grading approaches found to agree with both detection studies using real observers (Sund, Båth, Kheddache, Tylén, & Månsson, 2000) and physical calculations of image quality (Sandborg, Tingberg, Ullman, Dance, & Alm Carlson, 2006); 3) in comparison to the ROC studies, VGA experiments are easier to undertake, particularly when optimising equipment locally. This is beacuse with VGA less number of images are required and fewer observers amy be adequate than that of ROC; 4) the time required to implement VGA studies is relatively small, when the observer's workload is taken into account, meaning that it can be used in any hospital or clinic. Additionally, certain preparartions are required with ROC such as half of images should have lesions and specific software is necessary for the study to conduct; the latter issues are not required with VGA studies (Båth, 2010). There are two common types of VGA approaches which can be applied to assess an image:

Absolute VGA

In this approach the observer is asked to give his subjective opinion on the visibility of anatomical structures in the image. The collected data from this method is then computed to provide the visual grading analysis scores (VGAS$_{abs}$) using the following:

$$VGASabs = \frac{\sum_{1i=1}^{I}\sum_{s=1}^{s}\sum_{o=1}^{O} Gabs}{I \times S \times O}$$

where G$_{abs}$ represents the absolute rating for a given image (i), structure (s), and observer (O). The letters I, S and O refer to the number of images, structures and observers respectively.

Relative VGA

The relative VGA requires a rating of the visibility of anatomical structures against the same structures within a reference image. The observer should grade the visibility of the structure using a scale in which a value of 0, or equivalent, referring to visibility is equal to the reference image and therefore other values can represent the superiority and inferiority of the structures' clarity in comparison to the reference image. Scores can be computed using this expression:

$$VGASrel = \frac{\sum_{o=1}^{O} \sum_{i=1}^{I} \sum_{c=1}^{C} Grel}{I \times S \times O}$$

where G_{rel} represents the absolute rating for a given image (I), criterion (C), and observer (O). The letters I, S and O refer to the number of images, structures and observers, respectively. It is suggested that two images should be displayed on side by side monitors with same brightness, and the reference image must include well defined landmarks (Månsson, 2000; Zarb, Rainford, & McEntee, 2010 & Seeram, Bushong, Davidson, & Swan, 2014). The above scores allow for further statistical analysis and interpretation.

In summary, it becomes clear that by using a visual/clinical method such as VGA or ROC when quantifying image quality, the result can be more relevant than those of physical measures, since visual methods focus on how clearly each anatomical structure can be visualised by an observer (Månsson, 2000; Ludewig, Richter, & Frame, 2010). However, two main limitations can be identified with these clinical approaches. Firstly, they reflect observer opinion and therefore can be highly susceptible to inter-observer variability (Sund, Båth, Kheddache, & Månsson, 2004); secondly, with these approaches the anatomical structures under evaluation must be pre-specified. No formal and validated guidelines on this exist, and it is likely that these will be highly variable between published literatures, therefore making comparisons difficult (Li, Poulos, McLean, & Rickard, 2010; Shet, Chen, & Siegel, 2011).

1.2.4. Variability in assessing visual image quality
In diagnostic radiology, the variability in image quality evaluation has been widely recognised as a common phenomenon. Accordingly, a noticeable body of research has been created to address this phenomenon and improve consistency in relation to dose levels and image quality (Johnston and Brennan, 2000; Elmore, Wells, Lee, Howard, & Feinstein, 1994; Freedman & Osicka, 2006; Garland, 1949; Tudor, Finlay, & Taub, 1997; Shet, Chen, & Siegel, 2011). In the context of image quality assessment, system performance may not only be the sole reason behind diagnostic variations. Observer variability could also have a significant contribution on the overall diagnostic accuracy (Manning, Gale, & Krupinski, 2005). This issue could influence the reliability of the results obtained from visually based image quality assessment methods. Variability in determination of image quality has been investigated since the 1940s (Kundel, 2006). This variation in image quality assessment may result from a lack of standards, including those in reference to visual grading scales. In this context, Krupinski and Jiang (2008) have identified two important issues which need to be considered when addressing variability: 1) that systems are required to minimise the variation between observer interpretations; 2) that approaches are required to assess the systems and their influence on observer interpretation. The European Guidelines for image quality criteria (CEC, 1996) could be one measure used to address the variability in image quality assessment.

1.2.5. European image quality criteria establishment (1996)

Having taken the problems of assessing visual image quality into consideration, two decades ago it was decided that new standards would be needed (Schibilla & Moores, 1995). In 1987, a team from the Commissions of European Communities/ Radiation Protection Programme launched a project to identify radiographic criteria which could help medical imaging professionals make more well-informed judgements in evaluating image quality. These criteria included technical, physical and radiological parameters (Maccia, Ariche-Cohen, Nadeau, & Severo, 1995). Once the quality criteria had been established, two clinical trials were conducted within 24 European countries. The purpose behind these trials was to instill a set of guidelines for the implementation of uniformed strategies for the standard conventional radiographic examinations in Europe to aid in the obtaining of acceptable image quality with a low radiation dose. Initially, six routine X-ray examinations were considered, including skull, chest, lumbar spine, pelvis, urinary tract and breast (EC, 1990). Other important reasons for selecting these radiographic examinations within the European initiative were due to their frequency and the radiation dose which they were administering to patients.

The first European intitiative (1987) has resulted in that a work document to be issued (EC, 1990). Afterthat, in order to validite the proposed criteria another trial was conducted in 1991. The second trial was focused on chest, lumbar and breast radiography only. Accordingly, three seprate questionares were designed for each of the three exmainations. These questionares were then sent to the participating radiology deprtments. Image quality criteria used by the depratments was one of the items requested within the questionare. Then, questionare were gathered with corresponding films. Thses films were sent to a group of fifteen experts for data analysis (five experts for each examination). Their task was to evaluate the films using the same criteria used by departments with same questionares. Data analysis includes how experts' opinion was comparable to those who locally evaluate the same criteria. The reliability of the data, however, was tested by comparing the agreements of independent experts with that of the local radiologists using illustrations of vertical bars (Maccia, Ariche-Cohen, Nadeau, & Severo, 1995). Therefore the criteria were chosen according to the level of agreement existed between two groups of reviewers.

The findings from these two trials, which aimed to assess the relevance of the criteria in 1987 and 1991, revealed there was a significant variation in using exposure factors and patient dose for radiographic examinations (e.g. kVp and FFD), and this led to different image quality. However, about fifty percent of the participating centres demonstrated good compliance with the CEC's suggestions. This indicates that a quality assurance scheme and radiation protection training programme can result in improved radiographic practice (Maccia, 1995, EC, 1990). Nevertheless, the 1991 trial concluded that the criteria should be adopted and will result in an improvement of image quality. After this, large numbers of radiography departments began considering the criteria when assessing image quality; this resulted in the issuing of the final version of the Guidelines in 1996 (CEC, 1996). This version (1996) contains an updated list of

quality criteria; these guidelines mainly address these three issues: 1) the diagnostic quality of radiographic image 2) patient radiation absorbed dose 3) the selection of radiographic techniques.

The 1996 image quality criteria focused on how clearly the anatomical structures are visualised within a specified radiographic image and how this aids in making an accurate diagnosis. Some of the criteria, however, rely on the correct positioning of the patient, whereas others are dependent on the technical performance of the imaging system (CEC, 1996). This was supported by providing a quantitative guide to explain the minimum size at which the important anatomical structures should become visible on the radiograph. In addition to this, the degree of visibility of anatomical structures were categorised into three major definitions: 1) Visibility, *characteristic features are detectable but details are not fully reproduced; features just visible*; 2) Reproduction, *details of anatomical structures are visible but not necessarily clearly defined; details emerging*; 3) Visually Sharp Reproduction, *anatomical details are clearly defined; details clear* (Jessen, 2001; BIR, 1989b). They also excluded all pathological considerations or abnormalities in the establishment of the quality criteria. This was due to the extent and nature of pathology being distinctive, and interchangeable for any specified disease and for any particular patient (EC, 1990). This CEC (1996) project is considered as the foundation on which further work on quality assessment criteria can be built by the radiological community (CEC, 1996). Overall, the purpose behind these criteria was to standardise practice and reduce the variability in radiation dose, and, most importantly, in the evaluation of image quality.

1.2.6. Other literature associated with image quality criteria

A number of researchers have reviewed image quality criteria between 1990 and 1996 (Vaňo, Guibelalde, Morillo, Alvarez-Pedrosa, & Fernandez, 1995; Maccia, Ariche-Cohen, Nadeau, & Severo, 1995; Schibilla & Moores, 1995). Although six common radiographic projections were involved in the CEC guidelines, the work focused mainly on chest and lumbar spine. An early study by Vaňo *et al* (1995) evaluated the EC quality criteria of the chest X-ray. This could be considered as an important step in investigating the applicability of the criteria for research and clinical work. Vaňo *et al* proposed new criteria, and modified the CEC criteria, to make something capable of evaluating the acceptability of chest radiographs for the subjective identification of image quality. In 1996, the CEC funded a project for a joint proposal by British, German and Swedish titled 'Predictivity and Optimisation in Diagnostic Radiology', which was the fourth frame of CEC 1996. This project investigated the relationships between the technical and physical parameters of radiographic examination, the image quality as visually perceived by an observer, and patient radiation dose. One of the main objectives of this project was to further improve the existing quality criteria for a wide range of radiographic procedures. It was focused, however, on the clinical radiographic procedures for assessing the quality of an image, as this would reflect the clinical advantages of image quality criteria (Moores, Mattsson, Månsson, & Panzer, 2000).

The European Commission had issued and published a document for presenting and analysing the results obtained from the two European trials in 1987 and 1990 on the quality criteria. This work was undertaken by Maccia *et al*., (1997) as a part of the CEC project, and considered three main aspects: patient dose, radiographic techniques and image quality criteria. In regards to their findings on image quality, they found some difficulty in having the criteria interpreted by radiologists, specifically criteria that involved the evaluation of symmetry. Moreover, they also noted that some definitions, such as 'full' and 'symmetric', were too vague when used without limits for acceptable deviation, or even without having set any measurement techniques. It was found that some of the criteria can be interpreted in two ways (non-exclusive criteria), which would in turn increase the amount of observer variability in the assessment method. To illustrate, a criterion includes two anatomical structures of different densities, whereby the rating process may mean scoring both anatomical structures, or scoring one of them- ''*Visualisation of the retrocardiac lung and mediastinum*''. Additionally, the amount of film blackening is an example of the highly subjective criterion that has been noted (Vaňo, Guibelalde, Morillo, Alvarez-Pedrosa, & Fernandez, 1995).

Similarly, two other papers considered the evaluation of criteria validity for image quality appraisal (Tingberg *et al*., (2004); Almén *et al*., (2000)). Tingberg *et al*., considered how the European guidelines had addressed the choice of film characteristic curve (H and D-radiographic contrast). The findings of this research showed that although the quality criteria had practical implications for image quality improvements, inter- and intra-observer variation was a significant problem. Almén *et al*., (2000) concentrated on the evaluation of CEC quality criteria for lumbar spine image quality. From this study, conclusions were drawn which were similar to Maccia *et al.* (1995), in relation to how the quality criteria can lead to inter and intra-observer variability. Therefore, they concluded that an explanation of the criteria's meaning, prior to using them, is required for the observers. A recent study focused on developing a set of diagnostic radiographic criteria that would help in the diagnosis of lumbar spinal stenosis, and although this study did not achieve its goals (due to reliability issues), it indicated that the CEC quality criteria did not cover every radiographic projection (Mamisch *et al*., 2012).

On the ther hand, application of CEC image quality criteria to digital radiography is an important issue which needs to be considered. The advent of digital radiography has accompanied by new imaging concepts. Concepts include signal, noise, signal to noise ratio and wide dynamic range. These in fact reflect the capability of digital radiography to convey information about body parts, and the new characteristics of imaging detector (Busch, Faulkner, & Malone, 1995).This imposes that the new techmology would certainly influence the way with which image information such CEC quality criteria (CEC, 1996) could be displayed and visulaised. Accordingly, radiographers should be familiar with digital interface since features such as blackening and film density may not be longer applied. In this context, the digital characterisics would suggest that although CEC criteria may still workable, a revision or even upgrading of thses criteria is necessary to check how thses are fit with the new imaging feature. This is true especially when new option such

post-processing is available which would allow for quality manipulation and dose reduction (Busch & Jaschke, 1998). Accordingly, an EU project (DIMOND) was proposed to upgrade/establish new criteria for digital radiography (Busch, 2004). Others have recommended that CEC criteria should be reviewed to meet the criteria of new techmology (Hemdal *et al*., 2005; Li, Poulos, McLean, & Rickard, 2010).

Taking into account the aforementioned studies, one should be able to draw a number of noteworthy conclusions.For example, that the European guidelines on quality criteria were not future proof because of digital technology replacing analogue, and that professionals are prone to errors which arise from intra- and inter-observer variability (interpreting the criteria differently). From the literature review it can be concluded that no study has been focused on developing image quality criteria for the evaluation of AP pelvis radiograph. Also, no systematic and robust method for determining image quality criteria for AP pelvis has been created. Having realised that in order to optimise radiographic practice for this projection, it is necessary to measure the radiation dose and to quantify the quality of the obtained images. The evaluation of image quality necessitates a valid approach which should be associated with standardised image quality criteria, whilst covering all the factors that may affect the quality of AP pelvis. Given the paucity of literature associated with AP pelvis image quality criteria/visual assessment, it seemed necessary to establish a criteria and method of using them in a valid and reliable fashion. In the next subsection there will be a review of the literature related to research papers which have considered AP pelvis image quality.

1.2.7. Variations in using quality criteria for AP pelvis (Literature Review)
The search for relevant literature was undertaken using peer review journals. The literature search was conducted using ScienceDirect, Medline databases with full text and CINAHL. The relevant key words used in the search included 'image quality of AP pelvis radiograph', 'AP pelvis quality criteria', 'AP pelvis optimisation using CR and DR'; and the major journals searched were 'Radiology','Radiography','Radiographic','Medical physics', 'Radiation protection dosimetry', ' Radiologic technology' , 'European Journal of Radiology', 'Paediatric radiology' and the 'British journal of radiology. Also, CEC guidelines on quality criteria and othe relevant EU reports were reviewed.

An AP pelvis was selected for radiation dose and image quality optimisation within this thesis for two reasons: One reason relates to the purpose of Section I, which is that no valid method for assessing AP pelvis image quality has been reported in the literature; and the other is related to the radiation dose and the frequency of the AP pelvis examination, and will be described in further details in section II of this PhD thesis (subsection 5.2.6 page 123).

It is well known that the formation of images may involve a complex interrelation over many factors, including *technical* and *procedural*. Human observation of the medical image as part of the diagnostic process can also be considered as an essential factor in dose/image quality optimisation (Jessen, 2004). Therefore when developing/upgrading image quality assessment standards, observer effect should be considered to reduce the subjectivity since this has been

proven to have a direct effect on the reliability of the results. Hence, a lack of standards for assessing the image quality of the AP pelvis radiographs has led to significant variations; in some literature the CEC criteria has been used, whereas others have established their own criteria (e.g. noise level). For instance, in 2004, Al Khalifah and Brindhaban compared different exposure factors (i.e. kVp and mAs) and the quality of AP pelvis radiographs obtained by analogue and computed radiography. They utilised the overall diagnostic quality of an image, in terms of the amount of contrast, optical density and noise as an indicator for evaluating image quality. Another AP pelvis study by Brindhaban and Al Khalifah (2005) compared the effective dose and image quality using the same radiographic settings. Image quality assessment was conducted using image noise and the ability of the observer to differentiate between the bony pelvis and soft tissues. However, depending on the overall diagnostic quality to assess the image quality, as mentioned in the above two studies, would liable the assessment of the IQ into high level of subjectivity as based on the individual's experience and opinoin. This in turn would lead to marked variability across the same radiograph observers.

Persliden *et al*., (2002) also conducted a study to optimise the radiation dose and image quality for AP pelvis. In this study, image quality was assessed by two senior radiologists initially using CEC quality criteria for scoring the images. However, the radiologists found that CEC criteria were not suitable to be used for evaluating the quality, and instead they considered the diagnostic usefulness of the images. Diagnostic usefulness was expressed by the amount of noise that each image had and how that affected the clarity of the information in the images (Persliden, Beckman, Geijer, & Andersson, 2002). Again using a general criterion such as 'usefulness for diagnosis' is highly susceptible for variability since it highly based on observer opinion. Others have utilised optical density, density differences, visibility of quantum noise and the overall diagnostic quality as image quality characteristics to assess the AP pelvis radiographs acquired with DR imaging system (Fauber, Cohen, & Dem psey 2011). Regading Fuaber *et al*.(2011) work, there may be two issues when assessing the IQ; first it was based on the overall quality which is highly subjective criterion, and using optical density which may no longer be feasible with digital image as it with analogue since the SNR is the appropriate measure for digital IQ.

Two other studies aimed to develop an optimisation framework, or to find optimum techniques for AP pelvis projections. In one study (Manning-Stanley, Ward, & England, 2012) the authors used the CEC (1996) quality criteria for assessing image quality; whereas in the other study (Heath *et al*., 2011) the authors used additional criteria (i.e. sharpness and contrast) to the CEC criteria. Finally, Tingberg and Sjöström (2005) evaluated AP pelvis radiographs using a modified version of the CEC criteria for pelvis; they believed that these criteria needed to be improved. Reflecting on the latter three studies, the authors have used modified CEC criteria for the AP pelvis radiograph, however, it was not clear how these criteria have been modified and whether they would be valid and reliable or not escpially when additional 'physcal crietria' have been added to the evaluation process. To facilitate the comparison between above literature, table 1-1 summarise the main aspects of these literature.

Table 1-1. A summary of main aspects of the AP pelvis studies which have used different image quality criteria

Authors (year)	Type of study	Imaging system	Evaluation method	Image quality criteria
Al Khalifah & Brindhaban (2004)	- Phantom based - Comparing the IQ across analogue and CR	- Analogue (GE medical system) - CR(Agfa)	- Images and films were scored by 6 radiographers and 1 radiologist. - Five Likert point scale used (1to5).	- Overall diagnostic quality (contrast and optical density) - With CR radiographs only, noise was added to evaluating criteria
Brindhaban & Al Khalifah (2005)	- Phantom based - Comparing the radiation doses across analogue and CR	- Analogue (GE Adavantx -CR (Agfa)	- Hard copies of images were evaluated by 5 technologists, 1 medical physicist and 1 radiologist - Five point Likert scale used (1to5)	- Overall diagnostic quality (differentiation between bones and soft tissues and quantum noise)
Persliden *et al*. (2002)	- Phantom based (Anthropomorphic) - Dose optimisation using direct digital radiography.	- DR (Philips)	- Image were evaluated by two radiologists - Five point Likert scale was used(1to5)	- Usefulness of diagnosis
Fauber, Cohen, & Dem psey (2011)	- Phantom based (Anthropomorphic) - Explore the impact of exposure factors on dose, IE and IQ	- DR (Siemens)	- No details were mentioned on how has evaluated the images	- Measuring optical density, density difference, noise visibility and overall diagnostic quality
-Manning-Stanley, Ward, & England(2012)	- Phantom based (Anthropomorphic) - Study the effect of phantom orientation and AEC selection on IQ and dose	- DR (GE Medical systems)	- Two observers were evaluated the images on workstation monitor(3-MPX) - Relative VGA(against reference image) - Grading system 1to 3 was used	- Modified CEC criteria of AP pelvis radiograph plus three physical inclusion criteria.
Heath *et al*. (2011)	- Phantom based (Anthropomorphic) -Study the effect of increasing the SID on IQ and dose	- DR (GE Medical systems)	-Four radiographers were evaluated the images - VGA (against	- Modified CEC criteria for AP pelvis plus physical inclusion criteria (e.g. sharpness, contrast)

			reference image)	
Tingberg & Söström (2005)	- Explore the the kVp that results in high IQ per E for pelvis and chest - Anthropomorphic phantoms based	- CR (Fuji)	- Six radiologists were evaluated the images. - Two workstation monitors were used - VGA (against reference image)	- Modified CEC criteria for AP pelvis

According to above analysis, different researchers have used different IQ criteria for the AP pelvis radiograph. Additionally, the subjective nature of some of the criteria which have been used is highly susceptible for inter and intra-observer variability. Consquently, it is apparent that there is a complete lack of common standards for assessing image quality for AP pelvis. This no doubt results in a large variation of method and conclusions for image quality analysis, which leads to conflicting results (Seeram, Davidson, Bushong, & Swan, 2013; Shet, Chen, & Siegel, 2011).

In addition to the variability in using quality criteria for assessing AP pelvis, there are other issues that need to be considered, such as the process of evaluation itself, which is psychophysical in nature. Psychophysics in radiology refers to the way in which the relationship between the visual/physical stimuli and human response can be studied quantitatively (Kundel, 2006). This process comprises of two fundamental elements: the human observer, and the displayed image. An observer is required to perceive the information carried by an image and therefore analyse it to institute the required decision (Figure 1-3) (Månsson, 2000).
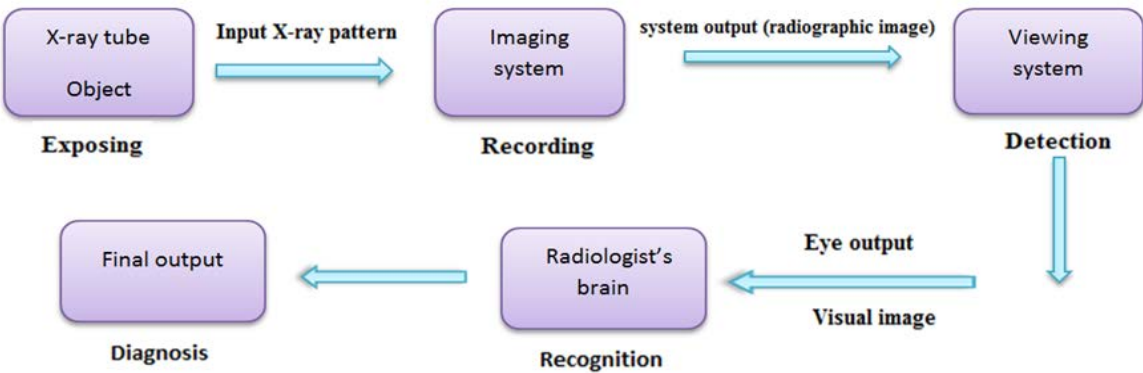
Figure 1-3. Radiological Imaging Procedure (Adapted from Rossmann and Wiley, 1970)

It may not be practical to separate the physical/visual effects from the psychological ones, in the sense of recognising image contents (Sharp, 1990). For this purpose, it could be concluded that, in order to achieve appropriate clinical judgment for the visual quality of an image, it is

necessary to address all factors that may impact on an observer's response. These factors can be represented by anatomical and physical landmarks of the visualised body parts in the X-ray image. This may contribute to the reduction of observer variability by focusing their attention upon certain features in the image (Dobbins, 2000; Tapiovaara, 2006; Thornbury, Fryback, Patterson, & Chiavarini, 1977).

In addition to this, Kundel emphasised the role of an observer alongside the physical measures. Kundel recommended a model be used for image quality assessment which would be based on physical measures and visual appearances which are both important to clinical performance. The latter of the two would evidence the active role that the observer has in extracting the diagnostic information from an image. Therefore, for the best image quality assessment strategies, it may be better to focus on the image's visual factors and how the observer sees them in the first order, while place the image information carriers (pixels that form the features) in the second order. To do this, Kundel suggested there to be a need for more collaboration with other disciplines, in particular psychology, and specifically for those interested in the analysis of an observer's perception of image information and the subsequent decision making; since "*such collaboration may require a large leap across a communication gap on both sides; but there may be great rewards both intellectually and clinically for those willing to jump*". (Kundel, 1979, p.271).

In conclusion, and with respect to literature which has investigated AP pelvis image quality, it has become evident that there is no validated published visual image quality scale for AP pelvis. Knowing that observer, both intra- and inter-, variability exists for all methods described to date it seems paramount that a suitable *image quality scale* be developed. The scale can generally be defined as a psycho-perceptual approach comprising of all those factors that influence the visual assessment of image quality which would in turn contribute to reduce the variability (Shet, Chen, & Siegel, 2011). Further information on the scale and its development can be seen in the next sub-sections (e.g. 1.4, p. 24).

1.3. Rationale for creating a scale to assess AP pelvis image quality

The primary focus of this thesis is to optimise dose and image quality for AP pelvis. So far it has been established that no robust method for assessing visual image quality exists. Because of this, within the first and part of the second year of my PhD, a novel approach to assessing image quality, resulting in the production of a new image quality scale, took place. Production of the visual image quality scale became a secondary focus of the thesis. The purpose behind the need to produce a visual image quality scale is outlined in following points:

1. No method exists for developing or validating a visual scale for assessing clinical image quality.
 2. Evaluating the image quality of acquired images would be slightly complicated with no common image quality scale for AP pelvis radiographs with which to make reference. In addition to this, the literature review has shown that there was significant variability in adopting the quality criteria when assessing the quality which could, in turn, lead to questionable image quality measure.

3. Within this research computed radiography equipment will be used, this would create further need for the employment of a specific quality criteria appropriate for evaluation of a digital image. This fact has been suggested by one of the ICRP publications (2004), where it was stated that some of the Guidelines criteria (e.g. CEC 1996) can be used, whereas others are deemed inappropriate for digital imaging.

4. The importance of developing or upgrading the quality criteria for digital technology may have been confirmed by the DIMOND project, when its focus was on the developing of clinical criteria for digital imaging (Busch, 2004).

In summary, developing a scale for evaluating the quality of AP pelvis radiographic images has been motivated by the need to establish new standards or criteria as an important step in the journey to standardisation within the radiographic practice, and, most interestingly, in addressing the *gap* in the published literature interested in optimising the radiologic procedures. Finally, this scale would serve to fulfil the main objectives of the overall study.

1.4. Measurement scale development- Literature review

The main aim of this literature review is to identify a theoretical framework which would be suited to the development and validation of a scale for assessing visual image quality. The philosophy behind establishing the image quality scales will be discussed. A series of arguments will be presented on why psychometric theory, supported by Bandura's guidelines, is suited in an adapted form for image quality scale development and validation. An explanation will be given on how to create and validate a (psychometric) scale. The search for relevant publications was undertaken using peer review journals and books related to self-efficacy and psychometric scale development. The literature review was conducted using ScienceDirect, Medline, CINAHL and psychologically-related SAGE-journals. For this literature survey, the key words that were used include 'image quality', 'computed or digital radiography', 'self-efficacy', 'psychometric scale and 'image quality for AP pelvis radiographic examination'.

Measurement is an essential element in scientific research within the health sciences as in other disciplines. However, some research work involves measuring things (e.g. human attitude) that cannot be measured directly (Streiner & Norman, 2008); an example of this is the measurement of an observer's perception of an image in diagnostic radiology. In fact, image quality measurements are highly related to amount of diagnostic information *perceived* by the observer in the image. Therefore, it may be necessary to quantify the observer's perception as a clinical metric for the image quality.

Measurement of image quality can either be made directly (e.g. physical measurement of image attributes e.g. SNR) or indirectly (e.g. visual perception). Visual assessment of image quality can be done simply (e.g. no criteria, simply asking for an impression from a clinician) or by using validated image quality criteria within a scale (Burgess, 1995; Kundel, 1979). In this context, a scale can be defined as an instrument whose main function is to measure a variety of visual characteristics/structures. These characteristics are represented as individual items (image quality

criteria) within the scale. Specifically, a scale represents a set of items that aim to measure different dimensions of the specified construct; in this case, 'image quality' (Panagiotakos, 2009). The construct refers to the charactristics that are not directly observable (latent concepts) for which the scale is designed to measure (Abell, Springer, & Kamata, 2009). In statistics, scale items are considered either as continuous or discrete random factors that are often scored using arbitrary rules and therefore summed so as to generate the overall score that describes an observer/individual's perception.

However, the scale development process is often concerned with the accuracy of measurements resulting from the use of scale. In other words, the scale is a measuremental instrument, and should therefore measure what it is designed to, in order to do so consistently and with minimal error. This point is crucial, especially when measurements are related to subjective judgment (e.g. human perception, attitude…etc). The latter arguments refer to the reliability and validity of scale. Therefore, to construct a scale which measure things such as human perception successfully, it must be built on a *scientific basis (framework)* to ensure the reliability and validity which results in a meaningful outcome (McDowell, 2006). An example for the scientific basis could be the adaptation of the psychometric theory (also known by psychometrics) (Abell, Springer, & Kamata, 2009). Further information on this can be found in subsection 1.5.

Having recognised that assessing image quality is an essential step in the optimisation of radiation dose and image quality, developing a scale which is valid and reliable becomes a necessity for medical imaging and radiation protection. Psychometric theory, supported by Bandura's guidelines for creating self-efficacy measurement scales, is likely to be a good theoretical framework for visual assessment scale creation and validation. This is because the evaluation of image quality involves the interaction between observer perception and image information. As a result, observers rate image factors in relation to whether they agree something is visualised clearly or not (Kundel, 1993).

1.5. Psychometric theory (Psychometrics)

Measuring human perception may necessitate the adoption of a scientific approach which would lead to a more reliable outcome (Striener and Norman, 2008). Within this context, using psychometric theory is likely to be a good option for obtaining scientific measurements of perception. Psychometrics is a branch of psychology that deals with measuring attributes that cannot be measured directly; it was established to make measurements (Coaley, 2010). Generally, it concerns itself with evaluating a measurement's problems in a given situation, and then developing methods that overcome or minimise the adverse effect that these have on the measurement. As such, it aims to reduce the amount of error and improve the quality of measurement. In this context, psychometric theory provides a common framework that can be adopted for measurement scale development, revision and modification. In fact, this theory is based on general statistical and mathematical methods that are valid for wide range of measurement applications (Raykov & Marcoulides, 2011). Evidence for the successful application of the psychometric theory is available within the literature. For example, Koutra *et*

al., (2012) have proved that the validity of the Youth Social Capital Scale in Greece using psychometric theory; and Parsian and Dunning (2009) have developed and validated a scale to measure spirituality following a psychometric process. Three publications have described the process of scale development and psychometric validation. One of them developed a scale to measure patients' satisfaction when taking insulin (Cappelleri, Gerber, Kourides, & Gelfand, 2000); whereas the second article successfully developed and validated a scale for measuring depression for people with learning disabilities (Cuthill, Espie, & Cooper, 2003). Finally, Rose *et al.*, developed and validated a scale to measure an individual's distrust in a health care system. The scale was developed in two phases: one phase, to generate the scale items and have them revised by experts, and another phase, to validate using a sample of participants. The psychometric testing has proven that the scale has high level of reliability and validity (Rose, Peters, Shea, & Armstrong, 2004). Therefore, psychometric principles have been proven to be a powerful approach for measuring an individual's psychological construct (e.g. attitude, perception…etc) that cannot be measured directly.

The major applications of the psychometric theory in this thesis are to develop a scale for assessing image quality perception and to test its characteristics (reliability and validity). However, developing a scale with sound psychometric properties (e.g. reliability) necessitates the careful consideration of a number of issues. These issues include the purpose behind constructing the scale (structural options), items content and response format. The latter are essential since they aim to quantify, using numbers/scores, a subjective opinion. Previous psychometric literature has provided some guidelines on how to construct scale (Abell *et al.*, 2009; Spector, 1992). Nevertheless, a literature review has identified that Bandura's guidelines for developing and validating self-efficacy scale could also be adopted as another robust theoretical framework to create a visual grading scale for assessing image quality perception. Further details on these guidelines and Bandura theory will be provided in the next sub-section.

1.6. Self-efficacy and Bandura's guidelines for scale construction

1.6.1. Introduction

This sub-section describes how self-efficacy was developed, and how publications from different disciplines have created scales with high reliability and validity to quantify self-efficacy using Bandura guidelines. The reason for this section is to check whether these guidelines are suitable for the development of a valid and reliable scale to use for assessing image quality perception or not. The concept of self-efficacy was founded as an important construct in the social learning theory. This theory was proposed by Miller and Dollard in 1941. However, it was found that social learning theory failed to consider what the novel responses could lead to as a creative action (Pajares, 2008). After that, Bandura and Walter (1963) wrote Social Learning and Personality Development which aimed to broaden the confines of social learning theory, taking into account the principles of vicarious reinforcement and observational learning. In the 1970s, Bandura realised there was an element missing from contemporary learning theories and from

his own learning theory too (Ashford & LeCroy, 2010). Subsequently, in 1977, Bandura identified this element in his own social learning theory through his publication "*Self efficacy: Toward a Unifying Theory of Behavioral Change*'', which is self-belief. This is widely known as self-efficacy.

Albert Bandura, in his Social Foundations of Thought and Action publication (1986), confirmed that people possess their own self system that can enable their execution of a measure of control over their notions, feelings and actions. This system holds individual cognitive structure and the abilities to plan, learn from others and regulate behaviour. This plays an essential role in providing the requirements for evaluating and regulating personal behaviour, which comes as a result of the interaction between the self-system and environmental roots of influences (Pajares, 1996).

From the social cognitive theory (Bandura, 1986), it was found that self-referent ideas mediate between the amount of knowledge and the required action. However, skills, information and previous achievements are poor predictors for subsequent achievements compared with that of individual thoughts of their ability to execute the required behaviour for achieving a given task (Bandura, 1977). An individual's belief in their ability to successfully achieve a specific task is known as self-efficacy.

1.6.1.1. Self-efficacy and outcome expectation

Bandura made a clear distinction between the outcome and efficacy expectations, and the difference between both can be seen in the schematic diagram below, see figure1-4.
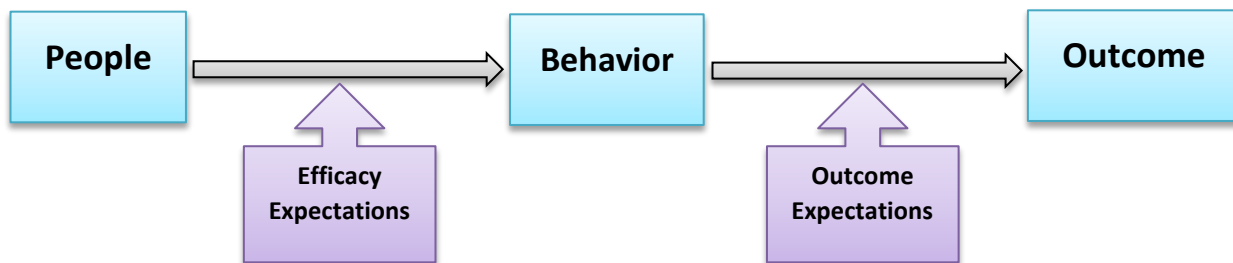
Figure 1-4. The Relationship between Outcome and Efficacy Expectations (Adapted from Bandura, 1977).

Expectation of outcome refers to the individual's estimation that a specific behaviour will lead to a given attainment or outcome. In contrast, efficacy expectation can be expressed as an individual's belief in his or her capability to execute the required course of action in obtaining certain outcomes (Wu *et al*, 2007). To illustrate, an individuals' self-efficacy belief should not be confused with their judgment of which behaviour will lead to a given outcome. As a result, self-

efficacy has the power to provide a level of confidence adequate enough to overcome barriers, whereas outcome expectancy provides the motivation for a given behaviour (Bandura, 1995).

1.6.2. Sources of self-efficacy

According to social learning theory analysis (Bandura, 1977 and 1986), Bandura suggested that self-efficacy relies on four major sources for information: 1) performance accomplishments; 2) vicarious experience; 3) verbal persuasion; and 4) physiological states. These sources will be described in brief as follows:

1.6.2.1. Performance accomplishment:

This can also be referred to as master experience; this source of information was considered as the most powerful factor in affecting efficacy. This is because when people frequently experience success, their incident failure will have no influence on their efficacy belief that they will complete their course perfectly. Furthermore, the interpretation of results for any activity with a successful outcome will help in developing and raising self-efficacy (Pajares, 2008).

1.6.2.2. Vicarious experience:

With this, one can obtain information through observing other people perform a given activity. (Joet *et al.,* 2011). This source of information is considered to be less effective than mastery experience in developing a self-efficacy belief (Pajares, 2008). However, vicarious experience can be more sensitive and relevant for those who are uncertain about their ability, or have a limited previous experience.

1.6.2.3. Verbal persuasion:

Feedback from others, such as parents, managers and teachers can alter a person's confidence for achieving in an activity. Encouragement, or even discouragement, can have a significant impact. Positive persuasion may lead the individual to put more effort and can lead to a higher chance of succeeding. Alternatively, introducing a negative persuasion may lead to a doubt about one's chance of succeeding (Bandura, 1977).

1.6.2.4. Physiological and emotional states:

These sources can play an important role in developing self-efficacy expectations (Bandura, 1977, 1986, 1997). Bandura stated that an individual's interpretation of their emotions, such as stress, anxiety and mood, can be considered as an indicator of self-efficacy level. Strong emotional responses can provide useful information about peoples' subsequent success or failure.

1.6.3. Self-efficacy structure

Bandura identified self-efficacy as the key element of his social cognitive theory, and described it as a person's belief in his or her capability to organise and carry out the required course of action, with the aim of achieving the desired goals (Bandura, 1977 & 1997). Having been given such a crucial role for self-efficacy in determining an individual's outcome, and in order to support his empirical experiment in studying the relationship between expectations and performance, Bandura sought to measure this construct with a task-specific scale (Bandura,

1977). Accordingly, Bandura (1997) realised that there are three main dimensions affecting the efficacy expectations of individuals: magnitude, generality and strength. Magnitude refers to measuring how difficult this particular task is, and this can be classified into simple, moderate and mostly difficult (Bandura, 1977). By generality, he meant that some activities or experiences might lead to generate efficacy beliefs that are domain specific, whereas others could create a self-efficacy that can be widely generalised among different domains.

Finally, the strength of self-efficacy can be represented by the amount of conviction (strong or weak) a person has towards successfully completing an activity, and a person with strong self-efficacy would continue to persevere, thereby challenging all obstacles that he/she will face in attaining the designated goals (Lunenburg, 2011). For this purpose, Bandura in 1977 mentioned that, in order to have an adequate self-efficacy analysis, one should assess the above dimensions in detail, considering the required level of precision that is to be expected within the measurement of behavioural processes.

1.6.4. Self -efficacy measurements

It is important to note that a number of issues must be considered when there is an attempt for a self-efficacy evaluation in any discipline. One essential issue is that self-efficacy, as derived from the Bandura's generic definition, is a domain, or task specific construct and therefore any self-efficacy measure should be designed with this having been taken into account (Bandura, 1977 & 1997). In addition to this fact, measuring a psychological component such as self-efficacy would require the assessment to be *valid* and *reliable,* aiming to make the required contribution from the obtained findings. To achieve the required level of reliability and validity, Bandura suggested conceptual guidelines, and that their adoption would ensure a developing scale with adequate psychometric properties. These guidelines cover the scale development from the point of generating the scale items to last step, when data analysis is required and therefore the reliability and validity of the scale is tested by the entire process (Bandura, 2006). Although the required scale for this thesis is not to measure the self-efficacy, these guidelines together with previous psychometric literatures could be essential for developing a psychometric scale for assessing image quality perception for the first time in medical imaging.

Bandura's guidelines outline the importance of the generated items accurately reflecting the construct to be evaluated; in this case image quality of AP pelvis. Items should have certain challenges for an individual to give a better performance, alongside measures for reducing affirmation bias. Also, items should only have one idea, to reduce confusion and therefore reduce measurement error. Ultimately, the degree to which people are confident about their feeling that they can answer certain questions, or do a given action to perform a given task, should be recorded using suitable response scale. The latter of these is important for measuring image quality perception because it is known that, in order to obtain information about image perception from an observer, the only way is to take a response to a question or image report. However, the reliability of the response, or self-reported measure, is strongly linked to the appropriately framed question within a well-designed scale (Kundel, 1993).

In practice, self-efficacy is assessed by asking individuals to record the strength, magnitude and generality of their beliefs to perform an activity. After that, it is necessary to translate the belief/confidence of an individual into a numerical format using a Likert scale as a reliable and valid measuring system. Finally, the value of self-efficacy will be obtained by totaling, or summating, the reported scores by each respondent to give the overall score for the measured construct (Stajkovic & Luthans, 1998). Bandura recommended assessing all items in relation to their scores that are ready to be tested for reliability and validity, so that any item found to adversely affect the measurement can either be addressed or discarded from scale. According to what has been aforementioned, following these guidelines could positively improve the characteristics of the scale under development.

1.6.5. Self-efficacy measurement scale– Application in different disciplines

This sub-section focuses on other work that followed Bandura's guidelines, in order to develop and validate scales. Bandura's self-efficacy and social cognitive theory has provided propositions for a large number of applications. This is because the validity and reliability are adequate and clear guidelines on how to develop and assess human attitude for a given action, have been provided (Bandura, 1995). Therefore, it gives a self-reported measure of an individual's perception as to how confident they feel in relation to performing a specific task.

Building on Bandura's theory, fields as diverse as psychology, medicine, politics, athletics and education have all gone on to create psychometric scales. For the purpose of this research it was decided to that the focus be on the application of Bandura principles in the education and health spheres. This is because these two domains have relevance to developing and validating a psychometric scale for image quality perception in medical imaging. For example, a breast feeding scale development and validation using psychometric principles and Bandura's guidelines was attempted by by Dennis and Faux (1999). The authors started with conceptual analysis of breast feeding to identify the main aspect of the construct; and they then generated a pool of items to form the scale draft ready for validation process (scoring), which was done using study samples. The results demonstrated that the developed scale had excellent psychometric properties. This suggested that the scale had value for clinical work. Another project aimed at developing and validating a psychometric scale for assessing women's confidence to regularly attend mammographic screenings. In this work the procedure of scale development and validation followed Bandura's guidelines. They started by defining the factors which influence the construct (women's confidence) and introduced them to experts, to add face validity to the scale. They validated the scale using an adequate sample size (>500 volunteers) to score the scale items; this procedure resulted in a scale with high psychometric properties (reliability and validity) (Champion, Skinner, & Menon, 2005).

Wolf and colleagues (2005) developed and validated a psychometrically sound scale for assessing a patient's attitudes to communication about cancer. Again, the research processes were guided by Bandura guidelines. Aside from the final scale produced, this work has offered clear guidance about the steps required to develop and validate a psychometric scale. The steps

covered the entire procedure, from generating and testing the scale items to the sample size and validation process ready to finalise the scale (Wolf, Chang, Davis, & Makoul, 2005). Others have followed their scale developing format to reduce the number of originally validated scale items (breast feeding scale) and to assess their characteristics psychometrically. The results demonstrated that the new scale version has an excellent reliability and they therefore suggested the scale to be valid for clinical assessment (Dennis, 2003).

On the other hand, the education sector includes many attempts for developing and validating a psychometric scale based on Bandura's guidelines. A research published by Kitching *et al.*, in 2011 aimed to develop and validate a psychometric scale for radiography students. In fact, the scale was intended to measure self-efficay of students' radiographers in the clinical placement. Therefore it was aimed to predict the level of the skills the students gained throughout their training course. According to the scale evaluation, action can then be made especially with those students who had low training skills. The research was conducted through two phases: a development phase that included item generation and focus group analysis to improve scale validity; and a validation phase, which included the sample size scoring of the scale draft. Item analysis, reliability and validity testing demonstrated that the scale had high psychometric properties which suggested it had value for educational purposes. Cassidy and Simon (2002) have, in their paper, described the procedure required to develop and validate a computer-user self-efficacy scale. The procedure was conducted in similar format to that conducted in the aforementioned reports. The reliability and validity of scale items were tested using relevant psychometric metrics. The results indicated that the developed scale had a high level of internal reliability and validity. From the literature review, it is apparent that Bandura's principles are a rigorous framework to guide the methodology of creating and validating psychometric scales for measuring an individual's confidence to achieve a given task in different disciplines. Therefore, it provides a robust theoretical background to guide the methodology for creating and validating a perceptual image quality measurement scale.

1.6.6. Self-efficacy measurement in diagnostic radiography
The literature review revealed a paucity of literature regarding the operationalisation of self-efficacy principles in radiology, and particularly in radiography. Nevertheless, one study was recognised as relevant and utilised Bandura's guidelines and psychometric theory to develop a scale for assessing the image quality of mammographic film (Moran, 2012). This work aimed to develop a psychometric scale for image quality assessment in mammography (based on analogue equipment). In this, the scale was developed following Bandura's principles, as mentioned in the previous sub-sections (1.6.4 and 1.6.5). However, for the purpose of developing an image quality assessment scale, reference images must be used for scoring purposes, and this is because image quality scales regard items which reflect certain anatomical and technical features to be factors that affect the quality of an image.

Although Bandura's guidelines with psychometric principles were adopted in the development of the mammography scale (Moran, 2012), there are a number of issues that need to be considered.

First, the sample size used to score the analougue images could not be deemed adequate for testing the scale psychometric properties (n=79). Evidence for this comes from scale development literature, where sample sizes in excess of 100 are required for scale development and validation (Spector, 1992). Second, the number of reference analogue images used was small (only 3), so does not reflect a good range of the quality that a scale must be validated against. Finally, the procedure used to select the reference analogue images was questionable. It was based on subjective opinions from only a few professionals, and there was no adequate consensus on the determination of their quality.

According to the previous passages, the principles of Bandura are best introduced to develop a scale for the purpose of self-efficacy assessment in different disciplines. Therefore, these principles can guide the process of scale item generation and formulation, taking into account their *psychometric impact* on the overall evaluation of image quality perception. Individual perception assessment is essential in identifying the most important and influential factors deemed effective enough to be retained in the final scale. For this cause, the volunteers' scores would help in identifying to what extent the scale is valid for assessing the perception of the image quality, since they would score their agreement on the applicability of each item for a given image quality assessment.

1.7. Conclusion
The presented literature has been used to argue a case for using psychometric scale development and validation theory in assessing visual image quality. Specifically, the psychometric theory will be adopted as a robust theoretical framework to guide the methodology of scale creation and validation. Bandura's guidelines will be used extensively to inform the aforementioned approach and to allow the development of a visual image quality assessment scale for AP pelvis radiographs.

1.8. Objectives of producing a valid and reliable image quality perception assessment scale for AP pelvis radiograph

1. To identify a theoretical framework which can be then used to create and validate a scale to assess visual image quality.

2. To adapt the theoretical framework to create and validate the scale.

3. To develop and validate the scale.

4. To reflect on the (adapted) theoretical framework for its suitability to develop and validate scales for assessing visual image quality.

5. To use the validated scale to assess the images acquired for the optimisiation purposes (section II of this PhD thesis).

Chapter 2: Scale creation and validation methodology

2.1. Methodology overview

This chapter describes how the image quality scale was developed and validated using images. The description is preceded by an explanation of the study design. To start with, the main domain(s) of the image quality will be defined using published literature. Once the image quality construct is identified, a draft scale will be produced comprising of a set of items that would cover the domains (themes). A focus group was then formed to review the generated items. Next, the reviewed scale was drafted and finally reviewed by an expert, prior to administration. Concurrently, a set of reference images were produced for the two validation phases (phantom & cadaveric). The appropriate method for administering the image quality scale will be discussed as well alongside an explanation regarding the required sample size necessary to generating reliable findings for the scale validation (figure 2-1). After collecting the data from both validation phases, it is important to understand the statistical analysis process for interpreting the outcomes; this would provide the final conclusions regarding the reliability and validity of the scale and therefore allow the publishing of the final visual image quality assessment scale.
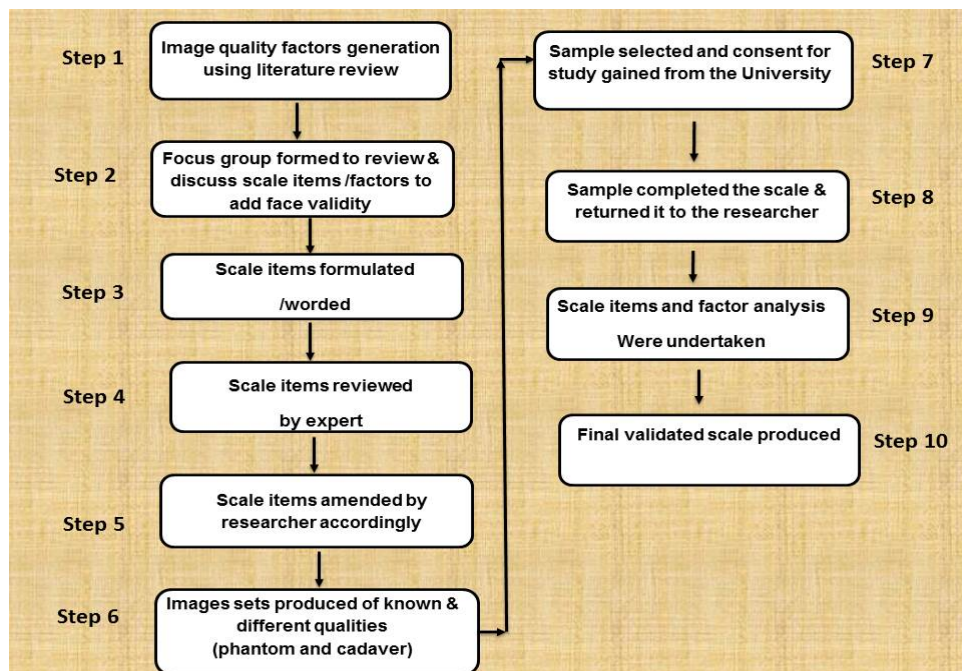
Figure 2-1. Key steps in the scale development and validation process.

2.2. Study design

Perception as a construct can be assessed in various ways. It may be measured either quantitatively, qualitatively, or both depending on the underlying purpose of the study.The literature review (see pages 25 and 30-31) demonstrated that the vast majority of published studies which developed a psychometric scale used a quantitative approach to meet their proposed objectives. Accordingly, to best meet the objectives of visual IQ assessment scale development and validation, a quantitative based experimental approach has been adopted. The justification for this is due to the research procedures involving volunteers scoring phantom and cadaver images of known quality using the AP pelvis image quality scale developed within this thesis. This is essential for the secondary focus of this thesis, since the volunteers will score their opinion/confidence in numerical form to give an indication regarding the quality of the images that can later being analysed statistically.

2.3. Domain identification and image quality factor generation

Setting a clear definition of the domains leads to the generation of a pool of items, item refinement and then item selection, based upon standard psychometric principles and statistical testing (Bandura, 2006). Careful delineation of the construct is essential, and could otherwise lead to difficulty in the defining of the items. Several themes/domains normally represent different aspects of a construct; when combined they make up the whole construct (overall image quality) (Spector, 1992). In this context, it is recommended that the best way to define the construct be to base it on similar work, at least as a starting point. If the scale construct is totally new, Streiner and Norman (2008) suggest that a literature search be conducted and a focus group held to identify the domains and scale items. Since no scales were found in the literature, the searching process focused on identifying factors deemed crucial in affecting the quality of an AP pelvis radiographic image. After these factors were identified, the next phase included the discussing of their correspondence with an underlying construct (i.e. image quality of AP pelvis), ready for item generation.

2.3.1. Main sources of image quality factors

This subsection focuses on how the image quality factors were identified. The factors found to be essential in defining the quality of an AP pelvis radiograph were acquired from different sources. One of the most important sources was that of the European Guidelines on the quality criteria for radiographic images (CEC, 1996). The CEC criteria comprised of anatomical and poisoning factors that are considered to be effective in determining the image quality of AP pelvis projections (table 2-1).

Table 2-1. European quality criteria for AP pelvis radiography (CEC, 1996)	
No.	Criteria
1	Symmetric reproduction of pelvis as judged by the imposition of symphysis pubis over the midline of sacrum
2	Visually sharp reproduction of the sacrum and its intervertebral foramin
3	Visually sharp reproduction of pubic and ischial rami
4	Visually sharp reproduction of sacroiliac joints
5	Visually sharp reproduction of the necks of femora which should not be distorted by foreshortening or rotation
6	Visually sharp reproduction of the spongiosa and corticalis, and of the trochanters

Published studies that have used AP pelvis as a topic for investigation were the second source for obtaining the quality factors. Some factors/criteria were identified in the literature using the CEC criteria with slight modification, whereas the rest used other (different) criteria established for the purposes of their studies (Al Khalifah and Brindhaban, 2004; Brindhaban and Al Khalifah , 2005 ; Persliden et al., 2002 ; Fauber, Cohen, & Dempsey 2011; Heath et al., 2011). Most of these studies were cited in subsection (1.2.7). Furthermore, Rainford *et al.,* (2007) have classified the pelvis quality criteria into *technical* and *procedural*, to study the effect of these factors on the image quality. Finally, radiographic positioning books were also examined as they contain radiographic criteria about image quality. In summary, there are three domains (themes): physical, technical and anatomical/procedural.

2.4. Scale item creation

There was no literature found which used Bandura's guidelines and the psychometric theory to develop an image quality scale for use in medical imaging. However, there are a considerable number of studies which developed scales for other applications. Therefore, in order to generate scale items for this thesis, it was necessary to review the methodology sections of various published studies to establish a theoretical framework capable of guiding the process of proposing the items (Kitching, Cassidy, & Hogg, 2011). The existing literature served as a guideline to identify the number of items that should be produced (Spector, 1992).

The literature review also revealed that the majority of relevant publications did follow Bandura's guidelines in their attempts to generate and word their items within their developed scales (Champion, Skinner, & Menon, 2005; Rose, Peters, Shea, & Armstrong, 2004; Wolf, Chang, Davis, & Makoul, 2005; Kitching, Cassidy, & Hogg, 2011). Bandura's guidelines emphasise two points: domain specificity (i.e. image quality of a particular radiograph), and that the proposed items be designed to measure how confident an observer is for a particular item in a given image set. Finally, within this thesis, twenty seven items were generated from the previously suggested image quality factors.

2.4.1. Content validity of scale items

Content validity can be defined as being the extent to which the scale items comprehensively represent the (main) construct of interest (Streiner & Norman, 2008). Once the scale items have been generated, it is important to ensure they cover the construct adequately. Any item that does not relate to the construct could lead to an error in measurement. This, therefore, results in

discrimination on certain different dimensions. Three important points have been suggested to support the content validity: 1) using large numbers of items, 2) using items generated from a broad literature review, 3) including a broad range of cognitive strategies (Strickland & Dilorio, 2003). The scale items were first tested by experts (radiographers) alongside researcher and then reviewed by focus group members.

2.5. Ethical issues

When research requires human involvement, special care must be paid to volunteers' rights (Polit and Beck, 2003). Three ethical approvals were sought for this thesis. Two were provided by the University of Salford (UOS), one for each phase of the research (i.e. phantom and cadavers) to enable radiography students and qualified radiographers to review images (Appendix I). Focus group members' recruitment and participation was included within the first ethical approval only, since no focus group was required for the second validation phase. And another was provided by Human Ethics Committee of the Canton de Vaud (Switzerland) to produce sets of images from cadavers (Appendix II). All volunteers in this study were required to sign a consent form before conducting any related task (Appendix III).

2.6. Focus group

A focus group can be defined as a group discussion designed to obtain thoughts on a defined area of interest in a permissive, non-threatening environment. Group sizes often range from six to twelve people (Puchta & Potter, 2004). A focus group was formed for the purpose of developing/agreeing image quality scale items. The main function of this focus group was to add *face validity* to the proposed scale items. Most of the volunteers were recruited from radiography staff, from University of Salford and local clinical departments.

The focus group comprised of a consultant radiologist with over twenty five years' experience, and two clinical radiographers with experience of 25 and 33 years, respectively. The rest of focus group members were University-based staff with between five and ten years' experience. Within the University staff there was a medical physicist and four diagnostic radiographers. The number of focus group members was deemed adequate to acquire the required information and to give each member the chance to have his/her own role in the discussion. According to this, homogeneity has been reached in the focus group, as per recommendations (Sim & Wright, 2000). Focus group homogeneity refers to the level of experience focus group memebrs should have to provide a thorough and balanced contribution to discussion. If, however, focus members recruited with big experience gap, then main contribution would have been reached by little members (i.e.most experience members).

2.6.1. Focus group discussion and analysis

Generally, the role of the focus group was to review the proposed items and improve their validity in measuring what they are designed to measure. Two steps were accomplished before the holding of the focus group. Firstly, a background information letter was sent to all of the participants of the focus group. This letter comprised of a brief overview about the nature of the study at hand, and the aims behind constituting the focus group. This information, in turn, would

give volunteers an understanding of what they were going to do. Secondly, all of the focus members were asked to sign a consent form, ensuring they were prepared to comply with the ethical issue requirements (see appendix III).

The focus group started with a brief explanation on how the image quality factors list had been generated; this was from an extensive literature search which provided details on factors deemed important when assessing the image quality of an AP pelvis radiograph. Focus group members then discussed the proposed items, analysing each from different perspectives, e.g. whether any factors could be considered as anatomical or procedural in terms of theme. The focus group was provided with an AP pelvis radiograph to help facilitate discussion. The appropriateness of each item was discussed, with the aim of attributing each item representing a factor to one of the themes/domains mentioned in literature (procedural and technical). Accordingly, the following pivots points were discussed:

1. The applicability of scale items for clinical work in addition to their utility for research purposes. This is due to any lack in the standardisation in diagnostic radiology having the potential to affect the diagnostic efficacy, and this would in turn affect how a patient's problem is managed.

2. The designing of a psychometric scale for assessing the image quality of digital image should be clearly defined, primarily for normal and non-pathologic imaging as this scale is to be validated for the first time in diagnostic radiology (EC, 1990). Therefore, all items that could reflect any clinical case should be removed from the proposed scale.

3. According to Bandura's guidelines (Bandura, 2006), each item should be carefully worded, so that it reflects one single idea in order to avoid confusion in the statement's reflecting two or more ideas. This would address some of confusion within the CEC criteria (1996).

Focus group members suggested that some of the items should be removed. Five items were removed because of inappropriateness, and that they may cause some structures to be visualised inadequately. One item was deleted because it is not frequently used in the clinical practice, and thus may confuse the observer (the level of the SNR on the image). However, it was suggested that this item should be substituted by another item with a similar meaning, as an appropriate alternative. One further item was deleted because it was considered redundant, as there was a similar item which would give the same result.

Other items needed modification. As a result, it was suggested that each anatomical structure (mostly bones) in the pelvis should have a separate item in order to reduce confusion that might arise from the inclusion of two identical items in one item. For example, the left iliac crest should have in its own item, instead of wording both iliac crests in one. Six items were generated and added to the proposed scale. This expansion in the number of items may increase the generality of the scale (Bandura, 1986, Bandura, 1997).

A final review to the draft scale was made by an experienced radiographer who is an expert in the field of psychometric theory. A review of the literature, combined with the focus group, lead to the production of a twenty nine item (draft) scale.This covered physical, procedural and technical domains (image quality themes).

2.7. Image set production

Producing (AP pelvis) images of predefined quality was a key step in scale validation. In order to create an image quality scale, it is essential to produce images of both known and different quality. The quality of the images needed to range from very poor to very good. The images were ranked from good to poor using qualitative (consensus opinion – 6 experience radiographers with minimum 5 years experience) and objective measures. The image production process was preceded by a literature review to identify guidance as to how a clear definition for the quality of the radiographic image can be given. There were two sources used: Radiological Society of North America (RSNA) lexicon and International Labour Office (ILO, 2002; RSNA, 2010). Also, Lehnert *et al*., (2011) provided five definitions for the quality of an image in terms of satisfaction for medical diagnosis. All these sources provided a subjective definition to help identify image features which are consistent with the most common disorders that pelvis radiology is tasked with diagnosing. The image features refer to most common anatomical landmarks within pelvis region; the common disorders may include routine follow up studies after fracture, arthroplasty, trauma and orthopedic measurement (Völk *et al*., 2003). However, the image quality still needed to be confirmed objectively. The purpose for this is to produce images with true (high) quality, and also minimise the subjective bias. As a result, SNR, as a figure of merit for image quality, was used for this purpose (Tapiovaara, 2006). This figure refers to the ratio of the amount of useful information (signal) in a given image, to that of useless information presented at the same image (noise). Therefore, to meet the objectives of the preliminary study, two sets of images of known quality were produced. One set produced using phantom, and the other using cadavers. The procedures conducted for both will be explained in subsequent sections.

2.7.1. Production of phantom images

A series of experiments were conducted to define the images of varying quality. Initially, it was intended to identify the image with highest SNR to be used accordingly as a reference for acquiring the subsequent images with lesser quality. To produce the highest SNR image, images were acquired by systematically varying kVp from its lowest available setting (e.g.40) to 120 kVp. The varying of the kVp was done initially in three steps (increments) till 60 kVp and then varied at 5 steps, according to the equipment's available settings and the kVp range that trigger change in SNR. This procedure was repeated three times but with three different commonly used mAs - 10, 20 and 30 respectively. The same procedure was conducted to acquire images, but with varying the mAs from its lowest available setting (e.g. 1.2) to 100 at three commonly used kVps - 70, 80 and 90 respectively. The mAs was increased in 2 steps, according to the equipment's available settings. The reason behind repeating the procedure three times for each

acquisition factors was to identify the average high quality image. The previous experiments were conducted to identify at which kVp and mAs the SNR was at its highest and lowest levels (see figures 2-2 and 2-3 as typical examples). Details on specifications of the X-ray equipment used for these experiments can be seen in section II (6.2.1; p.134) since the same equipment were used to acquire images in both thesis sections. Equipment performance was tested via the conducting of quality control measures, to see whether their performance fell within the manufacturer's specifications or not. The experiments were conducted using an opague anthropomorphic pelvis phantom (Alderson) to acquire the images. Nevertheless, the phantom used for scale development was different to that used for optimisation work (i.e. availability reason). The phantom was positioned in relation to standard radiographic positioning (Whitley, Sloane, Hoadley, Moore, & Alsop, 2005).
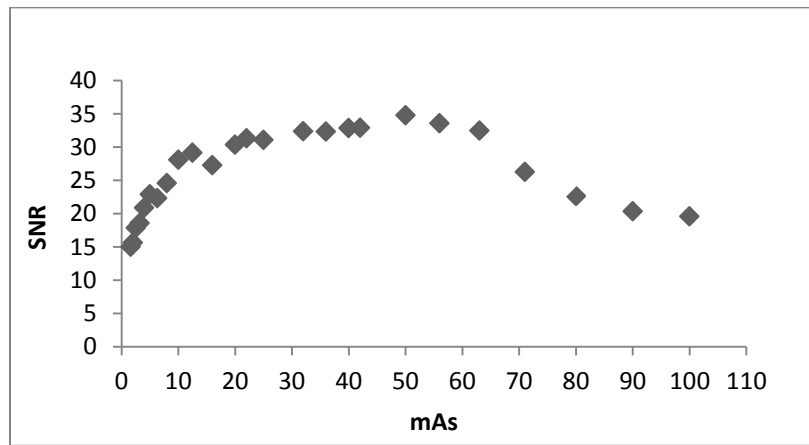
Figure 2-2. This figure presents the trend of SNR of the acquired images when mAs varies from its lowest available setting to its highest, at a constant kVp (70). This helped in identifying at which mAs setting the SNR is highest and vice versa.
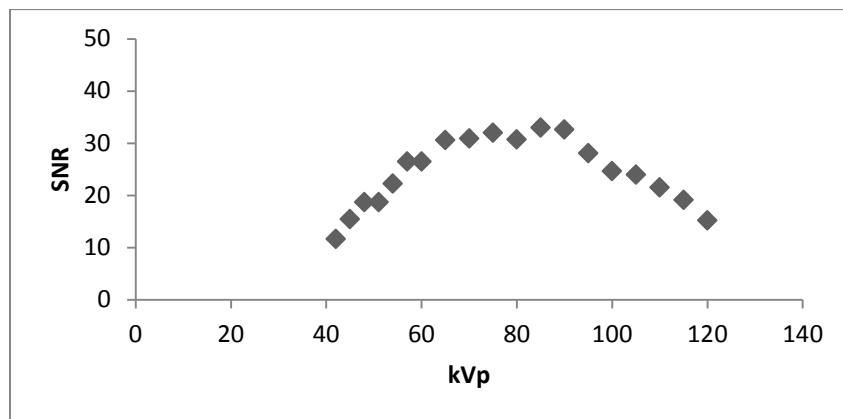
Figure 2-3. This figure presents the trend of SNR of the acquired images when kVp varies from its lowest available setting to its highest, at constant mAs (20). This helped in identifying at which kVp setting the SNR is highest and vice versa.

As a result, three different values for each of the kVp and mAs were obtained at which the SNR was highest. After that, a factorial experiment ($3 \times 3 = 9$) was undertaken to identify the best SNR image (highest average IQ image), see table 2-2 for combination of settings used. Middle quality images were then produced by varying the exposure factors (kVp and mAs) systematically (i.e. through definite steps for each of them), see figure 2-4.
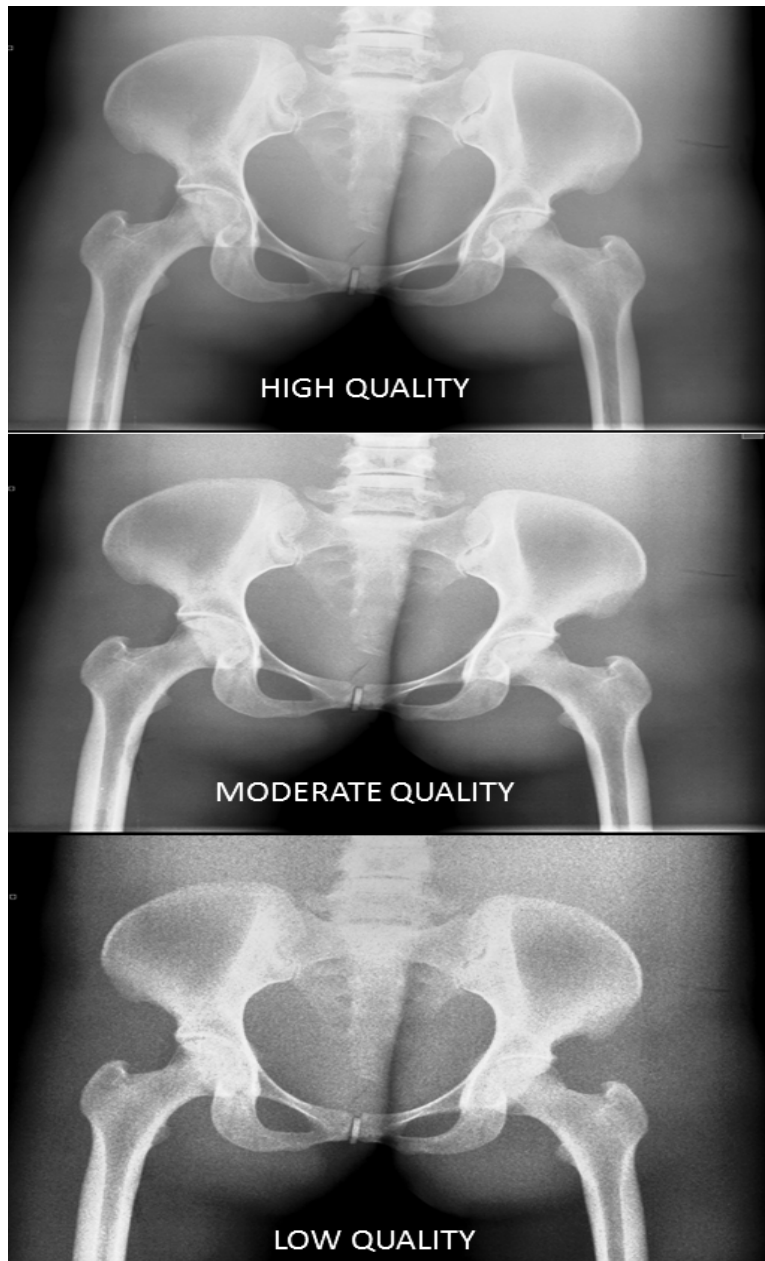
Figure 2-4. Samples of the reference images produced using phantom.

Table 2-2. This presents the combinations of settings used to identify the highest SNR image allwere at 110 cm.									
kVp	105	105	85	105	75	75	75	85	85
mAs	50	32	50	20	32	20	50	32	20

Seven images were eventually created, ranked in term of SNR from low to high quality; table 2-3 summaries their acquisition parameters. The SNR was measured by drawing four ROIs to calculate the average signal value from, and one ROI to identify the noise value, see figure 2-5.
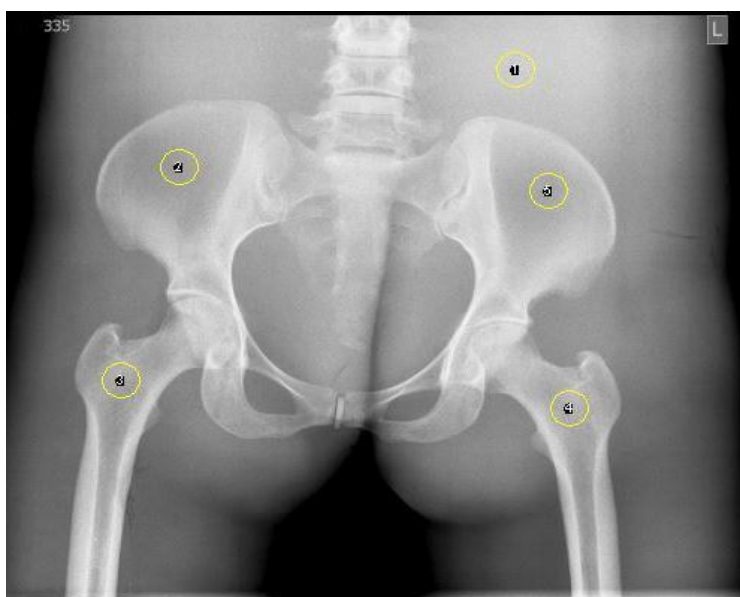
Figure 2-5. This figure illustrates the four ROIs used to calculate the mean signal values across bony pelvis and the fifth ROI (uniform area) used to calculate noise value for the purpose of SNR measurement (i.e. SNR= mean signal value/ noise)

The rationale behind having 'seven images' was to comply with the domains definition requirements (task difficulty) (Bandura, 1997), and so that the scale can be tested/validated against a wide range of image quality (utility). This measure, therefore, enhances the validity and the generality of scale, lending it more credibility for its future use in research and clinical practice. The quality of these images were then checked and confirmed subjectively through a group consensus with the help of the subjective quality definitions. Group consensus was achieved by presenting the set of seven images with different quality, in term of SNR, to agroup of experience radiographers. The task of radiographers was to see how they would agree that these images are well differentiated from each other, and to make sure whether that the SNR ranking is agreeing with their subjective ranking or not (from high to low). If, however, they did not agree, then another images acquisition and manipulation would have been made.

Table 2-3. This illustrates the SNR values for each image (ordered from highest to lowest), associated radiation doses (dose area product (mGy.cm^2) and acquistion factors.

Image rank	kVp	mAs	SID	DAP (mGy.cm^2)	SNR Mean	95% CI for mean	
1	85	20	110	1161	60.1	56.7	63.6
2	80	16	110	776	42.7	40.2	45.2
3	75	12	110	335	34.4	32.7	36.2
4	70	9	110	325	29.9	28.3	31.5
5	65	7.1	110	236	23.1	21.8	24.4
6	57	5	110	118	16.7	15.5	17.8
7	50	4	110	63	11.6	10.7	12.5

2.7.2. Production of cadaver images

The cadaver images were then used to further validate the scale. Unlike phantom images, cadaver images can demonstrate anatomical variance, structured noise, and soft tissue shadow variation. Acquisition factors that had led to the final seven phantom images were used as a guidance to acquire the reference images for the second validation phase, using cadavers. However, manipulation of the said acquisition factors was allowed to meet the challeges imposed by different body sizes and conditions to acquire images with different quality, similar to that of phantom images. In addition, to simulate the clinical situation certain positioning and technical problems were included. Images were acquired using CR system (Carestream 800). Four cadavers were imaged; two of them were males and two were females. Different cadavers were used to best test the scale in a clinical simulated environment. The cadvers were chosen to have an average adult body size. Seven images from each of these four cadavers were acquired; in total, twenty eight cadaveric images were acquired. For the purpose of choosing seven images with different quality, SNR was calculated for all images using the same protocol as that of phantom (i.e. four ROIs for calculating signals values and one ROI for noise) see figure 2-5. After that all images presented to a focus group of six radiographers to identify seven images of different and known quality (high to poor). This process was conducted using images SNRs' values together with focus group's subjective opinion to compromise between the both approaches, namely subjective and objective approaches. This was so to make sure that the quality of chosen images is well defined subjectively and objectively. The role of focus group was essential with cadaveric images ranking due to the inclusion of the postioning and technical issues. The characteristics of each of the seven images are described below.

2.7.2.1. High quality cadaver image (Rank =1)

The highest quality image was produced with a low noise level (Figure 2-6). This image was produced without positioning problems, or any other procedural error, and was meant to be the best compared with rest images of the same cadaver, but with different acquisition factors. The

signal to noise ration of this was 49.5 SD 4.6. Visually, it was confirmed to have a good contrast and almost all anatomical structures were visible.

Figure 2-6. The highest quality cadaveric image.

2.7.2.2. Second quality cadaver image (Rank =2)
The second ranked cadaveric image's features were closely comparable to the highest one in terms of noise and positioning. Nevertheless, its SNR was 30.7 SD 2.45. The reason behind this, though all images were presented randomly to volunteers, was to add certain task challenges in order to test the utility of scale items across quality with small differences (Figure 2-7). Visually, its contrast was slightly lower than the first ranked image. No positioning or technical problems were included.

Figure 2-7. The second ranked quality cadaveric image.

2.7.2.3. Third quality cadaver image (Rank =3)

This image was chosen to have some positioning errors. The imaged body was slightly rotated to right side, and, in addition, a technical fault exists in tight collimation near the proximal femora. However, it was still classed as good image in terms SNR 25.6 SD 6.12, and the anatomical structure visualisation was generally good, together with appropriate tissue differentiation (Figure 2-8).

Figure 2-8. The third ranked quality cadaveric image

2.7.2.4. Fourth quality cadaver image (Rank =4)

This image includes a technical collimation fault nearer to the right femoral side. However, no positioning issues were associated with this image (symmetrical). It was deemed to have a high noise level compared with the previous images. Hence, the SNR was 24.53 SD 2.8, meaning that its quality was slightly lower than the third image (Figure 2-9).

Figure 2-9. The fourth ranked quality cadaveric image.

2.7.2.5. Fifth quality cadaver image (Rank =5)

The fifth ranked image had technical and positioning errors; a collimation and a slight body rotation. This image had a low SNR value (20.7 SD 2.87), and the sacrum, along with its intervertebral foramina were almost hidden (Figure 2-10).

Figure 2-10. The fifth ranked quality cadaveric image.

2.7.2.6. Sixth quality cadaver image (Rank =6)

This image had a high noise level and therefore low SNR value (14.9 SD 1.04). The latter value was the lowest compared with all of the other images. No positioning errors or technical faults were included. Overall, the subject contrast of this image was low (Figure 2-11).

Figure 2-11. The sixth ranked cadaveric quality image.

2.7.2.7. Seventh quality cadaver image (Rank =7)

This was the poorest quality image, with the highest noise level; an artificial artifact (button) exists on the right hand side together with a collimation fault at the lower side of the image. Tissue differentiation was poor due to the high noise level (SNR 12.1 SD 1.65; Figure 2-12).

Figure 2-12. The seventh ranked cadaveric quality image.

Overall, the seven cadaveric images were ranked in terms of quality, both subjectively and objectively similar to phantom images.

2.8. Construction of draft scale

Once scale items have been reviewed by the focus group and an expert, the draft scale was constructed. The scale included 29 items, and the items were randomised across domains to reduce the information bias. A 5 point Likert scale was used to rate scale items (i.e. a score of 1 means the responder strongly disagrees and a score of 5 means they strongly agree), resulting in a numerical format for individual agreements. (Appendix IV). Some of the scale items were worded negatively and the rest positively, to lessen acquiescence in affirmation (Presser *et al.*, 2004).

2.9. Preparations for completing the scale

In order to validate the scale, volunteers were required to score it against reference images. This includes volunteers completing one scale for each image. Prior to starting any scoring process for the two phases, it was deemed essential to perform the measures below:

1. Prior to image scoring all participants undertook a 1 hour tutorial on image quality in which the scale was explained. The purpose of performing the tutorial for all BSc (Hons) Diagnostic Radiography students (YI, II, and III) is to bring their knowledge and understanding to a standardised and known level prior to undertaking the imaging scoring scale. This training has direct relevance to the BSc Radiography curriculum and the competencies of a newly qualified radiographer. The training elemments are focusing on defining the IQ and how this is essential in diagnostic radiography, physical aspects of image quality (e.g. contrast), how acquisition factors are affecting the IQ, CEC Guidelines on quality criteria and explainging some physical measuers of the IQ such as SNR. Students' radiographers start studying pelvis radiography at Y1 of their course programme.

2. Three mega-pixel PC monitors (22 inch Iiyama ProLite liquid crystal display monitors - B2206WS) were used to display the images; these monitors were calibrated to the DICOM Gray scale Standard Display Function (GSDF).

3. Ambient light was kept dimmed at 20-38 Lux during the scoring process (Norweck *et al.*, 2013).

4. No image manipulation was permitted; volunteers were blind to image acquisition factors.

5. All monitors were cleaned at regular intervals.

6. The seven images were randomised for image quality review in order to reduce observer scoring bias.

2.10. Pilot study

Accordingly, a pilot study (Balnaves & Caputi, 2001) was performed with 23 radiography students; the initial results were found to closely conform to the predefined quality of the images, and there was no problem with the wording of the scale items.

2.11. Selection of the observer sample and sample size

Volunteer sample size is an important element in scale validation. This is because it is directly related to the number of random errors that might arise. Reliability assessment and factor analysis (the statistics used for scale validation) require a minimum sample size. Spector (1992) recommended a sample of 100-200. Brenowitz & Tutle (2003) argued that a sample size of less than 100 would compromise the results. Therefore a sample with 100 volunteers, and greater, could have the same effectiveness of factor analysis, and the distinct differences in the scale could be appreciated. Other investigators argued that 150 participants would be adequate. Some suggest a rule of five participants per item (Tabachnick & Fidell 2013). Consequuently, 151 volunteers scored the phantom images, and 184 scored the cadaver images. These are considered to be adequate sample sizes in relation to the work cited within the literature. Volunteers comprised of qualified radiographers and student radiographers from several higher education institutions. In this research, groups of students' radiographer were sought from four high education institutions throughout Europe to score the images. Those students (i.e. Eu) were almost studying at their finishing year (e.g. 3rd or 4th).

2.12. Scale administration method

There are many ways by which the scale can be administered to the sample. These methods include internet and paper-based (Streiner and Norman, 2008). After considering the appropriateness of each approach for this study, it was found that, to best meet the purposes of the current research, it would be best to use the paper based approach for a variety of aforementioned reasons relating to the measuring of the image quality requirements (e.g. PC screens; ambient room light conditions).

2.13. Data collection period

The period of collecting data from the administered scales using phantom images was four months. However, when cadaveric images were used, it took around 5 months. The period was so long because it took time to get volunteers into the lab at convenient times, according to their studies and other duties.

2.14. Factor analysis

Factor analysis can be defined as a statistical data reduction method to condense a large number of items into a small group of underlying factors which characterise the most important information (Coakes, 2005). A factor refers to a cluster of items that represents a unitary feature. Thus, this analysis provides another approach for examining the validity of a large set of items (Polit & Beck, 2003). In addition, this analysis can be used as a validating tool for both one-dimensional and multi-dimensional scales. Scale dimensionality expresses whether the created scale is assessing a single image quality theme (e.g. anatomical features) or multiple themes (e.g. anatomical and technical) (Spector, 1992). Therefore, factor analysis was undertaken for both sets of data (phantom and cadaver) to test the underlying structure of scale.

2.15. Reliability

Reliability is defined as the measuring system's ability to consistently measure the feature it is designed to assess. Therefore, reliability is an indicator for testing consistency (Ho, 2006). Methods for establishing the reliability of instrument can be divided into two main classes, namely internal and external consistency. For the external, they rely on the cumulative test results versus themselves as an approach of verifying the reliability of the measurement. By contrast, internal consistency refers to how well individual items within a scale consistently measure the same common underlying construct.

Internal consistency reliability therefore enables investigators to identify those items that are inconsistent within the measuring of the phenomenon under study; these items can then be removed to improve scale reliability (Spector, 1992 & Ho, 2006). The most common statistic used to measure the internal consistency is Cronbach's alpha coefficient. It should be noted that reliability is an important and perquisite component for validity.

2.16. Validity

Validity refers to the adequacy of the scale in measuring a specific attribute. Essentially, there are three kinds of validity: content validity, criterion validity and construct validity.

2.16.1. Content validity:

Streiner and Norman (2008) differentiated between the ways of testing content validity and other forms of validation. For instance, the content validity cannot be determined by the scores from the scales, or people's performance variations. Rather, it relies solely on the judgments of expert panels or focus group members.

2.16.2. Criterion validity:

This refers to the extent to which the results from a particular scale are closely related to that of a gold standard one. However, there is no other similar scale with the same construct (i.e. image quality) published in the literature which could be considered as "gold standard". Therefore, this cannot be tested (Streiner and Norman, 2008).

2.16.3. Construct validity:

This refers to the most stringent way of establishing the validity. Defining the construct clearly can lead to accurate expectations about how the scale will behave if it is proven to be valid. Construct validity comprises of the comparison between the domains, and also tests the logical relationship between the image quality factors (items) and underlying domains (e.g. procedural or technical measures) (Guyatt, Feeny, & Patrick, 1993; Streiner and Norman, 2008). Factor analysis can be used as an appropriate statistical analysis for examining the construct validity of the scale.

Chapter 3: Results and analysis

3.1. Chapter overview

In this chapter the results from the phantom and cadaver validation phases will be presented. Initially, this chapter will describe how the data was collected from the research volunteers. After that, the scores from each volunteer will be aggregated. The data analysis will start by looking for any outliers. Next, the data will be tested to see if it conforms to the normal distribution, before going into further data analysis. Item analysis will be used to determine which items are robust enough to be retained within the final version of the scale. The last subsection will assess the reliability of the remaining items. Finally, factor analysis will be undertaken to identify the underlying factors (themes) of clustered items. To order to simply, phantom data will be considered first, followed by cadaver data.

3.2. Phantom data

3.2.1. Data collection

Data was collected from the volunteers over a four month period using a self-reporting approach. This process took place in a room with PCs and computer screens dedicated to medical image analysis at the University of Salford. One thousand fifty seven (1057) completed scales were collected from the volunteers, including their scores on the image quality of the seven different phantom images. The target population of this research were radiography students (Years I, II and III), studying at the University of Salford/ Radiography Directorate and qualified radiographers (i.e. staff members from University of Salford and other NHS departments). The composition of volunteers are shown in figure 3-1
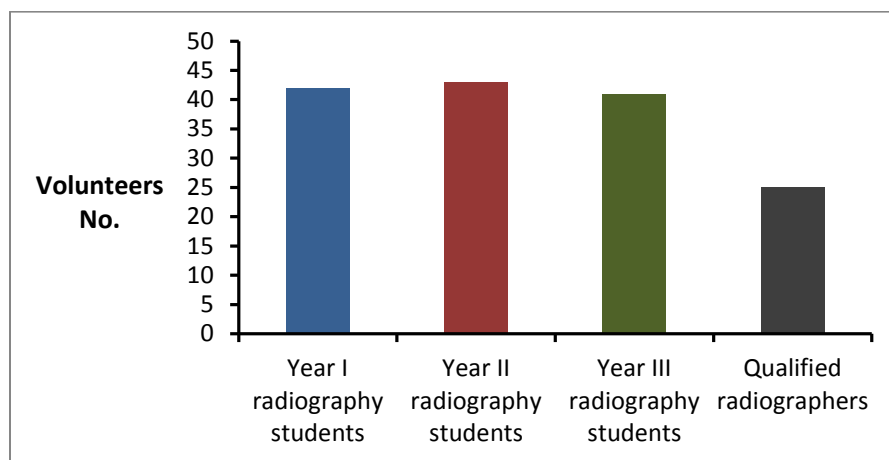
Figure 3-1. Volunteer characteristics – phantom image dataset.

3.2.2. Draft scale format
The (draft) scale that seen in appendix (IV) initially comprised of 29 items with a 5-point Likert scale. The responses from the negatively worded items were reversed so that all the obtained responses were uni-directonal (i.e. score 5 refers to a high agreement level and therefore high volunteers agreement on a particular image quality factor).

3.2.3. Total scale score calculation
The overall scores for each volunteer were calculated for each of the 29 items in the scale. The process of summating the scores from individual items is crucial for two main reasons. Firstly, measuring a psychological construct such as perception is difficult, and cannot be represented by a single item, therefore a multiple itemed scale would be necessary for obtaing the overall estimation of the construct under investigation (Spector, 1992). Secondly, image quality perception, being the main construct of this research, is often estimated radiologically by summing the scores of the corresponding radiographic criteria alongside the specified images. Consquently, the main focus in the initial analysis is on the overall score for each volunteer, as it represents the value of the image quality of an image set. The aggregation process revealed that there were three uncompleted scales and therefore these were removed from the data set, leaving 151 completed scales.

3.2.4. Outlier removal
Outliers can be defined as unusual values in the set of data from a given volunteer that seems to be inconsistent compared with the values of other volunteers (Shaughnessy, Zechmeister, & Zechmeister, 2012). Detecting outliers is an important step, and must happen before going into full data analysis as they may lead to either type I or type II errors. There are many methods for outlier detection; common methods include the identification of outliers using a scatter plot, Grubb's equation, or both (Filliben, 2012). For the current research, the data from the seven images was examined for any outliers using both approaches.

The data for images (6), (7) and (5) was investigated, and no outliers were found. In contrast, for image set 2 there was a single outlier. The scores for this respondent were seen to be low (70) compared with overall mean value for the scores from other volunteers (107). With regards to the data from image set 4, two outliers were detected. The detected scores were low (61, 60) in relation to the overall mean value (101). In image set 3, two outliers were identified and they were low (60 ,64) when compared with the rest of the responses (mean value = 105). Finally, a single outlier was detected with a value of 65 for image set 1, whereas the overall mean value for the scores from this image set was 112. When all of these cases were reviewed it was found that respondents rated the items in the scale with low scores, although most of the images were of a high, predefined quality (e.g.image set 1,3,2 and 4). So, they may either have been rushed, or have not the required skill to apprise the particular image. Accordingly, it was decided to remove them from any subsquent analysis.

3.2.4.1. Overall scale scores (Initial rating)

Table 3-1 below presents the overall mean scale scores for each of the seven images after removing all the detected outliers mentioned above.

Table 3-1. Initial image quality scale scores for the seven images of known quality.				
	Image quality scale scores			
Image quality rank*	Man scale score	SD	95% confidential intervals for mean	
1	111.9	12.6	109.9	113.9
2	107.3	10.9	105.3	109.3
3	105.9	10.6	103.9	107.9
4	101.9	11.5	99.9	103.9
5	97.2	13.1	95.2	99.2
6	80	12.4	78.0	82.0
7	62.8	11.9	60.8	64.8
*Rank number 1 = Very good image quality; 7= Very poor image quality.				

3.2.5. Testing normality of the data

Testing data normality from the seven images may be necessary to examine the appropriateness of the overall data for further analysis (e.g. item analysis). Given that the level of the data is ordinal (non-parametric), adopting a Kolmogorov-Smirnov test, or measuring the skewness, could therefore be the most appropriate method for testing the normality of this type of data.

For the given data, the Kolmogorov-Smirnov test demonstrated that the data of six of the image sets conformed to the normal distribution with $P \geq 0.05$, as shown in table 3-2. Image set (6) had P value of ≤ 0.05 , and it was found to be more suitable to study its skewness level instead. Testing this indicates the appropriateness of its data for further item analysis (Field, 2000).

Table 3-2.Values of Kolmogorov-Smirnov normality test for the data sets of the seven images.			
Image No.	**Statistic**	**df**	**Sig.**
1	0.056	148	0.200
2	0.054	148	0.200
3	0.071	148	0.069
4	0.075	148	0.062
5	0.051	148	0.200
6	0.100	148	0.001
7	0.072	148	0.056

3.2.6. Item analysis

This sub-section provides the opportunity to examine the features of each item in the scale, with an aim to improve scale reliability (Kitching, Cassidy, & Hogg, 2011). This step is directed by published guidelines within the literature (Bandura, 2006). Initially, item analysis is achieved by examining the descriptive statistics (e.g. mean, standard deviation) for each item, and for the seven images separately using SPSS software. This was done to eliminate any item which could introduce an excessive level of error or does not contribute any useful information to the study (Field, 2005).

The item analysis began with determining the amount of missing data (missed scores). A high amount of missing data may indicate problems either with the wording of response choices, or with the wording of the items (Bjorner, Damsgaard, Watt, & Groenvold, 1998). By investigating the current data (i.e. for 7 images), it was revealed that the percentage of missing data was considerably low and would not affect the research outcome.

It has been suggested that any scale item which does not have all of the response choices of the Likert scale (i.e.1 to 5) can be eliminated (Ware and Gandek, 1998). This means that the scale items do not measure image quality as a construct differently by the volunteers. For this reason, all items had all the responses (i.e.1 to 5) to each of the the seven images, because image quality cannot be limited to a particular quality of one image and rather should be tested across a wide range of quality, as is so in this research. As a result no item was removed for this reason.

According to Field's (2005) suggestion, items which have extreme mean scores (i.e. either 1 or 5) can also be eliminated. This would mean that a volunteer chosing either higher or lower scores may add no considerable meaningful data. The range of means for all items varied between 1.2 and 4.3 across all image sets. The item which had score (1.2) was retained for further analysis, after it was examined, beacues the image it appeared with was with very poor quality and therefore all other items were also scored low. Consequently, no items were deleted because of this criterion.

Ware and Gandek (1998) suggested, for five point response scales, the standard deviation for any item should roughly be around 1.0. The standard deviations for all items for the seven images ranged from 0.6 to 1.2 except one (image set 7), where item 8 had a standard deviation of ± 1.50. This item was removed from subsequent analysis.

Field (2005) suggested that each item should introduce low skewed scores among volunteers (i.e. the responses should be normally distributed for each item). Accordingly, after all items had been examined for their skewness alongside all images sets, the following items were removed from further statistical analysis as they had either more than +1 or below than -1 for skewness and. See table 3-3 for a complete list of these.

Image Rank	Item deleted due to high skewness
1	1, 3, 4, 5, 12, 14, 15, 17, 23, 24, 29
2	3, 5, 9, 10, 12, 13, 17, 20, 29
3	1, 2, 3, 4, 5, 9, 12, 17, 28
4	3, 4, 5, 10, 13, 15, 17, 24, 28, 29
5	4
6	6, 7, 25, 27
7	1, 2, 3, 5, 6, 7, 8, 9, 14, 21, 25, 26, 27

Table 3-3. This table presents the items that were removed due to their skew of scale responses.

After eliminating the above items for each image set, it is now appropriate to test the inter-item correlation and reliability, to prepare all scale items for achieving factor analysis.

3.2.7. Inter-item correlation

Inter-item correlation within a particular domain has a significant impact on reliability (Nunnally and Bernstein, 1994). This is because it could be expected that each single item has a certain amount of specificity. Therefore, it was necessary to examine the inter-item correlation to eliminate low correlated items, improving the reliability of the scale. According to Nunnally and Bernstein (1994), a value ranging between 0.2 and 0.4 could be adequate for retaining the items ready for factor analysis. Removing low correlated items in this phase led to the improving of the reliability of the scale for whole images sets. Table (3-4) below illustrates the deleted items.

Image Rank	Item deleted due to low inter-item correlation
1	8,18, 25
2	8, 18, 25
3	18, 19, 25
4	18, 25
5	18, 25
6	8, 18,19, 20, 29
7	17, 18, 19

Table 3-4. This table demonstrates which items were removed because of their low correlations.

Now, the item characteristic testing was complete. After that, all items that had introduced a high level of error, or added no meaningful contribution to the results, were removed.

3.2.8. Cronbach alpha

Cronbach alpha is a statistical coefficient used to measure the internal consistency (reliability) of a scale. It directly relates the number of items in the scale and their inter-correlation magnitude (Spector, 1992). The value of the alpha coefficient ranged from 0-1, and a value of 0.6 was placed as a standard cut off point for each extracted factor (Cronbach, 1951). The internal reliability coefficient for the current scale was calculated to be within 0.8, especially after removing the skewed and low inter-correlated items- see table (3-5).

Table 3-5. Values of Cronbach alpha for the seven phantom images.	
Image rank	**Alpha coefficients**
1	0.883
2	0.846
3	0.823
4	0.878
5	0.913
6	0.891
7	0.803

After it was clear that the scale items were consistent in measuring the image quality of AP pelvis, the next phase of analysis began. Factor analysis is often preceded by the examination of sample adequacy and an item pattern correlation through calculating Kaiser-Meyer-Olkin (KMO) values using SPSS software.

3.2.9. Sampling adequacy (KMO).

Kaiser–Meyer–Olkin (KMO) is known as an alternative metric used to measure the adequacy of a sample for performing factor analysis. The value of KMO ranged from 0 to 1, where 1 indicated a perfect sample size for extracting factors from a particular set of data (Field, 2013). The lower limit of the KMO value should be >0.5 to be able to start working with factor analysis (Kaiser, 1974).

Bartlett's test gives information about data sphericity (i.e. the correlation between items), and for the test to be significant its value should be closer to zero (Field, 2005). KMO and Bartlett's test results can be seen in table (3-6).

Table 3-6. This table demonstrates the KMO values for the seven images.		
Image rank	**KMO**	**Bartlett's test**
1	0.855	000
2	0.861	000
3	0.857	000
4	0.888	000
5	0.867	000
6	0.823	000
7	0.868	000

Considering table 3-6, it could be argued that the sample size, and the number of correlating items, is robust enough to proceed to factor analysis.

3.2.10. Factor analysis

The main function of factor analysis is to help researchers explore how many latent factors/themes underlie a group of items. After removing the redundant items, factor analysis can determine whether there is single broad factor, or several more definite factors (DeVellis, 2012). This analysis is essential in identifying scale construct validity (Dennis, 1999). There are two types of factor analysis, namely principle component analysis and rotated factor analysis (varimax).

The factor based principle component analysis was initially conducted across the seven image data sets to identify the main underlying structure(s) of image quality. However, principle component analysis often explores many factors that are hard to interpret, especially when items have high loading (correlation) into more than one factor (Koutra et al., 2012). Therefore, to simplify the extraction process, a rotated factor analysis based with a varimax mode was done on all 7 images separately.

Item factor loading values greater than 0.32 were considered to be the lower limit for the item to be retained. This therefore means that these items play an essential role in the interpretation and labeling of the image quality factor they are used on. Factors to be considered for interpretation should have an eigenvalue limit ≥ 1 (Tabachnick & Fidell, 2013). An eigenvalue refers to the amount of information explained by a specific factor; the higher the value, the higher the contribution to the overall scale. The results from factor analyses will be described below for each image independently.

3.2.10.1. Image set 1 (1st Ranked quality image)

Conducting the principle factor analysis on the data of a high quality image with the retained items from the previous analyses revealed that there were 3 factors with an eigenvalue greater than 1- *see table 3-7*. It should be noted that all tables from this image set (1) analysis will be presented as examples for the subsequent analysis, which will be copied for the other image sets' data. However, for the other image set analyses, only the main tables from factor analysis will be presented.

Table 3-7. This illustrates the number of factors extracted from the principle component analysis of image set (1) data			
Factor No	Total Variance Explained		
	Total	% of Variance	Cumulative %
1	6.031	40.208	40.208
2	1.427	9.512	49.72
3	1.182	7.882	57.602

From the above, it is clear that the first factor accounted for the majority of variance at 40%, with a considerable number of high loaded items (≥ 0.32) - *see table 3-8*[*]. The next largest factor accounted for 9% of variance.

Item	Factor number		
number	**1**	**2**	**3**
Item_2	0.684	-0.013	0.18
Item_6	0.704	0.153	0.05
Item_7	0.604	-0.172	0.231
Item_9	0.747	-0.029	-0.372
Item_10	0.752	-0.005	-0.512
Item_11	0.509	-0.277	0.191
Item_13	0.801	-0.2	-0.256
Item_16	0.661	0.263	0.353
Item_19	0.339	0.682	-0.212
Item_20	0.44	0.518	-0.069
Item_21	0.68	-0.027	0.264
Item_22	0.664	-0.168	0.119
Item_26	0.68	-0.19	0.352
Item_27	0.628	0.077	0.337
Item_28	0.734	-0.123	-0.309

Table 3-8. This table illustrates how items were loaded (correlated) to each of the extracted factors.

[*]This table presented as a typical example for tables obtained from principle component analysis for the rest image sets.

Rotated factor analysis was performed to investigate whether there is a single factor or several specific factors from the data of this image. The rotated factor analysis demonstrated three factors; the first two were with a comparable total variance percentage, namely, 24.9% and 20.3% respectively, and the third was for a variance of 12.2 %, *see table 3-9*.

Table 3-9. This table illustrates the number of factors extracted from the rotated analysis of image set (1) scores			
Factor No	Total Variance Explained		
	Total	% of Variance	Cumulative %
1	3.738	24.92	24.92
2	3.05	20.333	45.253
3	1.852	12.349	57.602

However, the third factor was deleted because it only had two clustered items, and may not reflect good psychometric properties (Field, 2005; Suhr, 2006). This therefore meant eliminating two items from the analysis, 16 and 20. Finally, table 3-10 demonstrates how the retained items were loaded across factor 1 and 2 respectively.

.

Table 3-10. This table illustrates the retained factors with their items that highly loaded into them.		
	Factor number	
Item number	**1**	**2**
Item_2	0.612	
Item_6	0.498	
Item_7	0.631	
Item_9		0.755
Item_10		0.862
Item_11	0.566	
Item_13		0.722
Item_16		
Item_20		
Item_21	0.666	
Item_22	0.603	
Item_26	0.767	
Item_27	0.646	
Item_28		0.711

3.2.10.2. Image set 2 (2nd Ranked quality image)

Principle component analysis resulted in four main factors with greater than 1 eigenvalue. It was shown from this analysis that there was a single prominent factor which accounted for 33.1% of

variance. A considerable number of items that had a factorial loading ≥0.4 loaded into this factor. By contrast, the second largest factor accounted for 9.3% of total variance, *see table 3-11*

Factor No	Total Variance Explained		
	Total	% of Variance	Cumulative %
1	5.63	33.1	33.1
2	1.584	9.3	42.4
3	1.371	8.1	50.5
4	1.19	7.0	57.5

Table 3-11. This table illustrates the number of factors extracted from the principle analysis of image set (2) data

Once again, a factor analysis was carried out with a varimax rotation to see if another different factorial structure could be revealed, *see table 3-12*. This solution demonstrated that there were three factors with a comparable amount of variance (e.g. around 15% each), as is shown in below table 3-12.

Table 3-12. This table illustrates the four factors extracted from the rotated analysis of image set (2) scores

Factor No	Total Variance Explained		
	Total	% of Variance	Cumulative %
1	2.847	16.8	16.8
2	2.781	16.4	33.1
3	2.635	15.5	48.6
4	1.512	8.9	57.5

Items that had high factor loadings across the above three factors can be demonstrated in the following table 3-13.

Table 3-13. This table illustrates the retained factors with their items that highly loaded into them		
Factor number		
Items number	**1**	**2**	**3**
Item_1			0.757
Item_2			0.598
Item_4			0.686
Item_6			0.557
Item_7		0.703	
Item_11		0.602	
Item_14			0.577
Item_15	0.575		
Item_16			
Item_19	0.353		
Item_21		0.617	
Item_22		0.626	
Item_23	0.722		
Item_24	0.653		
Item_26		0.556	
Item_27		0.582	
Item_28	0.76		

One item was deleted from this analysis (16) due to it's having a low factor loading ≤ 0.32.

3.2.10.3. Image set 3 (3rd Ranked quality image)

Within the initial analysis, it was revealed that there were five factors with an eigenvalue greater than 1. Factor number one accounted for the highest percentage of variance, compared with the others at 28.8 %; the second largest factor accounted for 9.6 % of total variance. This therefore led to most of the items having a high factor loading into this factor. On the other hand, investigating the factor structure alongside rotated factor analysis has demonstrated that there were five factors. Factor number 1, 2 and 3 had a comparable variance at an average of 13.2%, *see table (3-14) below*.

Table 3-14. This table presents the five factors extracted from the rotated analysis of image set (3) scores.			
	Total Variance Explained		
Factor No	Total	% of Variance	Cumulative %
1	2.65	15.6	15.6
2	2.28	13.4	29.0
3	1.813	10.6	39.7
4	1.777	10.4	50.1
5	1.673	9.8	60.0

This analysis resulted in items with high factor loading values clustering around the first three factors, namely 1, 2 and 3, *see table 3-15*.

Table 3-15. This table illustrates the retained factors with their items that had high factor loadings of image set (3) scores			
	Factor number		
Item number	1	2	3
Item_6	0.447		
Item_7			0.557
Item_8			
Item_10	0.861		
Item_11			0.417
Item_13	0.763		
Item_14	0.427		
Item_15	0.495		
Item_16			
Item_20		0.518	
Item_21			0.519
Item_22		0.592	
Item_23		0.772	
Item_24	0.656		
Item_26		0.653	
Item_27			0.788
Item_29			

Accordingly, three items demonstrated poor psychometric properties across the three factors and were deleted.

3.2.10.4. Image set 4 (4th Ranked quality image)

The principle factor analysis (un-rotated) yielded four factors with an eigenvalue greater than 1. The first factor accounted for 36.5% of total variance, confirming the prevailing characteristics of this factor. The second factor accounted for 8.8% variance. This analysis showed that the majority of items had a higher loading level into factor number 1. Performing the rotated factor solution gave rise to four main factors. The latter factors extracted with a variance percentage are illustrated at below table, *see table (3-16).*

Factor No	Total Variance Explained		
	Total	% of Variance	Cumulative %
1	3.465	20.4	20.4
2	2.651	15.6	36.0
3	2.003	11.8	47.8
4	1.834	10.8	58.6

Table 3-16. This table shows the four extracted factors after having undertaken varimax factor analysis of image set (4) scores

The rotated analysis for the image that ranked as fourth has led to the retained items that loaded highly across the first three extracted factors, *see table (3-17).*

Items number	Factor number		
	1	2	3
Item_1	0.753		
Item_2	0.810		
Item_6		0.631	
Item_7		0.561	
Item_8			0.660
Item_9	0.737		
Item_11			0.577
Item_12	0.760		
Item_14		0.437	
Item_16			
Item_19			
Item_20		0.377	
Item_21	0.458		
Item_22			0.549
Item_23			0.549
Item_26		0.622	
Item_27		0.744	

Table 3-17. This table illustrates the retained factors with their items that had high factor loadings

Two items were deleted due to having low factor loading values.

3.2.10.5. Image set 5 (5th Ranked quality image)

Seven factors were extracted after performing the principle component analysis on the image set 5 responses. Factor number 1 accounted for largest variance at 34.4%, whereas the second largest factor accounted for 7 % of total variance. It was found that the vast majority of the items had higher factor loading onto factor number 1.

However, another attempt was undertaken to check the factor structure with a varimax rotated factor analysis. The latter analysis revealed that the first two factors (1st and 2nd) accounted for around 12% of variance each, whereas the second two factors (3rd and 4th) accounted for about 8% of variance each. Regarding the number of highly loaded items, it was found that there were twenty one items loaded onto the main four factors and can be shown in the table below (3-18).

Item number	Factor number				Item number	Factor number			
	1	2	3	4		1	2	3	4
Item_1		0.753			Item_15				
Item_2		0.507			Item_16				0.316
Item_3		0.782			Item_17		0.348		
Item_5				0.454	Item_19				
Item_6				0.591	Item_20				
Item_7				0.647	Item_21	0.551			
Item_8					Item_22	0.453			
Item_9			0.790		Item_23	0.731			
Item_10	0.508				Item_24	0.735			
Item_11			0.415		Item_26				0.404
Item_12			0.67		Item_27				0.758
Item_13			0.494		Item_28	0.755			
Item_14		0.641			Item_29				

Table 3-18. This table shows the distribution of items with high loading values across the 4 factors of image set (5) scores

Five items were eliminated as a result of this analysis due to the low loading values they had.

3.2.10.6. Image set 6 (6th Ranked quality image)

Conducting the principle factor analysis for the data of this image has shown that there were five factors with an eigenvalue ≥ 1. However, it was found that there was a single dominant factor accounting for 34.8% of variance, whereas the second largest factor accounted for 8% of total variance.

Factor analysis was done once again to examine whether there was another factorial structure using varimax rotation. The analysis revealed that there may be three prominent factors that

accounted for 48.1% of total variance together. For each factor there were more than three items with considerable factor loading, *see table (3-19).*

Item number	Factors number		
	1	2	3
Item_1		0.800	
Item_2		0.540	
Item_3		0.809	
Item_4	0.724		
Item_5		0.579	
Item_9	0.703		
Item_10	0.840		
Item_11			0.366
Item_12	0.769		
Item_13	0.648		
Item_14			0.610
Item_15			0.509
Item_16			0.735
Item_17			
Item_21			
Item_22			0.426
Item_23	0.739		
Item_24	0.694		
Item_26		0.321	
Item_28	0.795		

Table 3-19. This table illustrates the items that had high loadings values across the three extracted factors using varimax rotation of image set (6) scores

In brief, this analysis led to the elimination of two items, namely, 17 and 21, due to their loading values being ≤ 0.32.

3.2.10.7. Image set 7 (7th Ranked quality image)
The last principle factor analysis was carried out on the obtained scores from this image. Principle factor analysis resulted in four factors; the first factor accounted for the majority of total variance at 38.7%, whereas the second largest factor accounted for 11.6% of variance. Studying the factor loading for each item revealed that the majority of items had higher loading values onto factor number 1.

Again, a rotated factor analysis was performed to search for different factor structures. This analysis confirmed the prevailing role that factor 1 had in terms of its variance index, *see table (3-20) and (3-21) below.*

Table 3-20. This table shows the four extracted factors adopting varimax factor analysis of image set (7) scores.			
Factor No	Total Variance Explained		
	Total	% of Variance	Cumulative %
1	4.836	37.2	37.2
2	1.492	11.5	48.7
3	1.433	11.0	59.7
4	1.149	8.8	68.5

According to the table 3-21(below), two factors were deleted because they have less than three items each and their variance was not significant for their retainment (Field, 2005; Suhr, 2006). So, five items were deleted, namely, 11, 15, 16, 20 and 29, respectively

Table 3-21. This table demonstrates the items factor loading among the first three factors of image set (7) scores.			
Item number	Factor number		
	1	2	3
Item_4	0.828		
Item_10	0.810		
Item_11		0.775	
Item_12	0.847		
Item_13	0.828		
Item_15			
Item_16			0.827
Item_20			0.814
Item_22	0.648		
Item_23	0.741		
Item_24	0.746		
Item_28	0.681		
Item_29		0.854	

Finally, twenty four items loaded highly (correlation) onto the extracted factors from the rotated factor analysis of each of the seven images' data. These items were therefore retained to form different subscales from this validation phase across all of the seven images. Interpretation of the resulted data will be discussed in the later discussion chapter.

3.3. Cadaver data

3.3.1. Data collection

The data obtained from cadaveric images was analysed following the same format as that for the phantom. Volunteers scored the images over a five month period; at the end of this period, 184 volunteers had completed the process for the whole scale. The volunteers used for this phase were radiography students (Years I, II and III) studying at the University of Salford/ Radiography Directorate and qualified radiographers (i.e. staff members from University of Salford and other NHS department). Details of the constitution of the volunteers are presented in figure 3-2.
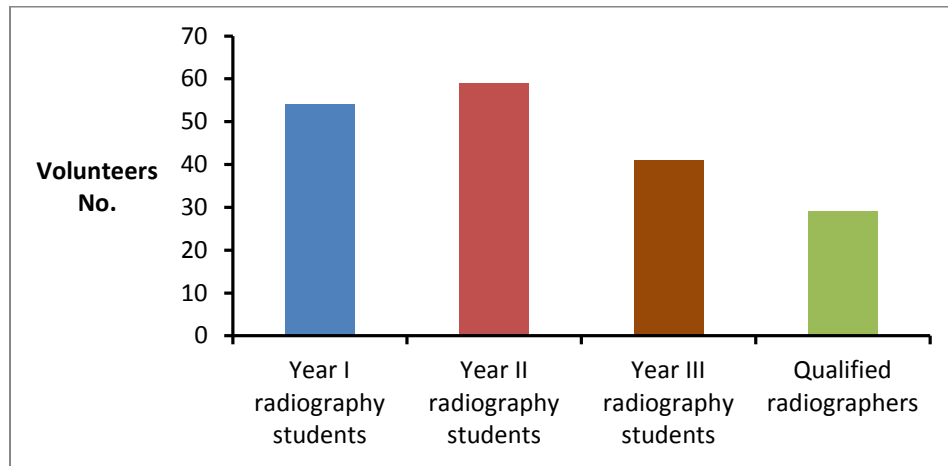
Figure 3-2. Volunteer characteristics – cadaver images dataset.

3.3.2. Scores Aggregation and outlier detection

The scores given to each item by the volunteers were aggregated into the scale, to obtain the overall scale score for each image of specified quality. One outlier was detected from image set 1. The scores for this respondent were seen to be low (i.e. 59) compared with overall mean value for the scores from other volunteers (95). This was therefore removed from the data for the subsequent analysis to minimise error. The overall scores for each image, together with the corresponding image rank, are presented in table 3-22, after the removal of the outlier.

Table 3-22. Scale scores for the 7 images of known quality[*] (Initial rating).				
	Image quality scale scores			
Image rank	**Mean**	**SD**	**95% confidence intervals for the mean**	
1	97.5	9.5	96.1	98.9
2	89.9	10	88.5	91.3
3	82.3	9	81.0	83.6
4	81.0	10	79.6	82.4
5	74.0	9	72.7	75.3
6	76.3	10	74.9	77.7
7	63	11	61.4	64.6

[*]Rank number 1 = Very good image quality; 7= Very poor image quality.

The data sets for the 7 images were then compared to a normal distribution; and they conformed to it (see table 3-23).

Table 3-23. The values of the Kolmogorov-Smirnov normality test for data sets of the seven cadaver images.			
Image Rank	Statistic	df	Sig.
1	0.978	183	0.295
2	0.913	183	0.375
3	1.098	183	0.179
4	1.052	183	0.219
5	0.767	183	0.598
6	0.629	183	0.824
7	1.026	183	0.243

The above test indicates the data was appropriate for further analysis, which will include item analysis, internal reliability and factor analysis.

3.3.3. Item analysis
The item analysis began with determining the amount of missing data (missed scores). By investigating the current data (i.e. for 7 images), it was revealed that the percentage of missing data was considerably low and would not affect the research outcome.

Before conducting internal reliability and factor analysis, item characteristics were investigated individually for each image set (Bandura, 2006). This was conducted by adopting the same approach as for phantom images. No item was removed because of the amount of error they may introduce through a score's SD. The SD range for all items across the 7 images was 0.6 to 1.2

and therefore was within published limit (Field, 2005). Items that had high skewed scores were removed to improve the scale's reliability.

Inter-item correlation was investigated for each image, ready for calculating Cronbach's alpha. This led to the removal of all items which had very low inter-item correlation (e.g. ≤ 0.2) with the rest of scale items, *see table* 3-24.

Image Rank	Item eliminated due to low inter-item correlation
1	21,24
2	9,24
3	9 , 10 , 15, 24
4	9,21,24
5	7 ,8 ,9, 24
6	9 ,16,21,23
7	23,24

Table 3-24. This table demonstrates which items were removed because of their low correlations.

3.3.4. Cronbach alpha (Reliability)

Following this, internal reliability was tested for each image set through the calculating of Cronbach's alpha coefficient, see table 3-25.

Image rank	Alpha coefficients
1	0.889
2	0.872
3	0.826
4	0.837
5	0.811
6	0.863
7	0.870

Table 3-25. The values of Cronbach alpha for the 7 cadaver images.

3.3.5. Factor analysis

The KMO statistic was calculated first to test the correlation pattern of the scale items and sample adequacy. The KMO ranged from 0.710 to 0.838 (i.e. minimum acceptable ≥0.5). Factor analysis was undertaken for all the images scores separately. Details of these analyses will be described below for each image set.

3.3.5.1. Image set 1(1st Ranked quality image)

The principle component factor analysis was first undertaken on the retained items of this image. The data demonstrated that there are five factors with greater an eigenvalue >1. The first factor

accounted for the largest amount of total variance at 32.7%. The next largest factor accounted for 9.8% of total variance, *see table 3-26.*

Table 3-26. This table illustrates the number of factors extracted from the principle analysis of image set 1 data			
	Total Variance Explained		
Factor No	Total	% of Variance**	Cumulative %
1	7.204	32.7	32.7
2	2.147	9.8	42.5
3	1.633	7.4	49.9
4	1.245	5.7	55.6
5	1.164	5.3	60.9

*Minimum value required to consider any extracted factor   ** Refers to percentage of information explained by a given factor.

Within factor 1, twenty one items were highly loaded (≥ 0.458) compared to the rest of the extracted factors. Rotated factor analysis results demonstrated that the factor numbers 1, 2, 3 and 4 each accounted for around 12.8 ±1.6 % of total variance, *see table 3-27*.

Table 3-27. This table illustrates the number of factors extracted from the rotated analysis of image set (1) scores.			
Factor No	Total Variance Explained		
	Total	% of Variance	Cumulative %
1	3.242	14.7	14.7
2	2.827	12.9	27.6
3	2.771	12.6	40.2
4	2.391	10.9	51.1
5	2.161	9.8	60.9

 The retained scale items from the analyses were loaded onto the five factors with high factor loadings, (i.e. 0.40 to 0.87), see table 3-28.

Item Number	Factor number				
	1	**2**	**3**	**4**	**5**
Item_1					0.874
Item_2					0.818
Item_3	0.789				
Item_4	0.782				
Item_5	0.793				
Item_6	0.722				
Item_7			0.757		
Item_8			0.813		
Item_9		0.414			
Item_10			0.347		
Item_11		0.794			
Item_12		0.747			
Item_13			0.548		
Item_14			0.654		
Item_15				0.505	
Item_16				0.691	
Item_17				0.536	
Item_18		0.578			
Item_19				0.631	
Item_20				0.467	
Item_22					0.495
Item_23		0.686			

Table 3-28. This table illustrates the retained factors with their items that highly loaded into them

3.3.5.2. Image set 2(2nd Ranked quality image)

The principle component analysis was conducted on the second ranked image scores, resulting in 6 factors with an eigenvalue ≥1. The first factor accounted for 28.8% of the total variance; and the second largest factor accounted for 10 % of the total variance. More than 90% of items were highly loaded (correlated) onto factor number 1 with a factor loading ≥0.4, except two items loaded with 0.355 and 0.382.

Rotated factor analysis demonstrated that factor numbers 1 and 2 accounted for 12.3% and 11.9% of the total variance compared to the remaining four factors which each accounted for around 9% of the variance. Finally, two factors were eliminated because they had only two items each, *see table 3-29*.

| Item | Factor number | | | |
number	1	2	3	4
Item_1	0.752			
Item_2	0.572			
Item_3			0.674	
Item_4			0.758	
Item_5				0.818
Item_6				0.761
Item_7				
Item_8				
Item_10				0.446
Item_11				
Item_12				
Item_13	0.692			
Item_14	0.689			
Item_15			0.487	
Item_16		0.746		
Item_17		0.667		
Item_18		0.707		
Item_19		0.451		
Item_20	0.547			
Item_21			0.385	
Item_22		0.593		
Item_23		0.336		

Table 3-29. This table presents the retained factors with their loaded items

3.3.5.3. Image set 3 (3rd Ranked quality image)

Seven factors with an eigenvalue ≥1 were extracted after undertaking the principle component analysis on the image set 3 scores. 24% of the total variance was explained by factor number 1, whereas factor number 2 accounted for 14.4% of variance, *see table* 3-30. Eighteen items out of a total of twenty loaded very highly onto factor number 1 (e.g. range 0.415-0.573), compared with two items loading at round 0.32.

Table 3-30. This table presents the number of factors extracted from the principle component analysis of image set (3) scores

Factor No	Total Variance Explained		
	Total	% of Variance	Cumulative %
1	4.804	24.0	24.0
2	2.879	14.4	38.4
3	1.731	8.7	47.1
4	1.358	6.8	53.9
5	1.297	6.5	60.3
6	1.263	6.3	66.7
7	1.01	5.1	71.7

Another attempt was undertaken to check the factor structure with a varimax rotated factor analysis. The latter analysis resulted in seven factors with closely comparable variance percentages (e.g. 10% ±1 %), *see table 3-31*.

Table 3-31. This table presents the number of factors extracted from the rotated analysis of image set (3) scores

Factor No	Total Variance Explained		
	Total	% of Variance	Cumulative %
1	2.391	12.0	12.0
2	2.165	10.8	22.8
3	2.092	10.5	33.2
4	2.03	10.2	43.4
5	2.012	10.1	53.4
6	1.852	9.3	62.7
7	1.801	9.0	71.7

Five factors were retained based on the standard criteria that related to the number of items together with their loadings (Suhr, 2006). Two factors were eliminated as they had only two items loaded into each of them (i.e. 4 items in total), namely factor 6 and 7 (*see table 3-32*).

Item number	Factor number				
	1	**2**	**3**	**4**	**5**
Item_1		0.895			
Item_2		0.888			
Item_3					
Item_4					
Item_5					0.786
Item_6					0.874
Item_7			0.881		
Item_8			0.899		
Item_11					
Item_12					
Item_13				0.811	
Item_14				0.77	
Item_16	0.633				
Item_17	0.863				
Item_18	0.745				
Item_19	0.578				
Item_20			0.381		
Item_21				0.519	
Item_22		0.581			
Item_23					0.486

Table 3-32. This table presents the retained factors with their loaded items.

3.3.5.4. Image set 4 (4th Ranked quality image)

Conducting the principle factor analysis for the data of image set 4 has shown that there were seven factors with an eigenvalue ≥1. However, it was found that factor number 1 accounted for 24.8% of variance, whereas the second largest factor accounted for 13% of the total variance. The rest of this factor's variance percentage can be seen in table 3-33. Twenty items were highly loaded onto factor number 1 with a range of 0.335 to 0.672 factor loadings, compared with a single item loaded with a 0.297 onto this factor.

Table 3-33. This table presents the number of factors extracted from the principle component analysis of image set (4) scores.

Factor No	Total Variance Explained		
	Total	% of Variance	Cumulative %
1	5.202	24.7	24.7
2	2.775	13.2	38.0
3	1.964	9.4	47.3
4	1.503	7.2	54.5
5	1.249	6.0	60.4
6	1.099	5.2	65.7
7	1.033	4.9	70.6

Another factor analysis was undertaken, but with varimax rotation, searching for another factor structure. The resulted data demonstrated that factor numbers 1, 2, and 3 accounted for the largest percentage of variance altogether, 15%, 12.8% and 9.7%. Accordingly, three factors were retained whilst the rest were eliminated. Some of these included only two items, whereas others cross loaded into more than one factor see table 3-34.

Table 3-34. This table presents the retained factors together with their loaded items.

Item number	Factor number			Item number	Factor number		
	1	2	3		1	2	3
Item_1				Item_13			0.836
Item_2				Item_14			0.842
Item_3				Item_15			0.562
Item_4				Item_16		0.7	
Item_5	0.697			Item_17		0.813	
Item_6	0.67			Item_18		0.546	
Item_7				Item_19		0.679	
Item_8				Item_20		0.465	
Item_10	0.546			Item_22		0.408	
Item_11	0.839			Item_23	0.603		
Item_12	0.832						

3.3.5.5. Image set 5 (5th Ranked quality image)

The principle factor analysis (un-rotated) yielded 6 factors with ≥1 an eigenvalue. The first factor accounted for 24% of the total variance; the second factor accounted for 14.9% of variance. The

rest of the four factors' variance percentage ranged from 5% to 8%. Fourteen items of the twenty were highly loaded with a considerable factor loading of ≥0.4. However, the left six items were highly loaded onto the second factor.

Performing the rotated factor analysis gave rise for six main factors with ≥1 an eigenvalue. The latter factors extracted with percentage variance are displayed in the table below (3-35).

Table 3-35. This table presents the number of factors extracted from the rotated analysis of image set (5) scores

Factor No	Total Variance Explained		
	Total	% of Variance	Cumulative %
1	2.814	14.1	14.1
2	2.726	13.6	27.7
3	2.152	10.8	38.4
4	2.128	10.6	49.1
5	2.127	10.6	59.7
6	1.131	5.7	65.4

As a result, five factors were retained based on the number of items that loaded high onto them together with their variance (%), *see table 3-36*.

Table 3-36. This table presents the retained factors together with their loaded items

Item number	Factor number					Item number	Factor number				
	1	2	3	4	5		1	2	3	4	5
Item_1			0.846			Item_14		0.84			
Item_2			0.833			Item_15		0.703			
Item_3	0.778					Item_16				0.430	
Item_4	0.762					Item_17					0.803
Item_5	0.837					Item_18					0.794
Item_6	0.753					Item_19					0.627
Item_10		0.525				Item_20		0.598			
Item_11				0.789		Item_21					
Item_12				0.796		Item_22			0.635		
Item_13		0.808				Item_23				0.562	

3.3.5.6. Image set 6 (6th Ranked quality image)
Principle component analysis resulted in six factors with an eigenvalue ≥1. It was shown from this analysis that there was a single prominent factor which accounted for 29.5% of the variance. A considerable number of items (17) had a factorial loading of more than 0.4 with this factor. By contrast, the second largest accounted for 11.9% of total variance, *see table 3-37*.

Table 3-37. This table illustrates the number of factors extracted from the principle component analysis of image set 6 data			
Factor No	Total Variance Explained		
	Total	% of Variance	Cumulative %
1	5.899	29.5	29.5
2	2.38	11.9	41.4
3	1.518	7.6	49.0
4	1.33	6.7	55.6
5	1.118	5.6	61.2
6	1.016	5.1	66.3

Once again, a rotated factor analysis was carried out to see if another different factor structure could be revealed, *see table 3-38.*

Table 3-38. This table presents the number of factors extracted from the rotated analysis of image set (6) data			
Factor No	Total Variance Explained		
	Total	% of Variance	Cumulative %
1	2.982	14.9	14.9
2	2.662	13.3	28.2
3	2.048	10.2	38.5
4	1.892	9.5	47.9
5	1.842	9.2	57.1
6	1.835	9.2	66.3

Table 3-39 presents the retained factors from the rotated analysis, with their corresponding items. Two factors had their loaded items eliminated because they had less than three items in each, and this therefore shows their having low psychometric properties.

Item	Factor number			
number	**1**	**2**	**3**	**4**
Item_1		0.606		
Item_2		0.485		
Item_3				
Item_4				
Item_5				
Item_6				
Item_7		0.822		
Item_8		0.782		
Item_10			0.748	
Item_11			0.708	
Item_12			0.744	
Item_13	0.745			
Item_14	0.798			
Item_15	0.695			
Item_17	0.584			
Item_18	0.459			
Item_19	0.616			
Item_20				0.392
Item_22				0.437
Item_24				0.787

Table 3-39. This table presents the retained factors together with their loaded items of image set (6) scores.

3.3.5.7. Image set 7 (7th Ranked quality image)

The principle component analysis resulted in six factors; the first factor accounted for majority of variance at 28.2%; whereas the second largest factor accounted for 10.9% of it. Studying the factor loading for each item revealed that the majority of items loaded highly onto factor number 1 (i.e. 21 items out of 22 with ≥0.4). The variance percentage range of the remaining 4 factors was from 5.6 to 8.0%.

Once again, a rotated factor analysis was performed to search for different factor structure. This analysis demonstrated that factor numbers 1, 2, 3, and 4 accounted for 13.9, 12, 11.3 and 10.9% of the total variance, respectively. Accordingly, five factors were retained with their items, see table 3-40.

Item No.	Factor number				
	1	2	3	4	5
Item_1			0.831		
Item_2			0.836		
Item_3					
Item_4					
Item_5	0.718				
Item_6	0.712				
Item_7					0.495
Item_8					0.524
Item_9				0.685	
Item_10	0.463				
Item_11	0.846				
Item_12	0.839				
Item_13		0.845			
Item_14		0.86			
Item_15		0.466			
Item_16				0.47	
Item_17				0.612	
Item_18				0.463	
Item_19				0.57	
Item_20		0.459			
Item_21					0.681
Item_22			0.665		

Table 3-40. This table presents the retained factors resulted from rotated analysis of image set (7) scores.

Overall, the majority of the twenty four items from validation phase 1 all loaded considerably highly onto the extracted factors, and for the seven image sets forming different sub-scales, taking into account the differing amount of correlation they had in regards to the different qualitiy of the cadaveric images. An interpretation of the resulted data will be discussed in the following discussion chapter.

Chapter 4: Discussion

4.1. Discussion overview

This chapter individually discusses the scale validation results from the phantom and cadaver tests. Then, common points from the phantom and cadaver data will be discussed to help draw conclusions, where applicable. For phantom and cadaver data, points reflecting the internal reliability, together with points that can theoretically and practically support scale validity, will be outlined. Factor analysis will be discussed to see whether the scale is uni- or multi-dimensional. Scale utility will then be discussed based on the given results. Finally, conclusions will be drawn regarding the principle value of the scale in research and clinical work; these will be mentioned in chapter nine.

4.2. Phantom data

Bandura's guidelines, supported by psychometric literature, provided the theoretical basis for the successful development and validation of a scale. The validity and reliability were assessed by the investigation of scale psychometric properties, including internal reliability (Cronbach alpha), KMO (items correlation pattern), and item factor loading through factor analysis. The scale demonstrated a high reliability (Cronbach alpha ≥ 0.8); and scale item correlation patterns were compact (KMO 0.7 to 0.9). The scale can therefore assess anatomical and technical quality, reflecting its construct validity.

To generalise the findings, two important issues were initially considered: the size and demography of the research sample. Sample size was chosen to comply with the rule of 'five subjects per item'. This meant that 145 subjects were required. However, 151 volunteers were recruited to score the seven phantom images in this phase. As a result, 1057 completed scales (151 volunteers $\times$ 7 images) were collected, each with twenty nine items scored. The sample was chosen to include volunteers of different levels (i.e. YI, YII, YIII radiography students and qualified radiographers), to ensure that the number of random errors from human variations was as low as possible, thus improving the precision. The sample volunteers were selected from within a field in which the quality of an image was a topic of interest, hence the radiography students and radiography professionals. This also ensured the scale would work similarly across a range of experience levels.

Aggregating scale scores allowed an overall score for each of the 7 images. The agreement between an images' rank and mean scores was investigated. This showed there to be an excellent agreement between the predefined image rank and the overall scores (i.e. 62.8 to 111.9, $r^2=0.94$, $p\leq 0.001$), supporting the principle value of the scale in quantifying the quality of an image using phantom.

Cronbach's alpha across the seven images demonstrated (0.8-0.9) consistency. This confirms the strong correlation between the scale items in measuring what they were intended to measure, and may give an indication for the uni-dimentionality of the scale, meaning that it is measuring a single domain of the phantom images (Nunnally& Bernstein, 1994). Eliminating the redundant items did not substantially lower the scale internal reliability (Dennis & Faux, 1999).

4.2.1. Factor analysis

One essential application of the factor analysis was to systematically reduce a large number of items into small number of meaningful scale items (Spector, 1992). Also, it also examines how the underlying factors affect the responses on a number of items (DeCoster, 1998). Initially, the KMO statistic was applied across all phantom images (table 3-6, p.55), indicating that the correlation is compact (Field, 2013). This confirmed that data was ready for factor analysis.

Principle component analysis demonstrated there to be a single dominant factor among all of the images. This was because factor number 1 in each of the 7 images accounted for the largest amount of variance (%). This means that this factor includes the most important information about the image quality of an AP pelvis radiograph. In addition, this factor (dominant) loaded highly into the majority of scale items with factor loadings exceeding a value of 0.45 (e.g. range 0.45 to 0.8). By contrast, the rest of extracted the factors (2nd, 3rd, etc…..) accounted for small variance percentages across the 7 images, and loaded highly onto very few scale items (e.g. two items), with most of them being extracted with a very low factor loading (e.g. ≤ 0.3). Similar findings were found by other researchers throughout their scale development and validation (Kitching, Cassidy, & Hogg, 2011).

Whilst principle analysis (unrotated) is capable of achieving the objective of data reduction, it would not provide information offering the most adequate interpretation of the items (i.e. image quality factors). Rotated factor analysis provided a simpler and theoretically meaningful factor solution. As such, factor rotation facilitates interpretation through reducing ambiguities associated with unrotated analysis (Hair, Black, Babin, & Andersson, 2009).

Factor analysis was undertaken using rotated factor analysis to search for the different factor structures of the images. The analysis revealed that extracted factors across most image sets (five out of seven images) had comparable variance percentages, excluding two sets (1 and 7) which were extracted with different variance pattern. This might indicate the scale could measure more than one image quality theme (e.g. anatomical and technical).

Examining the items which loaded onto the factors for each image set demonstrated that they would not singularly reflect any clear physical, procedural or anatomical dimension, because each factor included a mixture of items that varied from anatomical to the other themes. However, the anatomical items formed a high percentage of each factor, with some different item(s) not from the anatomical dimension. Fifteen of the twenty four items were anatomically related on the final scale. These items display how clearly a given structure is visualised in an image. The other nine items varied between procedural (relating to correct radiographic positioning) and technical/physical (relating to the appropriateness of the acquisition factors). The latter may suggest the scale measures a single factor (uni-dimensional) for the phantom. To illustrate, the scale is assessing the image quality perception in relation to the visualisation of anatomical structures of AP pelvis radiographs. The explanation for this could be that the phantom images were quite uniform, apart from having different noise and contrast levels. It could be argued that the scale was fairly efficient in characterising different image quality as related to noise and contrast. Accordingly, phantoms have a place in the validation of visual grading scales.

In contrast, the nine non-anatomical items assessing image quality features are already in favor of visualisation of anatomical pelvis features (i.e. fifteen anatomical items). For instance, item number 17 ("The exposure factors used for this image are correct") reflects whether the acquisitions are appropriate, and, if so, the pelvic anatomical structures would clearly be imaged.

Another analysis was undertaken to investigate the impact of removing the nine items on the scale reliability and for all image sets. The analysis was showed that Cronbach's alpha was still high (≥ 0.8) and even improved it for some image sets. This means that these items, for phantom use, can be eliminated without adversely affecting the scale psychometric properties; this argument is supported by extisting literature (Cassidy & Eachus, 2002; Kitching, Cassidy, & Hogg, 2011). However, in order to obtain a broader assessment from this scale when assessing the perception of image quality, and to provide balance, it was decided to retain the twenty four items from this validation, with the possibility of using a set of fifteen anatomical items as a sub-scale to assess phantom images, and a seperate whole scale for the clinical work .

4.3. Cadaver data

As it mentioned earlier, the purpose of the second validation phase was to provide further testing (validating) of the scale using images of an AP pelvis taken from a cadaver. These images were produced to have certain positional problems, further to the natural anatomical variation. Therefore, this would provide a clinical environment for the scale to be validated and to translate the results into the clinical situation.

Once again the sample size for this phase was of high priority, aiming to reduce the amount of random error. Therefore, the sample size recruited to score the cadaveric images could be deemed more than adequate when applying the rule "five subjects/item" (Tabachnick & Fidell 2013). This means that 120 (i.e. 24 items × 5 subjects) volunteers were required to score the images adequately. Nevertheless, 184 volunteers completed the scale for each of the seven images. This led to 1288 completed questionnaires (184 ×7) each with twent four items scored. Again, the sample included volunteers of different levels (i.e. YI, YII, YIII students and qualified radiographers) for the same reasons as with phantom phase.

Data from the total scores for each image set revealed that there was a considerable agreement between the image quality rank and volunteers scores (i.e. 63 to 97, $r^2=0.95$, $P\leq 0.001$). This could reflect that the scale was, to a certain extent, sensitive to different image quality. Next, the internal reliability of the scale was investigated after all the items' characteristics were tested and redundant items removed. Cronbach's alpha for the seven images demonstrated that the scale items were consistent in measuring the quality of an AP pelvis when normal human variation was present (i.e. $\alpha \geq 0.8$). This also indicated high scale reliability. KMO values (≥ 0.5) demonstrated that data correlation patterns were adequate for achieving factor analysis as another tool of validity.

4.3.1. Factor analysis

To investigate the items which correlated among the extracted factors, factor analysis was conducted on the scale responses. Principle component analysis data demonstrated that there was a single dominant factor in each of the seven images, which accounted for the largest variance percentage (%). This factor, similar to phantom phase, was highly loaded on the vast majority of the scale items (i.e. refined from phantom), with factor loadings ranging from 0.5 to 0.8, excluding the few items loaded with 0.35 to 0.45. This kind of loading would indicate high correlation between this factor (i.e. dominant) and their items in measuring image quality perception. Similarly, a rotated factor analysis was undertaken with the scores obtained from cadaveric images, seeking another structure. This was especially necessary in this case, being that there were different anatomical variations of different bodies, together with certain positioning problems. For this, the correlation map (i.e. items' loadings) across the seven images was expected to be varied slightly compared with that of the phantom images.

The scale items (i.e. anatomical and others) loaded amongst different factors of different images, almost in the same manner as with the phantom. As such, anatomically related items constituted the majority of the items in each factor, except in some image sets where there were two factors extracted, not including the anatomical ones (i.e. three items each). However, this could not be enough to consider the scale to be multi-dimensional (i.e. measuring more than one quality theme). Therefore, further analysis may be required to confirm whether the scale assessed is singular, broad or has several small definite factors (anatomical and technical).

Internal reliability was tested again after the removal of the nine items (non-anatomical), and for the seven images, the findings demonstrated that alpha coefficients decreased slightly, although still acceptably, compared with that of phantom phase. This may be explained by the existence of anatomical variation, and positional defects of the imaged bodies. This would suggest that it is necessary to use the whole scale when in clinical assessment, or even the majority of items (e.g. >15 anatomical items). This is because the nine items (technical items) cover important points related to positional and technical issues often associated with clinical practice. For example, "symmetrical visualisation of obturator foramina" depends on how the pelvis is positioned without rotation, and the visualisation of L5 is related to an appropriate collimation.

4.4. Combining cadaver and phantom data

To improve the performance of factor analysis in identifying how many factors (themes) the scale can assess, further analysis was conducted after the volunteers' scores from both phantom and cadaver phase were combined. This provided scores for 335 volunteers to be analysed (14x335=2345 completed scales). Prior to this, the t test was conducted to see if phantom and cadaver scores were significantly different; no significant difference existed ($p \geq 0.05$). Table 4-1 shows the Cronbach's alpha and KMO values, the high values suggest the scale has excellent internal consistency and validity.

Table 4-1. Alpha coefficients and KMO values (combined phantom and cadaveric data).

Image rank	1st	2nd	3rd	4th	5th	6th	7th
Cronbach alpha	0.903	0.867	0.849	0.857	0.786	0.889	0.907
KMO	0.906	0.858	0.809	0.826	0.734	0.866	0.894

Data from un-rotated factor analysis was similar in its themes to that of phantom and cadaver. Specifically, factor number 1 accounted for largest variance (%), 38%, 31%, 27%, 28.6%, 21.8%, 35% and 37.6 %. The second largest factor accounted for 7.6 %, 9%, 11%, 13.9%, 13.6%, 8.7% and 9.3%. This un-rotated analysis did not provide a clear understanding of the factorial structure of the scale.

Rotated analysis demonstrated the patterns of variance (%) were similar for phantom and cadaver. For instance, some factors extracted with comparable variance (%), excluding some image sets where some factor(s) extracted with low variance (%) see table 4-2 for a typical example of this.

Table 4-2. This table presents the extracted factors from rotated factor analysis for image set (1) (combined data).

Total Variance Explained			
Factor No	Total	% of Variance	Cumulative %
1	3.831	17.413	17.413
2	2.979	13.539	30.952
3	2.853	12.967	43.918
4	2.653	12.058	55.976

Examining the items that loaded highly onto all extracted factors demonstrated that, for all seven images (except the 7th ranked one), there was a clear factor identified relating to how *technical* factors can affect the image quality e.g. over collimation, inability to visualise L5. Accordingly, this provides evidence for the scale's ability to assess how clearly the anatomical structure of the AP pelvis radiograph can be visualised, and how technical and procedural issues can affect the quality of an image.

4.5. Technical considerations

There are certain issues which need to be considered when creating and validating a scale using phantom or cadaveric images. For example, phantoms might not have a suitable range of realistic features (e.g. anatomical variations), and this could be addressed by choosing a set of phantoms which possess a suitable range of anatomical features. For the cadavers, the anatomical structures should be visualised across different image sets randomly, because obscuring any of them from all images, for any reason, may bias the results and erroneously cause some items to be eliminated. Therefore, both phantoms and cadavers present opportunities and challenges.

It was found that the number of items with skewed scores were higher in the phantom when compared to the cadaver. The reason behind this was that with phantom images, especially the very good and very poor quality ones, the anatomical items were either very clearly or poorly visualised. This was practically expected and could be recognised by the "endorsement frequency", such that it discriminates across the volunteers' scores with very high or very poor quality (Streiner & Norman, 2008). Nevertheless, skewed items were removed from further analysis (i.e. almost ranked 1st or 7th), because they may be detected as errors that prevent some of the analyses from being conducted (i.e. factor analysis), or affect the psychometric properties of the scale.

The effect of anatomical and positional problems (e.g. positioning errors) associated with cadaveric images were clearly recognised on the correlation patterns among items' scores. For instance, the correlation among item scores with those images with positional problems was lower than those images that did not have any anatomical and positional problems. This was evidenced by the relatively low KMO statistics. This may indicate that positioning errors had an impact on the quality of an image, and, in addition to that, the effect was also clear on inter-item correlation. However, the KMO and other statistics were within acceptable ranges.

4.6. Scale validity

Validity refers to the degree to which the scale is measuring what it supposed to measure. The scale was validated by applying the same approach used for measuring the scale's psychometric properties, such Cronbach alpha and KMO. But, within this scale validation, there was another indicator of validity which was 'to what extent the overall scores of different image sets agree with predefined ranks of image quality'. For this, good agreement was found between the volunteers' scores and the predefined image quality measures, with both phantom and cadaver images. This confirms the capability of the scale to discriminate across a wide range of image quality.

The scale shows a high level of internal reliability (Cronbach alpha within 0.8). This figure indicates that the scale has a good level of internal reliability when compared with the acceptable level of internal reliability (i.e. 0.6 - 0.7). The majority of items had an acceptable range of inter-item correlation (i.e. ≥0.2) which would in turn reflect that the scale items were consistent in measuring the perception of image quality. Finally, the considerable factor loadings of the items in each image set would also support the construct validity of the scale (i.e. as it was detailed

before). The content validity of the scale was mentioned earlier (subsection 2.16.1, p.48), as it was confirmed by a focus group. Regarding scale *criterion validity*, it is not possible to discuss this within this research. The reason behind this is that the scale discussed in this thesis is the first ever to have been developed within medical imaging for AP pelvis radiographs. No similar scale exists, so it is impossible to prove its criterion validity. In this case, to prove the validity of the scale, further validation is highly encouraged, and further supporting evidence should be gathered from literature.

4.7. Scale application in radiography

This sub-section describes the philosophical points behind the creation of this scale, and how this attempt would contribute to fill a gap in the current literature through developing an innovative psycho-perceptual approach to assessing image quality perception. In addition to this, justification for this methodology as a model for creating and validating a scale for other radiographic projections will be discussed.

The main aim of this thesis is to optimise dose and image quality for the AP pelvis radiographic examination. According to the ALARA principle, radiation dose should be lowest without compromising the quality of an image. Therefore, special attention, as was previously mentioned, must be paid to image quality when dose reduction is required. This is because, in order to maintain the diagnostic efficacy of an image, it is necessary to understand how the radiation exposure influences image quality (Shet, Chen, & Siegel, 2011). To bring this balance into radiographic practice, radiation dose, as well as image quality, needs to be evaluated with adequate reliability.

The reliability and validity of image quality assessment methods are crucial in medical imaging. Reliability refers to precision of a given assessment, and therefore high reliability requires a small amount of random error. By contrast, validity represents the ability of measures to define the phenomenon, and a high validity necessitates low systematic error (Båth, 2010). In medical imaging, image quality is a phenomenon of considerable complexity. This is because, as mentioned above, the diversity of radiographic projections that have different physical and anatomical features is huge. These features would in turn define the quality limits of a specific task. Besides, it is important to note that the continuous improvement in imaging technology has imposed further challenges for diagnostic efficacy. Accordingly, it is easy to recognise the difficulty in find out an image quality measure that has high validity. On the other hand, having a high validity for measuring a specific task may result in the findings being less generalisable. The difficulty in successfully operationalising image quality measurement has resulted in the adoption of a wide range of quality assessments methods in the current imaging practice (Yoshiura, 2012, Båth, 2010).

A literature review revealed that there are two main types of image quality assessment methods (Seeram, Bushong, Davidson, & Swan, 2014). First, objective approaches which include physical and psychophysical. These approaches are likely to be used to test system performance

through a QA programme. However, it has been agreed that some of the physical metrics, such as SNR/CNR, can be used as a figure of merit for predicting the quality of the clinical images through what is called "structure SNR or conspicuity (Båth, 2010; Sund, Båth, Kheddache, & Månsson, 2004). Second, ROC and VGA, classed as diagnostic or clinical approaches. In regards to the ROC method, it has been considered to be the "gold standard" method for testing the diagnostic performance of the observer. Also, it can be used to investigate system diagnostic performance with high accuracy, because it can be implemented on clinical images (Zarb, Rainford, & McEntee, 2010). Well-controlled studies, such as ROC analysis, would lead to findings with high statistical power and clinical relevance. The important issue here is that almost all of the pitfalls within this approach have been studies and addressed. This was done throughout the development of different ROC-related methods, as mentioned above (subsection 1.2.3.3, p.13), together with the developing of certain analytical software to obtain reliable data (Båth, 2010).

A visual grading analysis is widely used to assess the image quality of images taken from patients or phantoms. This approach is often implemented in conjunction with CEC quality criteria. The CEC criteria were used with the hope of reducing subjectivity, and improving assessment accuracy (Ludewig, Richter, & Frame, 2010). Nevertheless, it has been seen that these criteria were used variably across different researches. According to our literature analysis, there may be several reasons why variation is associated with VGA-based CEC criteria. For instance, some of the criteria are ambiguous, allowing for different interpretations (inter- and intra-observer variability) (Maccia, Moores, & Wall, 1997); the criteria was established in film era and their application to digital imaging may require some modernization (Hemdal *et al*., 2005); some of the necessary criteria are missing; and, most importantly, no validated data was ever published against the CEC criteria. Accordingly, this illustrates the existence of a gap in the literature in relation to the application of VGA along with the CEC criteria. However, no published work attempted to address this gap, until now (Shet, Chen, & Siegel, 2011).

This current attempt aims to create and validate a visual grading assessment scale that will contribute to fill this gap and therefore reduce observer variability. This variation in image quality assessment is a common phenomenon in medical imaging, and many researchers have commented upon and some have suggested principles to address it (Krupinski, 2011 & Kundel, 2006). Amongst these suggestions was one to devise a psycho-perceptual system to assess image quality (Shet, Chen, & Siegel, 2011; Kundel, 1979). This is because visual image quality evaluation requires interaction between human perception and the physical/visual attributes of an image. This then demands a human observer to be one component of the imaging chain, and considered in the process of any creation of standards. Building on this, it was found that, to create a visual grading scale, it is best to adopt psychometric principles for scale creation and validation, to ensure the reliability and validity of the measure required. In fact, the philosophy behind opting the psychometrics to create a visual image quality assessment scale is that for many years psychometric theory has been used extensively to develop and validate scales in psychology, in order to create new scales (questionnaires). This theory has been adopted and applied in a novel fashion in this section of the thesis. Bandura's guidelines have been used

extensively to inform the approach mentioned above. Therefore, a new theoretical framework has been developed for the first time, which can be used to develop and validate a new scale. Based on the above, the scale was created against validated data. This work is completely original, since no validated scale exists for visually assessing the image quality of any radiographic examination (Shet, Chen, & Siegel, 2011). This is crucial for medical imaging because, for the first time, we have a scale that should be able to visually measure image quality for an AP pelvis radiograph.

By way of comparison, one important aspect of the current validated scale as compared with other grading scales exit in literature is the scale creation and validation process supported by validation data. The validated data include statistics regarding the scale reliability and validity which are not provided with other existed IQ assessment grading scales.   Several statistics are used to indicate for scale reliability and validity. For example, Cronbach's alpha refers to how scale items *are consistent* in measuring the image quality perception (≥ 0.7), providing an objective measure for the scale reliability; KMO coefficient indicates whether the items' correlation pattern is compact or not; finally, factor analysis provides an evidence about construct validity, and is a way of eliminating redundant items (≤ 0.32), and retaining those items which add meaningful contribution to the overall scale value. Another feature which is worth mentioning with this scale is that psychometric scale development and validation necessitates that the scale items, once validated, cannot then be modified because their validation has based on a robust psychometric procedure/evaluation and therefore any attempt to modify them necessitates another validation process. This in fact would likely to contribute to reduce the variability in image quality perception assessment since using validated scale demands that all researchers/observers use the same terminology of the items. Additionally, scale psychometric properties provide evidence regarding how clear these items are in reflecting a singular aim with less ambiguity. The said evidence regarding the clarity of scale item can be illustrated by a number of measures; these include items scores' descriptive statistcs. As such this would ensure that the scale is less ambiguous and this therefore reduces the possibility of different interpretation by an observer(s).

The data analysis resulted in several scales (sub-scales), and these were produced either from the analysis of the data of the different images independently, or resulted from the analysis of a single image's data. Examples of this include: 1) using the scale to assess the anatomical structures of interest within the AP pelvis radiograph; 2) using a whole scale to assess the anatomical structures with technical parameters; 3) using shorter scales with fewer items, from "1" and "2". Further research can be conducted on the current scale to further test its reliability and validity. The latter measure is usual in psychometrics and is based on the fact that construct validating is an ongoing process (Bandura, 2006; Cappelleri, Gerber, Kourides, & Gelfand, 2000). This step may include a larger and more diverse sample size of experience observers. Finally, data (scores) arising from this scale application can be converted into visual grading points where possible, and then plotted on a graph to compare the image quality of two different conditions. The resulted data can be analysed in similar manner to that of ROC (Båth & Månsson, 2007).

By creating and validating this scale systematically (see Appendix V) it could be argued that we have achieved the following:

1. Proving that the psychometric theory and Bandura's guidelines appear to be robust theoretical frameworks to create a methodology that can be used to develop and validate a visual grading scale for image quality assessment.
2. Proposing a methodology to develop and validate other visual grading scales for other radiographic projections.
3. Providing, with the scale, a perceptual-based standard, used to evaluate the image quality in digital imaging. Thus filling a gap in the current literature where no previous work is available on the development of a visual grading scale, presented alongside validation data.
4. Identifying that 50% of errors made in radiology are related to perception (Krupinski, Kundel, Judy, & Nodine, 1998) and realising that this scale may help reduce the errors because the scale items were psychometrically tested against human observer scores of different image quality. Therefore, inter and intra observer variation would likely to be reduced to an acceptable level.

Section II

Optimisation of the radiation dose and image quality

(*Major focus of the PhD thesis*)

Chapter 5: Introduction and background

5.1. Introduction

A major concern in medical imaging arises from the use of ionising radiation. The use of X-radiation has been associated with the risk of developing harmful genetic changes, such as cancer (Seo *et al.,* 2014). During radiological imaging, a variety of conditions may determine the amount of the radiation risk a patient is exposed to. Such conditions include the nature of the diagnostic information required, patient size, the imaging system and the skill of the imaging practitioner. The increasing use of X-ray imaging techniques in the healthcare sector generates challenges in controlling the risks to patients (Sezdi, 2011). Controlling radiation exposure during X-ray imaging is a central focus involved in radiation protection. This minimises the radiation risk, and can be achieved through the reduction of a patient's radiation dose. However, reducing the radiation dose may compromise the image quality, since it would reduce the amount of photons/penetrating power required to carry specific anatomical information to the imaging detector. Therefore, the minimisation of the radiation dose should be *optimised* to maintain an image quality level necessary for making an accurate medical diagnosis (Hogg & Lança, 2015).

Optimisation in medical imaging is considered to be a key component in radiation protection research (ICRP, 2006). This matter has been discussed extensively by the International Commission on Radiological Protection since the 1980s. Accordingly, a number of recommendations have been issued by the ICRP on how to apply the optimisation principle. The aim of the optimisation principle is to provide the required level of protection through continual and iterative processes including the regular monitoring of radiation exposure; the identification of the appropriate reference level value; and the identification of the best possible protection option to implement (ICRP, 2007a). It is important to have iterative processes available to allow for the optimisation of any X-ray practice. Such processes should continue to exploit the potential capabilities of modern imaging systems and further reduce the radiation risk (Matthews & Brennan, 2009). The identification of an appropriate approach to optimising the radiation dose , without compromising the image quality, is an essential step for diagnostic radiography to consider.

Having taken these principles into account, the focus of this PhD thesis was decided to be an attempt to identify/develop a framework that systematically optimises the radiation dose and image quality. For the purpose of this thesis, an AP pelvis radiographic examination was chosen. There are two major reasons behind the selection of an AP pelvis projection. First, that there are frequent examinations of the AP pelvis in current radiographic practice; and second, that there is a relatively high radiation dose associated with radiography of the pelvis (further information on this can be found in subsection 5.2.6, p.123). Optimisation of the AP pelvis' radiographic examination means identifying a radiographic practice capable of producing images with suitable quality at the lowest possible radiation dose (Al Qaroot, Hogg, Twiste, & Howard, 2014; ICRP, 1991). Suitable image quality is defined in this thesis as the adequate visualisation of all anatomical structures listed in AP pelvis image quality scale (See appendix V). Linking the suitability of image quality to the adequate visualisation of all the APPS anatomical structures would help explore the efficiency of the optimisation framework in reducing the radiation dose,

without compromising the image quality (Joyce, McEntee, Brennan, & O'Leary, 2013). Optimising radiation dose and image quality systematically has not yet been fully described in literature. This is undoubtedly one innovative aspect of this PhD thesis. Additionally, this thesis could provide a range of acquisition parameters which could be used as guidance to produce images with an optimised dose alongside suitable image quality.

The second part of this thesis was conducted in three successive stages. In the first stage (stage 1), a method was used to optimise AP pelvis radiographic practice using manual mode (non-AEC), a CR imaging system and an anthropomorphic pelvis phantom. The method comprised of three consecutive steps through which the impact of the primary acquisition factors on radiation dose and image quality (perceptual and physical) were investigated systematically.This permitted the identification of the optimum acquisition combination settings from a ranked list. These were based on radiation dose, and further explored the main effect of each of the acquisition factors on different response variables (e.g. radiation dose and image quality scores). The optimum combination setting was identified according to the lowest radiation dose which produced a suitable image quality from the ranked list.

In stage two, another method was conducted to optimise AP pelvis practice, but using automatic exposure control (AEC). In this stage the same anthropomorphic phantom and CR imaging system were used. However, the method comprised of 4 consecutive steps in which the impact of the acquisition factors (excluding mAs) on radiation dose and image quality was investigated systematically. Similarly to the manual mode, a ranked list of acquisition settings (based on the radiation dose) that produced suitable quality images was generated. Accordingly, the optimum combination setting with lowest dose was identified, and the main effects of the different acquisition factors on response variables were further explored.

Finally, in stage three, a method was used to investigate whether post-processing options available on the CR imaging system could improve images which deemed unsuitable during stage one and two. In this final stage, the effect had on the perceptual image quality when the latitude and density of the images were manipulated was systematically investigated. A ranked list based on the image quality scores was generated to check whether the manipulation had improved or degraded the post processed images.

The current section (II) of this thesis consists of 4 chapters. **In chapter five**, comprehensive information in relation to the optimisation of radiation dose and image quality will be described. This will start by describing the percentage of projection radiography use in relation to other areas of radiology. Then, the possible radiation risks which may result from exposure to radiation in projection radiography will be explored. This will then be followed by an explanation of the different radiation protection options (e.g. optimisation) established by the national and international bodies to protect individuals from radiation risks.

Different aspects of the optimisation process which have been reported in literature will be reviewed. This is preceded by a description of the common differences between analogue and digital systems followed by a brief identification of the advantages which led to digital systems taking over from analogue. Different strategies for optimising digital imaging systems, reported

in the literature, will also be discussed, as will the physical characteristics of the CR detector. This will be followed by a literature review on the different acquisition factors that have been used to optimise X-ray practices. Finally, published optimisation papers for AP pelvis radiography will be reviewed and discussed.

In chapter six, the methodology behind the optimisation procedure will be described. This chapter begins by describing the equipment which was used in this thesis, together with relevant quality control tests. Following this, an overview of the whole methodology will be described. A description of the study design which was used to optimise AP pelvis radiography will then be described, before a final detailing of each of the 3 stages in the optimisation study.

In chapter seven the results will be presented. Subheadings within this chapter will be similar to those in the corresponding sub-sections in the methodology chapter.

Finally, **in chapter eight**, the results from the optimisation experiments will be discussed. This chapter will begin with a general overview, followed by a more in-depth discussion of the different sections. These sections will, in turn, discuss the results generated from the different optimisation experiments. However, each section consists of two sub-sections; one is related to optimum technique identification from a given experiment, whereas the second relates to the 'main effect analysis'.

5.2. Literature review (Background)

The literature review will be focussed upon two points: 1) exploring and explaining key concepts essential for radiation protection in medical imaging; 2) critically analysing the available literature that concerns the optimisation of projectional radiography examination. The aim of the latter is to review the different approaches used to reduce radiation dose and maintain image quality.

The search for relevant publications was undertaken using peer review journals and textbooks relating to patient dose management and image quality. The literature search was conducted using ScienceDirect, Medline databases with full text and CINAHL. The relevant key words used in the search included 'image quality', 'patient dose in radiology', 'digital radiography (CR & DR)', and 'optimisation'; and the major journals searched were 'Radiology', 'Radiography', 'Medical physics', 'Radiation Protection Dosimetry', 'Physics in Biology and Medicine', 'European Journal of Radiology', 'Paediatric Radiology' and the 'British Journal of Radiology'. A number of key reports were also reviewed such as ICRP reports, and those from the American Association of Physics in Medicine. Finally, legislation and guidance were also reviewed.

5.2.1. Optimising projection radiography

It is well known that the main function of an X-ray's being used in medical imaging is to produce images which could help with diagnosis (Seeram & Brennan, 2006). The quality of the information within these images is, however, highly dependent upon the radiation dose administered to patient (Oliveira *et al.,* 2013). Within radiology departments, approximately 60 to 70% of examinations fall into the category of projection radiography. By contrast, images acquired from other 30 to 40 % of radiologic investigations include 'computed radiography', 'nuclear medicne', 'single photon emission computed tomography (SPECT)', 'magnetic resonance imaging (MRI)' and 'ultrasound'(Huang, 2010). Projectional radiography is the process of projecting a three-dimensional (3-D) body part into a two-dimensional (2-D) image/radiograph. Examples of body parts which may be captured on film, computed radiography (CR) and digital radiography (DR) technologies include chest, pelvis, breast, skull, and abdomen. In X-ray imaging, different body parts require different radiation doses. This is attributed to the different physical characteristics of the tissues being exposed, implying different attenuation characteristics (Martin, 2007).

With reference to the beneficial role of using X-radiation in projection radiography, the problem of exposing patients to a radiation risk must always be considered. The radiation risk is resulted from inappropriate use of radiography equipment or from subjecting the patients to unnecessary radiation exposure that exceeds the required level (Sezdi, 2011). One of the main objectives of medical imaging is to minimise a patient's radiation dose, and therefore risk, without compromising the quality needed to establish an accurate medical diagnosis. Findings from more than one hundred years of radiation protection and radiobiological research can confirm that ionising radiation can cause cancer and other genetic effects (Sherer, Visconti, Ritenour, & Haynes, 2014).

The main biological effects of ionising radiation are stochastic and deterministic (Bushberg, Seibert, Leidholdt, & Boone, 2012). Stochastic effects are more likely to occur by chance,

meaning that there is no threshold of radiation dose at which they will occur. To illustrate, any level of radiation dose, irrespective of how small it is, has the potential to be a source of harm (Little, Wakeford, Tawn, Bouffler, & Gonzalez, 2009). In this case, if the harmful effect occurs, damage may be apparent years after the radiation exposure. These kinds of effects are also termed 'late effects'. Typical examples of such effects include leukaemia and other genetic effects. Accordingly, stochastic effects can be regarded as a fundamental health risk which results from low radiation exposure. As such, this involves the exposure to diagnostic radiography (Seeram & Brennan, 2006).

In contrast, deterministic effects are related to high radiation doses and therefore are always accompanied by a threshold exposure level. Increasing the radiation dose means increasing the severity of the effect, rather than the probability (Bushberg, Seibert, Leidholdt, & Boone, 2012). Examples of the deterministic effects include skin injuries, bone marrow suppression and cataract formation. These sorts of effects are also referred to as 'early effects', which are caused by high level of radiation exposure. However, effects such as these are unlikely to occur in diagnostic radiology, with certain exceptions such as interventional cardiology procedures (Brenner *et al*., 2003; Little, Wakeford, Tawn, & Bouffler, 2009).

Accordingly, it is clear that any radiation risk to the public from medical radiation exposures must be considered, no matter how small (Cohen, 2008). For this, concepts, principles and standards of radiation protection have been established worldwide. In radiography, practicing radiation protection can be regarded as protecting patients and the general public from unnecessary radiation risks; this process has no contribution to image quality improvement (Brusin, 2007). Also, different techniques for protecting workers and patients from radiation exposure have been used in medicine. This is done to ensure that the least amount of radiation dose is absorbed by human tissues, thereby reducing the probability of unwanted radiobiological effects (Sherer, Visconti, Ritenour, & Haynes, 2014). In this context, a major goal for radiation protection within radiography is to prevent any deterministic effects by reducing the absorbed dose below threshold levels and to minimise the probability of stochastic effects (Bouzarjomehri, 2004). Achieving this goal, therefore, requires radiation protection actions to be upheld. These actions include controlling the exposure time, increasing distance from the radiation source and using shielding where appropriate (Seeram & Brennan, 2006).

Minimising the exposure time can also contribute to reduced patient motion (blur) and, therefore, improve the quality of an image. Increasing the distance between the patient and X-ray tube would certainly reduce the absorbed dose, according to the inverse square law (Bushong, 2013). Finally, the use of shielding can have a significant role in keeping the exposure level at a low and safe level. Nevertheless, to achieve radiation protection goals, three actions should be considered equally with the radiation protection principles, dealing with concepts of justification, optimisation and dose limitation. The latter can be guided by the two triads of the radiation protection (see figure 5-1) (Seeram, 2001).
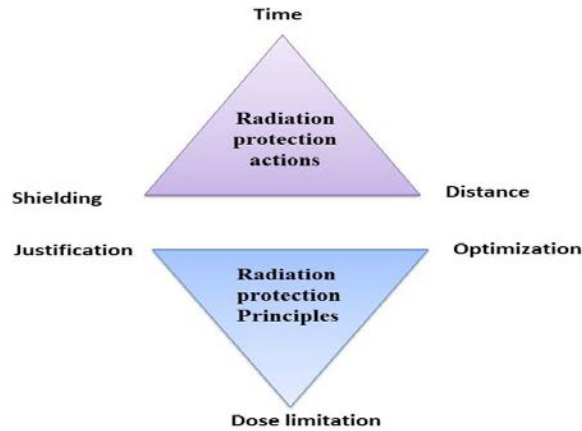
Figure 5-1. This figure illustrates the two triads of radiation protection (Adapted from Seeram, 2001).

Continuing the above discussion, justification involves linking the practice of exposing patients to radiation by considering the "*benefit to risk ratio*". When a patient is ill, or has sustained an injury, then they may need to undergo a justified amount of risk from radiation exposure in order to obtain the essential diagnostic information. In this context, the benefit from the radiographic examination outweighs the risk associated with x-radiation exposure (Figure 5-2) (ICRP,1991; Sherer, Visconti, Ritenour, & Haynes, 2014).
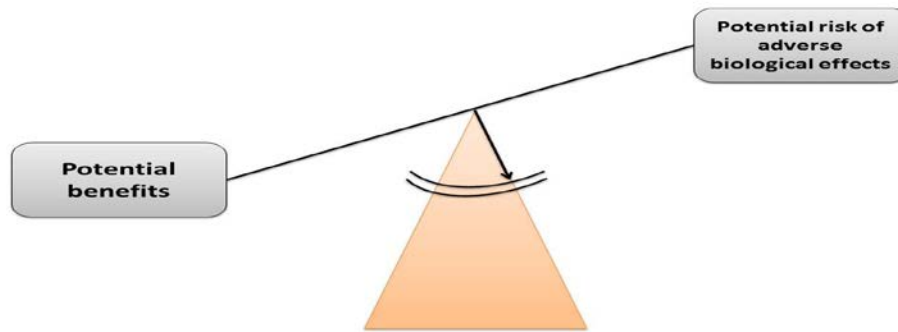
Figure 5-2. This shows the required potential benefit versus potential harm (Adapted from Sherer, Visconti, Ritenour, & Haynes, 2014).

Justification involves considering the appropriateness of radiological examination in obtaining the required clinical information. In diagnostic radiography, this almost always lies within the responsibility of radiographers. Nevertheless, the principle of justification also deals with making a decision regarding the issue of reducing the radiation dose. For instance, a reduction in the radiation dose may adversely influence the quality of an image, which in turn reduces the benefit gained from the exposure in managing the patient's clinical condition (ICRP, 2007a; Matthews & Brennan, 2008).

Therefore, in certain situations when high quality images are required, using a higher dose could be justifiable.

Whilst the principle of justification provides a substantial standpoint for the prudent use of radiation, dose limits have been suggested by the ICRP (2007a) for occupationally exposed people as well as the general public. In this sense, it is important to note that there is no dose limit for patients in diagnostic radiography, since the goal is to the deliver the lowest possible radiation dose for every patient (ICRP, 2007b; Seeram & Brennan, 2006). Additionally, in radiography, setting a dose limit may restrict the use of X-rays in some situations where variations in body habitus and clinical conditions may necessitate different exposure levels, which may not comply with an established dose limit.

Optimisation aims to keep the radiation dose administered to patients from all radiographic exposures to its lowest possible level. Dose optimising works in favour of maximising the margin of benefit over the harm in diagnostic radiology, taking into account the social and economic context. The principle of optimisation has been mentioned by ICRP, IAEA and other independent organisations as the most important radiation protection concept, when compared to justification and dose limits (IAEA, 1997, 2002; ICRP, 1991). Optimisation is also known by the acronym 'ALARA', standing for *as low as reasonably achievable,* which means keeping the radiation dose as low as reasonably achievable. The root of this principle dates back to 1977 when it was initially stated by ICRP (publication number 26, 1977). After that, the ALARA principle has undergone a series of revisions to comply with technological advances.

The ALARA principle sought to minimise the patient radiation dose by introducing a guideline to the field of the radiation protection. This would, in turn, confirm that the optimisation principle in diagnostic radiography is linked to the philosophy of ALARA (Grupen, 2010; ICRP, 1977, 2003). In fact, the rationale behind this principle comes from the evidence collected by researchers over the last hundred years (National Research Council, 1990). Therefore, the *as low as reasonable achievable* philosophy must be a major item in every healthcare facility's personnel radiation monitoring scheme (Sherer, Visconti, Ritenour, & Haynes, 2014).

In addition, whilst there is no dose limit for the amount of radiation that the patient may incur from any radiographic examination, the ALARA principle should be instituted, maintained and used to ensure imaging professionals have taken the required actions to minimise patient radiation dose. This is so because, as mentioned earlier, there is no threshold value at which cancer may be induced, meaning there is no definite level of exposure below which people would have no probability of developing such a disease. Overall, having recognised that there is no safe dose at which radiation exposure should be kept, all imaging professionals should follow the ALARA as guidance for the selection of appropriate radiographic practice (Don, 2004; (Sherer, Visconti, Ritenour, & Haynes, 2014)).

In addition to the above radiation protection principles, diagnostic reference levels (DRL) can be considered as another measure utilised to protect the patients from unnecessary radiation dose. This concept was first introduced by the ICRP publication No 73 in 1996 (ICRP, 1996). The DRL was established to be an optimisation supplementary tool for medical exposure. The major

goal of the DRL is to protect the patients undergoing radiographic examinations from unnecessary radiation dose which does not contribute to the overall goal of imaging task (Seeram & Brennan, 2006). The application of DRL in diagnostic radiology is based on defining a dose levels/values for the most common diagnostic procedures to be used as a benchmark above which a review should be undertaken (Suliman & Mohammedzein, 2014). Nevertheless, these levels are not a dose constraint rather they just act as a base line through which professionals can judge the level of radiation protection. It is advised that the DRL established at the local institute or departments by 'professionals' bodies in conjunction with radiation protection authorties (ICRP, 2007a). The DRL values identification is based on a percentile point on observed dose distribution to patients or patient equivalent. These values usually expressed by an easily measurable dosimetric quantity such dose in air (ICRP, 1996).

In Europe, the implementation of ALARA was done through two directives produced following the published ICRP recommendation (Pub.60) in 1990, namely The Basic Safety Standards Directive (EC, 1996) and The Medical Exposure Directive (EC, 1997). The former directive (BSS) considers the protection of staff and members of the public, and was applied to the UK by the Ionizing Radiations Regulations 1999. In contrast, the Medical Exposure Directive specified in protecting patients from unnecessary radiation exposure. This was implemented in the UK in 2000. This statute is recognised as The Ionizing Radiation (Medical Exposure) Regulations 2000 (IR (ME)(MedicalExposure), 2000; King, Pitcher, & Smail, 2002).

The terminology of the ALARA principle has undergone modifications. For example, in 1999, Clarke suggested that the terminology of ALARA *as low as reasonably achievable* should be replaced by ALARP - *as low as reasonably practical*. This was an attempt to change the requirements of achieving the optimisation of protection, to ensure that the residual radiation doses, after the application of Protective Action Levels, are as low as reasonably practical. Protective action levels refer to the doses above which there should be a requirement to consider all reasonable steps to reduce the radiation. Moreover, changing the ALARA to ALARP was intended to be the basis for developing ICRP work, which involved a suggestion to change the emphasis on the optimisation and use the new term. In the UK, the phrase "*reasonably practicable*" has a specific meaning which was derived from the health care and safety case legislation (ICRP, 2001b). However, Robinson (2002) has suggested that, in order to avoid any confusion that may occur with changing of terminology from ALARA to ALARP, it would be better for the ICRP to continue using ALARA, bearing in mind the current proposal for developing the principle of optimisation. Also, Robinson suggested that, for any change in terminology, the new ICRP recommendations should be made only when the benefits from said change outweigh the expected costs of its implementation, and would not introduce any interpretational difficulties. Nevertheless, safety consideration's being integrated into any process is highly advocated.

Overall, one could draw two main conclusions from the above discussion: 1) there is no safe radiation dose, no matter how small, from any radiographically or radiologically based X-radiation procedure; and 2) working continuously on *controlling and monitoring* the radiation

risk that patients may receive from medical exposure is mandatory for the implementation of radiation protection rules (e.g. optimisation).

5.2.2. Aspects of optimisation in digital radiography (CR & DR)
Although it is true that the main goal of optimisation in medical imaging is to keep the radiation dose as low as reasonably practical (ALARP), this does not mean reducing the radiation dose to a value of zero. What is required by ALARP is to reduce the dose to an acceptable level whereby the stochastic risk is decreased while the deterministic is eliminated (Sezdi, 2011). Alongside this, it should also be noted that one aspect of optimisiation is to address the quality of an image. Thus, one must consider that dose optimisation must not compromise the image quality required to make an accurate medical diagnosis (Seeram & Brennan, 2006). This builds on the relationship by which the radiation dose from an examination and the resultant image quality are linked. This should therefore imply that the higher the radiation dose, the higher the quality of the information within a given image (ICRP, 2004). Such a correlation between image quality and radiation dose could be more prominent in the digital imaging system than with the analogue. This is in fact owing to the characteristic of digital detector material which has the ability to accurately response to various degrees of exposures. This characteristic is known by linear response of digital detector (Murphey *et al.*, 1992). Further details on the differences between the analogue and digital, along with recent advances in technology, will be discussed in the subsequent sections of this chapter.

It is notable that both patient absorbed dose monitoring and image quality assessment in diagnostic radiography (analogue or digital) are important steps within quality assurance programmes (Kumar, Kumar, & Malleswararao, 2011). Therefore, the optimisation of radiographic practice is an essential element within the quality assurance programme, to which its contribution, if properly implemented, could enhance the entire health care system (Vaňo *et al.*, 2002). Projection radiography has undergone massive technological development over the last few decades. The principle change within diagnostic radiography was the introduction of digital radiography, known as computed radiography (CR) or digital radiography (DR). The most important aspects of DR and CR development are based around detector technology (Cowen, Davies, & Kengyelics, 2007). The dominant features of digital detectors far outweighed those of analogue radiography. This, in turn, has led to the rapid transition from analogue technology to digital radiography (Lança & Silva, 2009). In order to understand the differences between analogue and digital, it may be necessary to discuss the following: 1) the comparative differences between digital and analogue modalities which would clarify the potential capabilities of both; and 2) the main advantages of digital radiography over analogue, together with the associated challenges. Finally, a review the available options and strategies which manage patient dose without compromising the image quality will be given.

5.2.2.1. Computed versus analogue radiography
Despite the numerous differences between CR and analogue, they share one feature in common: their response to radiation exposure. Anatomical information is acquired in analogue radiography after the X-ray photons pass through the object and carry information concerning the region of interest. Following this, a screen absorbs the photons' energy, releasing multiple visible photons

which strike an emulsion layer built onto the film, to finally depict the internal body structure. In contrast, CR detector, unlike film screen, is made up of photo-stimulable phosphor material. Their exposure to radiation occurs in the same way as that of the X-ray film. However, this CR detector stores the photon energy within a trap in the phosphor crystal. The trapped energy is then released after it has been stimulated by a laser present in the reader (Khattak, Sajjad, & Alam, 2010). Further details on the physical characteristics of digital detectors and the imaging process will be described in sub-section (5.2.3, p.111).

The detection efficiency of digital detectors is high compared with that of film. The efficiency refers to ability of imaging detector to convert high percentage of photons into image information, so the higher the efficiency is the better the image quality (further information can be seen in p.113) (Lança & Silva, 2008). Film includes an inverse relationship between image quality and radiation dose; this feature is eliminated with digital imaging, and the image can be manipulated independently. For digital imaging, unlike film, there is a possibility for image auto processing which can correct an error with exposure problems. High radiation doses in film screen radiography cause film blackening, whereas this feature has been eliminated from the digital radiography. (ICRP, 2004; Uffmann & Schaefer-Prokop, 2009). In this context, the transition from analogue to digital technology has cleared the way for further research into the two modes and their radiation dose. The reason behind these comparison studies may be due to the introduction of new technology in medical imaging being accompanied by new technical options which were not available for analogue radiography. These studies provide information regarding whether the traditional acquisition factors used for analogue are still applicable with digital imaging or not. Therefore, investigating the differences between the analogue and digital systems may contribute to dose reduction and image quality enhancement, but are still necessary. Examples of the recent options in digital radiography are the wide dynamic range of detectors and the advanced post-processing tools available at the workstation (Kottamasu, Kuhns, & Stringer, 1997; Tylén, 1997).

An earlier work, published by Pettersson *et al.,* in 1988, aimed to compare the abilities of analogue and CR in visualising anatomical structures in musculoskeletal radiography. Their findings demonstrated that the quality of digital images was superior to that of analogue and the radiation dose could be reduced by 50% without compromising the quality of the diagnostic information. However, the dose values from the CR system were contrasted with a 140 speed film system, whereas the usual speed at which film screen combination systems are likely to work is 400. This therefore makes the comparison difficult in regards to using the CR for dose saving (Pettersson, Aspelin, Boijsen, Herrlin, & Egund, 1988). Sandmayr and Wallentin conducted a pilot project in 1997 (Sandmayr & Wallentin, 1997) to study a number of radiologic issues, and one of these was to compare digital with analogue modalities. Exposure values from both modalities revealed that the radiation dose can be reduced by 50% for CR. In this study, the speed of the film screen combination was 200 and the resultant radiation doses measurement was conducted using a solid-state dosimeter (Unfors). However, comparing the CR performance to analogue with a speed of 200 may be difficult due to that the usual film screen speed used is 400.

Busch (1997) described the experience obtained from the application of a storage phosphor CR system in a number of radiologic examinations including skeletal radiography. He found that, for the majority of applications with CR, slightly more information could be obtained when compared with 400 speed film screen. Furthermore, this was associated with a dose reduction due to the wide dynamic range of CR and reduced images retakes. However, for certain applications, the CR and analogue are comparable in terms of image quality and exposure factors (Busch, 1997). Lu *et al*., compared CR (200 speed) and 400 speed film screen combination in relation to skin dose, techniques and the detectability of contrast details. Within this study, a contrast detail phantom (CDRAD) was used, and a Lucite sheet of different thicknesses was utilised to simulate scattering tissues. Researchers applied a tube potential range from 60 to 120 kVp for both modalities, and added a 2 mm Al filter to the CR to determine whether it could reduce skin dose or not. The results from this study suggested that using high tube potential with added Al filtration would reduce the skin dose without affecting the contrast detail detectability when using CR technology with contrast manipulation (Lu, Nickoloff, So, & Dutta, 2003). Although using CDRAD is valuable for physical identification of contrast detectability, it simulation for the clinical situation may be questioned since there are no anatomical variations. Also, the CR system speed was 200 when the usual speed is 400; this may allow for more dose reduction if it would have been used. Therefore, this would limit the generality of the findings and adds difficult to comparison. Further phantom based work has been undertaken to investigate how far the radiation dose can be reduced when using a new CR system without losing diagnostic accuracy of angle measurement, when compared with the analogue. The researchers found that, at a lower exposure using CR, there was a 98% dose reduction from that of the analogue. Finally, the authors found that, with a CR system, the possibility of manipulating the acquisition factors to reduce a patient's dose was higher than that of analogue, taking into account the aim behind the radiographic examination. (Sanfridsson, Holje, Svahn, Ryd, & Jonsson, 2000). In addition, other researchers have found that there was an acheivable dose reduction of 25-50%, without significant loss in diagnostic accuracy, when compared with analogue. Consequently, they concluded that CR can be considered as an efficient alternative to analogue without significant alteration of diagnostic quality of musculoskeletal images (Murphey *et al*., 1992).

According to the literature, in a good proportion of clinical applications, the radiation doses from CR are either the same or higher than that of analogue. For example, Weatherburn *et al*., (2000) reported that adult patient doses were approximately the same as those for a 300 speed film screen when using mobile CR in chest imaging. Nevertheless, they also anticipated that the doses for adult patients would be higher when a storage phosphor computed radiography imaging plate replaced the analogue with *a speed higher than* 300 for these kind of examinations (Weatherburn, Bryan, & Davies, 2000). The reason why similar dose was found between the two modalities may be due radiographers have used the same exposure factors used with analogue. By doing so one might ignore the wide dynamic range and post processing capabilities which featured the CR system. Also, the radiographers may not be well familiar with the new technology due to lack of training and knowkdege. Others have reported that the percentage of dose increase with CR imaging systems is around 50% compared with that of analogue

(Bragg, Murray, & Tripp, 1997). They attributed the increase to the speed class of CR (200), whereas the minimum film speed was almost 400.

Weatherburn and Bryan studied how far using a CR integrated picture archiving and communication system (PACS) can reduce patient radiation dose when undertaking lateral lumbar spine examinations.They found that the introduction of PACS with computed radiography has little or no effect on patient dose reduction compared to that of analogue radiography (Weatherburn & Bryan, 1999). In this work the authors have put a clear emphasis on the effect of PACS on the dose where the PACS function is to store and transmit images throughout radiology department. Nevertheless, it is noted that one of the hypothysis made was to investigate the effect of wide dynamic range CR system on the dose reduction which is the major hypothesis that should clearly be made in this study. Also, it was not clear whether the authors have considered the image quality as a parameter for comparison across the CR and analogue. In 2006, Compagnone *et al.,* compared the radiation dose received by patients from three different modalities, CR, DR and analogue. Within this study, six common radiographic examinations were considered. In this study the same standard exposure factors were used in all of the three modalities. The findings of study demonstrated that the radiation doses from CR were *higher* than those of other systems (i.e. DR and analogue) (Compagnone *et al.,* 2006). From this study the reason why CR dose higher than other may be due to the same exposure factors used with analogue were transposed to CR. This however works against the potential advantage of wide dynamic range of CR which requires lower exposure factors.

Another similar comparative study was conducted in 2006. It aimed to compare the patient exposures across three common examinations: pelvis, chest and abdomen using CR, DR and analogue. The initial measurements of the radiation doses (i.e. just at the equipment installation time) using CR were similar or higher than those of analogue. However, after the authors manipulated the exposure factors as an attempt to optimise the practice, they found that dose from CR became similar to the published diagnostic reference levels (Aldrich, Duran, Dunlop, & Mayo, 2006). Finally, a clinical study compared CR to analogue in regards to the evaluation and recognition of interstitial lung diseases. No radiation dose measurements were conducted in this study and the results indicate that, with adequate attention to the acquisition parameters and softcopy display, comparable findings can be obtained from both imaging modalities (Laney, Petsonk, Wolfe, & Attfield, 2010). Table 5-1 presents the main elements of the key papers mentioned in the above literature review to facilitate comparison.

Table 5-1. This table presents the main aspects of key papers mentioned above which includes comparison between the digital radiography and analogue in term of dose and image quality

Authors (year)	Anatomy	Imaging system	Study design/ evaluation	Findings/conclusions
Pettersson, Aspelin, Boijsen, Herrlin, & Egund (1988)	- Phantom (Hip, shoulder) - Patients (Knee, ankle)	- CR (Philps) - Analogue (Dupont), film speed 140	- Assessment the accuracy of visualising anatomical landmarks, digital images acquired by reducing dose from 100, 50, 20, 10 and 5 % (phantom)	- CR has advantage of contrast and density manipulation of soft tissue (good visualisation); slightly lower spatial resolution

			- Assessment the accuracy of detecting images lesions of patients, images acquired by reducing the dose by 50% of original - Assessment was conducted by two of authors through consensus	- Analogue has higher spatial resolution than CR - Dose could be reduced by 50 % without compromise IQ
Sandmayr & Wallentin (1997)	- Thorax	- CR (ADC 70) - Analogue (200 speed)	- Ninety intensive thorax images were collected for comparison. - evaluation criteria: tube, stomach tube, central venous catheter, Pneumothorax and Rib fractures - Images were evaluated by specialist and trainee specialist -Dosimetry (Unfors)	- CR system presents slightly better image quality than analogue due to image post processing options (Windowing) - Dose can be reduced by 50 %
Busch (1997)	- Chest (stand and beside), skeletal, gastrointestinal and Urogenital radiography	-CR -Analogue (400 speed)	- Survey - Evaluation based on gathered experience from hospital and clinic (survey)	- CR: little more information can obtained across different areas compared with analogue; number image retakes reduced more than analogue; reducing the dose highly affected the analogue images compared digital images. - CR post processing options shows promise. - Dose reduction due to less image retakes
Lu, Nickoloff, So, & Dutta, (2003)	- No specific anatomy defined	- CR(Kodak Model 400 reader) - Analogue (Fuji HG-1 intensifying screen and Kodak TMG-RA-1 film)	- CDRAD was used to acquire images from both systems; Lucite sheets of different thicknesses were used to simulate different scattering levels (5,10,15,20,25 cm) - Images were evaluated by 5 physicists - kVp (60 to 120) - ESE was used as dosimetric quantity - Three exposure taken by adjusting mAs (0.5, 1 and 1.5mR) - Same procedure repeated but 2 mm Al filter and high kVp	- Increasing the kVp leads to increase scatter and then image noise -Increase tissue thickness increase scatter - Adding extra 2 mm filter can reduce skin dose without compromise the contrast detectability as compensated by post processing manipulation
Sanfridsson,	- Knee (angle	- CR (Fuji,	- Anthropomorphic phantom	- CR: radiation dose can

102

Holje, Svahn, Ryd, & Jonsson (2000)	measurement in weight bearing) and hip - Leg	FCR 900) - Analogue (Sterling quanta	(pelvis and leg) -Images acquired by reducing dose successively -CR: kVp (hip/knee), (80/61); mAs (hip, 0.8, 1.3, 2, 3.2, 5, 12.5, 32 and 125); mAs knee, 0.5, 0.8, 1.3, 2.3, 2,5, 12.5 and 50) - Analogue (80 kVp and 81 mAs) for whole imaging - Images were evaluated by three technicians, two radiologists and orthopaedic surgeons for angle measurement	be reduced (94% Reduction level) without loss in diagnostic accuracy compared with analogue - Relative risk with CR is 2% less than analogue - With CR high possibility manipulate the acquisition factors
Weatherburn, Bryan, & Davies (2000)	-Bedside chest examination	- CR (Kodak Ektascan Storage Phosphor Reader) - Analogue (TMat LRA; Kodak) with screens (Lanex Regular; Kodak)	- Randomised controlled trial - The only satisfactory images were chosen. - Dosimetry (TLD):surface dose was measured to calculate E(mSv)	- The effective dose with CR radiography was found to be the same as that of analogue - The surface dose was found to be significantly higher
Weatherburn & Bryan (1999)	- Lateral lumbar spine	- CR - Analogue (Kodak-300 speed)	- Comparison of patient dose before and after CR integrated PACS is operated - Dose measurement was conducted using TLD -Effective dose also estimated	- Patients doses were found to be comparable for both analogue and CR
Compagnone *et al.,* (2006)	- Abdomen, chest, pelvis, lumbar, lumbosacral joint, skull and urinary tract radiography	- Analogue (Kodak, Rochester, NY) - CR (Kodak) - DR	- Images acquired using all modalities were reported by radiologist using CEC criteria - ESD was measured and E was estimated -Approximately the same acquisition factors were used for analogue and CR	- Dose from CR was higher than analogue and DR - DR was the lowest radiation dose modality

The above literature analysis reveals that there was a controversy regarding the potential advantage of using CR to reduce the radiation dose. To illustrate, some researchers have reported that the CR introduced similar or even higher dose than analogue; whereas others have reported that CR dose could be lower than that of analogue. Little have been mentioned regarding the corresponding image quality across the majority of the above literature (table 5-1). Nevertheless, the majority of publications considered in this review confirmed that there is the possibility for dose reduction when using CR. This could be attributed to the use of added filtration and image

post-processing tools. However, for those authors who have reported CR radiation exposures as being the same, or even higher, than that of analogue, acquisition parameters previously used for analogue were simply transposed to CR. This approach leads to higher or equivalent radiation doses and goes against the core advantages of CR as advocated by the manufacturers and the radiological community. Also, the clinical applications almost always involve patients and, as such, there is often insufficient opportunity to attempt any dose optimisation, because this takes time. Finally, using traditional exposure factors may overlook a key feature associated with the new digital detectors, such as absorption efficiency and wide dynamic range. This is one of the reasons that may cause the dose creep (next sub-section). Therefore, different exposure factors may be more suitable for obtaining an adequate image quality with a lower radiation dose.

5.2.2.2. Dose creep

It is worth mentioning that the introduction of DR and CR has not only facilitated communication between radiology professionals and clinicians (i.e. through ease of images transition and information quality matter), but also helped improve image quality (Schaefer-Prokop & Neitzel, 2006). This characteristic may allow for further reduction in patient radiation exposure.The main attributes for this are related to the wide dynamic range and detection efficiency of digital detectors. Thus, the concern regarding the image quality of digital images is becoming of less importance when compared with analogue. Radiographers now have a considerable exposure range by which image quality can be diagnostically acceptable (Honey & Hogg, 2012; Samei, 2003).

However, the possibility of exposing patients to an unnecessary radiation dose with digital radiography is undoubtedly high, meaning that the increment in radiation dose may go undetected by radiographers. This phenomenon is termed in digital radiography as "*dose*" or "*exposure creep*". This issue is currently considered to be a very important concept in radiation protection using digital radiography. Dose creep results from radiographers raise concerns about noise levels in CR images when the exposure factors are less than the required level for a diagnostic image. It should be noted that overexposure artefacts may not be apparent in CR images until the radiation dose level is >10 times what is required. Equally important within CR imaging are the feedback mechanisms of analogue for over- and underexposure (e.g. blackening or whitening), which are not present. Therefore, overexposing the image detector may not affect the acceptability of image quality. However, underexposure is likely to lead to a noisy image appearance (Willis, 2002; Willis & Slovis, 2005).

Another contributing factor to dose creep is the uncoupling of image acquisition and image displayment in digital radiography.This allows for the automatic rescaling of an image to compensate for any variation in the exposure factors, leading to consistent image quality. The latter automatic optimisation function makes it hard to determine whether an image is under or overexposed by assessing its density (Willis & Slovis, 2004). In order to compensate for this, operators have shown a tendency to practice on the side of caution, thereby overexposing patients to ionising radiation.Trends have shown that the radiation dose for standard examinations has started to rise. Nevertheless, the magnitude of dose creep for a single exposure with low expected radiation risk would be of less importance than those requiring multiple

exposures for follow up investigations, those examining highly sensitive organs, and for people deemed highly vulnerable (e.g. paediatrics) (Schaefer-Prokop, Neitzel, Venema, Uffmanna, & Prokop, 2008).

Evidence for dose creep is not adequately addressed in the literature.For example, an early study was conducted to investigate how using computed radiography contributes to increased patient exposure in certain radiographic examinations, without a radiographer's knowledge (Freedman, Pe, Mun, Lo, & Nelson, 1993).The first investigations of Freedman *et al*., demonstrated that radiographers can apply 32 different exposure combinations whilst obtaining an acceptable image quality for chest examinations. In contrast, for pelvis imaging, they found that it is possible to produce acceptable images, with exposure ranges that can reach the upper available limit of their equipment. This therefore means that, with digital technology, exposing patients to unnecessary radiation is possible. In a study conducted by Weatherburn *et al,* to compare the surface doses from CR and analogue radiography, for patients admitted into an intensive care unit (around 270 patients). They found that the surface dose for CR was significantly high when compared with that of analogue (i.e. median 0.21 versus 0.16 mSv) (Weatherburn, Bryan, & Davies, 2000).

However, Eisenhuber *et al*., concluded that, with standard CR imaging technology, an increase in patient dose would not improve catheter detection beyond that of a 400 speed analogue radiographic system (Eisenhuber *et al*., 2003). Others have reported that, with the transition from analogue to digital radiography, the motivation to move the collimation to an appropriate area of the body within patients has been significantly reduced due to the availability of digital masking options (processing programmes) for the unnecessarily irradiated areas. This has led to considerably larger areas of the body being exposed to radiation (Zetterberg & Espeland, 2011).

Gibson and Davidson (2012) defined exposure creep as "*the gradual increase over time of the radiographers 'usual' exposures for a given radiographic anatomical projection*". They conducted a longitudinal study to test whether "*exposure creep*" was a critical issue for CR and DR. They also sought to determine if there were any measures which could be adopted to halt the creep. Findings from this study demonstrated that exposure creep did exist, and one way to address it would be to train the operators on how to deal with digital systems (Gibson & Davidson, 2012). In the same way, a phantom study was conducted by Ma *et al* to investigate how much image quality and lesion detectability in chest radiography could be affected by applying wide range of exposure factors. The findings demonstrated the potential existence of overexposure in digital practice, while still obtaining adequate image quality (Ma *et al*., 2013). Finally, a study was conducted by Butler *et al*., (2010) to see how exposure indices of different versions of CR and DR are consistent so that they can be used as a measure to monitor the dose creep. This study includes different radiographic examinations including AP pelvis. They ultimately found that the exposure indices with CR were highly variable compared with the DR ones which were highly consistent. Although this attempt is valuable in finding a dose creep control at the local level, different kinds of exposure indices across different manufactures may make it hard for radiographers to be trained on for their diversity (Butler, Rainford, Last, & Brennan, 2010).

Overall, it is clear that the potential risk of increasing exposure factors, and therefore increasing a patient's dose over time using CR or DR, is considerably high. Therefore, continual research work in this field, together with regular dose audits, should be adequate to provide feedback on dose level and exposure parameters for a variety of radiographic examinations. This could then identify an *appropriate strategy* for reducing dose without compromising image quality. Also, establishing a trainging programme for all qualified radiographers and students' radiographer (through their course) may contribute to reduce the probability of dose creep (Vaňo *et al*., 2007). This programme may include improve the knowledge of trainees on the extent of exposure factors to which image quality is still acceptable, and the extent of exposure at which the quality starts to decline. Therefore, they would have ability to identify a range through which patient overexposure can be avoided and the image quality is maintained. These measures could contribute to reducing the probability of the dose creep; this is a legal requirement in the UK (IR (ME), 2000).

5.2.2.3. Optimisation strategies in digital radiography (CR & DR)
This sub-section will review the literature focussed on optimising digital radiographic practice. It will discuss potential strategies to reduce radiation dose whilst maintaining diagnostically acceptable image quality. The overall aim of this literature review is to form a synopsis that will help guide developing the methodology for this thesis.

It has already been established that the transition from analogue to digital radiography was accompanied by an increase in patient radiation dose. With new developments in technology, new radiation protection frameworks have been required to deal with current challenges, in order to meet the requirement of ALARA (Vaňo *et al*., 2007). Imaging professionals must understand the relationship between radiation dose and image quality. This, in turn, has led to a number of events and publications which have aimed to educate imaging professionals about the nature of this relationship. For example, the International Commission on Radiological Protection established a working group in 2001 to produce a document on how to manage patient radiation dose in digital radiography (ICRP, 2004; Vaňo, 2005). Moreover, other guidance documents have been published by the American Association of Physicists in Medicine (AAPM) and the American College of Radiology to inform radiographers on dose issues to consider when imaging patients. The efforts aimed to minimise the likelihood of stochastic risks without compromising the quality of an image; this would confirm the necessity to operationalise the radiation protection concepts in medical radiography.

Not only is understanding the relationship between radiation dose and image quality a prerequisite for optimisation, realising the physical contribution of each of the available options within digital imaging is also extremely important (Graham, Cloke, & Vosper, 2011). This means that optimisation should be guided by a specific strategy which would exploit the advantage of varying one parameter at a time (e.g. kVp), or in combination with others, to reduce the dose whilst maintaining adequate image quality. For this to be clear, it is essential to review literature that focuses on strategies which can be adopted to achieve the required balance between image quality and dose (Seeram, Davidson, Bushong, & Swan, 2013). Some of the literature focused on discussing optimisation strategies, pointing out their possible influence in

reducing radiation dose, whereas others have examined the effect of specific approaches on dose and image quality using either phantoms or humans. Nevertheless, for the purpose of achieving a comprehensive literature analysis on this topic, it may initially be feasible to review the guidelines established earlier for protecting patients from unnecessary radiation dose. For instance, NCRP reports No 105 "*Radiation protection for medical and allied health personnel*" (NCRP, 1989) and No 68 "*Radiation protection in paediatric radiography*" (NCRP, 1994) both provide useful radiation protection considerations, and most of them are still applicable to digital radiography. Thus, following these codes of practice in digital radiography can still reduce radiation dose and improve the radiographic image quality produced by CR or analogue (Willis, 2009). Examples of these guidelines are: appropriate collimation, correct selection of filtration, exposure factors (e.g. kVp & mAs), anode-heel orientation and dose monitoring using dosimetric instruments (e.g.TLD). In addition, it was recommended in the NCRP reports that radiologic professionals should realise the effect of different exposure factors and technological parameters (e.g. beam diaphragm) on both image quality and patient exposure.

The ICRP mentioned, in Publication No 73, that the optimisation of radiation protection is often applied in two main levels: one of them is related to the construction and design of radiographic equipment, and one deals with the optimisation of daily radiography working practice (ICRP, 1996). To illustrate, the first level focuses on how equipment design conforms to radiation protection standards, while the second directly links the manner by which the radiographic procedure is conducted to the optimisation goals, allowing professions to modify practice in favour of reducing dose and thereby improving image quality. This follows the fundamental principle of ALARA's philosophy (Seeram, Davidson, Bushong, & Swan, 2013). The application of the optimisation principles in medical exposure undergoes continual reviewing by the ICRP to meet recent advances in medical technology. The current recommendations of the ICRP have confirmed that the implementation of optimisation should be done via an on-going process which includes the following (ICRP, 2007b): 1) identifying the requirement for an action in relation to the context of the exposure; 2) choosing an appropriate reference level; 3) selecting the possible protecting actions to keep the radiation exposure ALARA; 4) identifying the best options; 5) employing the best option; 6) carrying out regular reviews for exposure situations to implement correction actions if required; 7) planning how to avoid emergencies and unnecessary exposures. Matthews and Brennan, on the other hand, have noted that only three points out of the seven are usually considered, namely the 3rd, 4th and 5th. They also suggest that the majority of research around optimisation has focused either on how to reduce the dose without affecting the image quality, or how to improve the image quality without increasing the dose (Matthews & Brennan, 2009).

A number of publications have described options to reduce radiation dose whilst keeping image quality acceptable, or improving it. For example, Willis (2009) grouped the required measures to address patient radiation dose into three categories: alternating imaging practice, modifying how the examination is conducted and altering imaging technology. In this context, changing imaging practice means choosing the appropriate imaging modality, fitting the radiographic examination to the clinical purpose of the procedure, and avoiding too many images per procedure. Appropriate collimation, geometry, positioning, and projection are all actions related to the

principle of changing the examination, and are controlled by radiographers. Finally, choosing the appropriate imaging detector, utilising suitable filtration, and image processing are all technological issues to which a medical physicist, radiographer or technologist could contribute.

With reference to dose reduction, the literature suggests there are five technological strategies which can be used. Each of these strategies has practical limitations. First, the high efficiency (DQE) of digital detector allows for using low exposure factors; this can reduce the image detector dose and, in turn, patient dose. However, reducing the dose may lead to an increase in image noise, and reduce the number of useful signals. In digital imaging, the remaining signals can be amplified by image processing (Khattak, Sajjad, & Alam, 2010; Martin, 2007).

Second, increasing the conversion efficiency of an image detector would contribute to a decrease in radiation dose. This is because the signals will increase, with the same amount of exposure reaching the image detector. Noise level, in turn, will decrease as the percentage of signals increases; therefore the acquisition parameters can be decreased while the noise level at the detector is kept the same. However, image sharpness may be slightly affected. It has been argued that DR has a better conversion efficiency compared with that of CR. Nevertheless, the recent advances in CR manufacturing have made the conversion efficiency for both DR and CR detectors nearly comparable (Leblans, Struye, & Willems, 2000). Consequently, high reduction in patient dose can be achieved.

Third, patient exposure can be reduced by increasing the mean energy of the X-ray beam administered during imaging; this means increasing the penetrating power of the X-ray beam and, therefore, reducing the amount of radiation energy absorbed by the human body, and reducing patient dose. There are two main ways to increase the average energy of a beam: 1) through setting a high kVp and 2) by using additional filtration thicknesses of either aluminium or copper. However, increasing the penetrating power of an X-ray beam may cause degradation in the physical image contrast. Specifically, soft tissue is highly vulnerable for this case due to the low absorption characteristics they have. Also, using high energy beams may cause more image noise because fewer photons reach the image detector. Some studies have also reported that, while using additional filtration during radiographic examination, tube potential can still be maintained at a high level. This tactic can lead to a significant dose reduction (e.g. 33% reduction) (Hamer *et al.*, 2004; Lu *et al.*, 2003).

Fourth, through reducing the amount of scatter produced from the interactions between the X-ray photons and the patient's body. One way to reduce scatter is through collimation. Reducing the field size will decrease the amount of scattered radiation (Honey & Hogg, 2012). The scattered photons are almost all with low energy and the probability of their absorption by the body is high. In addition, scattered radiation not only increases the dose, but also negatively affects image quality. Nevertheless, the collimation strategy is dependent on patient size, diagnostic task and operator skills (Uffmann & Schaefer-Prokop, 2009).

The fifth and final way to address the scatter is by using an anti-scatter radiation grid. When a grid is in use, the amount of dose reduction is more than offset by the grid Bucky factor, which is the proportion of increased dose required to penetrate the grid. In this sense, it has been reported

that an increase in dose in CR is less than the conventional Bucky factor. This is because only the primary beam blocked by the grid needs to be compensated to achieve the same signal to noise ratio, rather than compensating for the lack of both the primary and scatter (Fetterly & Schueler, 2007). Another approach that can be used to reduce the radiation dose known as noisy images combination technique. This includes constructing a composite image with less noise from a number of noisy images (Willis, 2009). Acquiring the stimulated signal from both sides of the CR image detector is an example of this approach and was developed by Arakawa *et al.*, (1999).

Other researchers have discussed strategies related to image quality improvement when dose optimisation is attempted. The strategies include dose control mechanisms, such as 'exposure index', and possible ways of optimising tube potential using an anti-scatter grid, filtration, image post-processing, and speed class (Schaefer-Prokop & Neitzel, 2006). These strategies are likely to be influenced by the imaging professionals and their decisions during the examinations. For example, a patient's body size and whether the patient is an adult or child. Using anti-scatter radiation grids during radiographic procedures can improve image quality. The grid's function is to attenuate non-useful photons, so they do not reach the image detector. Therefore, this reduces the amount of noise and enhances the percentage of diagnostic information (i.e. signal) in an image (Fetterly & Schueler, 2007).

Limiting the X-ray field dimensions to the anatomical region of interest helps to improve image quality. The reason behind this is to reduce the amount of scatter generated from a large field size. However, large patient size may limit the collimation to the area of interest, and may lead to the need to expose the patient several times to cover all areas (Willis, 2009). Furthermore, adopting high exposure factors can result in a larger amount of radiation reaching image detector. As a result, the percentage of signal to noise will be improved, thus improving image quality. This measure may be necessary for large adult patients. However, this practice is associated with an increased radiation dose.

The quality of an image can be manipulated through what is known as image post-processing. This facility is available for CR and DR and provides imaging professionals with a number of options by which they can manipulate the noise, latitude, contrast and sharpness of an image. Aldrich et al., (Aldrich, Duran, Dunlop, & Mayo, 2006) reported that, when changing certain processing algorithms within CR, image quality can be modified when low exposure parameters are adopted. Nevertheless, the level of image post-processing is dependent upon the values of the signal to noise ratio; thus in order to allow for high levels of image processing and avoid artefacts, an adequate exposure in the detector is required. All these measures can be categorised as operational approaches to improving the quality of an image (Uffmanna & Schaefer-Prokop, 2009).

It is worthwhile considering other operational strategies for managing patient dose. For instance, automatic exposure control (AEC) or manual modes are measures that can be adopted for optimising different radiographic examinations. Using AEC can help in controlling the exposure factors where an excessive radiation dose may not be permitted once the AEC detectors gain enough radiation to produce an image of adequate quality. However, one important issue with

AEC needs to be considered: a regular calibration of the ion chambers is necessary to ensure consistent, accurate radiation detection. This is necessary for digital radiography because of the difference in energy dependence between CR and DR detectors to analogue (Christodoulou, Goodsitt, & Chan, 2000).

In contrast, and in order to use manual mode in optimising practice, attention should be paid to the new characteristics associated with digital detectors. For example, the energy dependence of image digital detectors is completely different compared with analogue modality. In addition, the availability of post-processing tools in CR/DR allows for image quality modification, so could influence the selection of required techniques by imaging professionals.

The optimisation of radiographic practice using digital radiography has been widely investigated in the literature. The key aim was to discover the optimum exposure factors that could lead to a balance between radiation dose and image quality. A recent article reviewed literature focused on optimisation processes for different radiographic procedures using CR (Seeram, Davidson, Bushong, & Swan, 2013). The review includes the period from 2005 to 2013. The authors concluded a number of important points: most of the studies were focused on optimising kVp, and on optimising practice for chest radiography using different kinds of CR (e.g. Kodak, Fuji and Agfa); they almost all used automatic exposure control and constant effective dose; and, finally, they adopted DAP as a common dosimetric quantity. Another article, published by Schaefer-Prokop and Neitzel (Schaefer-Prokop & Neitzel, 2006), summarised the literature that described the relationship between image quality and radiation dose; this article reviewed the literature from 2000 to 2005, and the number of publications in this review was seventy five. The authors discussed a variety of different strategies for dose management and image quality improvement. Conflicting results were evident in the literature reviewed on the topic of radiation dose and image quality optimisation.

Overall, and according to this review, it is clear that there are two types of strategies which could be considered for the purpose of image quality and dose optimisation. First, technical strategies, which are based on the technology itself, detector efficiency, and whereby their manipulation could be practically limited; however, the choosing of the most efficient imaging detector, amongst other things, could be attributed to the imaging professionals for the purpose of the ALARA principle. The seond type includes operational strategies which their application margin is much wider than the technical ones, since the professionals are able to manipulate the acquisition factors. This, in turn, allows for a wide range of approaches to optimise dose and image quality.

Generally speaking, the literature review revealed that researchers almost always have limited options when optimising practice (Pina *et al*., 2004; Vassileva, 2002). Therefore, these attempts may have not met the challenges brought about by the new digital technologies. It should be noted that the implementation of digital detectors can lead to two outcomes: first, protecting patients from unnecessary exposure, since high exposure is no longer required, as was the case with analogue modality; second, since they have high detection efficiencies, radiation dose can rise in an undetected fashion due to image quality no longer being affected by high exposure as it was with film. Therefore, on-going research work in this field is necessary to explore the

inherent characteristics of digital detectors (Hogg & Honey, 2012). For this, the next subsection will review the physical characteristics of the imaging detector, which will provide a comprehensive understanding on how new advances affect radiation and image quality.

5.2.3. Computed radiography-detector (physical overview)

This thesis seeks to optimise the radiation dose and image quality for AP pelvis radiographic examinations using CR. Therefore, it may be advantageous to review some of the physical characteristics of this imaging system. In addition, comparing certain features and operations of CR technology to analogue may be useful in understanding the nature of the recent advances of CR systems, and how these might be employed to optimise practice. The physical composition of film materials, and how the image is produced, will thus be briefly described.

In analogue radiography, film/screen detector is constructed from a thin layer of active silver halide crystals, sandwiched between two phosphor screens (see figure 5-3). The phosphor is a powder of an inorganic luminescent crystalline, its main function is to convert X-ray photons into visible light. The phosphor converts the X-ray image into light which creates a latent image in the film. After X-ray exposure, the film is developed. Drawbacks of film include limited exposure latitude and the low sensitivity of its silver halide crystals. This means a high radiation dose is required to produce high quality images (Leblans, Vandenbroucke, & Willems, 2011; Seggern, 1999).
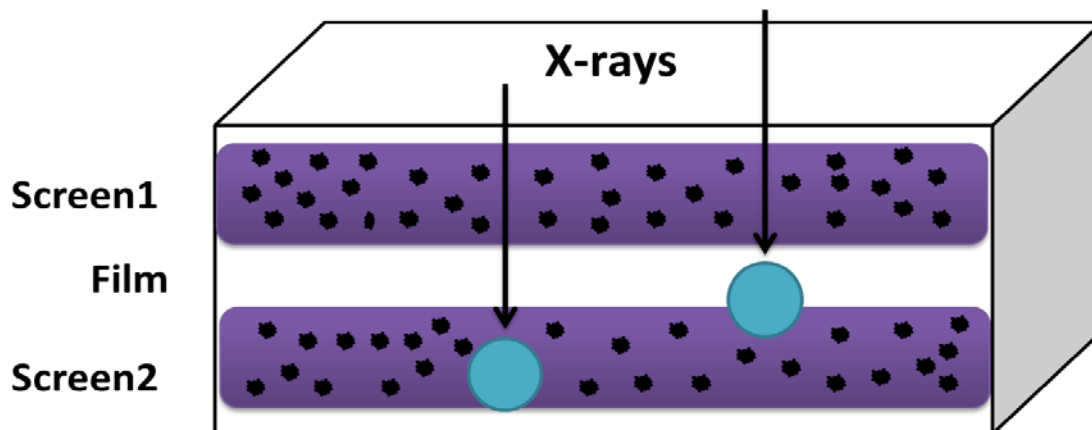
Figure 5-3. Film screen construction used in conventional radiography (adapted from Leblans, Vandenbroucke, & Willems, 2011).

By contrast, CR, being a newer technology, was first introduced in 1983. CR consists of a passive, independent, cassette based X-ray detector of various physical dimensions, similar to that of X-ray film screen cassettes. The CR image plate is constructed in the same way as the film-screen combination, where it consists of a polymeric support film coated with a thin layer of organic binder, in which the phosphor grains are stored. Unlike film screen, the main principles of the CR image plate is not the radiation-induced generation of simultaneous luminescence, but radiation-induced photo-stimulable luminescence (PSL), which is the key phenomenon of CR digital technology (Seibert, 2004). The phosphor used in the CR image plate is photostimulable storage phosphor (PSP). Specifically, the PSP material comprises a family of phosphor $BaFX$: Eu, where X can be any of the halogens, such as Cl, Br and I (Lança & Silva, 2009).

A PSL process can be described as follows: radiations incident on CR detector electron and a hole is generated, these are then captured in the electron and hole traps (i.e. metastable state) (see figure 5-4). Pairs of electron-holes will not be able to recombine, as with film, unless they are exposed to heat or light. Therefore, the phosphor stores energy from incident X-ray photons in the crystal structure, which in turn leads to the creation of a latent image. The latent image produced at the higher energy levels in the crystal lattice is proportional to density of the carriers of the hole and electron (Leblans, Vandenbroucke, & Willems, 2011). The efficiency of the CR detective layer in absorbing X-ray energy is dependent on three main points: the energy of X-ray photons, the thickness of PSP composite and the adjusted upper limits of detective quantum efficiency (DQE) associated with the CR imaging system(Seggern, 1999).
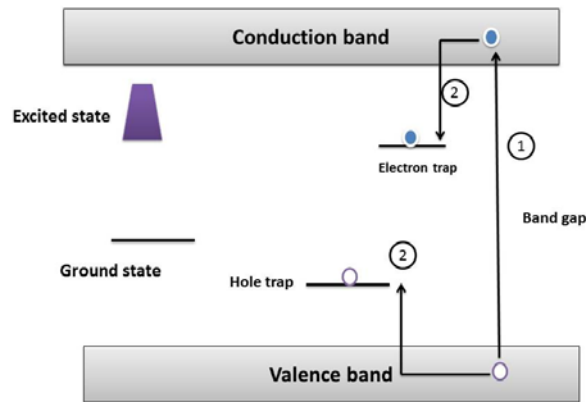
Figure 5-4. Diagram illustrates electron and hole traps in storage phosphor.

After the CR image plate (IP) is exposed to the X-radiation and the latent image has been created, the next step is to process the detector and produce the (digital) image. This is achieved by scanning the IP using a reader system. The photo-stimulable screen should be scanned by a laser beam to stimulate the emission of blue light photons. This triggers the process of photo-stimulable luminescence that can result in the emission of blue light in an amount proportionate to the quantity of X-rays which incident on the phosphor materials; this allows the free electron to return back to its lower energy state. Next, the emitted light is collected by a photodiode which is then converted into electric charge. Finally, the analogue to digital converter transforms the electric charge into the (digital) image (see figure 5-5) (Leblans, Vandenbroucke, & Willems, 2011; Lança & Silva, 2009).
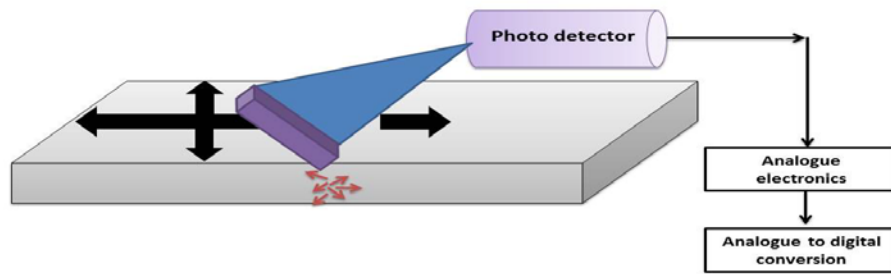
Figure 5-5. Shows the process of scanning the exposed image detector.

The last step in the CR imaging cycle is to erase the residual signal in the image detector. This step is necessary because there is a residual latent image of electrons trapped at high energy levels after the readout process. The residual energy is erased by using a high intensity white light source that removes the traps without re-exciting electrons from the ground energy level (AAPM, 2006).

The advent of CR systems has brought many advantages to medical imaging over analogue. One of these advantages is the quality of the diagnostic information carried by its image (Seggern, 1999). In this context, there are a number of physical aspects which characterise the CR detector performance, ultimately influencing image quality. These include: dynamic range, spatial resolution, contrast, and dose efficiency. The dynamic range can be described as the range of incident radiation dose that an image detector can accommodate whilst still producing adequate diagnostic image quality. This range is limited in analogue radiography and is only determined by the radiographic exposure, whereas in CR the dynamic range is almost dependent on the detector medium itself and on the readout process (Lança & Silva, 2008). Similarly, the minimal signal capability is determined by image noise and the grey scale differentiation capability of the digital system. The CR dynamic range is four hundred times wider than that of analogue, which would enable the CR detector to acquire image information over a wide range of entrance doses (see figure 5-6). Due to this wide dynamic range and normalisation of signal, image quality becomes less dependent on dose, and thus would produce more consistent image quality, in terms of contrast and density (Schaefer-Prokop, De Boo, Uffmanna, & Prokop, 2009).
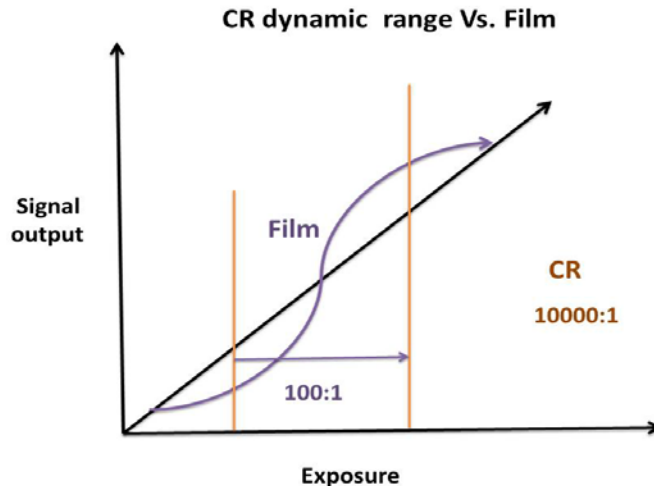
Figure 5-6. This illustrates the dynamic range trends for both CR and film screen technology.

Spatial resolution refers to the ability of an imaging system in discriminating between two close, small objects in an image. The spatial resolution can be affected by a number of factors, such as detector medium, thickness of detector materials, laser beam size and pixel size (Weiser, 1997). However, it has been reported that the spatial resolution of the CR image is limited when compared with X-ray film. This may be attributed to the scatter of light from the storage phosphor grains during the readout process (Seggern, 1999).

Another essential figure that correlates with the detail's size and contrast is modulation transfer function (MTF), which is important for visual recognition. A higher MTF means fine detail visualisation, in relation to other image details, can be achieved. Equally important is detective quantum efficiency (DQE), and is considered to be the best physical indicator for digital system performance. Of course, the higher the DQE, the higher the performance of the imaging detector in recording the required information. Ideally, this value would be 100%, but it is reliant on the amount of noise and thus the expected DQE is less than 100% (Cowen, Davies, & Kengyelics, 2007). These aspects of CR images were found to be generally high over wide range of exposures (Schaefer-Prokop, De Boo, Uffmanna, & Prokop, 2009).

With reference to these physical characteristics of the CR detector, producing an image with inadequate image quality is becoming less of a concern. However, this has possibly given rise to another concern - dose creep. Measures should therefore be taken to optimise dose and image quality, taking into account all available acquisition factors. One of the measures suggested to counter the risk of dose creep is the "*technique creep*" strategy, alongside various digital imaging modalities. The results of this strategy would ensure the required reduction in patient dose (Bushong, 2013, p. 312).

5.2.4. Radiographic acquisition factors (Technological and Operational)

In diagnostic radiography, the formation of an image includes a complex interrelation of many factors. These factors control the quantity and energy of the X-ray beams reaching the image detector. Some of these factors are under the direct control of the operator, whereas others are

114

purely technological and already set by manufacturers (Martin, Sutton, & Sharp, 1999). Understanding the effects of each of the acquisition factors is necessary in order to produce images with adequate diagnostic quality, and with the lowest possible radiation dose. Acquisition factors include the anode target angle, beam restriction and centring, beam filtration, anode heel effect, tube voltage (kVp), tube loading (mA), exposure time(s), antiscatter radiation grid, focal spot size, source-to-image detector distance, air gap technique, image post-processing, and using the automatic exposure control technique (AEC) (Graham, Cloke, & Vosper, 2011; Schueler, 1998). In addition to the direct impact of each of these factors on radiation dose and image quality, they may also have indirect effects on each other when combined. In the following subsections, there will be an explanation of the function of each acquisition factor, and how they could contribute to optimising radiation dose and image quality.

5.2.4.1. Angle of anode target

This angle is referred to as the bevel; it is subtended at the surface edge of the anode, forming an angle with the central axis of the X-ray beam (Figure. 5-7). Anode angles typically range from 7° to 20° and they are set by manufacturers and cannot be changed during the imaging process (Schueler, 1998).
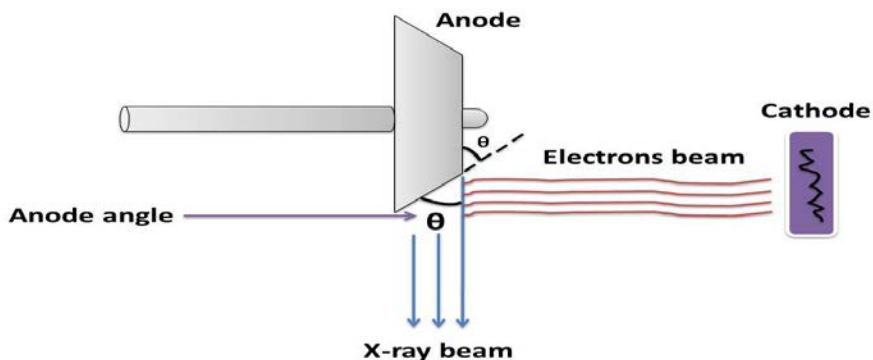
Figure 5-7. This shows anode angle set in the X-ray tube envelope.

The anode angle also determines the projected focal spot size of the X-ray field. If the anode angle is small, the focal track width will be increased, therefore also increasing the tube loading. Conversely, the larger the angle, the smaller the track width, permitting larger tube loading (Dowsett, Kenny, & Johnston, 2006). As the X-ray field size increases with the increasing anode angle, so does the effective focal spot size, which leads to an image with a large area and some degradation in the resolution. On the other hand, small anode angulation results in a small field size, but gives good image resolution. Finally, the selection of anode angle relies on the required application and on the source-to-detector distance (Schueler, 1998).

5.2.4.2. Beam collimation and centring

The collimation of the X-ray field size to the anatomy under examination is essential in diagnostic radiography for two main reasons, namely 1) collimation directly affects the patient

radiation dose, and 2) inappropriate collimation can degrade the image quality. Therefore, imaging professionals must pay special attention to reducing the field size to the required area. Collimation can be adjusted by shutters (Uffmann & Schaefer-Prokop, 2009). Appropriate collimation means that less body tissues will be included within the primary beam, thereby generating a smaller amount of scattered radiation which ultimately reaches the image detector. This, in turn, decreases the image noise and increases the amount of useful information. This would not negatively influence image contrast (Fauber, 2014).

There is another factor used to ensure the anatomy of interest is within the X-ray field - beam centring. Misalignment of the central beam can cause the individual photons' paths in the primary beam to be more divergent as the distance from the central beam increases. Therefore, adjusting the central ray's midpoint at the part of the body being radiographed can significantly reduce image distortion (Zetterberg & Espeland, 2011). It has been recommended that misalignment must not exceed 2% of the set source image detector distance. In modern radiography technology, centring can be inspected through a laser light fixed at the X-ray tube window. The concern of collimation may be more dominant in cassetteless technology (e.g. DR) than that dependent on cassette such CR. Finally, careful collimation and centring of the X-ray beam would ensure the necessary exposure (ALARAP) to the patient (Carroll, 2007).

5.2.4.3. Tube filtration
After the bombardment of electrons at the anode target has occurred, X-rays are produced and projected outside of the tube envelope to form the primary beam. The primary beam is responsible for recording information about body structures on the image detector. Generally, the primary beam comprises of X-ray photons with different energy levels, low, medium and high. The lower energy levels will not be able to penetrate the body, as these are completely absorbed by tissues and contribute significantly to the radiation dose (Fauber, 2014). They do not contribute to image formation. As a result, the lower energy photons must be removed from primary beam, whilst permitting the high energy photons to pass through; this is known as total filtration (To do this, a sheet of material such aluminium is usually placed in the path through which the X-ray beam passes on its way to the detector. Filtration is measured in units of aluminium equivalence (Al) millimetres (mm) (Carroll, 2007). The filtration can be divided into two categories - inherent and added. Inherent filtration is referred to as the glass envelope, the tube oil and the tube housing window. The typical value of the inherent filtration in most X-ray tubes is between 0.5 to 1.0 mm of aluminium equivalence. By contrast, added filtration represents any additional thickness of a specific material, usually aluminium, inserted into the tube port. Total filtration can be obtained from the summation of inherent and added; it commonly ranges from 1.5 to 2.5 mm, and depends on the highest tube potential at which the X-ray tubes are designed to work (Fauber, 2014; Graham *et al*., 2011). A value of 2.5 mm Al has formerly been suggested by the National Council on Radiation Protection as the minimum required level of filtration necessary to reduce patient exposure to acceptable levels (NCRP, 1968). In this context, the major role of filtration is to reduce the quantity whilst increasing the quality of the X-ray beam. As such, the filtration can contribute to improving the energy distribution of the radiographic output spectrum. In certain conditions, a specific type of filtration is required to alter the intensity of the beam and produce consistent exposure to the

detector, especially when the body structure is not uniform. This kind of filter is called a compensating filter, and an example is a wedge filter (Fauber, 2014). The possibility of using added filtration for the purpose of optimisation has been investigated extensively in literature. The majority of researchers have reported that, with added filtration, usually copper, a considerable dose reduction can be obtained without compromising the image quality (Brosi *et al.,* 2011; Ekpo *et al*., 2014; Hånsson *et al*., 1997). Finally, similar findings concerning the added filtration impact on radiation dose and image quality with analogue radiography were reported in previous literature (Kohn, Gooch, & Keller, 1988; Sandborg, Carlsson, & Carlsson, 1994; Staniszewska, Biegan´sk, Midel, & Baran´ska, 2000).

5.2.4.4. Anode heel effect

The anode heel effect refers to the unequal distribution in the intensity of X-ray photons down the axis of a line drawn from cathode to anode. This means that photon density is highest at the cathode and lowest at the anode (Figure 5-8) (Fauber, 2014). This phenomenon arises from the existence of the anode angle. After the X-rays are produced at the anode, they travel out equally in all directions. This means that X-rays produced at a point that is a few millimetres inside the anode's surface have to travel through the anode itself. This will cause attenuation for those X-rays (Fauber, 2014; Huda, 2010). The percentage difference in the beam intensity across the two sides of the tube has been estimated to be around 45%. The heel effect can be affected by anode angle, source-to-image-detector distance, and field size. This phenomenon can be utilised positively in two ways. Firstly, it acts like a wedge filter when imaging a non-uniform anatomical structure; also, the heel effect can clearly be considered as a filter on its own because of the attenuation caused by the anode material itself for the X-ray beam (Carroll, 2007; Graham *et al*., 2011).
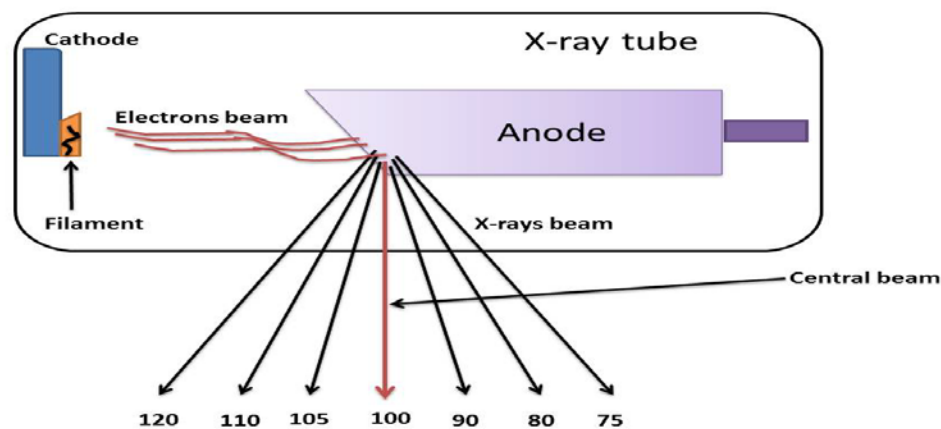
Figure 5-8. Demonstrates how the X-ray intensity (%) changes from cathode to anode inside the X-ray tube. The 120 to 75 illustrate the decrement in the photon percentage (adapted from Fauber, 2014).

Very few publications have investigated the value of the anode heel effect in imaging. Early work by Fung and Gilboy (2000) investigated the anode heel effect on gonad dose for lateral lumbar spine radiography. They found that, when the feet were orientated towards the anode, the male and female gonads doses were significantly reduced and thyroid, eye and breast doses were slightly increased (Fung & Gilboy, 2000). Another study was conducted by Mearon and Brennan (2006) to investigate whether appropriate positioning of the anode could improve the image quality of a thoracic spine. This study was conducted using an anthropomorphic chest phantom and conventional film. They ultimately found that correct positioning can slightly improve image quality (Mearon & Brennan, 2006). Two recent attempts by Soares *et al*., (2013) and Al Qaroot *et al*., (2014) considered the heel effect for lumbar spine radiography. Soares *et al.,* investigated the effect of adding filtration to the non-uniformity of radiation intensity caused by the anode heel, which resulted in the improvement in quality of lumbar spine images without an increase in exposure level. They concluded that noting the attenuating anodic effect demonstrated an improvement in the image quality along with a reduction in the entrance surface dose. In contrast, Al Qaroot *et al.,* investigated heel effect orientation on image quality and radiation dose during lateral lumbar spine X-ray procedures. They found that, when feet were positioned toward the cathode, the image quality was slightly better (Al Qaroot, Hogg, Twiste, & Howard, 2014; Soares *et al*., 2013).

5.2.4.5. Tube potential (kVp)

Tube potential refers to potential difference applied across the cathode and anode; kilovoltage peak (kVp) is the physical unit used to measure tube voltage. The Tube potential determines the speed at which the electron beam flows toward the anode. The energy of the X-ray beam also is dependent on the kinetic energy of the electrons that interact with the anode. Thus, an increase in the kVp results in an increase in the maximum photon energy. Whilst mean photon energy is approximately 30-50 % of maximum photon energy, the average can be increased when the maximum photon energy is increased too (Fauber, 2014; Graham, Cloke, & Vosper, 2011). Tube potential defines x-ray beam quantity and quality. Tube potential determines the capability of X-rays to penetrate the patient, affecting image quality. However, whilst a higher kVp increases photon penetration power, the physical object contrast will be low. Conversely, a low kVp setting would give a good image contrast, due to the low energy photons being easily absorbed by the body (Carroll, 2007; Dowsett, Kenny, & Johnston, 2006, 2006).

On the other hand, it has been argued that with certain radiographic examinations using a high tube potential could reduce patient radiation dose; although they have low contrast, the produced image are still diagnostically acceptable. This is because adopting a kVp which is less than recommended could lead to high radiation doses (Jessen, 2004). Similarly, Brindhaban *et al*., (2005), found that, by increasing the kVp and decreasing the mAs, a dose reduction of 25 to 50 % can be achieved in lumbar spine radiography using CR. However, they also noticed that both the SNR and CNR values decreased as the kVp increased. Selecting the optimum kVp depends on the body size of the patient under examination, the image detector, the type of information required and the image display.

5.2.4.6. Tube current (mA)

Tube current can be defined as the number of electrons flowing per unit of time from cathode to the anode; milliampere (mA) is the physical unit used to measure tube current. The mA determines the number of electrons generated which, in turn, determine the number of X-rays produced (Dowsett, Kenny, & Johnston, 2006, 2011; Fauber, 2014). Tube current can affect the quality of an image in relation to image density. It affects the quantity of photons required to carry information about the body structures being imaged. Too low an mA results in low image density, characterised in the form of noise. It should be noted that mA is the main source of patient exposure, so doubling it means doubling the absorbed dose, and vice versa (Carroll, 2007; Schueler, 1998).

5.2.4.7. Exposure time(s)

Exposure time is referred to as the length of time during which electrons flow and X-ray photons are produced. It is abbreviated to "s" and is measured by both seconds and milliseconds. This parameter can be set by the operator; the longer the exposure time is, the higher the quantity of electrons moving toward the anode (Fauber, 2014). Having established that mA is the 'rate of the flow of charge', the process of multiplying mA by exposure time would result in what is known as mAs. This quantity (mAs) gives an indication of the total intensity of the X-ray exposure. mAs controls the quantity of X-ray photons used during an exposure (Carroll, 2007). To obtain optimum image quality, there should be a trade-off between the tube current and exposure time, as the amount of X-rays reaching the image detector is highly reliant upon the mA and s. Short exposure times are strongly advised in radiography to minimise patient motion and image blur. However, very short times may require high tube currents; this, in turn, increases tube heating, which can have damaging consequences due to heat dissipation (Bushong, 2013; Dowsett, Kenny, & Johnston, 2006). Studying the effect of the mAs on radiation dose and image quality in the literature often shows that it comes together with a varying of the kVp (Gkanatsios, Huda, & Peters, 2002). For instance, two major roles for mAs are seen in literature: 1) to adjust the exposure factors and maintain a constant effective dose, and 2) to apply the 15% and 10 % rules in which the mAs is halved as the kVp increased by 15% and 10% respectively for the purpose of optimising the X-ray practice (Brindhaban & Al Khalifah, 2005; Allen, Hogg, Ma, & Szczepura, 2013).

5.2.4.8. Anti-scatter grid

The main function of this grid is to reduce the amount of scatter, in turn reducing image noise and improving image contrast. Using an anti-scatter grid is recommended when large body parts are being examined. Additionally, using the grid is also recommended with CR imaging. The reason for this is the high sensitivity of CR detector material to low energy scatter photons which, if absorbed, would lead to high noise levels (Tucker, Souto, & Barnes, 1993). In the same way, the grid permits a high percentage of the primary beam to be transmitted whilst absorbing the majority of the scattered photons (Figure 5-9) (Holmes, Elkington, & Harris, 2014; Jessen, 2004). However, a grid can also absorb some of the primary beam, resulting in the patient's radiation dose being increased to compensate.

Grids can be either stationary or reciprocating. The stationary grid can be mounted between the patient and the image detector. In contrast, the reciprocating or moving grid is located, or integrated, directly below the table top, where its movement is electrically controlled by an X-ray exposure switch. The grid is usually constructed of lead which is interspaced by carbon fibre to allow for primary beam transmission. Different grids types are characterised by the specifications they have. For example, they vary in relation to strip ratio, which is the ratio of strip height to the distance between them; strip frequency, which refers to the number of lead strips per unit length (i.e. inches, centimetres); strip pattern (e.g. linear and crossed lead lines) and strip focus (e.g. focused and parallel).
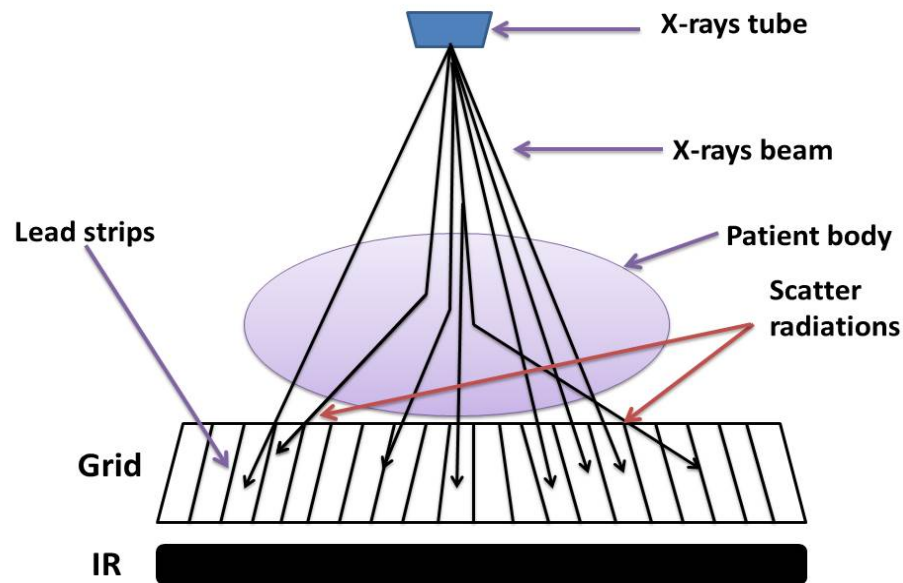
Figure 5-9. This shows how the focused grid absorbs scattered radiation.

Grid frequency ranges from 25 to 45 lines /cm, whereas the grid ratio typically ranges from 4:1 to 16:1 (Bushong, 2013; Fauber, 2014; Graham, Cloke, & Vosper, 2011). High grid ratio and frequency allow for high reduction in the scatter, lowering the noise level. Focused grids are characterised by their strips lines being canted; their orientation should be set to match the primary beam divergence angle. However, with parallel grids, the lead strips are perpendicular and parallel to one another. A focused grid is more beneficial than a parallel, because is permits more photon transmission through to the image detector. It is also worthwhile to consider the focal range, as this determines the source-to-image-detector distance at which there is no useful beam cut-off, due to the misalignment (Carroll, 2007; Fauber, 2014).

5.2.4.9. Focal spot
The focal spot is the area of the anode where electron bombardment occurs. The focal spot is physically described by what is known as the line focus principle. The line focus principle defines the relationship between two aspects of focal spot: the actual focal spot and the effective focal spot. The actual focal spot refers to the length of line in the anode that is actually struck by

electrons, and this depends on the length of cathode filament; the effective focal spot can be expressed as the size of the focal spot as estimated directly under the tube anode (Fauber, 2014). In radiography, there are two common focal spot sizes - small (fine), which ranges from 0.5 to 0.6 mm, and large (broad), which ranges from 1 to 1.2 mm. The focal spot sizes can be set by the operator, which is dependent on the filament size to be energised during X-ray exposure. Focal spot size can play a role in affecting the image sharpness. For example, using a fine focal spot will lead to a sharp image, whereas the using broad focal spot can degrade image sharpness. However, using a fine spot can be associated with the anode's overheating, due to the heat being concentrated in a small area of the anode. This issue can degrade the anode target and shorten its life (Graham, Cloke, & Vosper, 2011; Johnston & Fauber, 2012). It should be noted that the elongation of exposure time can cause patient movement, and can result in image blurring (Ball & Price, 1995).

Few publications have considered the value of changing the focal spot in optimisation research. Gorham & Brennan (2010) investigated the impact of focal spots sizes on image quality and radiation dose for different radiographic examinations; Ma *et al*., (2014) and Al Qaroot *et al*., (2014) investigated the focal spot size's effect on image quality and radiation dose during hand and lumbar spine radiography. The existing literature has found no significant differences in the image quality when switching to either focal spot size.

5.2.4.10. Source to image detector distance (SID)
SID is the distance between the X-Ray source and the image detector. The source-to-image-detector distance can be used to control the intensity of radiation reaching the patient and image detector. This can be explained by the inverse square law, which states that the intensity of radiation is inversely related to the square of the distance from the source. Accordingly, the greater the distance from the X-ray source, the larger the divergence of the radiation field. However, a larger the area of the field means a lesser intensity of radiation will reach the image detector (Graham, Cloke, & Vosper, 2011; Johnston & Fauber, 2012). The effect of this phenomenon on radiation dose and image quality has been investigated by some researchers. They found that when SID is increased from 100 to 130cm, while keeping object image distance at 0 cm, patient exposure is reduced and an acceptable image quality is maintained (Brennan, McDonnell, & O'Leary, 2004; Brennan & Nash, 1998). A number of other recent studies have been identified, but several of these will be discussed in sub-section (5.2.7.) since they are dedicated to the optimisation of AP pelvis radiography. Nevertheless, Joyce *et al*., (2013) investigated the varying of the SID (from 100 to 150 cm) as an option for optimising skull radiography. They found that the radiation dose administered to the patient was significantly reduced without a compromise in the image quality.

5.2.4.11. Air gap technique
Using an air gap in diagnostic radiography has been described as an alternative to a grid for reducing the number of scattered photons that reach the image detector. This contributes to improved image contrast whilst reducing the amount of noise that may be caused by the scattered radiations (Carlton & Adler, 2013; Bushong, 2013). The principle of this technique is based on creating a distance (cm) between the patient's body and image detector. As a result, a portion of

the scattered photons from a patient body would be lost before they strike the image detector. The created gap between the patient and image detector can range from 10 to 15 cm. The higher the gap is, the higher the reduction in the scattered photons reaching image detector. Using an air gap sometimes requires an increase in the mAs to compensate for the reduction in beam intensity. Some researchers have reported the radiation exposure with an air gap may be slightly lower than with that of a grid because of the grid's cut off (Bushong, 2013; Kottamasu & Kuhns, 1997). The major drawback of the air gap is the reduction in the visibility of fine detail, making its application limited. Also, it can cause image magnification, which may require an increase in the SID to compensate. However, this is not possible for every examination since it is limited by the permissible heights at which the x-ray tube can be raised, as these are set by manufacturers (Carrol, 2007).

5.2.4.12. Image post-processing
This option is currently available in all modern digital imaging systems and it represents a distinct advantage over analogue. It is considered to be an effective tool for adjusting anatomical detail within an image. However, it can only be used by the operator after the image acquisition process. Image post-processing software provides a number of image quality manipulating parameters such as contrast enhancement, latitude, noise reduction and windowing (Carroll, 2007).

The effectiveness of applying post-processing in x-ray imaging has not yet been widely investigated. Nevertheless, Moore *et al.*, (Moore, Liney, Beavis, & Saunderson, 2007) presented an approach to define which optimum post-processing algorithms could improve chest image quality. Others have explored ways of adapting specific post-processing algorithms to enhance image quality (Prokop, Neitzel, & Schaefer-Prokop, 2003). A recent study by Decoster *et al.* (2015) investigated the contribution of post-processing on image noise and contrast using a test phantom. Finally, it is important to note that image post-processing always results in information loss when compared with the original image. Therefore special attention needs to be paid when working with such processing algorithms (Carter & Vealé, 2014).

5.2.4.13. Automatic exposure control (AEC)
AEC is a common and widely used technique in projection radiography. Its importance comes from its ability to control the amount of exposure delivered to patients which can produce adequate and consistent quality image. This device assists operators when choosing the appropriate exposure factors for any examination (Johnston & Fauber, 2012). However, operators should be aware of the limitations of the AEC in ensuring consistent performance. In practice, the AEC consistently controls the quantity of the radiation reaching the image detectors; it terminates the exposure once enough radiation has been received. For this, the AEC's radiation detectors are used to determine the required amount of radiation. In AEC, two kinds of detector have been used: photo-timers and ionisation chambers. The former refers to the AEC device that utilises photo-multiplier tubes or photodiodes, and is uncommon today; whereas ionisation chamber based AECs are most common, and consist of three chambers, one in the centre and two at the lateral upper sides. The imaging professional should select the best configuration of the three chambers for optimal performance. Although ionisation chambers are less accurate and

complicated compared to photo-timers, they are also less liable to failure (Fauber, 2014; Holmes, Elkington, & Harris, 2014).

On the other hand, using an AEC device still necessitates the appropriate selection of kVp, mA, image detector and grid. This means that the main function of the AEC is to control the exposure time (Carroll, 2007). Therefore, the inappropriate setting of these other factors may lead to either overexposure or underexposure. For example, a low kVp setting requires long exposure times to reach the predefined amount of exposure. In contrast, a high kVp setting reduces the exposure time and the amount of predefined exposure required to reach the detector, and can ultimately decrease patient exposure. The predetermined amount of radiation necessary for good quality image is set either manually or automatically by the imaging professional (Carroll, 2007; Fauber, 2014). In this, the amount of exposure needed to produce an image is controlled by the backup time. This mechanism controls the maximum amount of exposure permitted by the AEC for given kVp and mAs settings. The backup time is adjusted by either the operator or manufacturer in order to keep the exposure within the tube load capacity. Its value ranges from 1 to 6 milliseconds. The backup timer protects the patients from unnecessary radiation dose and saves the tube from being damaged (Carlton & Adler, 2013).

Finally, it is important that imaging professionals consider some points when working with AECs such as the positioning and centring of patients, collimation, size and variation of detector. Equally, regular AEC calibration is necessary to ensure consistent performance (Mazzocchi *et al.,* 2005).

5.2.5. Clinical indications for pelvic radiography

This subsection describes the common clinical indications for AP pelvis radiography. It should be noted that projection radiography is still the preferred modality for obtaining clinical information on pelvis pathologies when compared to other available modalities (e.g. CT). Pelvic radiography plays an essential role in diagnosing and treating the corresponding pathologies within the pelvic region (Flemming & Walker, 2010). For example, trauma is one of the most common reasons for which the pelvis and hip are imaged (Carver & Carver, 2012). Another indication which requires radiographic imaging is to confirm the suspicion, or to follow-up patients with osteoarthritis. This is a degenerative joint disease and can be considered as the most common type of arthritis. This type of arthritis occurs normally as result of the aging process. Furthermore, the pelvis includes red bone marrow, and this makes it a metastatic site for tumour spread, again providing justification for imaging (Bontrager & Lampignano, 2014).

5.2.6. Rationale for selecting AP pelvis

The anterior-posterior (AP) pelvis projection has been selected as the focus of this thesis. From a radiation protection perspective, there are a number of reasons behind selecting this projection. First, the pelvic region includes the reproductive organs, which have been classified as the second most radiosensitive organ according to the ICRP publication 103, compared with other body organs (ICRP, 2007a). This means that, during pelvic imaging, the gonads are inevitably exposed to primary beam radiation and, therefore, the risk of inducing a late effect within future generations does exist (Frank, Long, & Smith, 2012). Second, AP pelvis and hip radiography has been reported to be the third most frequent examination when compared with the biggest dose

contribution examinations in the UK, with a 39 per 1000 of population annual frequency (Hart, Wall, Hillier, & Shrimpton, 2010). In this context, survey studies on radiation dose revealed that the average adult effective dose from AP pelvis radiography in the UK is 0.7 mSv, almost seven times as large as that of chest radiographic examinations (0.08 mSv) (Sherer, Visconti, Ritenour, & Haynes, 2014). Furthermore, no systematic attempt was found in literature to optimise the radiation dose and image quality of the AP pelvis radiography using either anthropomorphic phantom or real patient taken into account the primary and seconday acquisition factors. Finally, significant variations in the obtained results were seen from the previous optimisation attempts (Seeram, Davidson, Bushong, & Swan, 2013).

5.2.7. Previous optimisation attempts for AP pelvis examinations (Literature review)

There have been many attempts to reduce the patient radiation dose from AP pelvis examinations. The main focus of these attempts has been to identify the optimum technique that would produce suitable quality images with the lowest possible dose. This sub-section will review the literature on optimising AP pelvis radiography and explore the effect of different acquisition factors on radiation dose and image quality.

An early attempt to optimise image quality and dose for AP pelvis radiography using DR was conducted by Persliden *et al.*, (2002). They investigated the effect of varying mAs whilst maintaining a constant kVp, using an anthropomorphic phantom. In their study, image quality was measured in two ways: objective (noise level) and perceptual, through radiologists. They found that, when using low mAs, the dose was reduced from 1.4 mGy to 0.48 mGy and the quality of the images, although having slightly increased noise, was still acceptable for diagnostic purposes. They also suggested more dose reduction was possible if further optimisation was carried out, and that radiation dose levels of 0.24 mGy could be reached. These were only suggestions, since they limited their optimisation methodology, only varying the mAs. A comparison study was conducted to investigate the effect of various exposure factors (e.g. kVp and mAs) on the image quality of AP pelvis using CR and analogue modality (Al Khalifah & Brindhaban, 2004). In their study they used a phantom and various exposures factors similar to those used in the hospital. Their findings revealed that there were no significant differences between the image quality scores for both modalities. However, the authors acknowledged that they did not use all of the available optimising options for the CR system, such as adjusting image contrast and density, within the Look Up tables, which allows for the reduction of the mAs setting, and thus patient dose (Al Khalifah & Brindhaban, 2004). Nevertheless, no dose measurement was attempted alongside the IQ testing and the same acquisition factors were used for both modalities. This is therefore work against the expected advantage of CR in dose saving.

In another study (Brindhaban & Al Khalifah, 2005), the researchers studied the effect had on the quality of AP pelvis radiographs and radiation dose when the mAs was changed, with a fixed kVp, and the kVp was changed, whilst keeping mAs constant. For this they used a phantom, CR and analogue. In addition, they were also seeking to define at what radiation dose limit CR systems could still produce an acceptable image quality. Their results revealed that the effective dose and gonadal dose could be reduced by half, compared with analogue. They identified that 83 kVp with 5 mAs can produce acceptable quality image with a low dose. In another

optimisation study (Aldrich, Duran, Dunlop, & Mayo, 2006), the authors investigated the patient radiation doses using CR, DR and analogue for a number of common examinations, including AP pelvis. They found that patients' doses from AP pelvis were similar for all modalities (i.e. CR, DR and analogue). However, this finding contradicts that obtained by Brindhaban & Al Khalifah (2005) work mentioned above for AP pelvis. Nevertheless, the researchers have attributed this similarity to having used the same mAs in all systems. Accordingly, they argued that the mAs can be used as a good indicator for controlling the radiation dose and a further study was advised. There was no significant difference in image quality between CR and analogue; this would indicate that the same exposure factors used for X-ray film have been adapted for the CR.

In 2005, a research study was undertaken to find out which kVp would be suitable for acceptable AP pelvis image quality, whilst limiting the effective dose. In this study an anthropomorphic phantom was used, and the image acquisition was done with a CR system. One of the goals was to test the efficiency of the detector in reproducing a diagnostic quality image at a low kVp. The kVp range used in this study was from 50 to 120; and the image quality was assessed by six radiologists using a relative VGA against a reference image. The researchers found the VGA image quality score was superior when a low kVp was used. This could be attributed to the high detector efficiency of the CR imaging system. However, using low kVp increases skin dose, and decreases the effective dose. A common rule in radiography indicates that when kVp decreases, the mAs should be increased to compensate for the low radiation output yield (Tingberg & Sjöström, 2005).

Other researchers (Sandborg, Tingberg, Ullman, Dance, & Alm Carlson, 2006) have investigated the dependence of image quality of the AP pelvis imaging on kVp using CR. In this study the effective dose was kept constant by manipulating the mAs. The kVp was varied from 50 to 150 to include the values used with analogue systems. Radiologists scored the images using VGA, and the criteria were based on a refined EC one. The image quality was also assessed physically using SNR. This allowed for the calculation of a figure of merit (SNR^2/E). A subsequent aim was to find a correlation between SNR and VGA scores of image quality. The study had two important findings: first, that at a low kVp the image quality score and the overall SNR were highest, and vice versa; and second, that there was a positive correlation between the SNR and VGA measures of the image quality. Taking advantage of exploring the efficiency of CR detectors in accommodating for a low kVp into account, the findings of this study could be limited for use in optimisation research, because of the constant E adapted.

Other investigators (Butler, Rainford, Last, & Brennan, 2009) have adopted the exposure index (EI) of CR systems as an indicator for optimisation in the radiographic examinations of the pelvis. The intention was to establish the optimum EI in relation to dose and image quality, and compare them with manufacturers' recommended values. Images were obtained using human cadavers and ESD for the corresponding exposures. Images were assessed by clinicians using CEC anatomic criteria against a reference image. They found that, with a dose reduction of 38% of that recommended by manufacturers, the image quality of AP pelvis is still acceptable. Therefore, researchers have recommended establishing a specific EI for each centre, instead of

relying on the manufacturer set value. Taking this into account, it becomes clear that using an exposure index for optimisation is currently difficult because of the diversity of the X-ray equipment, which have different exposure indices. This therefore makes the widespread applicability of the results to be significantly lessened.

Walker *et al.,* (2011) studied the effect of varying the kVp and mAs to optimise AP pelvis radiography using an acrylic pelvis phantom and CR. In this study, 60, 70, 81 and 90 kVp, each with 6 different mAs values, were adopted. Image quality was assessed using VGA with a 5-point Likert scale; image quality criteria were adapted from the Al Khalifah & Brindhaban study (2004). The dose area product (mGy.cm^2), entrance and exit detector doses were also measured using a solid state dosimeter. They found that, at high and low mAs, the image quality scores were high and low at each kVp setting, respectively (Walker, Allen, Burnside, & Small, 2011). However, using this kind of phantom may have reduced the clinical relevance of the findings, since the acquired images' have a lack of anatomical variation levels which would be provided by an anthropomorphic phantom to acquire images that simulate clinical situations. Others (Fauber, Cohen, & Dempsey, 2011) have studied the effect of varying the exposure factors (mainly mAs and kVp) on the radiation dose and image quality of AP pelvis. Gonad male dose was used as a corresponding parameter to the image quality in this study. Varying acquisition factors were undertaken, increasing the kVp by 15% and decreasing the mAs by a half to acquire a series of images. They found that it was possible to produce a suitable quality image of an AP pelvis with a low gonad dose at 93 kVp and 12.5 mAs using a DR system. However, the authors assessed the image quality in terms of optical density and overall diagnostic quality. The optical density may no longer be a suitable indicator for image quality with digital radiography, and, depending on the overall quality, may actually increase the subjectivity and bias of the results.

In another work, Heath *et al*., have reported that increasing the SID to a value of 147 cm (standard SID = 100 cm) will significantly reduce the ESD and E (i.e. at 147 cm = 2.56 mGy, 0.44 mSv; at 100 cm = 3 mGy, 0.51 mSv, respectively) when using DR. They also found that such an increase will not affect image quality. However, this study also tested removing the grid during the imaging process, and, although this led to a significant dose reduction, it also created a huge decrease in the image quality (Heath *et al*., 2011). It should be noted that authors used the AEC to acquire the images with a fixed 80 kVp setting. A similar study was conducted by Tugwell *et al*., (2014) to investigate the effect of varying the SID from 90 to 140 cm on the image quality and dose during AP pelvis examinations, using CR and anthropomorphic phantom. In their study, they used a 2AFC approach to assess the images visually and SNR to physically assess the image quality. At each SID two images were acquired- one using AEC and one not. Images were scored by experienced radiographers. The results demonstrated, at a SID range of 110 to 140, the E and the ESD were reduced by 3.7% and 17.3% with AEC; and 50.3% and 41.79% without using AEC. No significant difference was found in the image quality scores across the range of SIDs. Nevertheless, a slight reduction in the SNR was seen with the increase in the SID. In relation to the above two studies, using a high SID could not be achievable in every hospital due to limited available space and the interference with grid focal range.

In a recent clinical investigation (England *et al*., 2015), the authors considered the effect of SID changes on the radiation dose and image quality of AP pelvis radiographs acquired using DR. In this study, two groups of patients were recruited; one was acquired with images using an SID of 115 cm (97 patients), and another (99 patients) was acquired with the highest possible SID (i.e. either 135 cm or greater based on minimum table height). Images were scored by experienced radiographers using an established VGA scoring system across multiple anatomical locations. The results demonstrated that a dose reduction (significant, $P<0.01$) of 39% and 41% for each of ESD and E can be achieved when increasing SID, without a compromise in image quality. The images were acquired using AECs with two lateral chambers selected, and at a fixed 75 kVp.

Optimisation must be considered when using AECs for AP pelvis radiography. In this context, 2 phantom based works (Hawking & Elmore, 2009; Manning-Stanley, Ward, & England, 2012) were identified in literature. One study was conducted to investigate at which AEC chamber configuration the ESE is lowest, without compromising image quality for AP pelvis radiographs (Hawking & Elmore, 2009). The results demonstrated that the ESE is lowest when using the two outer chambers for AP pelvis without affecting the image quality, and highest when using the central chamber. However, although the dose associated with central chamber was high, the quality of the images was the lowest, using CR. However, using EI as an IQ indicator may make results comparison difficult since the majority of literatures have used CEC quality criteria to simulate the clinical situation. Also, using ESE could not be appropriate as with using E (mSv) as a patient radiation risk measure. The second study investigated the appropriate chamber selection and phantom orientation that delivers a low dose and suitable image quality for AP pelvis using CR and DR (Manning-Stanley, Ward, & England, 2012). In this study, kVp and SID were kept constant. The findings demonstrated that, when the phantom feet was positioned toward the two outer chambers (caudally) and the only two outer chambers were used, the radiation dose was at its lowest but still had an acceptable image quality. Similar to the previous study, the dose was highest when the central chamber was in use, but the image quality score decreased, yet still remained adequate.

A recent randomised study investigated the impact of patient orientation (i.e. head toward and away the 2 lateral AECs) on reducing the dose without compromising the image quality of AP pelvis using CR and DR. In this study, patients were divided into two groups: a standard group with the patient's head towards the outer two AECs, and a second group where the head was positioned away from the outer two AECs. The ESD and E were calculated and the images assessed by three observers using an adapted CEC criteria. The results demonstrated that, when patient orientation is switched to 'head away', the patient dose, using CR, was reduced greatly by 38%, compared with DR which had a 31% dose reduction (Harding *et al.,* 2014). Lança *et al.* (2014), have investigated the effect of varying the kVp (60 to 120) on the effective dose and perceptual image quality of AP pelvis radiographs using an anthropomorphic phantom and CR. The images were acquired by applying the '10 kVp rule' with AEC, and then without. Five assessors scored the images using a 2AFC approach. The criteria used in this study were adapted from the novel scale generated in section I of this thesis. Finally, Lança reported that, when the 10 kVp rule was applied, a significant reduction in effective dose was seen, whereas the

perceptual image quality, although reduced at 90 kVp, was not significantly different both before and after the rule had been applied (Lança *et al.,* 2014). However, a technical limitation associated with this work was that the desired half value of mAs, when kVp increased by 10 % with AEC, could have not been achieved in the same manner as with non-AEC experiments.

Finally, recent work by Chan and Fung (2015) aimed to investigate the appropriateness of replacing the grid with an air gap on reducing testes and ovary doses during AP pelvis radiography for CR and DR. In this study, an ATOM dosimetry phantom was used for image acquisition, along with dosimetry measurements. Images were acquired with/without grids and with/without an air gap using AEC outer chambers. The images were assessed by five radiographers using two scoring systems, namely the image quality score (IQS) and a VGA. They found that the optimum air gap would be at 10 cm, since this was the range whereby the effective dose reduced by 2 and 2.3 times for both CR and DR. In addition, a considerable reduction in the ovary and testes doses was seen when an air gap was in use. However, two issues are evident from this study: first, it is currently impractical to create an air gap between the patient and image detector; and second, the images have been acquired using the ATOM dosimetry phantom which caused a shadow of the phantom slices to appear in every image. This would ultimately affect the quality of the images and may also bias the image quality assessment (Chan & Fung, 2015). To facilitate comparing the literature mentioned above, table 5-2 summarise the main elements of the key papers which associated with AP pelvis optimisation attempts.

Table 5-2. This table summarise the main elements of the key papers concerned with optimising the AP pelvis radiographic examination

Authors'	Study design	Imaging system	Acquisition factors	Assessment approach	Findings/ Conclusion
Persliden *et al.* (2002)	- Dose and IQ optimisation - Pelvis anthropomorphic phantom - Varying mAs only to change noise level - ESD and E were used	- DR (Pixium 4600, Thales Electron Devices, Vélizy, France)	- kVp (77) kept constant	- IQ : physically through noise level calculation (1 ROI); Visually assessed by two radiologists based on usefulness for diagnosis. - Likert 1 to 5 - PCXMC used for E estimation	- Dose was reduced from 1.4 to 0.48 mGy - By decreasing mAs images noise increase but still acceptable for diagnosis - Varying mAs only good optimisation strategy
Al Khalifah & Brindhaban (2004)	- Effect of varying kVp and mAs on IQ for CR and analogue -15% kVp rule was used - Pelvis phantom	- CR(Kodak) - Analogue (Kodak)	-kVp (76,83, 90) -mAs (16,10,8)	-IQ: images and film were assessed using overall diagnostic quality (contrast, noise) - Images and films were scored by 6 radiographers and 1 radiologist.	- No significant changes in the IQ for two modalities across wide range of kVp (-15 to +30%) and mAs (-25% lower that standard) - Analogue

				- Five point Likert scale used (1to5).	exposure factors can be used for CR
Brindhaban & Al Khalifah (2005)	- Radiation dose at various kVp and mAs using CR and analogue - 15% kVp rule - Pelvis phantom - Dosimetry (organ dose, ESD and E)	- Analogue (GE Adavantx -CR (Agfa)	-kVp (76,83, 90) -mAs (16,10,8)	- E was estimated using XDOSE programme - ESD measured using ionisation chamber - IQ : Hard copies of images were evaluated by 5 technologists, 1 medical physicist and 1 radiologist - Five point Liker scale - Criteria: Overall diagnostic quality (contrast and noise)	- Dose can be reduced by 50% that of analogue with images still acceptable for diagnosis - CR lower exposure factors(83 kVp,5 mAs) - Analogue (90 kVp, 8 mAs)
Aldrich, Duran, Dunlop Mayo (2006)	- Optimisation of IQ and dose using analogue, CR and DR - Patients based - ESD and DAP readings -PACS used for CR and DR images dsiplay	- Analogue (Kodax Insight-300 speed) -CR (Fuji) -DR (Philips Diagnost)	- Pelvis (kVp): CR, 75; DR, 77; analogue,75 - Pelvis (mAs): CR, 21.8; DR, 10.17; analogue, 37	-IQ : DR and CR images were reported by radiologists on PACS -IQ assessment was subjective based on observer's experience and preference - Dose: ESE from TLD; E from conversion coefficient	- CR doses were similar or higher than that of analogue -It is possible to change the algorithm and reduce dose by 25% without IQ compromise; - IQ was similar across all modalities
Tingberg & Sjöström (2005)	- Kvp optimisation - Pelvis and chest as models - Anthropomorphic phantoms - Constant E	-CR (Fuji)	- Pelvis (kVp): 50 to 102 kVp (mAs, 8-112)	-IQ : Relative VGA ; CEC quality criteria; 6 observers (radiologists); scores (-2 to 2); Workstation monitor - Dose: E calculated from DA reading using conversion factors	- IQ can be improved using lower kVp (i.e. 50) than that was used with analogue
Sandborg, Tingberg, Ullman, Dance, & Alm Carlson (2006)	- Comparison between physical and clinical IQ measues - Pelvis and chest -Anthropomorphic phantoms -Constant E	-CR (Fuji)	- Pelvis (kVp): 50 to 102;	- IQ : relative VGA; CEC quality criteria; 6 observers (radiologists); scores (-2 to 2); SNR calculated using computer modelled pelvis phantom	- Strong correlation between clinical and physical IQ measures (VGA vs. SNR) - Optimum kVp was seen lower than that of analogue (i.e. 70

				- mAs adjusted to having constant E	kVp) for pelvis
Butler, Rainford, Last, & Brennan (2009)	- Optimisation of EI - AP pelvis and knee - Cadaver - ESD	-CR (Kodak)	- Pelvis: kVp, 80; mAs, 2-80	- IQ: Relative VGA; 5 clinicians; 4 point Likert scale; CEC quality criteria - Dose: TLD system	- EI reference values must be established for each clinical centre rather than relying on manufacturers' recommendations
Walker, Allen, Burnside, & Small (2011)	- Relationship between exposure factors, EI and dose - 15% kVp rule adopted - Acrylic pelvic phantom - Workstation monitor - DAP, ESD and E - EI	- CR : (Konica-Minolta Regius)	- kVp: 60, 70, 81, 90 - mAs : 6 different mAs for each kVp - 24 images at each kVp setting	- IQ: Images were scored by radiographer using 5 point Likert scale - EI was recorded for each image - Criteria : right neck of femur, left acetabulum and body of fifth lumbar vertebrae - Dose: PCXMC was used to estimate E from DAP readings	- Good quality image at high mAs, and poor quality image at low mAs with same kVp - EI is high at low dose and is low at high dose
Fauber, Cohen, & Dempsey (2011)	- Digital acquisitions effect on IQ, gonads dose and IE -15% kVp rule -Pelvis anthropomorphic phantom	- DR (Siemens AG, Munich, Germany)	-kVp, 70-121; mAs, 50	- 4 radiographers asked to score the image noise level on 1 to 3 scale; 2 radiologists asked to rank images from best to worse, acceptable or not, state amount of visible noise - EI recorded for each exposure - Gonads dose measured using TLD	-The optimum image produced at 93 kVp and 12.5 mAs indicating that high kVp can be used to reduce the gonads dose without compromise the quality of an image
Heath *et al.* (2011)	- Effect of the SID and dose and IQ - Anthropomorphic pelvic phantom -ESD and E used	- DR (GE Medical Systems)	- kVp, 80 -AEC -SID,100-147cm (10 cm interval)	-IQ: 4 observers; relative VGA; CEC quality criteria -Dose: E was calculated using QADDS software	- SID can be used as an effective tool to optimise the radiation dose and IQ for AP pelvis
Tugwell *et al.*	-Optimising the SID -Anthropomorphic	- CR (Agfa)	- kVp, 75; Two outer	- IQ: 2AFC for images	- SID can be used to reduce E and

(2014)	pelvis phantom - With and without AEC mode -ESD and E		chambers; -SID, 90 to 140 cm(5 cm interval) - mAs,16 for non AEC imaging	assessment; Quality criteria derived from CEC criteria and our novel scale criteria ;7 radiographers to score images; 5 point Likert scale(1-5) -SNR was calculated -Dose: - E wstimated using PCXMC; ESD (Unfors)	ESD without adversely affecting the IQ -SID a cost effective tool for dose optimisation
Hawking & Elmore (2011)	-Optimising AEC chambers configuration -Anthropomorphic pelvis phantom -Entrance skin exposure - Analogue and CR - Optical density and EI	-CR (Kodak) -Analogue (200 speed, GE health care)	-kVp, 70 - mA, 400 -SID, 100 cm	- Optical density was measured using densitometer -EI was recoded for each exposure - Films (only) were assessed visually using institution's established criteria	- Setting two outer AEC chambers can reduce ESE without affecting the IQ
Manning-Stanley, Ward, & England (2012)	- Optimising chambers selection and phantom orientations (cranially and caudally) -Anthropomorphic phantom -AEC only -E and ESD	- DR (GE Medical system)	- Fixed kVp at 80; SID at 100 cm	- IQ: Relative VGA; 2 observers scored the images using workstation monitor - CEC quality criteria and 3 point Likert scale -Dose: E was calculated using QAADS	- With cranial orientation, single chamber is preferred - With caudal orientation, two lateral chambers are preferred
Lança et al.(2014)	- Impact of 10% kVp rule on dose and IQ - Anthropomorphic phantom - AEC and manual modes - Different AEC combinations - E	- CR (Agfa)	-kVp, 60-120 (AEC and non AEC) -SID, 110 cm	IQ : 2AFC, 5 radiographers; 5 point Likert scale - Quality criteria derived from our novel scale -Dose : -E estimated using PCXMC MC software	- IQ was seen to be similar (no difference) before and after 10% kVp rule; significant E reduction was seen - 10 % kVp rule show promise for pelvis imaging with both AEC and manual modes
Chan & Fung (2015)	- Dose optimisation using air gap technique - Sectional Rando	- CR (Fuji) - DR (Siemens)	- kVp, 85 - SID, 100 cm - Two later AEC chambers	IQ: two evaluating systems were used 1. Relative VGA; CEC quality criteria; 5	- A 10 cm air gap would be the best option to produce image of

| phantom
- Gonads doses
- AEC
- Air gap adjustable device (wooden) was used
- SNR | | -Air gap range 0 to 25 cm
- mAs was adjusted to having consistent image density | observers (radiographers);
2. IQS, SNR level, contrast between tissues and sharpness of CEC quality criteria

- Dose:
Ovary and testes doses measured using TLD;
E estimated using PCXMC MC software | acceptable quality
- At 10 cm air gap, 70.7 % and 81.6 at CR, 68.6 and 79.4 % at DR ovary and testes dose reduction reached respectively compared with grid doses
- E was reduced by 2 and 2.3 times at CR and DR using 10 cm air gap |

In conclusion, with the reference to this literature review, the common approach for optimising radiographic practice has been achieved either through changing one acquisition factor at a time (e.g. kVp), or in combination with other factor such as kVp and mAs . Also, it was found that researchers have adopted different approaches for radiation dose assessment, and most importantly, different IQ assessment methods were used to score the same radiographic examination - AP pelvis. In the context of visual IQ assessment, the said methods have been associated with variable quality criteria, where some researchers have used CEC quality criteria, others have modified CEC criteria, and the remaining researchers have created their own criteria (e.g. physical or preference criteria). For those who have modified the CEC criteria or those who have created their own ones there was no clear supportive information regarding the validity and reliability of the created criteria for assessing IQ. The latter issues would indicate the magnitude of variation in the optimisation methodologies used with AP pelvis. This would of course lead to different findings and therefore 'conflicting results'. A major limitation of all the publications is that they have not used the effect of interplay between the different acquisition factors to further reduce the patient dose whilst maintaining, or even improving, the quality of an image. This may indicate that a number of technical options associated with recent technology have been ignored by researchers, and that the adaptation of traditional optimisation approaches is still a dominant methodology. To researcher knowledge, and with regard to extensive literature review made, no study has been published which systematically considered all acquisition factors (primary and secondary) using either anthropomorphic phantom or real patient/ cadaver to optimise the radiation dose and image quality of AP pelvis radiography. Therefore, in order to optimise the image quality and radiation dose systematically, using human simulated anthropomorphic phantom, for AP pelvis radiography, it is necessary to consider a range of acquisition factors (primary and secondary), and the full chain of the imaging system using reliable and validated approach (physical or visual) for image quality assessment (Neitzel, 2004; Uffmanna & Schaefer-Prokop, 2009; Al Qaroot, Hogg, Twiste, & Howard, 2014).

The work reported in this section (II) of the thesis aims to fill a gap in the literature by developing and conducting a systematic framework which involves all acquisition factors at their

available settings to optimise AP pelvis radiographic examination. For section II of this thesis, the work is novel because the thesis seeks to:-

1.   Propose a systematic framework to investigate the effect of all the possible combinations of acquisition factors on image quality and radiation dose.

2.   Use the novel validated psychometric scale to assess the image quality using a relative 2AFC approach.

5.3. Objectives of the main focus of PhD thesis (Optimisation)

1. To identify the required framework for conducting the optimisation procedures.

2. To adapt the framework to optimise the radiation dose and image quality of the AP pelvis radiographic examination (optimum technique).

3. To study the main effects of the primary acquisition factors on response variables (i.e. radiation dose, image quality and figure of merit).

4. To reflect on the applicability of the adapted framework in optimising the radiographic examination.

5. To study the correlation between physical and visual image quality assessment approaches.

Chapter 6: Materials and method

6.1. Overview

This chapter begins by presenting the equipment and tools used to acquire and display the images along with their quality control tests. Following this, the approaches for measuring the radiation dose and evaluating image quality, together with the relevant equipment, will be described independently. After that, researcher variability in image scoring will be detailed. An overview of the whole methodology to optimise the AP pelvis practice will then be explained. This sub-section will be followed by a detailing of the study design. Next, the methodology for optimising the manual and AEC modes will be detailed independently in separate sub-sections. Each of these sub-sections is preceded by method an overview. A final subsection will explain the method conducted to test the effect of post-processing options on image quality.

6.2. Images acquisition and display

6.2.1. X-ray equipment and tools

The experimental work was conducted in the medical imaging laboratory of the Radiography Directorate at the University of Salford. The X-ray equipment used in this study was a Wolverson Arcoma Arco Ceil general radiography system (Arcoma, Annavägen, Sweden), with a high frequency generator and a VARIAN 130 HS X-ray tube. The total filtration of this system is 3 mm Al (i.e. inherent 0.5 and added 2.5 mm).

An Agfa CR 35-X digitiser was used to read image detector data (Siemens, Munich, Germany), with a 10 pixels/mm spatial resolution and a grey scale of 12 bits/pixel resolution (HealthCare, 2009). The CR cassette size used in this study was a 35×43 cm AGFA CR MD 4.0 cassette (Siemens, Munich, Germany). The same cassette was used throughout all procedures in order to avoid any variations in the sensitivity.

A reciprocating grid with 10:1 ratio, 40 line/cm frequency, and focus and linear strips was used (Wolverson, Willenhall, UK). This kind of grid represents the commonly used grid in clinical radiography departments (Fauber, 2014).

6.2.2. Display monitors

Two 5 MP class monochrome liquid crystal (LCD) monitors were used in this study to display the acquired images - grey scale (Native resolution; 2560 x 2048), and RadiForce GS251 (21.3 inch). The viewable image size of these monitors was 23.2 inches. High resolution monitors were chosen to simulate the clinical situation and improve the displaying conditions recommended for better detection and interpretation (Norweck *et al.*, 2013).

6.2.3. Phantom

A sectional lower torso anthropomorphic phantom (Rando® SK250) was used for image acquisition. This phantom is made of tissue equivalent materials with a natural human skeleton embedded inside it to simulate a real human body. In addition, the opaque Rando® materials allow for the simulation of X-ray absorbency, atomic number and specific gravity of human soft tissue (Figure 6-1) (Phantoms, 2014). The latter specifications provide realistic conditions for the

medical imaging processes under evaluation, such as the testing of newly developed acquisition protocols and image processing technology (Inoue *et al*., 2009; Sjöström, 2002). It should be noted that the phantom used in dose optimisation work (Figure 6-1) was different to that used in section I for acquiring images for the purpose of scale creation and validation. The reasons behind using two phantoms are attributed to availability and more human representative issues (human body characteristics simulation).

Figure 6-1. Anthropomorphic pelvis phantom used in the current study.

6.2.4. Quality control testing

6.2.4.1. X-ray equipment
Image quality and radiation dose, as the main optimisation parameters, are highly dependent on the radiographic system output. The system performance, in turn, controls the quantity and quality of the X-ray beam (BIR, 1989a; Sezdi, 2011). To ensure consistent performance of the X-ray system, as well as its compliance with manufacturer's specifications, comprehensive quality control tests were conducted before and during the experimental work. The quality control protocols were adopted from two sources: the Institute of Physics and Engineering in Medicine's (IPEM) recommended standards for the routine performance assessment of diagnostic radiographic imaging system (Hiles, Mackenzie, Scally, & Wall, 2005), and European Medical Radiation Learning Development (1998-2001)(EMERALD, 2001).

These assessments included radiation dose output, kVp and timer consistency. In addition, kVp accuracy, timer accuracy, kVp linearity, dose output variation with mA, and kVp variation with mA were evaluated; the half value layer (HVL) was also measured for different tube filtrations. These quality control tests were performed for both broad and fine focal spots. Results from the quality control tests fell within the manufacturers' tolerance ranges. Finally, the light beam diaphragm alignment was tested, and the results demonstrated that there was good alignment with the X-ray beam (Appendices VI& VII).

6.2.4.2. Automatic exposure control (AEC)

A series of quality control tests were conducted in a similar manner to that of the X-ray equipment, as was indicated in sub-section (6.2.4.1). This was necessary in order to make sure that the AEC chambers of the X-ray system were performing consistently. Tests included AEC sensitivity, cassette interlocks, system feedback and guard timer. The results demonstrated that the AEC system was working consistently and within the recommended manufacturer's settings.

6.2.4.3. CR reader and image detector

CR reader consistency was tested through two measures: Dose Detector Indicator (DDI), based on the value of current CR exposure index (LGM); and limiting resolution, based on the line pairs/mm. The results from both tests were considered normal and consistent with the previous measurements ($<\pm 20\%$ of the baseline). The image detector was erased each time prior to its use for image acquisition.

6.2.4.4. Display monitor

Both monitors were calibrated to the Digital Imaging and Communications In Medicine (DICOM) grey scale standard display function (GSDF) prior to use (luminance of >400 cd/m^2). Also, acceptance tests were conducted every week using an EIZO UX1 Sensor and RadiCS software. Finally, constancy tests were conducted every day before image viewing using a pattern check (SMPTE) to the test contrast, brightness and resolution of the monitors.

6.3. Radiation dose assessment

Measuring the radiation dose is important for optimising protection in diagnostic radiography (Abdelhalim, 2010). Various options of radiation dosimetry were considered for this study, and the relevant purpose for which they were estimated or measured was taken into account. For example, the effective dose (E) was chosen as a dosimetric quantity in order to identify a suitable quality image. This was the case for most experiments, with the exception of investigations into the anode heel effect, and its relationship with image quality and radiation dose. For the anode heel effect, organs doses were used as a corresponding dosimetry measure for selecting the image with the suitable quality. The direct measurement of individual organ doses requires different methods and tools; these will be described in subsequent sections.

6.3.1. Effective dose (E)

The effective dose is an efficient measure of the overall risk patients are exposed to from medical radiation. Specifically, E is commonly accepted as an indicator for radiation induced malignancy, such as cancer; it can be calculated from the sum of the organ equivalent dose, which is then multiplied by its tissue weighting factor (Huda, 2010). A common way to estimate E is either by incident air kerma (IAK) or dose area product (DAP) using a Monte Carlo simulation approach (Theocharopoulos, Perisinakis, Damilakis, Varveris, & Gourtsoyiannis, 2002; Williams, Zankl, Abmayr, Veit, & Drexler, 1986).

Such an approach was utilised to estimate the effective dose in this thesis. The PCXMC Version 2 (STUK, Finnish Centre for Radiation and Nuclear Safety, Helsinki, Finland) was used to conduct the Monte Carlo simulations. Further details on the use of PCXMC and the calculation of E can be found in the publication by Servomaa & Tapiovaara (1998). The tissue weighting

factors used in the current version of PCXMC were in relation to the ICRP report 103 (ICRP, 2007a).

The incident air kerma (mGy) was measured at the point of intersection of the X-ray beam on the phantom's surface using the Unfors Mult-O-Meter 401 (Billdal, Sweden). The Unfors dosimeter working range was from 100 nGy to 9999 Gy; with an inaccuracy of 0.5 %. The minimum exposure for this dosimeter is 7 mA at 70 kVp, and at 50 cm. Three measurements were recoded for each exposure, and these measurements were averaged to minimise random error. Information about X-ray field length and width at the phantom surface and image detector borders (cm), focal phantom surface distance, and SID (cm) were recorded and entered into the PCXMC software. The X-ray field size was corrected to image detector borders each time the SID changed.

The dose area product (DAP) was also measured using a Kerma X plus model 120-131 meter (Scanditronix. Wellhöfer, Schwarzenbruck, Germany) located immediately after the X-ray tube exit window. The reason behind the recording of DAP measurements was as a quality control measure for checking the X-ray tube (output) and air kerma dosimeter (e.g. Unfors) performance.

6.3.1.1. Quality control testing
Both dosimeters (Unfors & DAP meters) were calibrated and tested regularly for compliance with the manufacturer's specifications; this was performed before and during the experiments. Testing included data recording using both dosimeters over three different days; this was to provide estimation for the reliability of the dosimeters (Intra class correlation-ICC). Results demonstrate that the ICC coefficients ranged from 0.999 to 1 (95% CI 0.998-1, <0.0001) for consistency, indicating an excellent level of performance. No statistical difference was found between the three measurements of dose for both the Unfors and DAP meter (P>0.05).

6.3.2. Organ dose measurement
Gonad doses (testes & ovaries) were measured using thermoluminescence dosimeters (TLDs) as the method for identifying the optimum technique, with regard to the anode heel effect. PCXMC could not be used in this instance because it does not consider the non-uniformity in the intensity of X-rays generated by the anode heel effect. Details about adapted methods and tools will be described later.

6.3.2.1. TLD organ dose measure and phantom
A CIRS ATOM dosimetry adult phantom model 701-B was used to directly measue the gonads doses (testes and ovaries) in section II of this thesis - see figure 6-2 (CIRS, 2013a, 2013b).This phantom is equipped with five millimetre diameter predrilled holes, filled with tissue equivalent plugs and spaced in a 30×30 matrix. This model of phantom consists of 39 contiguous sections of differing density epoxy resin (representing bone and soft tissue) that, when assembled together, make up the whole phantom body. The ATOM phantom was utilised to measure organs doses (i.e. testes and ovaries) by inserting 4 TLD chips (2× testes & 2× ovaries) within the predefined drilled holes. AP pelvis radiographic projections, using the ATOM phantom, were undertaken according to standard radiographic positioning- see figure 6-3 (Whitley, Sloane, Hoadley, Moore, & Alsop, 2005).

Figure 6-2. A CIRS ATOM adult phantom for direct organs' doses measurement using TLD.

To investigate the anode heel effect on gonad dose systematically, a factorial design was adopted to generate various combinations of kVp, mAs and SID. Details on the factorial design will be outlined in sub-section **(6.5.1)**. The radiographic projections were repeated for the two positioning orientations, one with the feet towards the anode and the other with the feet towards the cathode. Three exposures were made for each combination setting to allow for the averaging of the dose and to minimise random error. The mean dose was calculated for the two testes and two ovaries locations by reading each of the TLDs.
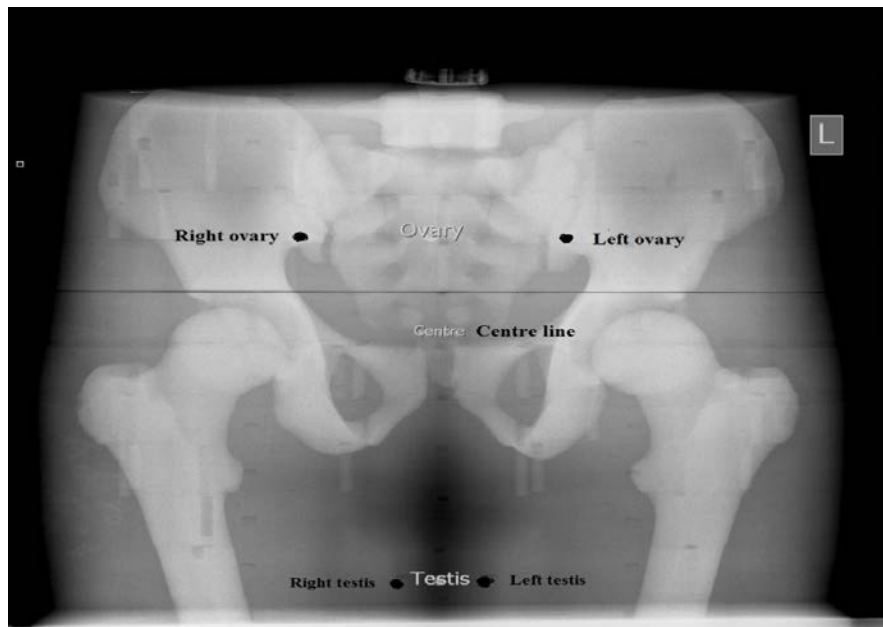
Figure 6-3. This figure shows the AP pelvis projection used to expose the ATOM phantom for the purpose of gonadal dose measurements, along with the locations of ovaries and testes within the phantom.

A Harshaw3500 TLD reader (Thermo Scientific, USA) was used to read the exposed TLD chips. The measurement range of this TLD reader is from 10μGy to 1 Gy; the repeatability for 1 mGy Cs^{137} doses is < 2% standard deviation of 10 sequential measurements; the working energies are >5 keV.

High sensitivity TLDs of LiF:Mg,Cu,P-100H, with $3.2\times3.2\times0.89$ mm^3 dimensions, an effective atomic number (Z*eff*) of 8.14, and a linearity of dose response (useful range) 10^{-12} to 10 Gy were used to measure the doses for each of the testes and ovaries, in relation to their corresponding predefined places within the ATOM phantom. A calibrated Unfors Mult-O-Meter 401 (Billdal, Sweden) was used for the calibration of the TLDs against a range of diagnostic X-ray beam energies.

6.3.2.2. Quality control testing for organ dose measurement

A variety of quality control tests were conducted in relation to different equipment and tools used for organ dose measurement. Unfors dosimeter quality control testing has been detailed in sub-section 6.3.1.1. Prior to the TLDs exposure, however, the repeatability of the TLDs was tested through exposing them to radiation over three different time periods. Results confirmed that the chosen TLDs were highly repeatable with a 0.992 (95% CI 0.989-0.994, P<0.001) consistency coefficient (intra-class correlation).

In addition, another measure was conducted to ensure that the TLDs were within a similar sensitivity (homogeneity) to reduce the amount of error which could arise. This involved exposing the TLDs to a uniform X-ray field, using the X-ray equipment indicated in sub-section 6.2.1 of this thesis and reading them using the TLD reader. After that, the TLDs were grouped into batches of similar response with the intention of having a homogenous group of TLDs; any TLD that deviated from the group mean (corresponding to 1.5 % SD) was removed (similar sensitivity; ≤ 3%). The linearity of the TLDs was tested over a range of doses (μGy to mGy), and the results demonstrated a good linearity fit with a coefficient of determination (R^2 =0.974) (Rivera, 2012; Zoetelief, Julius, & Christensen, 2000).

After each exposure the TLDs were annealed at 240 C^o for 10 min then cooled down to room temperature, according to the manufacturer's recommendations. This was done to ensure that the minimum residual dose was eliminated from the previous exposure. Ultimately, two batches were used, each with 64 TLD chips.

The calibration factors obtained from the exposure of 5 batches (5 TLDs each) had 10, 20, 30, 40 and 50 mAs for each kVp used in this study (i.e. 70, 75, 80 and 85 kVp). The TLD batches and the Unfors sensor were placed side by side during the exposure of the range of the kVps. This was necessary for improving the accuracy of the measurements. Accordingly, a graph of dose (mGy) measured by Unfors as a function of TLD response (nC) was plotted for each kVp. Then, the calibration factor was derived by conducting linear regression, forced through zero. This calibration factor represents the value of the slope (gradient) determined from the graph. Finally, the mean calibration factor was established from the data of all kVps. The accuracy of TLDs used for calibration purposes was estimated to be less than ±10 %. Five TLDs were kept aside for background correction for all of the TLDs exposure purposes (Tootell, Szczepura, & Hogg, 2013; Tootell, Lundie, Szczepura, & Hogg, 2013).

6.4. Image quality assessment

As indicated earlier, assessment of image quality can be made either directly via physical measurement of the image's attributes (e.g. SNR), or indirectly (e.g. visual) (Mraity, England, & Hogg, 2014). In this thesis, both methods are used, but special attention is granted to the visual approach in view of its importance in simulating image appraisal within the clinical environment. However, the objective measure was used to support the visual assessment, especially since the study was conducted using phantoms and digital images. Figure 6-4 summarises the whole process conducted in assessing the image quality. The following sub-sections detail how the image quality was assessed using both approaches.
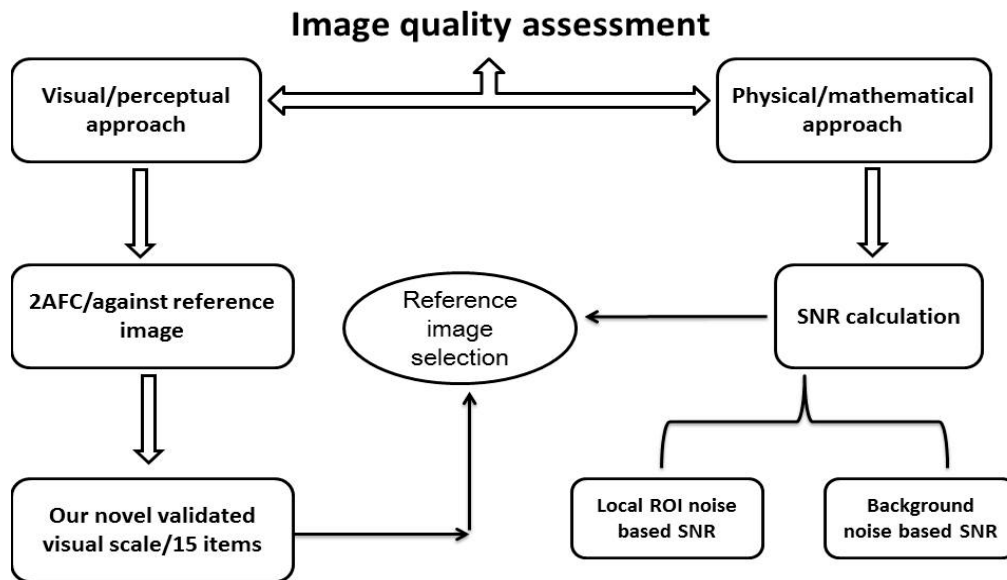
Figure 6-4. This diagram illustrates the processes of the image quality assessment of the acquired images (physical and visual), and the reference image selection which was based on both the SNR and visually using the novel visual scale.

6.4.1. Visual assessment of image quality.

Images were perceptually evaluated using a two alternative forced choice (2AFC) approach (Burgess, 2011). This approach was chosen because it has a high sensitivity to the small differences between images, and because it can help to minimise any subjective bias (Pelli & Farell, 1995). 2AFC requires all images to be appraised against a reference image; this means that the optimised (experimental) and reference images are displayed at the same time, side by side, on two separate monitors. The newly validated image quality scale (AAPS, see appendix V) was used to perceptually score the images and then identify the images with a suitable quality. Throughout this thesis, the term 'suitable' refers to any image that would be considered equal to, or greater, in quality than the reference image. Throughout the evaluation process, the observer was blinded to the image acquisition factors.

The APPS scale, described in section I of this thesis, consisted of 15 items which covered the most essential radiographic details within the pelvic region (Appendix V). A Likert scale (scored from 2 to 4; where a score of 2 refers to worse than, 3 equal to, and 4 better than the reference image) was used to capture the visual evaluation of the image by an observer. A three point Likert scale was chosen, as this approach aims to minimise any confusion that could arise from using a long (e.g. five point Likert) scale, whilst also reducing scoring errors. Images that scored a 3 or above on average were considered suitable in terms of their quality (with no individual item score <3). Java based bespoke software was used to display the images in a random order on dual screens (Hogg & Blindell, 2012); this software allows the reference image to be displayed on the same monitor throughout the course of the evaluation.

The reference image was first selected using an objective approach, to reduce subjective bias and help identify which image had an average quality. A reference image with an average quality is necessary for an observer to use the whole Likert scale and minimise the scores' skewness that may rise (Allen, Hogg, Ma, & Szczepura, 2013). Out of a pool of images (i.e. 64 images), the image with the median SNR value was first selected after the 64 images were ranked, in relation to the SNR values, from lowest to highest. The SNR calculation was detailed in section (6.4.2) which is the same approach used for calculating the SNR for each image (figure 6-4). This approach for selecting a reference image is supported by Carrol (2011), and more recently by Lança *et al.*, (2014). It is acknowledged that SNR only provides the quantification of one area of image quality, and for this reason the selected reference image was checked visually using the APPS criteria. The APPS criteria was used to score the reference image using a non-2AFC approach, and all items needed to be adequately visualised (have a score of 3 or more for each criterion) in order for the image to be selected as the reference. If the reference image initially included one item which was deemed to be poorly visualised (score <3) then the image with next highest SNR (in relation to median SNR image) was considered as a possible reference image. Suitable quality image can therefore be defined as an image which would provide optimum demonstration of image features consistent within the common disorders pelvic radiography is tasked with diagnosing, a definition supported by Joyce, McEntee, Brennan and O'Leary in 2013. To further simulate the clinical situation, images were appraised at the recommended ambient light (e.g. 30-40 Lux) (Norweck *et al.*, 2013). A calibrated Lux meter was used to check the ambient light level. Finally, to reduce the effect of tiredness, images were appraised in sessions, each with 20 images followed by a 15 minutes rest.

6.4.1.1. Figure of merit-FOM$_{IQ}$ (IQ/Dose)

The figure of merit calculations were based on the data obtained from the visual assessment of the optimised images (image quality score-IQ), and the estimated and measured dose (E & organ dose) (Williams, Hackney, Hogg, & Szczepura, 2014). The figure of merit was calculated by dividing the IQ by the radiation dose. This figure provides useful information on the exposure levels at which the IQ is highest, with the lowest possible dose (optimisation index). Also, it supports the optimum technique that produces a suitable quality image with a low dose.

6.4.2. Physical assessment of image quality.

Images were also evaluated physically by SNR. The SNR calculation followed a standard format which was based on the ratio of mean pixel value (Signal-N) to variation around this mean (Noise-σ) (Bushberg, Seibert, Leidholdt, & Boone, 2012). Two approaches were used for the region of interest (ROI). The first was based on drawing 4 ROI for the determination of the mean signal values plus one ROI (5th) for noise determination drawn over a uniform area within the image, see figure 6-5. The second was based on the same ROIs (four ones) but the noise value was taken from the same four ROIs themselves (not form the 5th ROI). The reason for this was to investigate how the local noise level of each ROI would affect the overall mean SNR value, taking into account the assumption that an observer could not be involved in comparing the anatomical structure to its background during a clinical visual assessment (Båth, Håkansson, Hansson, & Månsson, 2005). Additionally, to see the level of correlation between the two approaches, since they both adopted in literature to calculate the SNR. The ROIs were selected across the whole of the pelvic region and would, therefore, provide an overall objective measure for the image quality. This calculation of the overall SNR from several ROIs was similarly adopted by previous publications (Lin *et al.,* 2012; Sandborg, Tingberg, Ullman, Dance, & Alm Carlson, 2006).
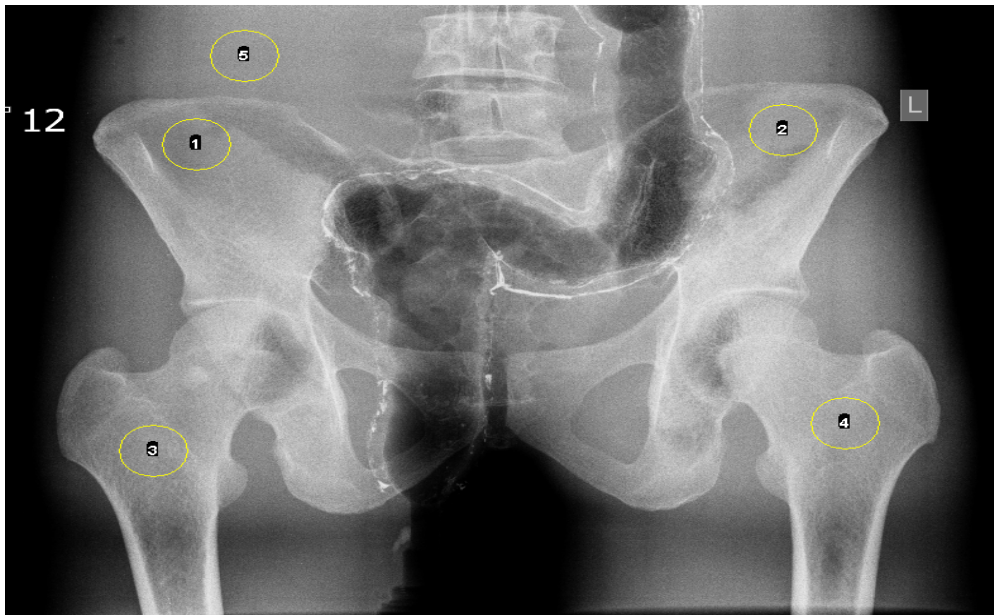
Figure 6-5. This figure presents the ROIs drawn across the pelvic regions to calculate the SNR. ROI number 1, 2, 3 and 4 were for determining the mean signal value at each ROI, whereas the 5th ROI was used to determine the noise value (σ).

Apart from the background noise ROI (5th), drawing more than four ROIs was not permitted due to the possible existence of an image artefact (e.g. bowel gas). The image J software was used to calculate the mean pixel value and standard deviation for the ROIs; the ROI manager was used to save the location of ROIs to improve the reliability of results (ImageJ, 2014).

6.4.2.1. Figure of merit-FOM$_{SNR}$ (SNR^2 /Dose)

This refers to the ratio of squared SNR to any dosimetric quantity (e.g. E). This figure is known as the 'dose to information conversion coefficient' (Ullman, Sandborg, Dance, Hunt, & Carlsson, 2004). The SNR^2/dose is often used to describe the efficiency of an imaging system in producing a high SNR image with a low radiation dose. In this thesis, this quantity was used to investigate how efficient the imaging system was in the optimisation techniques used to produce images with suitable quality and low dose.

6.4.3. Researcher variability/competence testing:

The experimental work to optimise the AP pelvis radiographic practice resulted in the production of a large number of images. It would have been practically impossible to ask a single experienced radiographer to scores all of the images, and it was therefore necessary that the PhD student score all of the images. The PhD student is a qualified medical physicist with a background in radiography (radiologic technologist), however, it was still felt important to test his competency and variability in scoring image quality against other experienced observers (i.e. radiographers with at least 10 years' experience), using the novel validated APPS (Figure 6-6).

Figure 6-6. Main steps of testing researcher variability and competency to score image quality.

143

Another reason for this study was to test the validity of the scale when using a visual grading analysis approach (i.e. 2AFC). Three experienced radiographers, together with the PhD student, were asked to score twenty AP pelvis radiographs. These images were selected objectively, depending on their SNR values, so as to have images with a range of different quality (i.e. poor, moderate and good). Intra-class correlation coefficients (ICC) were used to measure the agreement between observers. ICC values were generated for the overall scores (i.e. average score from 15 items), and also in relation to the individual scores for each item. Published guidelines have suggested that an ICC value of less than 0.40 indicates poor agreement; one of 0.40 to 0.75 indicates fair to very good agreement; and that one greater than 0.75 indicates excellent agreement (Rosner, 2010). The results from the observer variability (ICC) analysis are indicated as follows:

The ICC between the group of three radiographers, excluding the PhD student (overall image quality score), was 0.742 (95%CI 0.469 to 0.889). The ICC for the PhD student, when compared to the three radiographers (overall image quality score), was 0.839 (95%CI 0.683 to 0.929). The ICC for the individual items (i.e. each of the 15 scale items) when comparing the PhD student and the three radiographers ranged from 0.672 to 0.881 (worst case 95%CI 0.451 to 0.766). The ICC (consistency, repeat assessments by the same observer) for the PhD student was calculated three times across three weeks; and the resultant ICC values were, 0.891 (95%CI 0.725 to 0.957), 0.920 (95%CI 0.798 to 0.968) and 0.889 (95%CI 0.725 to 0.956, respectively). Figure 6-7 compares the overall scores for researcher to those of the individual experienced radiographers.
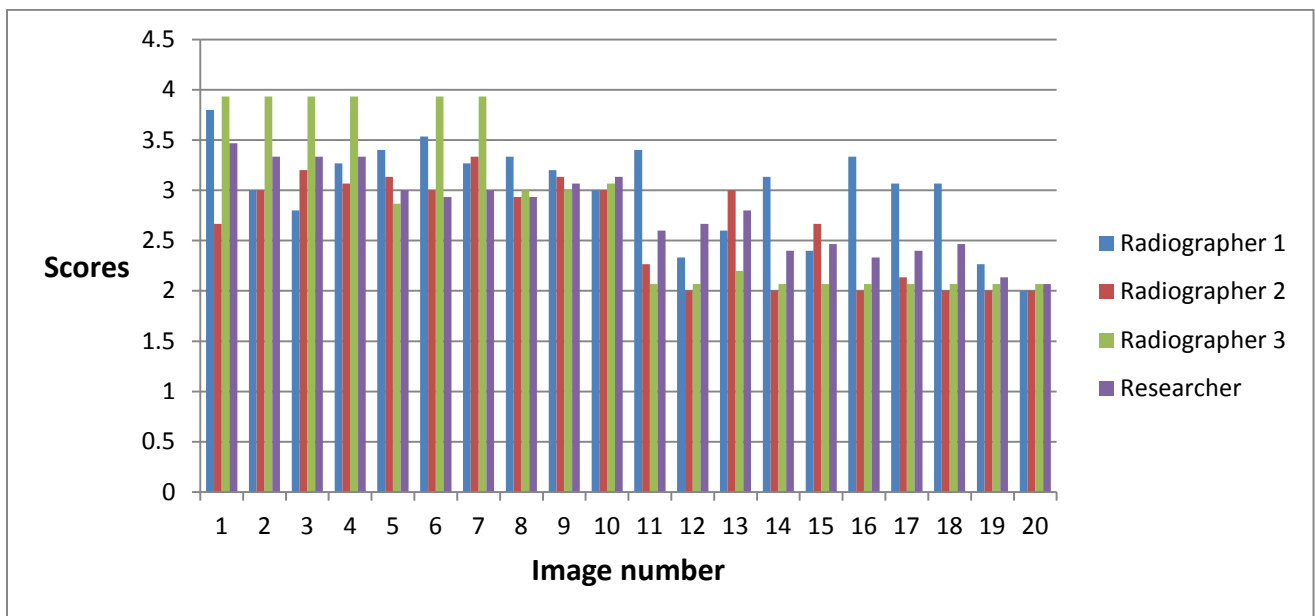
Figure 6-7. The overall scores of each of the three radiographers and the researcher from the scoring of twenty images.

To test the applicability of using APPS in visual grading analysis, the correlation between SNR and perceptual image quality scores for the twenty images were calculated. For this analysis

there was a strong correlation (r =0.908) between APPS scores and SNR, which was also found to be statistically significant (P<0.001).

In addition, further two observer variability tests were conducted, one during and another at the end of the scoring process (Figure 6-6). These additional assessments were conducted between the PhD student and two experienced radiographers. This was done by selecting 50 images at random from different images sets. The resultant ICC values ranged from fair to excellent, for both the overall and individual items scores (i.e. ICCs were ranged from 0.6 to 0.9). The above findings indicate that the PhD student was competent in appraising the images and demonstrated good reliability.

6.5. Optimisation of AP pelvis examination – Method overview

The aim of the optimisation process was to obtain images of suitable quality with the lowest possible dose. The process was conducted in three distinct and successive stages (Figure 6-8). Within this context, suitable quality images were identified according to the low E or gonad dose (i.e. testes and ovaries) using APPS. The image quality, or the defining of an image as suitable, was guided by the reference image, which was then used to appraise the quality of the optimised images. Images that scored as equal to (i.e. scored 3) or better than the reference image quality were ranked according to their dose (lowest to highest). Then, the lowest E image was identified with the corresponding acquisition factors (e.g. kVp, mAs and SID). Following this, the corresponding SNR was investigated for comparison and supportive purposes alongside the APPS assessment. The SNR was used in this thesis, as opposed to any other physical measure, such as CNR, because the SNR had a threshold value of 5 or greater, which is the minimum limit for a human eye to be able to visualise the anatomical details (reference value). This minimum SNR value has been experimentally proven by Albert Rose in his model for an ideal observer. (Bushberg, Seibert, Leidholdt, & Boone, 2012; Rose, 1973)
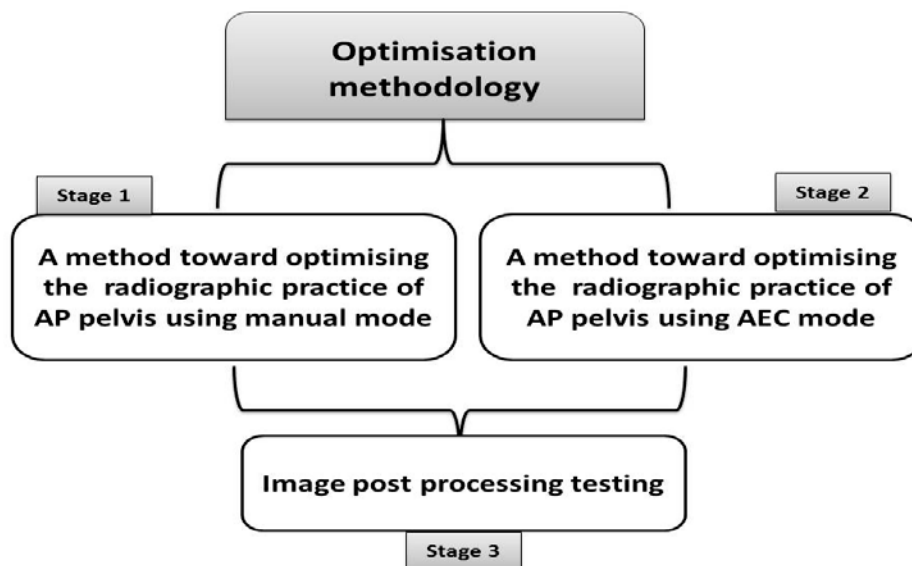
Figure 6-8. This schematic diagram is illustrating the main optimisation stages.

Each stage was conducted independently, regardless of the results obtained from each previous step. There was, however, one exception, which was the last stage (post-processing), as it is reliant on the outputs from the earlier two stages. Next is an overview of the three stages conducted to optimise the radiation dose and image quality for AP pelvis radiographic examination.

In stage 1 a method was developed to optimise AP pelvis radiographic practice, which would lead to images of suitable quality with the lowest possible radiation dose using the manual technique (non-AEC). This was undertaken using an anthropomorphic phantom and CR (see sub-sections 6.2.1 & 6.2.3). This stage also included a systematic investigation into the main effect of the primary acquisition factors on different response variables, such as image quality, radiation dose and figures of merit. Following this, a ranked list, based on the radiation dose values, was established to include the images that scored as suitable to identify the optimum combination setting which would lead to suitable quality image and the lowest possible dose.

In stage 2 a different method was developed to optimise the AP pelvis practice that would produce images of suitable quality with the lowest possible radiation dose, but using an AEC technique. The same phantom and CR system used in stage one were used in this stage. The basic combination settings of the available primary acquisition factors (kVp and SID) were adapted from stage one. Similarly, a systematic investigation into the main effect of the primary acquisition factors on the same response variables was undertaken. Finally, a ranked list, based on radiation dose, was established to include the images that scored as suitable and the combination setting that lead to suitable quality image and the lowest possible dose.

In stage 3 a procedure was developed to investigate the impact of post-processing options in improving the images scored as unsuitable. This stage was based on the results obtained from stage one. Following image post-processing completion, images that had their quality improved were compared with original image from which they were generated.

6.5.1. Study design
In order to systematically optimise the AP pelvis examinations, an investigation into the effect of all possible acquisition factor combinations was undertaken. To meet this requirement, a review of the literature revealed that adopting a factorial based experimental design would be the best choice (Matthews & Brennan, 2009; and Båth, Håkansson, Hånsson, & Månsson, 2005; Al Qaroot, Hogg, Twiste, & Howard, 2014). This approach was guided by the factorial design formula n^k, where k refers to number of factors under study (e.g. kVp, mAs….etc.), and n refers to the number of levels (e.g. kVp ranges) of each factor (Montgomery, 2013). The factorial approach allows for the testing of the effects (combined) of the primary acquisitions on both the radiation dose and image quality, instead of testing one factor at time and therefore missing the effect of other acquisitions.

Also, adopting a factorial experimental design allows for the systematic investigation into the *main effect* of kVp, mAs and SID (and their significance, *P*-value), each at its available settings, on different response variables (e.g. image quality score, FOM and E). The main effect testing explored which acquisition factor had a high impact on the different response variables (e.g. E)

compared with that of other factors when the setting changed from low to high levels (e.g. from 70 to 85 kVp). The main effect investigation included studying the effect of each level of a given acquisition factor (e.g. kVp) on a response variable when the levels of other acquisition factors (e.g. mAs and SID) systematically interacted with a previous level. The usual output of the main effect analysis is a trend plot in which the means of response variables (e.g. E) are plotted against different levels of each acquisition factor; the reference line (horizontal line) represents the grand mean (overall mean) of the response variable (see figure 6-9). The plot was constructed using Minitab statistical software rel.16 (Minitab Inc., Pine Hall Road, state college, PA).
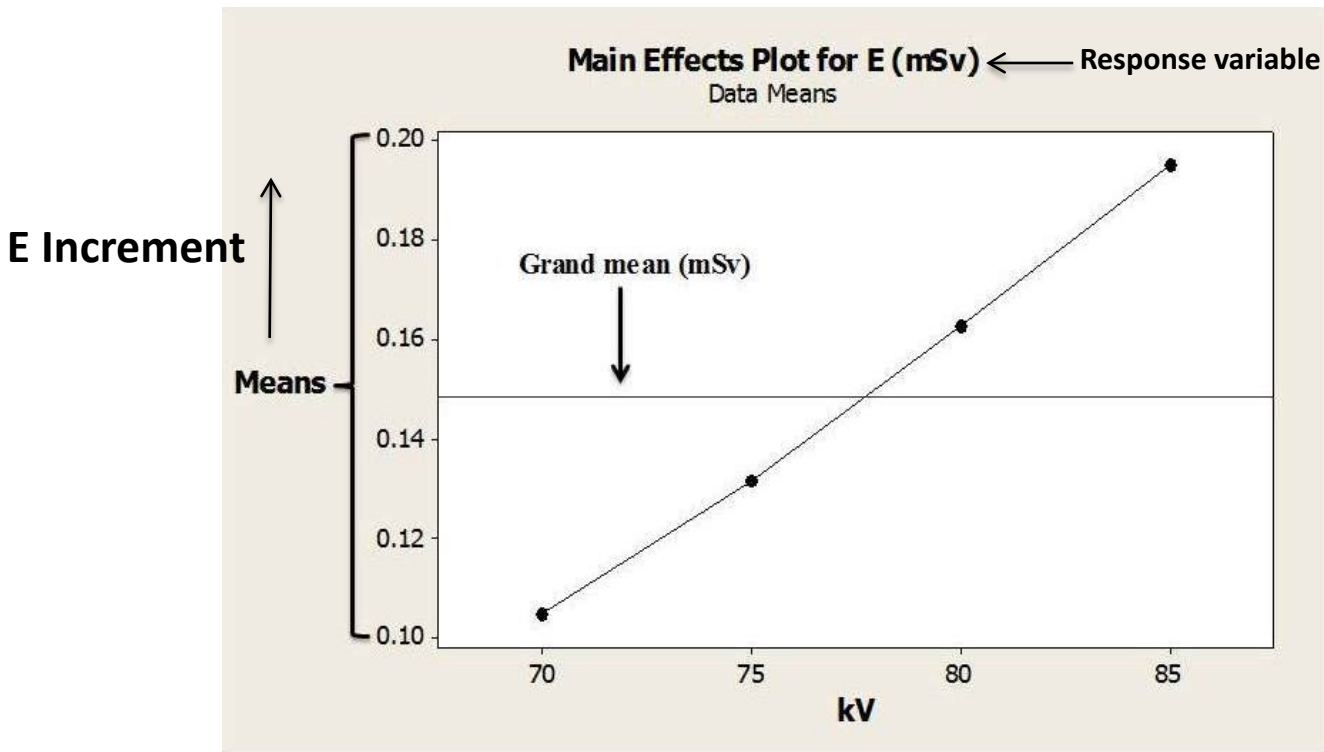
Figure 6-9. This provides an illustration of a main effect plot in which the Y-axis represents the mean values of the response variable (e.g. E (mSv)), whereas the X-axis represents the adopted values (levels) of given acquisition factors (e.g. kVp); the horizontal line represents the overall mean (grand mean) of the response variable, to be used as a reference line.

The main effect approach was conducted independently for each stage, depending on the available acquisition factors and their settings (manual and AEC modes).

For this experimental design the acquisition factors were divided into primary and secondary, according to the amount of effect they might have on image quality and dose. For Stage One and Stage Two, primary acquisition factors were kVp, mAs and SID; and secondary acquisition factors included anode heel effect, focal spot size and tube filtration thicknesses (Bushong, 2013; Fauber, 2014). The primary and secondary acquisition factors were used to facilitate the process of optimisation. Using a factorial set which would include all possible acquisition factors would be impossible since this would require a huge number of different combinations and would take

147

a very long time to conduct. It was therefore decided that a full factorial for the kVp, mAs and SID be conducted, with each of the secondary acquisition factors addressed separately.

6.5.2. Pre-Experimental preparations

The experimental work was preceded by preparation in relation to phantom positioning, cassette size and collimation. These were kept constant in order to avoid any source of error that might be caused by changing these parameters. Phantom positioning was set according to the standards recommended for AP pelvis, published in radiographic positioning textbooks (Frank, Long, & Smith, 2012; Whitley, Sloane, Hoadley, Moore, & Alsop, 2005). Following this, the phantom location on the table was marked to ensure a fixed phantom positioning throughout the experiments. Also the centring point on the phantom surface was marked to reduce any centring variations. X-ray field collimation was adjusted to the four borders of the cassette, irrespective of the SID setting (i.e. 35×43 cm). This was so because variation in the field collimation would influence dose and image quality, therefore biasing the results when optimising different acquisition factors.

6.6. Stage 1: Optimising the AP pelvis projection using manual (Non-AEC) technique

6.6.1. Method overview

The purpose behind this method was to optimise the AP pelvis practice that would produce images with suitable quality and a low radiation dose, using manual mode (without the AEC). This stage includes three distinct steps (Figure 6-10):

Step 1: This included creating the basic factorial setting of the kVp, mAs and SID combination upon which the acquisition factor combinations would be generated. The combination setting in this step was also considered for the purpose of optimising the X-ray practice using the AEC mode in stage 2.

Step 2: In this step, the secondary acquisition factors were optimised individually using a wide range of kVp, mAs and SID factorial combinations (established in step 1).

Step 3: In this final step, the AP pelvis radiographic practice was optimised through the extended factorial investigation of kVp, mAs and SID whilst the secondary acquisition factors were fixed in their optimised setting (according to step 2).

Method in stage one - Manual technique

	Step 1 (6.6.2)	**Creating the basic factorial set of kVp, mAs and SID combination.** **a**. One combination of kVp, mAs and SID identified from a broad range of combinations that can result in an acceptable quality image **b**. A factorial set of 64 kVp, mAs and SID combinations settings was created using a systematic approach (i.e. $n^k = 4^3 = 64$) derived from basic combination in (a).
Subheadings	Step 2 (6.6.3)	**Optimising secondary acquisition factors.** **a**. Images(i.e.64) were produced at each of the secondary factors at their available settings using the 64 kVp, mAs and SID combinations. **b**. The produced images were scored using APPS, and doses were estimated(E) and measured (gonads doses) accordingly. **c .** The optimised setting was identified
	Step 3 (6.6.4)	**Conducting an extended factrorial investigation of kVp, mAs and SID with secondary acquisition factors fixed at their optimised settings.** **a**. Image were produced using extended factorial settings (i.e. $n^k = 8^3$) while all secondary factors fixed at their optimizing settings. **b**. The produced images were scored using APPS, and doses were estimated(E) accordingly. **c**. Settings that produce suitable quality images with low dose were identified and ranked in relation the doses values.

Figure 6-10. An illustration for the three steps of stage one in optimising the AP pelvis practice using the manual technique.

6.6.2. Step 1: Creating the basic factorial set of kVp, mAs and SID combination

The purpose of this step was to identify the basic factorial combination set of the kVp, mAs and SID, through which the 64 factorial combinations settings of kVp, mAs and SID could be established. Accordingly, more than ten evenly distributed exposure techniques were chosen from the available range of settings. These settings were chosen to cover a broad range of available kVp, mAs and SID settings. Other acquisition factors were fixed in relation to European guidelines on the quality criteria for AP Pelvis examination (CEC, 1996). Combinations of the kVp, mAs and SID were selected from the above possibilities, and the images were acquired accordingly. Using the images, an image quality figure of merit (SNR) was calculated for five independent ROIs across the pelvis region. Four ROIs were used to identify mean signal value, whereas the fifth ROI was used to identify noise level (SD). The corresponding DAP and E values were also measured and estimated. The resultant images were then ranked in relation to their SNR, from the lowest to highest values, along with their corresponding dosimetric quantities. Finally, the basic combination of the kVp, mAs and SID was identified according to the image that produced a good SNR value when compared with the other images, and had a moderate radiation dose (less than the average adult AP pelvis E, 0.7 mSv as reported in Sherer *et al*., 2014 and UNSCEAR, 2010). This basic combination set was 75

kVp, 22 mAs and 110 cm SID. The image that led to this setting was visually checked using the APPS criteria to ensure the suitability of its quality (adequate visualisation of anatomy). The SNR was primarily used to reduce the subjective bias that could rise during the selection process. After that, more factorial combinations were derived from the basic combination using a systematic approach, opting for two settings above and one below the kVp, mAs and SID.

The justification for selecting two settings above and one setting below for the kVp and SID settings was as follows. Choosing two settings below and one setting above led to images of unsuitable quality. For the purpose of conducting Stage One of the optimisation experiment, lowering the kVp setting below 70 (i.e.65 if 2 settings chosen below 75) would produce an AP pelvis radiograph with slightly higher noise levels and a low signal value; this was the case even with high mAs and again led to an unsuitable quality. With regard to the mAs, selecting two settings above and one below was done because it was demonstrated that an mAs lower than 18 (i.e. 14) would lead to a noisy image inappropriate for the current stage in the investigation (i.e. Stage 1). In addition, this systematic approach led to 64 combinations based on 70, 75, 80 and 85 kVp; 18, 22, 27 and 32 mAs; and 105, 110, 115 and 120 cm SID. The 64 combinations created at this stage were deemed adequate for optimising the secondary acquisition factors (step 2), and would cover a broad range of settings that were generally used in the clinical practice and recommended within the literature (Bontrager & Lampignano, 2014; Carver & Carver, 2012). Furthermore, using 64 combination settings is labour intensive in terms of acquisition and overall investigation.

With respect to the range of exposure factors used (kVp, mAs and SID settings), a preliminary study was conducted to identify the interval for kVp, mAs and SID at which a change in the quality of an image was triggered. This was done using SNR because it was found to be difficult to accurately identify the required change visually. This was specifically the case for SID settings, where radiation dose values change markedly when increasing or decreasing the aforementioned settings.

6.6.3. Step 2: Secondary acquisition factors optimisation
In this step the secondary acquisition factors (i.e. anode heel effect, focal spot size and filter thicknesses) were optimised independently. Each secondary factor optimisation would remain unaffected by the results from the optimisation of another secondary factor, meaning that, when optimising one factor (e.g. focal spot), the others factors (e.g. filter type and phantom orientation) would be set according to the European Guidelines of the quality criteria for AP pelvis (CEC, 1996).

6.6.3.1. Anode heel effect
It is possible that the anode heel effect could reduce the radiation dose administered to the gonads during AP pelvic radiography, especially for the male gonads since they are located just below the border of the primary radiation field. This could mean that the radiation dose for the testes/ovaries should be lower compared with their respective doses when facing the cathode side of the X-ray tube. Details on the gonads dose measurement method using TLDs were explained in a previous sub-section (6.3.2.1).

Prior to starting to optimise the anode heel effect and measure the organ dose, a preliminary experiment was conducted to measure the radiation dose intensity across the anode-cathode line. Radiation dose intensity was measured at a distance of 2 cm intervals in order to ensure that the X-ray's intensity varied across the beam, and across a range of different SIDs (Figure 6-11).
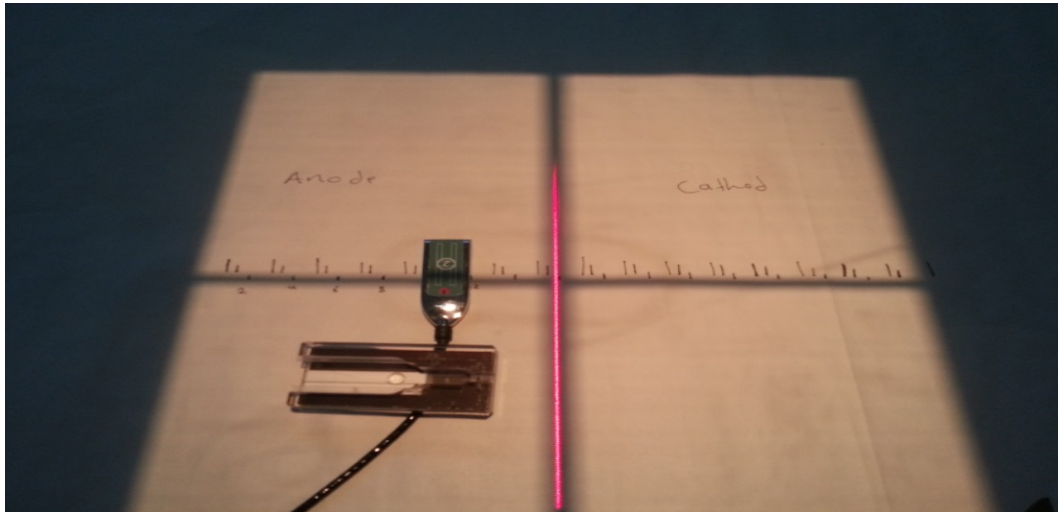
Figure 6-11. An experimental set up for testing the dose intensity across the anode-cathode line.

Results from this experiment demonstrated that radiation intensity towards the anode is less than those towards the cathode. Figure 6-12 provides a graphical illustration of the variation in the X-ray intensity profile along the anode-cathode line due to the anode heel effect.

Next, the anode heel effect was optimised using the 64 combinations of the kVp, mAs and SID created in step one to produce 64 images at each of the two orientations (128 images in total) of the anode heel effect, namely facing towards the feet, and towards the head. Based on the average testes and ovary doses, the optimum orientation, which led to suitable image quality with the lowest dose, was identified. However, this can lead to different optimised settings (orientations) for each of male and female patients; this is depending on the amount of effect this phenomenon has on the image quality and gonads doses. Although the PCXMC software does not consider the anode heel effect in its setup, the effective doses were estimated for the corresponding average gonad doses, for comparative and analytical purposes. Finally, the SNR was calculated for each image via a number of different regions across the AP pelvis radiographs (see sub-section 6.4.2).
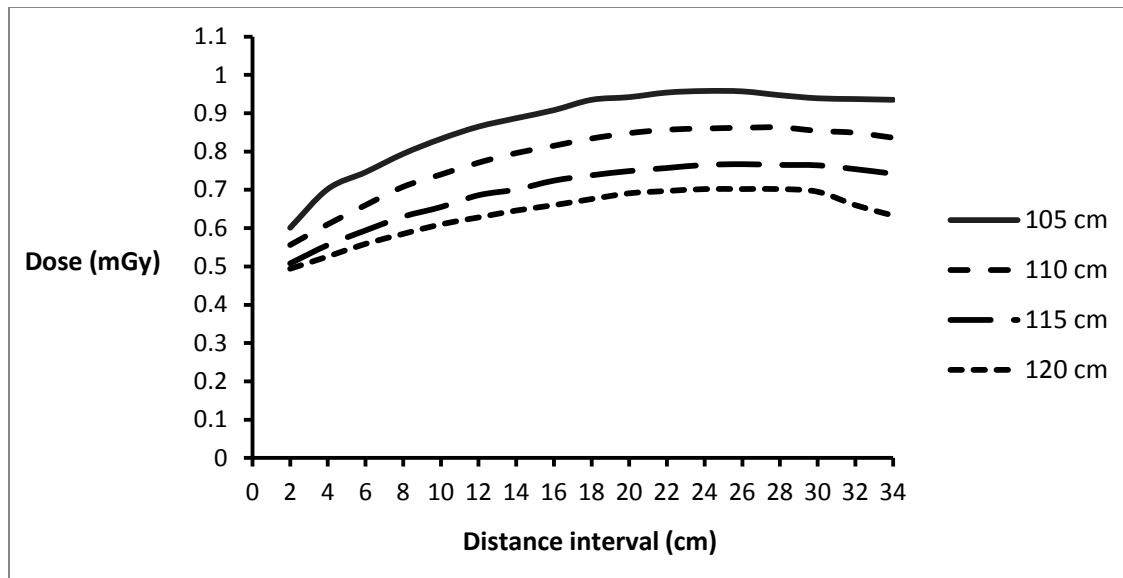
Figure 6-12. This shows the X-ray beam intensity variation along the anode-cathode line, as measured by Unfors using a 2 cm interval.

6.6.3.2. Focal spot size

Focal spot selection was optimised using the 64 factorial combinations of the kVp, mAs and SID established in Step One. Two available settings, namely the broad and fine focal spots, were tested and generated 128 images in total. Next, depending on E and the image quality score for each of the acquired images, the combination settings that associated with suitable image quality and a lowest possible dose image were identified; the secondary acquisition factors were fixed according to the European guidelines on quality criteria for AP pelvis. The signal to noise ratio was also calculated for all images produced using both settings. In addition, the optimisation of the focal spot was associated with an additional measurement of exposure time. This was the result of a radiographic theory wherein the focal spot size is said to influence the exposure time, for example, an exposure time with a broad focal spot is shorter than that of a fine focal spot (Ball & Pric, 1995). Also, according to pilot work within this thesis, this was shown to be the case and it was therefore necessary to track the exposure time. Finally, the exposure time as it appears on the panel screen of the X-ray equipment was recorded for all the images acquired, in relation to both foci.

6.6.3.3. Tube filtration thickness

Prior to starting the optimisation process for beam filtration, a preliminary study was conducted. This was undertaken to ascertain the effect of different added filtrations on image quality and radiation dose using a range of combined settings (kVp, mAs and SID). Preliminary work suggested that, for almost all the settings, an adequate quality image could be produced. No studies have been published within literature that have sought to investigate the effect of added filtration on radiation dose and quality for adult AP pelvis examinations. As a result it was decided that the effect of filtration on radiation dose and image quality be investigated. The different filter thicknesses (i.e. inherent filter, 2 mm Al, 0.1 mm Cu and 0.2 mm Cu) were optimised using the 64 combinations settings established in earlier steps. Sixty-four images were

acquired for each filter setting, yielding 256 images in total. The images were appraised using the APPS scale and the E was estimated. Based on the estimated E and the image quality of each image, the optimised filter thickness that produced the lowest dose with a suitable quality image was identified. However, the optimum combination setting(s) (i.e. kVp, mAs and SID) was also identified for each filter thickness as a step towards providing useful information about radiation protection from unnecessary exposures.

6.6.4. Step 3: Optimising the kVp, mAs and SID using an extended factorial settings (Secondary acquisition factors fixed at their optimised settings-step 2)

After the secondary acquisition factors were optimised individually, the kVp, mAs and SID were optimised using an extended factorial investigation in relation to the images produced at the extended ranges for each of the kVp, mAs and SID. The secondary acquisition factors were fixed at their optimised settings as identified earlier (see step 2). In this extended factorial analysis the kVp varied from 60 to 95 (i.e. at 5 increments give 60, 65, 70, 75, 80, 85, 90 and 95 kVp); the mAs varied from 10 to 40 (at 2 increments give 10, 14, 18, 22, 27, 32, 36 and 40 mAs), and the SID ranged from 95 to 130 cm (at 5 increments give 95, 100, 105, 110, 115, 120, 125 and 130 cm SID). It should be noted that the minimum and maximum limits for each of the kVp, mAs and SID were selected based on two settings above and two settings below of the minimum and maximum settings of the kVp, mAs and SID, as identified at step one. This experiment was conducted to check if there were more combinations below and above the minimum and maximum combinations settings of the kVp, mAs and SID, established in step one, associated with a suitable quality and low radiation dose based on the E estimation. The extended factorial set tested a total of 512 combinations (i.e. $8^3 = 8$ kVp $\times$ 8 mAs $\times$ 8 SID levels respectively = 512). However, with regard to the combination settings which were below and above the newly created ranges (extended ones): if the lower and upper limit led to suitable image quality, then lower and higher kVp, mAs and SID settings would have been used.

Due to the large number of acquisition factor combinations required, images were acquired in eight different batches, in relation to the SID ranges (i.e. 95, 100, 105, 110, 115, 120, 125 and 130 cm) to avoid any errors that may result from changing the SID each time. This means that, for each SID, a set of 64 images was produced, and within these ranges there was a wide spectrum of different image quality and radiation doses. This, in turn, allowed for a systematic investigation into the effect of the extended range of combinations. A reference image for each set/batch (e.g. 95 cm SID group), based on the median SNR for the respective batch, was selected, because using one reference image to appraise all 512 images could potentially bias the results (Sund, Båth, Kheddache, Tylén, & Månsson, 2000).

Accordingly, the combination settings of kVp, mAs and SID from each image batch that produced suitable image quality in relation to visual AAPS scores and SNR values were identified. The identification also included combination settings associated with the lowest possible radiation doses and suitable image quality.

This experiment was preceded by a quality control testing intended to make sure that going beyond the set focal range of current Bucky table (i.e.110 cm) would not lead to gridlines shadows to appear in an image (grid cutoff). This testing includes subjective visualisation of an

images acquired with different SID > 110 cm (i.e. at 120, 130 and 140). Testing images visually revealed that there was no gridlines appeared within those images acquired with SID > 110 cm. However, it could more reliable to adopt a physical measurement to test the gridlines appearance outside the focal range of Bucky table.

6.7. Stage 2: Method for optimising the AP pelvis projection using AEC mode

6.7.1. Overview
The procedure adopted for AEC optimisation differed slightly from the approach used in Stage One. The reason for this was that, with an AEC technique there would be different technical acquisition settings when compared with manual acquisitions (e.g. mAs eliminated). Radiation exposure using an AEC is based on the selection of chamber configurations (e.g. using a single, two chambers or all three chambers). As such, this required the creation of new dependent steps (Figure 6-13) which would need to be investigated systematically in order to understand their effects on image quality and radiation dose. However, it should be noted that the effect of the anode heel on the radiation intensity would still be the same, even with AEC. Since the AEC almost solely affects the exposure time, appropriate kVp manipulation and chamber positioning would be enough for optimisation purposes. The study of the effect of phantom orientation when using an AEC was also subject to further experiments. The method for AEC optimisation was conducted via 4 consecutive steps.

In step 1 the factorial combination settings of the kVp and SID were created. This was based on the basic factorial setting identified in stage 1, step 1 (6.6.2). In step 2, the phantom orientation was optimised in relation to the setting that produced suitable image quality and the lowest possible dose. In step 3, the AEC chamber configuration was optimised using a phantom orientation that was fixed based on the optimised setting identified in step 2. Finally, in step 4, the secondary acquisition factors (i.e. focal spot and tube filtration) were optimised when the chamber configuration and phantom orientation were fixed at their optimised settings from steps 2 and 3, see figure 6-13.

6.7.2. Step 1: Establishing factorial combinations (kVp & SID) for AEC optimisation
For the current stage of optimisation, mAs settings were eliminated as a primary acquisition factor because they were determined automatically by the AEC. Therefore, new factorial settings were created based on the kVp and SID ranges established in Stage 1, Step 1 (subsection 6.6.2). In order to produce the same number of combinations settings (i.e. 64), kVp ranges were extended by adding two settings below and two settings above (i.e. kVp range from 60 to 95), and the SID range was extended in the same manner (i.e. two settings above and 2 below) to give a range from 95 to 130 cm (at 5 cm increments). These combination settings would ensure the production of the same number of images and, most importantly, increase the statistical power when optimising the AEC. As in previous experiments, a preliminary study was conducted to provide a general idea about the effect of phantom orientations and AEC chamber configurations on the radiation dose when using an AEC.

Method in stage two_ AEC technique

(6.7.2)

Step 1

Creating the factorial set of kVp and SID combinations.
a. Based on kVp and SID combinations settings range established in step 1 stage 1, new combinations settings were created for AEC.

b. A factorial set of 64 kVp and SID combinations settings was created using a systematic approach (i.e. $n^k = 8^2 = 64$) derived from basic combinations in (a).

(6.7.3)

Step 2

Optimising phantom orientations (i.e. toward head or feet)
a. Images(i.e.64) were produced at each of the phantom orientation using the 64 of kVp and SID combinations settings, and chambers configuration was chosen according to published recommendation .
b. The produced images were scored using APPS, and doses were estimated(E) accordingly.
c. Combinations' settings that produce suitable quality with low dose were identified and ranked in relation to (E).

(6.7.4)

Step 3

Optimising chamber selection configurations
a. Images(i.e.64) were produced at each of the chambers configuration using the 64 of kVp and SID combinations settings.
b. The produced images were scored using APPS, and doses were estimated(E) accordingly.
c. The optimised configuration that produce suitable quality with low dose was identified.

(6.7.5)

Step 4

Optimising of focal spot and filtration factors
a. Images(i.e.64) were produced at each of the secondary acquisition factors using the 64 of kVp and SID combinations settings.
b. The produced images were scored using APPS, and doses were estimated(E) accordingly.
c. The optimised combination settings that produce suitable quality with low dose was identified.

Subheadings

Figure 6-13. An illustration of the steps required in optimising the AEC technique.

6.7.3. Step 2: Optimising the phantom orientations (toward head or feet)

The phantom orientation was optimised using the established combinations settings of the kVp and SID for two orientations: 1) head toward two outer chambers, and 2) feet toward two outer chambers (Figure 6-14), giving a total of 128 images. The other factors were set according to the recommendations within the literature (Bontrager & Lampignano, 2014; Frank *et al.,* 2012). The images were appraised using APPS and the E was estimated. Based on the estimated E and the image quality, the optimised orientation that gave suitable image quality and the lowest possible dose using APPS was identified. SNR was calculated for each of the 128 images to see how noise levels would vary across the different setting combinations using AEC.
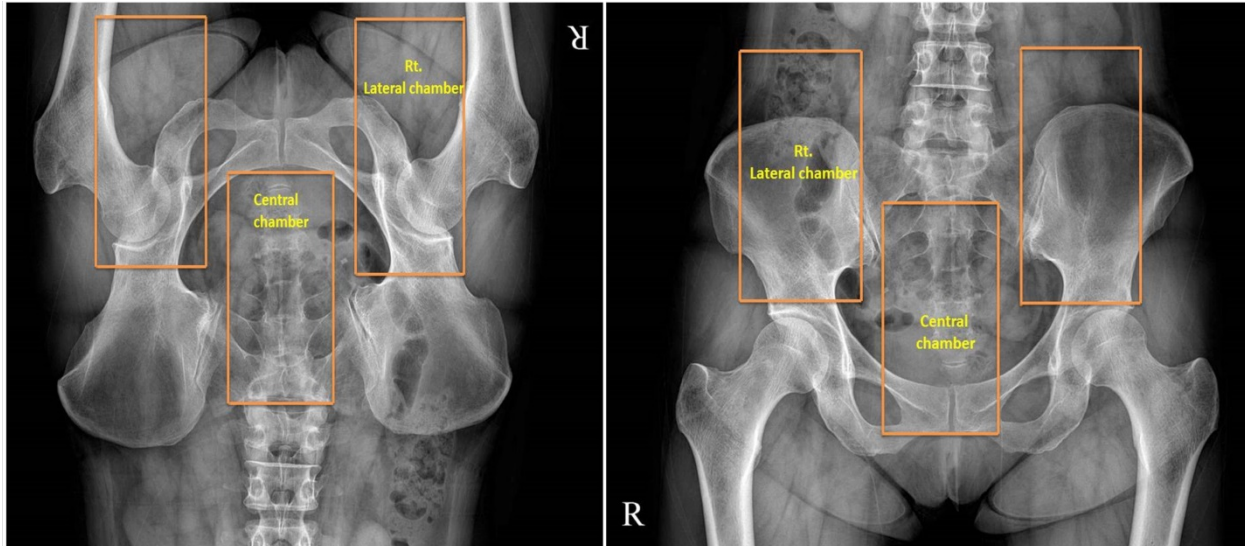
Figure 6-14. This illustrates the two phantom orientations set in this study; the left image represents feet toward two outer chambers (caudally), and the right represents head toward two outer chambers orientation (cranially).

6.7.4. Step 3: Optimising the AEC chamber configurations

It was also necessary to determine which chamber configurations produced images with suitable quality and a low radiation dose. The entire chamber selections (i.e. single chamber, two outer chambers and all three chambers respectively) were optimised individually (Figure 6-15). This used the 64 kVp and SID combination settings established in Stage 2, Step 1 (sub-section 6.7.2), to give 192 images (64×3). The images were appraised using APPS and the E was estimated. Based on the estimated E and the image quality score, the optimised chamber selection that produced suitable image quality and a low radiation dose was identified. Apart from the phantom orientation, the rest of the secondary acquisition factors were fixed according to the European guidelines on quality criteria for AP pelvis. The physical measure (SNR) of image quality was calculated for all images produced from the previous three experiments.
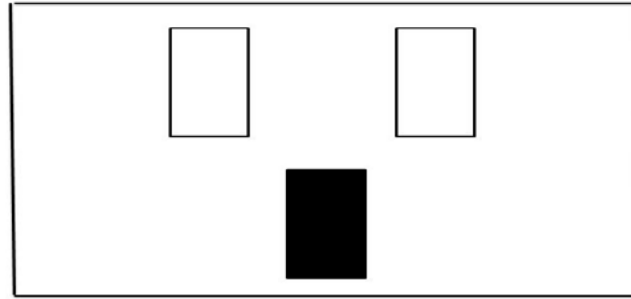
Figure 6-15. This shows an example of AEC chamber configurations.

6.7.5. Step 4: Optimising the focal spot and filtrations (AEC)

6.7.5.1. Focal spot optimisation (AEC)

Having identified the correct orientation and AEC chamber configuration, the focal spot was optimised using the 64 setting combinations of kVp and SID established in Stage 2, Step 1 (sub-section 6.7.2) at each of the two focal spots, broad and fine, to give 128 images. The rest of the acquisition factors were fixed according the European guidelines on quality criteria for AP pelvis. Images were appraised using APPS and the E was estimated. The optimised setting that produced suitable quality images, along with the lowest E, was identified. The SNR was also calculated for all of the images. In addition, as was done with the focal spot optimisation in Stage 1, the exposure times were recorded.

6.7.5.2. Filtration optimisation (AEC)

Prior to starting the optimisation process for tube filtration, when using AEC a preliminary experiment was conducted to check how different filtration thicknesses, across a range of kVp, would affect radiation dose and image quality. No published work in this area was identified within the literature. Several tube filtration settings were tested using the 64 combinations of kVp and SID, established in Stage 2, Step 1. This led to the acquisition of 64 images for each of the four filtration settings, namely inherent filtration, 2 mm Al, 0.1 mm Cu and 0.2 mm Cu, giving 256 (4×64) images in total. Based on the estimations of E, the optimum settings of kVp and SID that produced images of suitable quality and low dose were identified for each filtration type. Nevertheless, the tube filtration settings that produced suitable image quality and lower radiation doses were compared within, and between, different tube filtration settings. The images were appraised using APPS, and the SNR was calculated for all of the images.

It should be noted that there was no extended factorial investigation of the kVp and SID above or below the combination settings established in Stage 2, Step 1. This was because altering the factors to be above or below these limits of 60 and 95 kVp the X-ray tube would produce either a very low exposure time (i.e. at 95 kVp) to compensate for high kVp (i.e. set very low mAs), giving an image with high noise which obscured the essential AP pelvis details; or, with very low kVp (i.e. below 60 kVp) a very high exposure time would occur to compensate and therefore a higher dose with no image quality improvement would be expected. The latter (high exposure)

would also lead to high tube loading and potential damage to the tube if it was used over a long period of time.

6.8. Stage 3: Image post-processing investigations

The purpose of this study was to test the capability of post-processing options in order to enhance the quality of the images that were scored as unsuitable. Post-processing was conducted in relation to the density and contrast of the image, and these were adjusted by changing both the latitude and windowing. This study was based on six images scored as unsuitable. The criteria for selecting the images was based on preliminary work, and required each image to have a maximum of three scale items scored as worse than the reference image. This decision was based on the likelihood of choosing images with more than this being beyond the improvement of image post-processing parameters.

Image post-processing was conducted using an AGFA NX 2.00 workstation, by systematically manipulating the latitude and windowing using a range of 0 to 3.5 at increments of 0.5 (i.e. a full range of latitude from 0 to 6), and -0.05 to 0.25 at increments of 0.05 (i.e. full range of windowing -1 to 1). The limits for both latitude (i.e. 0 to 3.5) and windowing (i.e. -0.05 to 0.25) were determined following preliminary work, and were based on the limits through which image quality could be improved. In addition, the increments were selected based on their ability to trigger a change in the quality of images. However, it was found that ranges above or below these limits would either darken or whiten the images.

Combinations of latitude and windowing were generated using a systematic approach, to yield 56 settings. This resulted in the production of 336 post-processed images based on the original 6 images. Images were appraised using APPS against the original images from which the 336 images were generated (i.e. 56 images from each of the 6 images). Following this, images that were improved, when compared to their original form, would then be appraised against the reference image already used to evaluate the original batch of images (64 images) from which the unsuitable images were drawn from. A comparison study included how the individual items were improved or degraded against their previously unsuitable format, or against the original reference image (of suitable quality) for the original 64 batch images.

Chapter 7: Results

7.1. Results overview

This chapter presents the results from the optimisation experiments. The presentation of results is organised into two main themes. One theme focuses on identifying the optimum technique that would produce a suitable quality image with a low radiation dose. Due to an excessive amount of data, only the images that fit this criterion are included. This theme includes describing the radiation dose value (mGy or mSv) of the suitable quality images and their optimum techniques (i.e. kVp, mAs and SID). The SNR for optimised images is also presented in order to support the visual assessment of image quality using APPS.

Nevertheless, appendices (from VIII to XXXIII) present data on the full range of acquired images and their corresponding image quality scores, radiation dose values and SNRs. In addition, further images that scored as suitable, but their relevant radiation doses were up to 75% less than the average adult value of E for AP pelvis (0.7 mSv) (Sherer, Visconti, Ritenour, & Haynes, 2014; UNSCEAR, 2010), will be italicised to simplify their identification. The reason for this annotation was to provide a range of acquisition techniques that can be applied when a case of justification requires different techniques compared with what was identified in the research (suitable image quality with the lowest dose).

The second theme focuses on the main effect of the primary acquisition factors (kVp, mAs and SID) and their significance on the response variables. These response variables include image quality score (IQ), radiation dose and the figure of merits (FOM_{IQ}). The main effect on radiation dose, IQ and FOM_{IQ} will be presented using graphs to allow greater understanding into how acquisition factors influence the variables, with special attention given to the FOM_{IQ} trend, since it provides useful information on the optimisation index. In addition, the FOM_{SNR} will provide opportunities for discussion.

The two main themes outlined above will be considered for each experiment in order to explain the effect of each of the primary and the secondary acquisition factors on diagnostic efficacy. Finally, the subheadings are ordered in the same manner as that in the methods chapter, in order to facilitate navigation through the results.

7.2. Stage 1: Optimising the AP pelvis radiography using a manual mode

7.2.1. Step 1: Creating the Basic Factorial Set of kVp, mAs and SID Combinations.
This step resulted in 64 combinations of kVp, mAs and SID: kVp, 70, 75, 80 and 85; mAs, 18, 22, 27, and 32; and SID, 105, 110, 115 and 120 cm, respectively ($4^3 = 64$).

7.2.2. Step 2: Secondary acquisition factors optimisation

7.2.2.1. Tube Anode heel effect

7.2.2.1.1 Optimum technique
As was mentioned earlier, the standard dosimetric quantity used to determine the optimised setting (i.e. feet toward cathode or anode) was in relation to the male and female gonad dose (mGy). For testicular dose, there is a statistically significant difference between the two phantom orientations (P<0.001). This confirms that there was a significant reduction in dose received by the testes when feet placed towards the anode (mean 1.10 SD 0.38 mGy), compared to the feet being placed towards the cathode (mean 1.60 SD 0.59 mGy). No statistically significant difference was found with respect to anode heel orientation and female gonadal dose (P> 0.05).

Optimised settings which produced images equal or superior to the reference image, but had a lower testicular dose when feet were placed toward the anode (i.e. 0.84 mGy), were identified. A suitable quality image was produced when the head placed toward the anode and this gave a testicular dose of 0.99 mGy. This therefore means that the optimised setting for male AP pelvis radiography requires *orientating the feet towards the anode*. Also, although no significant differences were found for either orientations of the anode during female pelvic examination, the lowest dose with suitable quality image was achieved when head placed toward the anode (0.22 mGy). When feet placed toward the anode, the lowest dose for achieving a suitable quality image was 0.23 mGy. Acquisition factors that led to the above optimised images (male & female), with their relevant physical measures, are presented in table7-1. No significant differences were found between the effective dose estimations, either when the feet orientation was towards the cathode (0.15 SD 0.05 mSv) or when the phantom's feet were placed towards the anode (0.15 SD 0.05 mSv, P >0.05).

Orientation	Organs	Optimum acquisition Factors			dose(mGy)	SNR(SD)
		kVp	mAs	SID		
Feet toward cathode	Testes	80	22	120	0.99	34.0(2.0)
	Ovaries	_75_	_22_	_115_	_0.22_	_34.0(1.0)_
Feet toward anode	Testes	_80_	_18_	_110_	_0.80_	_38.0(2.9)_
	Ovaries	70	28	115	0.23	34.7(2.6)

Table7-1. This table presents the acquisitions factors that led to images with suitable image quality but lower organs doses when compared to the reference image.

*SD: Standard deviation; SNR: signal to noise ratio; *underline refers to the optimum technique upon which the optimum anode heel orientation was chosen for both male & female; optimum orientation will be used for the extended factorial experiment.

A full range of the acquired images; their corresponding image quality scores, radiation dose values, SNR are presented in appendices VIII and IX.

7.2.2.1.2 Factorial analysis (4^3)-Main effect

The main effect of each of the kVp, mAs and SID on radiation dose (testes & ovaries), image quality scores and FOM_{IQ} were investigated and illustrated in figures 7-1(A, B, C and D), 7-2 (A, B, C and D) and 7-3 (A, B, C and D). Analysis of the variance demonstrates that all acquisition factors (kVp, mAs and SID) had significant effects on testes and ovarian dose, IQ and FOM_{IQ} ($P<0.001$), and for both phantom orientations.
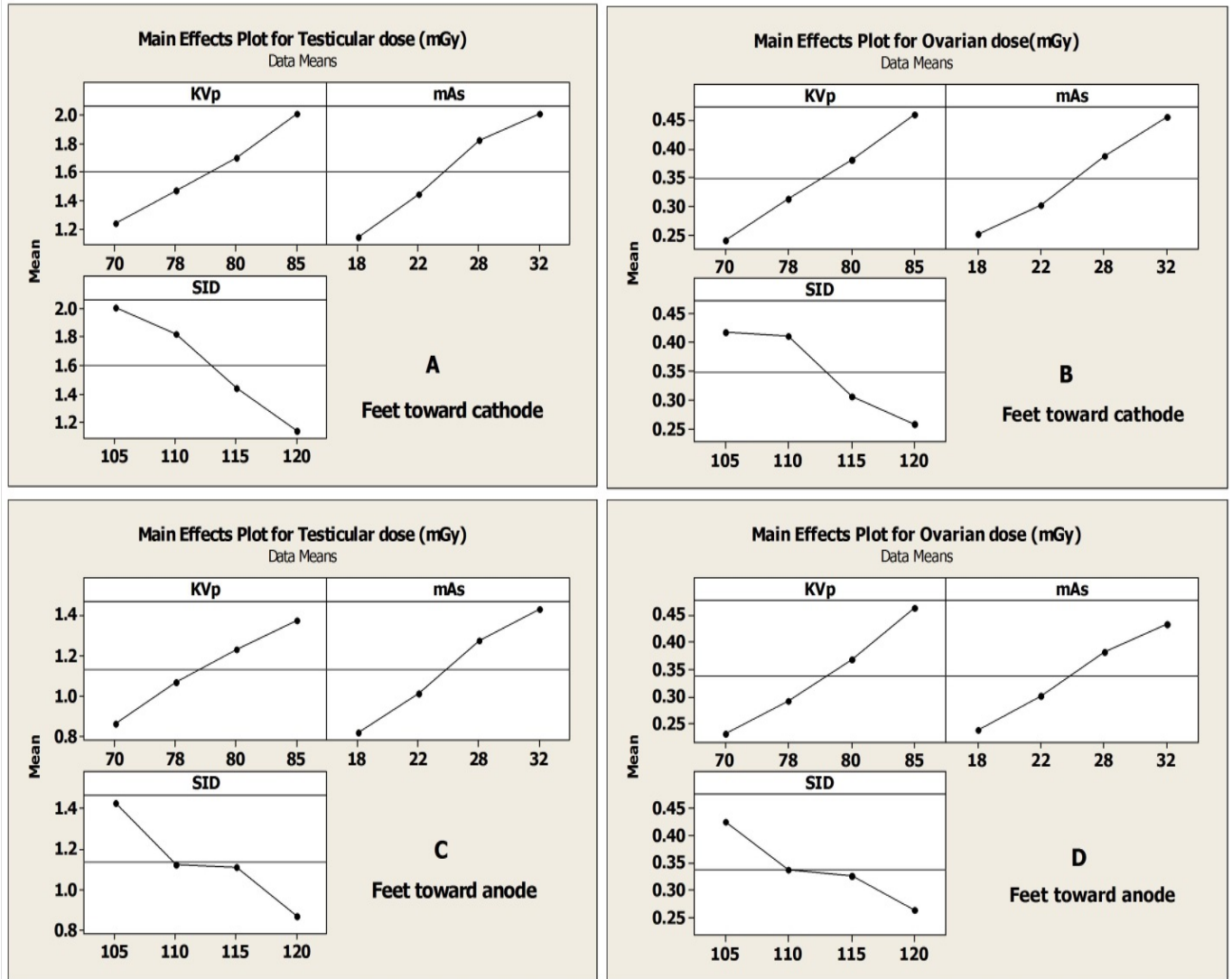
Figure 7-1. This shows the main effects on both testicular and ovarian organ doses (mGy) when the acquisition factor settings changed from lower to higher levels for both of the phantom orientations (A, B, C and D). The horizontal lines represent the grand mean (overall) of the organs doses.

Data in figure 7-1(A, B, C and D) illustrates which acquisition factors had a high effect on gonad dose, when changing from lower to higher settings (e.g. 70 to 85 kVp), compared with that of other factors and for both phantom orientations in relation to the anode heel effect. It can be seen that the mAs and SID had the biggest effects on testes doses by factor of ~1.7 for toward head orientation, compared with kVp effect (i.e. by factor of ~1.6). For the feet towards the anode orientation, the mAs still had the biggest effect compared with the kVp and the SID effects; the SID had the least effect on testes doses. In contrast, the kVp effect on ovarian doses was the biggest, causing an increase by a factor of 1.9 and 2 for both anode orientations, compared with same effect of the mAs. The SID appeared to have the least effect on the ovarian dose.

The main effect of the acquisition factors on IQ is presented in figure 7-2 (A and B) for both anode heel orientations. From this figure (7-2, A and B), it is clear that the kVp had the biggest

162

effect on the IQ since it caused the IQ to increase by ~24 and ~31% for both orientations, as opposed to the mAs effect which caused a ~19 and 23 % increase in the IQ when settings changed from lower to higher levels. The SID had the least effect on the IQ with ~ -7 and -9 % respectively.
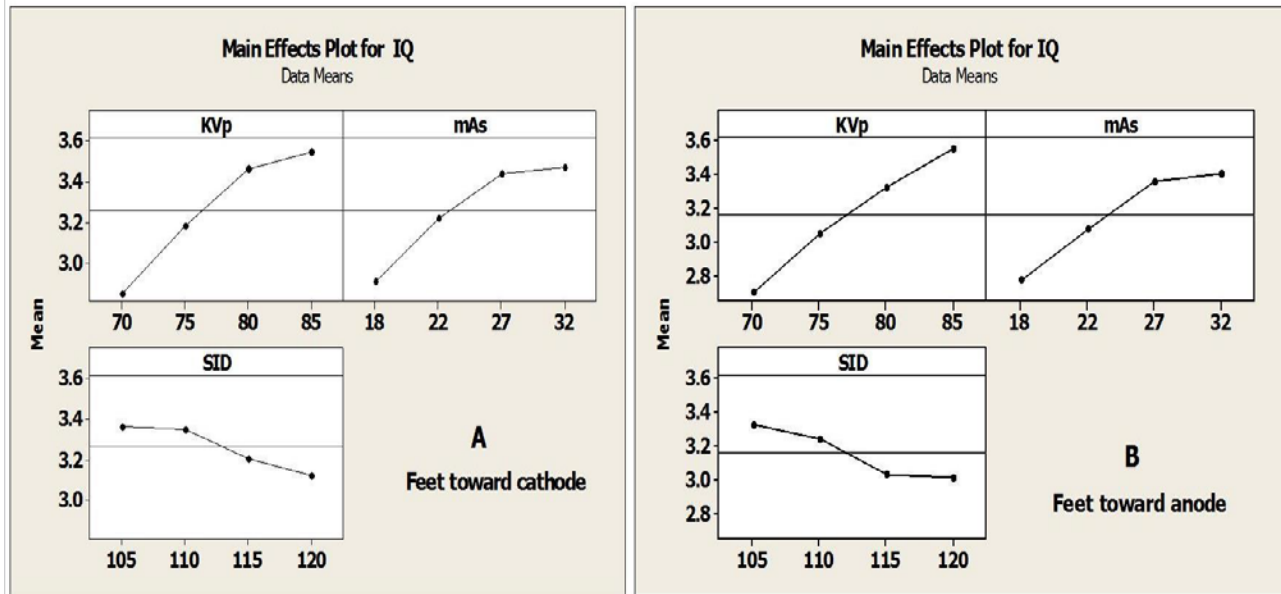
Figure 7-2. This shows the main effect on image quality when the acquisition factors settings changed from lower to higher levels for both phantom orientations, in relation to the heel effect (A and B). The horizontal lines represent the IQ grand mean (overall).

The impact of the same acquisition factors on FOM_{IQ} is illustrated in figure 7-3 (A, B, C and D). Note that there are two types of FOM_{IQ} generated from this experiment; one was derived from IQ scores and testicular doses, and the second FOM_{IQ} was based on the same IQ scores but with ovarian doses. For the testes based FOM_{IQ}, the SID and the mAs had the biggest effects, compared with the kVp, when settings changed from lower to higher levels for both orientations. However, the kVp had the biggest impact on FOM_{IQ} which based on ovarian doses, compared with mAs and SID effects.
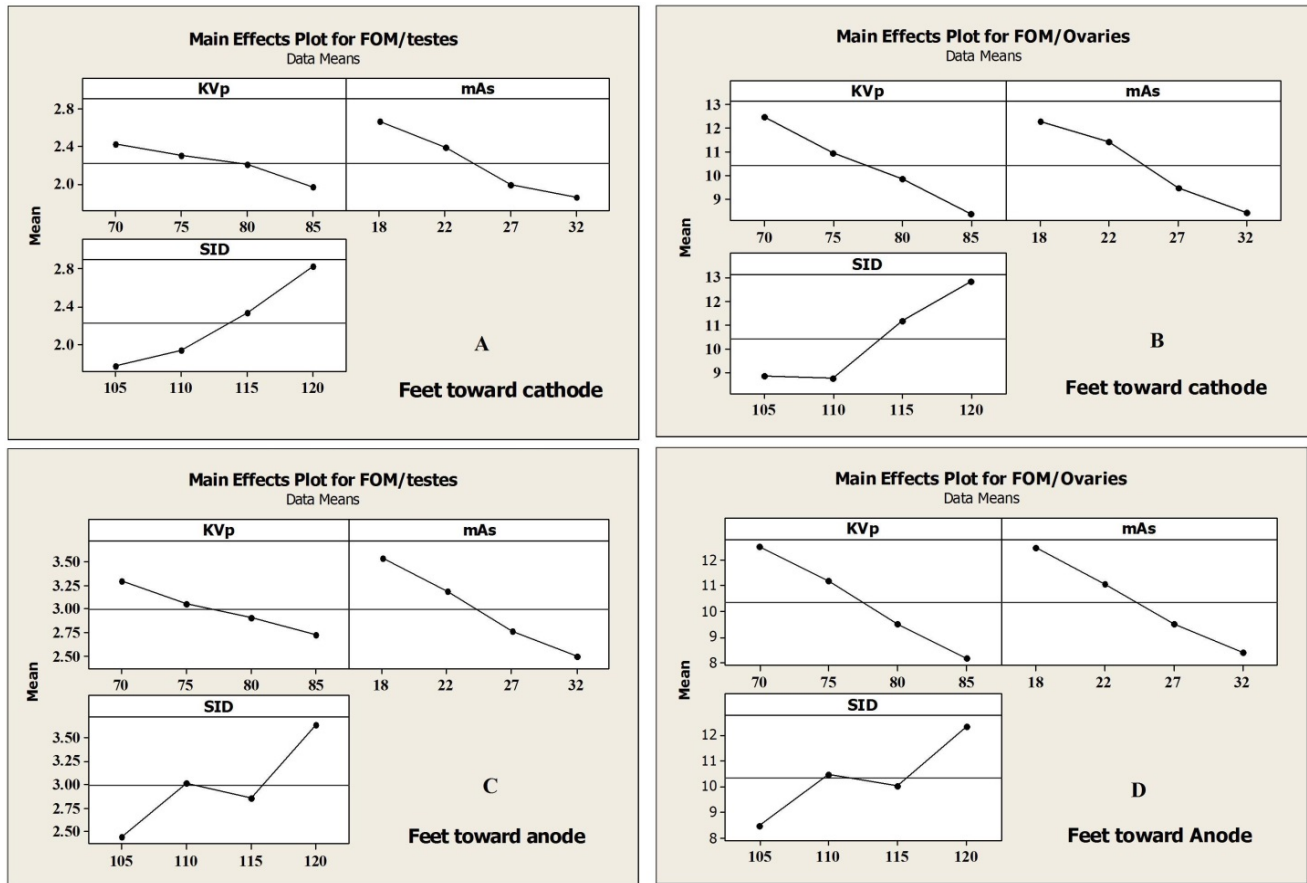
Figure 7-3. This shows the main effect of acquisition factors (kVp, mAs and SID) on FOM$_{IQ}$ when the settings changed from lower to higher levels. Figures A and B illustrate the effects on FOM$_{IQ}$ when the feet were towards the cathode; C and D illustrate the effects on FOM$_{IQ}$ when the feet were towards anode. The horizontal lines represent the FOM$_{IQ}$ grand mean (overall).

7.2.2.2. Focal Spot Size

7.2.2.2.1 Optimum technique

The dosimetric quantity used to rank the optimised images here was the effective dose (mSv). The results demonstrate that the lowest radiation dose which produced a suitable quality image (i.e. optimised image) had a broad focal spot with a radiation dose of 0.088 mSv. The lowest radiation dose with suitable image quality was produced using a fine focal spot at 0.100 mSv. Table 7-2 presents the acquisition factors that led to these optimised images, with their relevant SNRs for both foci.

Table7-2. This table presents the acquisitions factors that led to images with suitable image quality but lower E when compared to the reference image					
Focal spot type	**Optimum acquisition Factors**			**E(mSv)**	**SNR(SD)**
	kVp	**mAs**	**SID**		
Broad focus	75	18	115	0.088	33.1(1.13)
Fine focus	75	22	115	0.102	32.0(1.24)
*E, effective dose; SD, standard deviation, SNR, signal to noise ratio					

Investigating the exposure time associated with both focal spot sizes demonstrated that the mean exposure time with a fine focal spot (106.83 ms SD 26.82 ms) was significantly higher than the broad focal spot (55.55 SD 12.06 ms, P≤ 0.001). In addition, dose area product values were also tested, assuming that DAP might be higher with a broad, rather than with a fine focal spot, based on certain recordings. It was found that there were no statistically significant differences (P=0.752). Nevertheless, a full range of acquired images and their corresponding image quality scores, radiation dose values and SNRs are presented in appendices X and XI.

7.2.2.2.2 Factorial analysis (4^3)-Main effect

The main effect of the acquisition factors and their significant impact on the radiation dose (mSv), IQ and FOM_{IQ} for both focal spot sizes are presented in figures 7-4, 7-5 and 7-6 (each with A and B). Analysis of the variance demonstrates that all acquisition factors had significant effects on E, IQ and FOM_{IQ} (P<0.001), and for both foci.
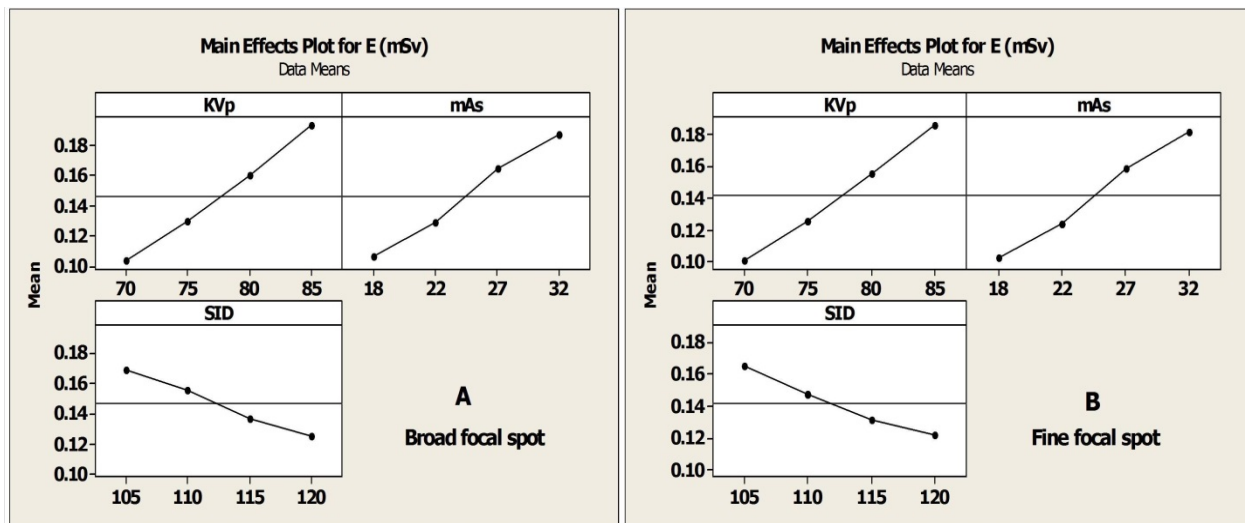
Figure 7-4. This shows the main effect on E when the acquisition factors settings changed from lower to higher levels, for both focal spot types (A and B). The horizontal lines represent the E grand mean (overall).

Figure 7-4 (A and B) demonstrates the acquisition factors that had a greater effect on E when changing from lower to higher levels (e.g. 70 to 85 kVp) compared with other factors and for both focal spot sizes. It can be seen that kVp had the biggest effect on E, for both the broad and

fine foci (caused ~ 86 and 85 % increase in E respectively), compared with the mAs and SID effects (~ 77 % increase; ~26 % decrease respectively), for both focal spot sizes when their settings changed from lower to higher levels.

Once again the main effect on the IQ, when acquisition factors change from lower to higher levels, can be seen in figure7-5, for both focal spot sizes (A and B). The kVp had the biggest effect on IQ when compared with mAs and SID effects for both focal spot sizes. For example, the kVp caused the IQ to increase by ~29 and 34 %; the mAs caused the IQ to increase ~23 and 31%; and the SID caused the IQ to decrease by ~ -18 and -11 % for the broad and fine spots respectively.

Figure 7-5. This shows the main effect on image quality when the acquisition factors settings changed from lower to higher levels, for both focal spot types (A and B). The horizontal lines represent IQ grand mean (overall).

The main effect of the acquisition factors on FOM_{IQ} can be seen in figures 7-6 (A and B), when their settings changed from lower to higher levels (for both foci). It can be seen that the kVp and mAs had comparable effects on the FOM_{IQ} for both focal spot sizes. By contrast, the SID had a slightly greater effect on the FOM_{IQ} with fine focal spot than with broad spot.
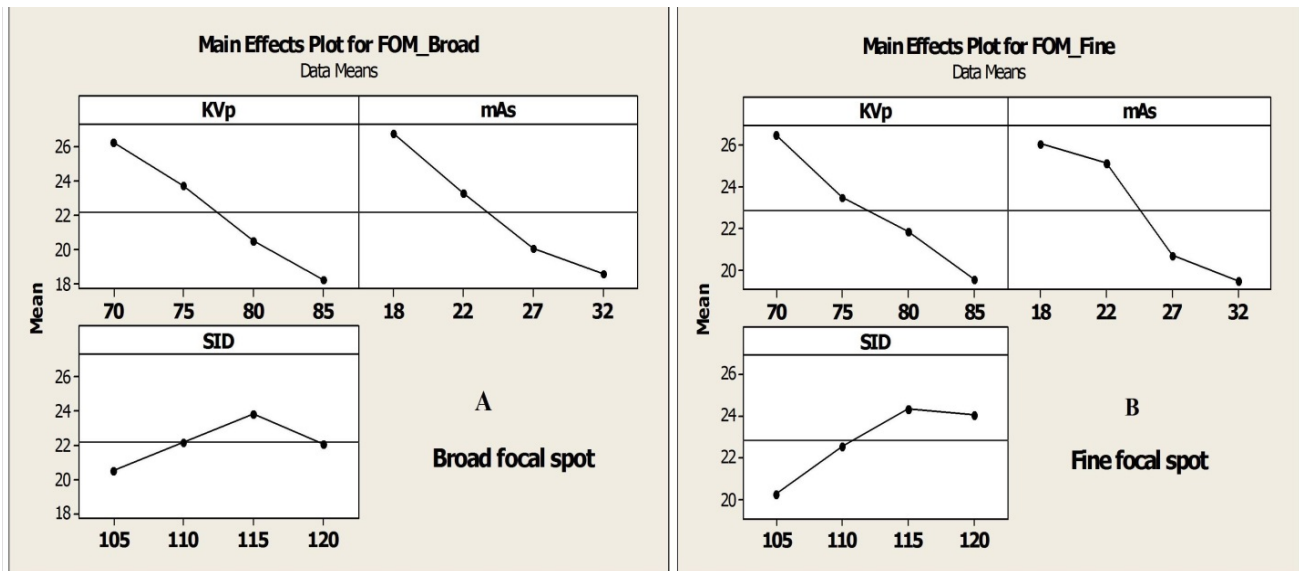
Figure 7-6. This shows the main effect of each of the kVp, mAs and SID on FOM_{IQ} when acquisition factors settings changed from lower to higher levels. Figure A illustrates the effects on FOM_{IQ} with a broad focal spot; figure B illustrates the effects on FOM_{IQ} with a fine focal spot. The horizontal lines represent the FOM_{IQ} grand mean (overall).

7.2.2.3. Tube Filtration optimisation

7.2.2.3.1 Optimum technique
In this study, the effect of added filtration on the quality of an image, and the corresponding radiation dose (E) was investigated. Four kinds of filtration were investigated individually, namely inherent filtration, 2 mm Al, 0.1 mm Cu and 0.2 mm Cu. The images for each filtration setting were appraised using APPS, and the E was estimated. Study findings demonstrated that the lowest radiation dose for an image with suitable image quality was produced when 0.2 mm Cu was added. The lowest dose was 0.050 mSv; this was 92% less when compared with the average adult AP pelvis E (0.7 mSv). To the author's knowledge, this was the first level of dose reduction for AP pelvis examinations reported for filtration. The corresponding SNR with this optimised image from 0.2 mm Cu was 28.0 SD 0.7. This may indicate that the level of noise in this image is likely to be lower than the reference image.

By way of comparison, the optimised combination setting that led to the suitable image quality and lowest dose, among other optimised settings produced using 0.1 mm Cu, yielded a dose of 0.065 mSv. The corresponding SNR for this image was 28.0 SD 0.9. The amount of radiation dose associated with 2 mm Al was higher than those of 0.2 mm Cu and 0.1 mm Cu at 0.085 mSv, with results of 37% and 18 % more than 0.2mm Cu and 0.1mm Cu optimised images, respectively.

Finally, the lowest dose optimised image produced from inherent filtration (i.e. no added filter) was 0.088 mSv. This value was close to that achieved when using 2 mm Al. Acquisition factors that led to the above optimised images and their relevant physical measures are demonstrated in table 7-3.

Table7-3. This table presents the acquisitions factors that led to images with suitable image quality but lower E when compared to the reference image

Filter type	Optimum acquisition Factors			E(mSv)	SNR(SD)
	kVp	mAs	SID		
Inherent	75	18	115	0.088	33.0(1.2)
2mm Al	75	18	105	0.085	31.8(2.0)
0.1mm Cu	75	18	110	0.060	28.0(0.9)
0.2mm Cu	*75*	*18*	*105*	*0.050*	*28.0(0.7)*

*E, effective dose, Al, aluminium, Cu, copper, SD, Standard deviation, SNR, signal to noise ratio; underline refers to the technique upon which the optimum filter thickness was chosen for the extended factorial experiment.

The full range of acquired images and their corresponding image quality scores; radiation dose values and physical measures for all filtration types are presented in appendices XII, XIII, XIV and XV.

7.2.2.3.2. Factorial analysis (4^3)-Main effect

The resultant data from the investigation into the main effect on E, IQ and FOM_{IQ} can be seen in figures 7-7 (A, B, C and D), 7-8 (A, B, C and D) and 7-9 (A, B, C and D), for the different filter thicknesses. An analysis of the variance demonstrated the acquisition factors which significantly affected the above response variables across all filter types, with the exception of SID which did not significantly affect the FOM_{IQ} for 2mm Al and 0.2 mm Cu filters, $P>0.05$.
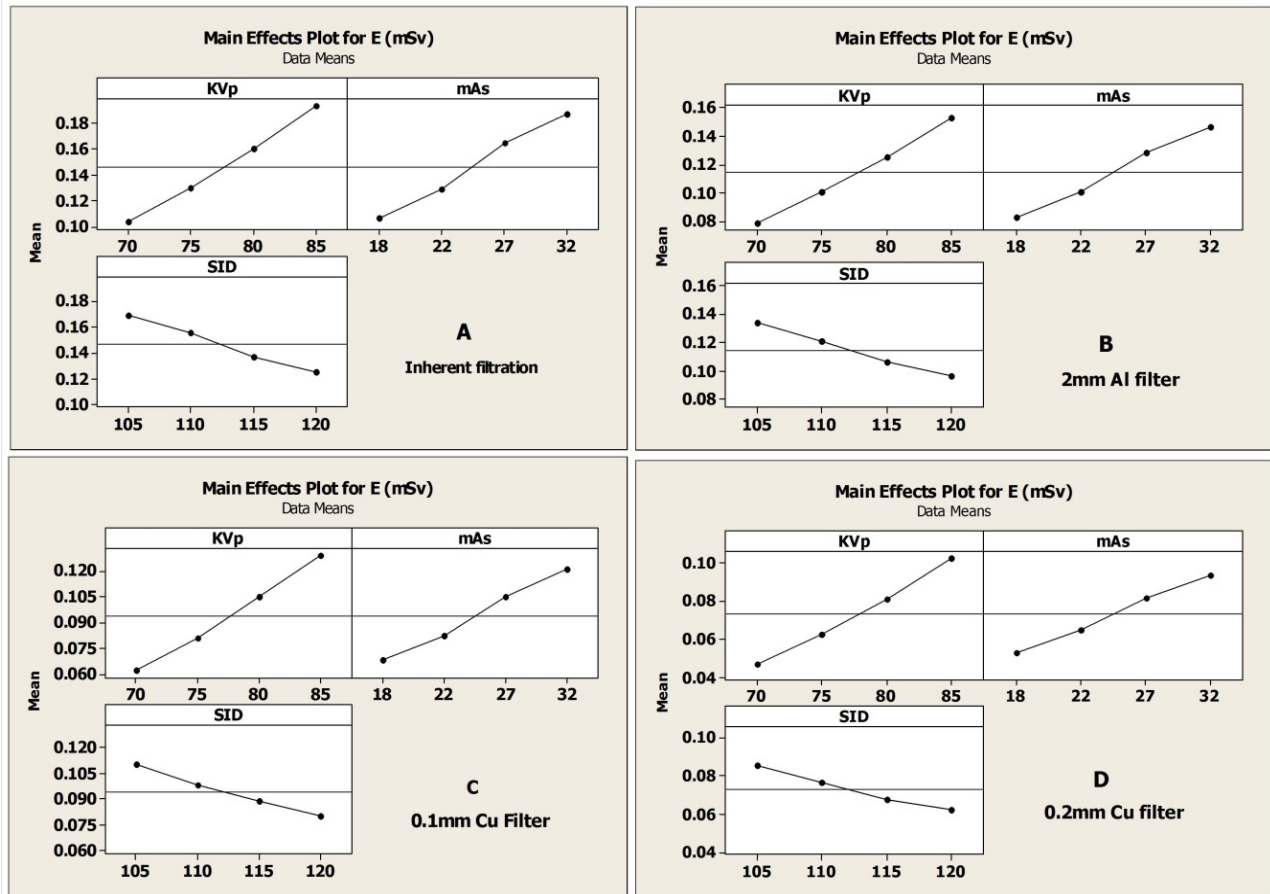
Figure 7-7. This shows the main effect on E (mSv) when the acquisition factors settings changed from lower to higher levels, for different filtration thicknesses (A, B, C and D). The horizontal lines represent the E grand mean (overall).

The data in figure 7-7 (A, B, C and D) shows the acquisition factors that had a higher effect on E, when changing from lower to higher levels, when compared with other factors and for all filter types. Clearly, the kVp had the biggest effect on the E when settings changed from lower to higher levels, compared with the mAs which had a comparable effect across all filter types (~ + 76%). Also, the kVp effect on E increases slightly as the filter thickness increases (i.e. ~ 86 to 120 %). The SID caused the lowest effect on the E when compared with the kVp and mAs effects (e.g. ~27% decrease).

Similarly, the main effect of the acquisition factors on the IQ in relation to different filters' types can be seen in figure 7-8 (A, B, C and D). According to this figure, kVp had the biggest effect on the IQ across all filter types; this effect increases as the filter thickness increases, in a similar trend to that of E. In contrast, the mAs effect was lower than that of the kVp, but higher than that of the SID, on the IQ for all filter types except those with a 0.2 mm Cu, where the SID effect was higher than the mAs effect and comparable to the relevant kVp effect, when settings changed from lower to higher levels.
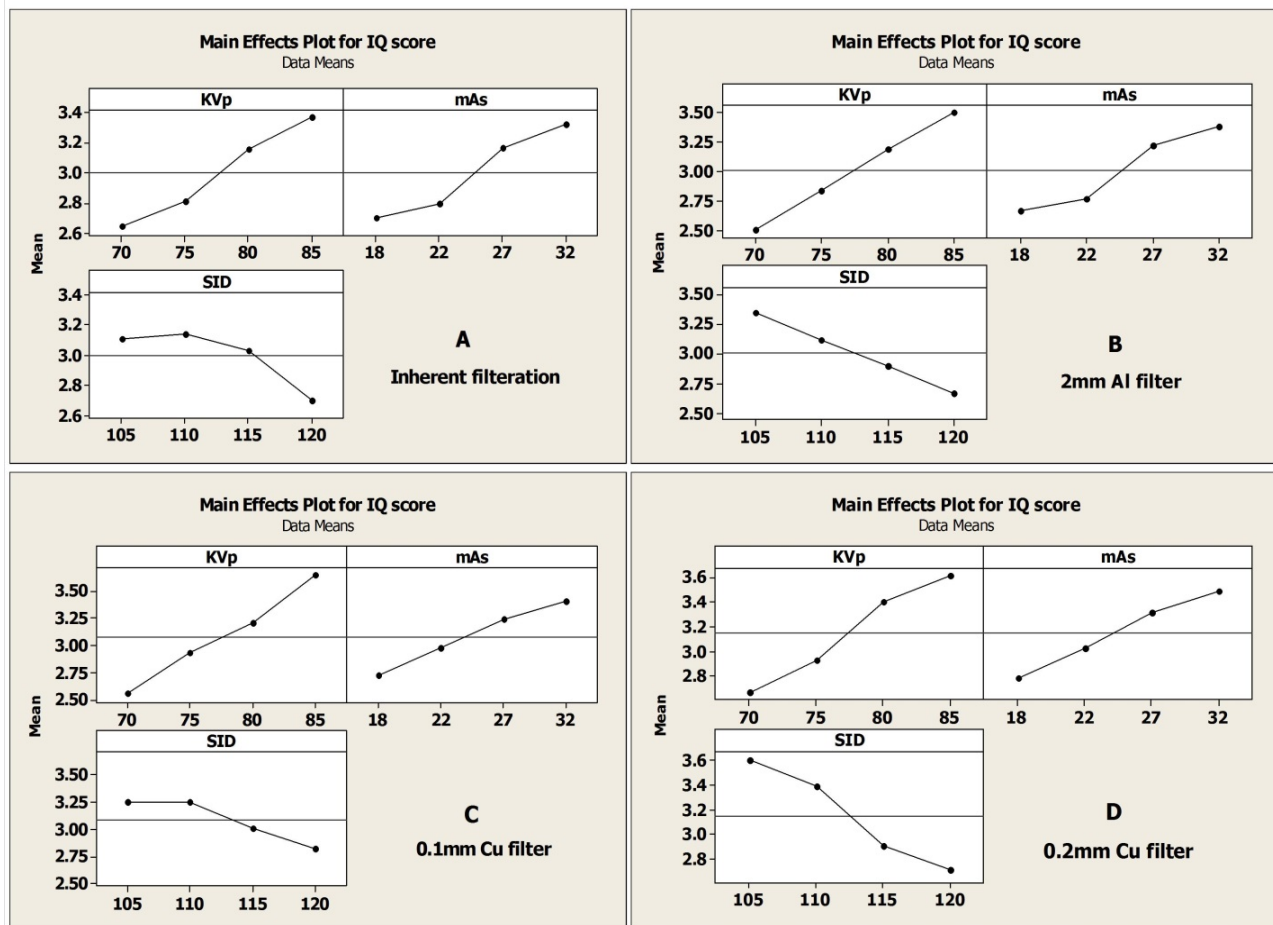
Figure 7-8. This shows the main effect on image quality when the acquisition factors settings changed from lower to higher levels, for different filtration thicknesses (A, B, C and D). The horizontal lines represent the IQ grand mean (overall).

The impact of the kVp, mAs and SID on the FOM_{IQ} in relation to inherent, 2mm Al, 0.1mm Cu and 0.2mm Cu filter types can be seen in figures7-9 (A, B, C and D). From this figure, it is clear that the effects of kVp and mAs on FOM_{IQ} are comparable with each other with inherent, 2 mm Al and 0.1 mm Cu filter types, however the kVp effect on the FOM_{IQ} with 0.2 mm Cu was higher than the effect of mAs since the kVp caused a ~ 35.5 % decrease in the FOM_{IQ}, whereas the mAs caused a ~28 % decrease in FOM_{IQ} when the settings changed from lower to higher levels. The least effective factor was the SID across all filter types.
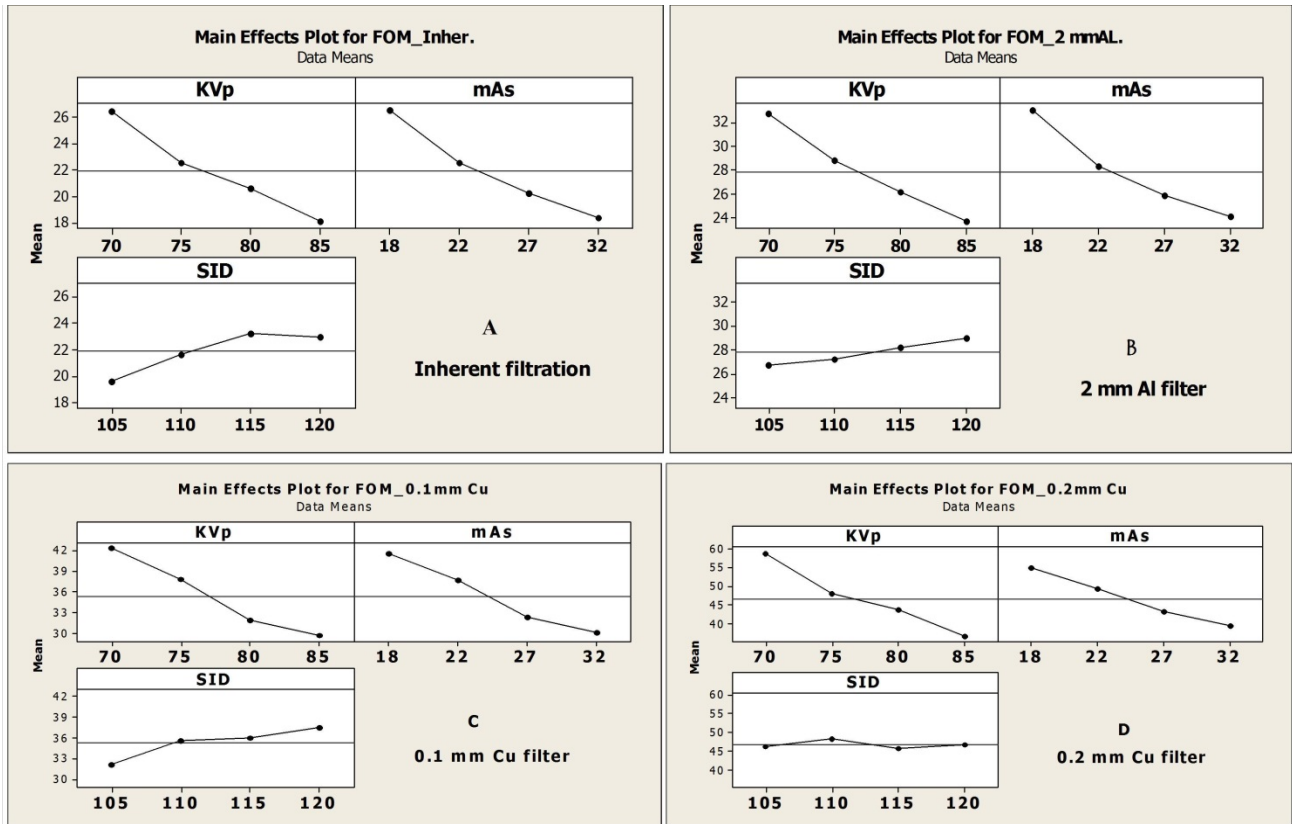
Figure 7-9. This shows the main effect of acquisition factors on FOM_{IQ} when the acquisition factors settings changed from lower to higher levels. A, B, C and D illustrate the effects on FOM_{IQ} with inherent filtration, 2mm Al, 0.1 mm Cu and 0.2 mm Cu filter types respectively. The horizontal lines represent the FOM_{IQ} grand mean (overall).

7.2.3 Step 3: Optimising kVp, mAs and SID using extended factorial settings (Secondary acquisition factors fixed at their optimised settings-step 2)

7.2.3.1. Optimum technique

The images were acquired using a wide range of kVp, mAs and SID to investigate the combinations that could produce suitable quality images with low radiation dose. In this sub-section those settings below and above the minimum and maximum settings of kVp, mAs and SID, which were not considered from Stage 1, Step 1 and 2, were used. The images were appraised using the APPS and the estimated E, to rank and identify the optimised combined settings. Since a large number of images were produced in this step, images were divided into 8 groups/batches, with 64 images in each according to the SID, in order to facilitate the presentation of results.

The lowest radiation dose with a suitable quality image was acquired at 0.04 mSv and a 130 cm SID when compared with other optimised images that were acquired within the other SID groups. The corresponding SNR for this image was 23.5, SD 1.7. The second lowest ranked optimised image was acquired at 0.043 mSv and with a 125 cm SID group. Full details on the

acquisition factors that led to the optimised images across all SIDs can be seen in table 7-4 along with the respective E and SNR values.

| SID group(cm)	Optimum acquisition Factors		E (mSv)	SNR (SD)
	kVp	mAs		
Table7-4. This table presents the acquisitions factors that led to images with suitable image quality but lower E(mSv) when compared to the reference image				
95	80	14	0.070	29.1(4.5)
100	70	22	0.056	26.2(3.7)
105	70	22	0.048	26.3(2.8)
110	70	22	0.045	24.4(2.6)
115	75	22	0.051	26.5(2.3)
120	75	22	0.046	25.0(1.8)
125	80	18	0.043	24.0(1.8)
130	_**80**_	_**18**_	_**0.040**_	_**23.5 (1.7)**_
E, effective dose SD, Standard deviation, SNR, signal to noise ratio; underline text refers to the final optimum technique identified for AP pelvis radiography when manual mode is in use.				

A small range of suitable quality images were acquired at the kVp and mAs settings, which were lower than the minimum settings (i.e. < 70 and 18 mAs) identified in Stage 1, Step 1 (subsection 6.6.2). However, a wide range of optimised images were acquired at various kVp and mAs values which were higher than the maximum settings (i.e. >85 kVp and 32 mAs). A full range of the acquired images and their corresponding image quality scores, radiation dose values and SNRs resulted from this step; they are presented in appendices XVI to XXII.

7.2.3.2. Factorial analysis (8^3) - Main effect

The main effect of the primary acquisition factors on radiation dose, IQ, FOM (which based on IQ and SNR)across a full range of kVp, mAs and SID established in Step 3 are presented in figures 7-10, 7-11(A and B), and 7-12 (A and B). An analysis of variance demonstrated that kVp and mAs had significant effects on all response variables, with the exception of the SID, which had little or no effect on the IQ of the acquired images. From figure 7-10, it can be seen that the kVp had the highest effect on the E, compared with that of the other acquisition factors when their settings changing from lower to higher levels.
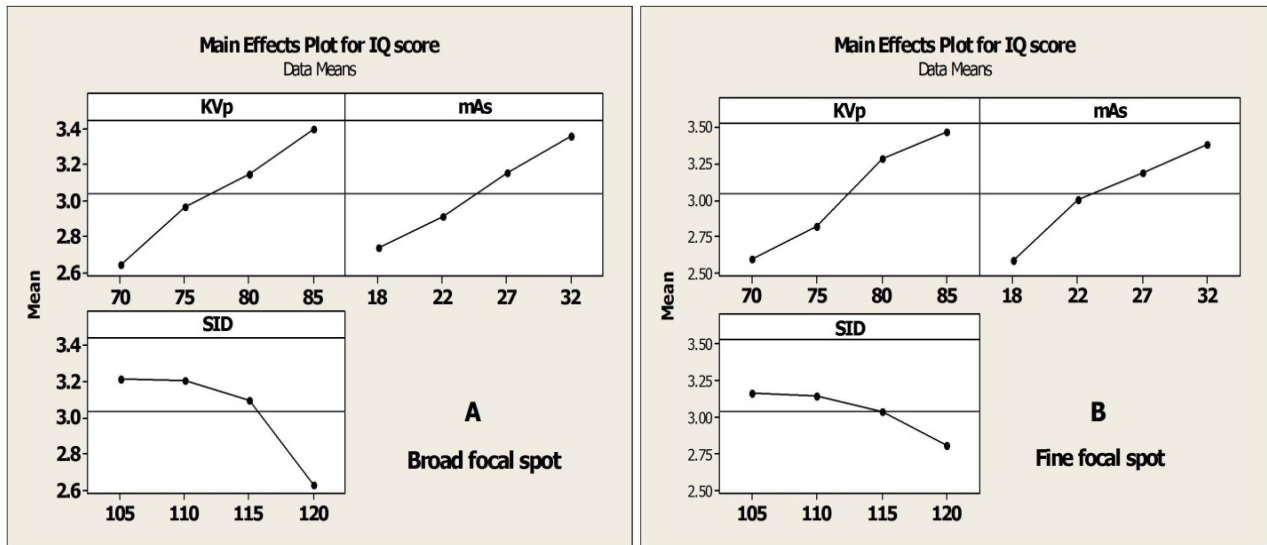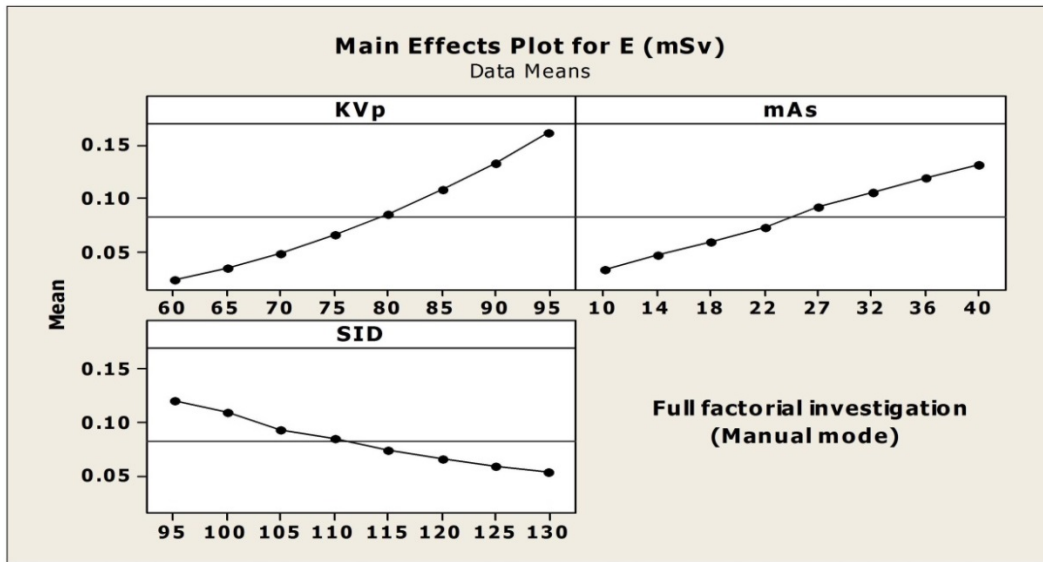
Figure 7-10. This shows the main effect on E when the acquisition factors settings changed from lower to higher levels, with the secondary acquisition factors were fixed at their optimised settings (Stage 1, Step 2). The horizontal lines represent the E grand mean (overall).

Figure 7-11 (A and B) illustrates the main effect of acquisition factors on the IQ and SNR in the same way as that of the E.
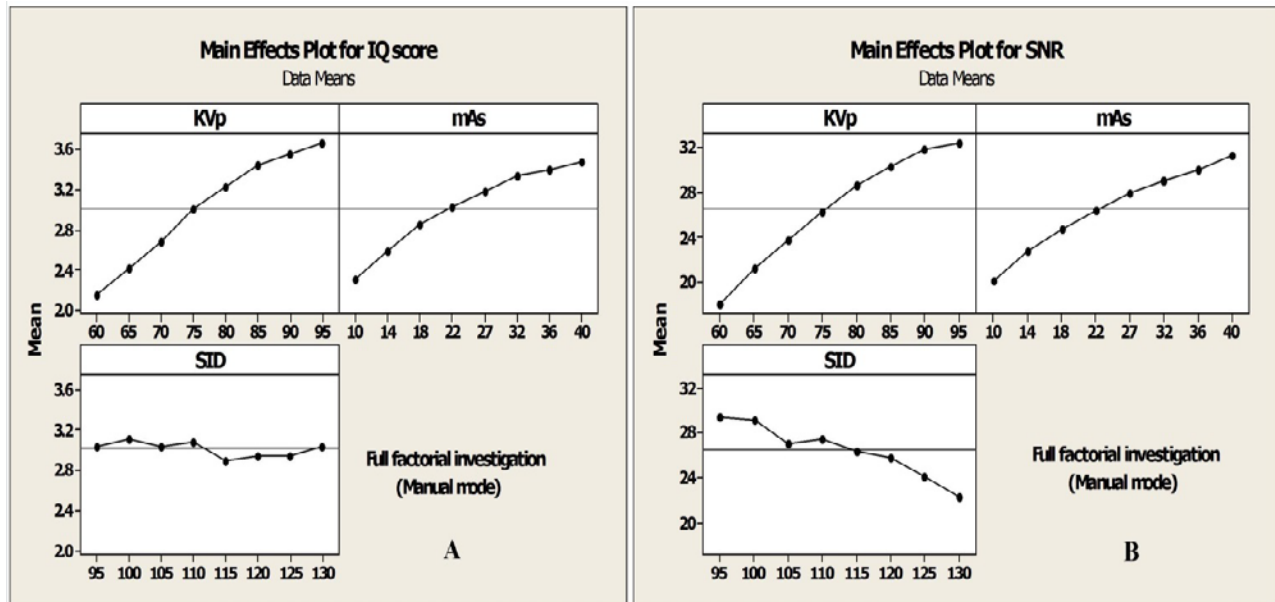
Figure 7-11. This shows the main effect on image quality (A) and SNR (B) when the acquisition factors settings changed from lower to higher levels, with the secondary acquisition factors were fixed at their optimised settings (Stage 1, Step 2). The horizontal lines represent the IQ and SNR grand means (overall).

The impact of kVp on the IQ and SNR is still the highest, whereas the SID appeared to be the least effective acquisition factor compared with others, such as mAs.

Figure 7-12 (A and B) shows how changing the kVp, mAs and SID from lower to higher settings affected the FOMs; one was based on the IQ scores and the other was based on SNR. According to this figure, it is clear that kVp had the biggest effect on the FOM_{IQ} by a factor of ~4.3, compared with that of mAs and SID. The kVp also had the highest effect on the FOM_{SNR} compared with that of the mAs and SID. Nevertheless, comparable trends for the effects of all acquisition factors were found for both FOMs when their settings changing from lower to higher levels.
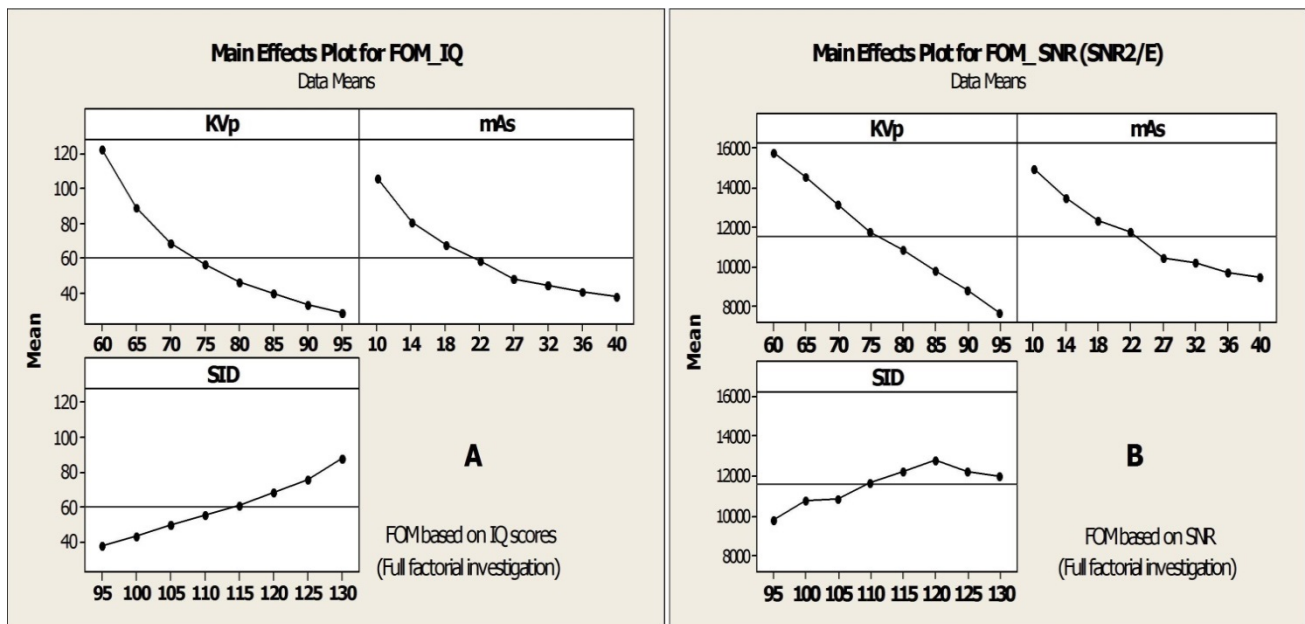
Figure 7-12. This shows the main effect of the acquisition factors on both FOMs, when settings changed from lower to higher levels; figure A illustrates the effects on FOM_{IQ}; figure B illustrates the effects on FOM_{SNR}; and the horizontal lines represent the FOM grand mean (overall).

The relationship between the radiation dose (E) and both the IQ and SNR as image quality metrics can be seen in figure 7-13 (A and B). It can be seen that, as the E increases, both the IQ and the SNR increase proportionately until the value of 0.3 mSv, where the IQ is levelled off and the SNR is reducing slightly. The latter trend would confirm the digital characteristics of the CR detector to accommodate a wide range of doses while the image quality is still within a suitable or higher level, during AP pelvis radiography. Also, a feature of detector saturation may be seen from the relationship between the E and SNR.
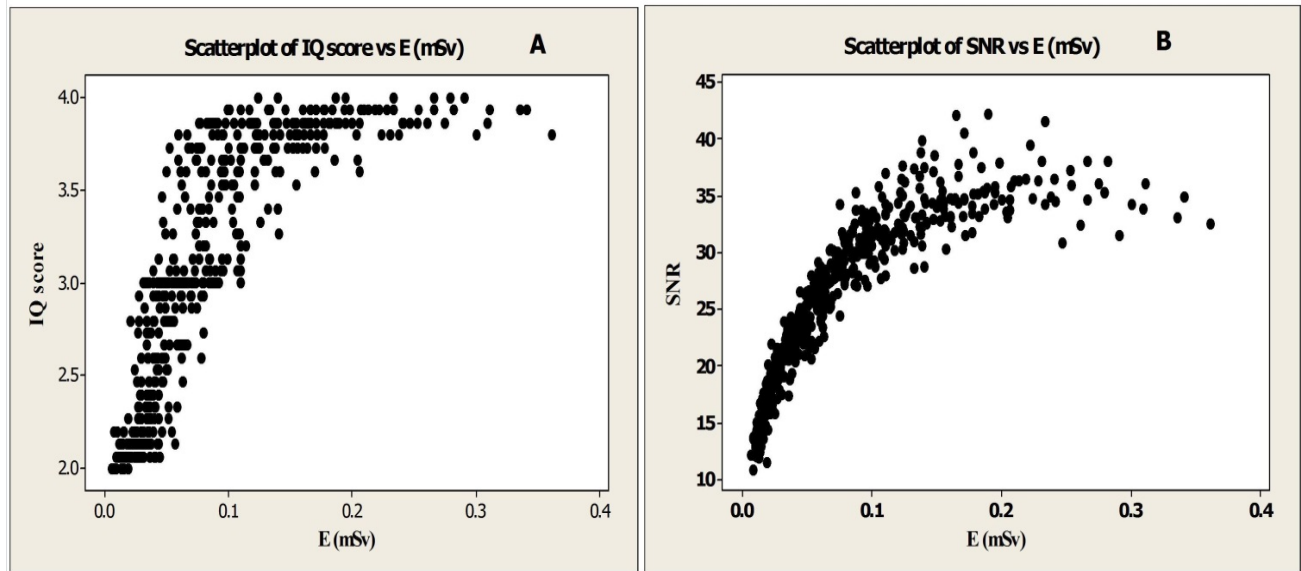
Figure 7-13. This figure illustrates the trends of each of the IQ scores (A) and SNR (B) in relation to E (mSv).

7.3. Stage 2: Optimising AP pelvis radiography using the AEC mode

In this sub-section of the resulting data, the optimisation of the AEC images is reported. All images were appraised with the APPS methodology; the E was estimated for all images and then they were then ranked according to the lowest and highest values. Only images which met the image quality criteria have been included in the results tables, in the same manner as in Stage 1. The SNR is also included.

7.3.1. Step 1: Creating the factorial set of kVp and SID combinations

64 combinations of kVp and SID were created based on 60, 65, 70, 75, 80, 85, 90 and 95 in relation to 95, 100, 105, 110, 115, 120, 125 and 130 cm SID (i.e. $8^2 = 64$ combination settings). The latter ranges for either kVp or SID would ensure systematic investigations of all possible combinations capable of producing optimised images.

7.3.2. Step2: Phantom orientation optimisation (AEC)

7.3.2.1. Optimum technique

The images were acquired at each of the two orientation settings (i.e. feet or head toward two outer chambers), using the 64 combinations settings of kVp and SID. The lowest radiation dose with suitable quality image in relation to the reference image for the feet toward two outer chamber (caudal) was 0.087 mSv, and the overall SNR measure for this image was 35.0 SD 3.6. In contrast, the optimised image with suitable quality and lowest radiation dose for the head toward two outer chambers (cranial) was produced with an effective dose of 0.134 mSv and a SNR of 30.4 SD 2.1. The optimised image from the cranial orientation was produced at a 54% higher dose than the caudal. Table 7-5 presents the acquisition factors that led to these optimised images for either orientation.

Table7-5. This table presents the acquisitions factors that led to images with suitable image quality but lower E(mSv) when compared to the reference image

Phantom orientation	Optimum acquisition Factors		E(mSv)	SNR(SD)
	kVp	SID		
Caudal orientation	*90*	*120*	*0.087*	*35.0(3.6)*
Cranial Orientation	75	125	0.134	30.4(2.1)
*SD, Standard deviation, E, effective dose, SNR, signal to noise ratio, underline refers to the optimum orientation to be used for the subsequent experiments				

A full range of acquired images; their relevant IQ scores, E (mSv) and SNRs which resulted from this experiment (for both orientations) are presented in appendices XXIII and XXIV. The SNR values from both orientations ranged from 26.2 to 50.5, and this level indicates that the amount of useful information (signal) in relation to the noise level is considerably high. This may be attributed to the automatic compensation implemented by AEC devices to produce a diagnostic image.

7.3.2.2. Factorial analysis (8^2) - Main effect

The main effects of the kVp and SID on the E, IQ and FOM_{IQ} are presented in figures 7-14, 7-15 and 7-16 (each with A and B), respectively. Variance analysis demonstrated that both the kVp and SID had a significant effect on the E, IQ and FOM_{IQ} for both orientations ($p<0.01$). Data in figure 7-14 demonstrates that kVp had the highest effect on E, compared with that caused by SID, when settings changed from lower to higher levels.
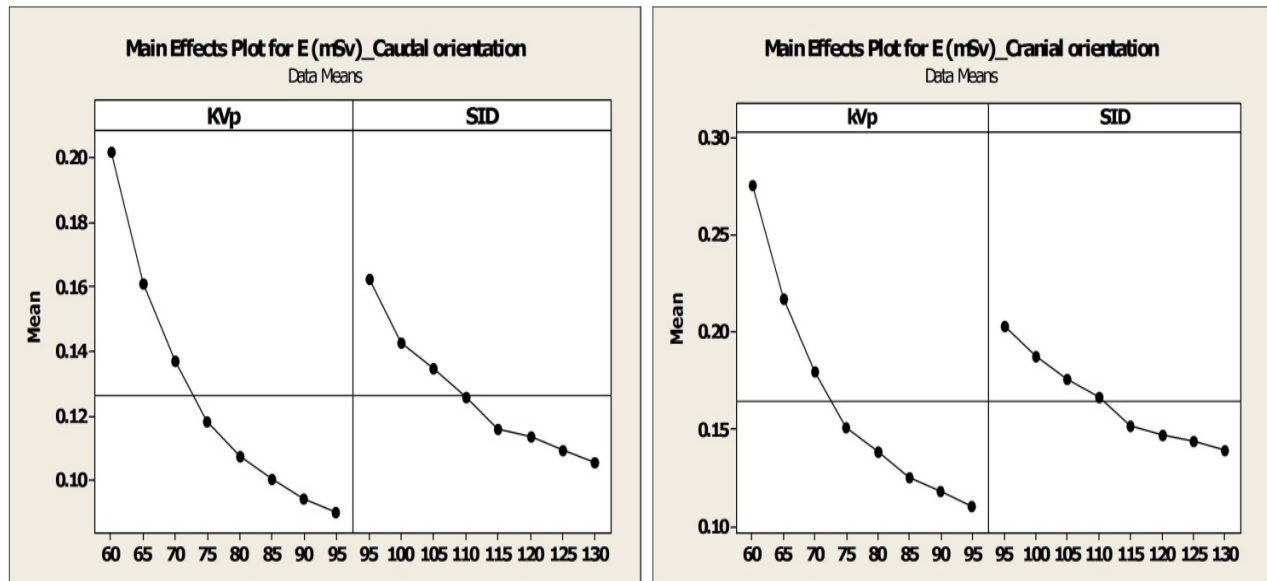
Figure 7-14. The main effect on E (mSv) when acquisition factors settings changed from lower to higher levels, for both phantom orientations using AEC; the horizontal lines represent E grand mean (overall).

Similarly, the main effect of the kVp on the IQ for both orientations was still the biggest compared with the SID effect when AEC was in use; see figure 7-15.
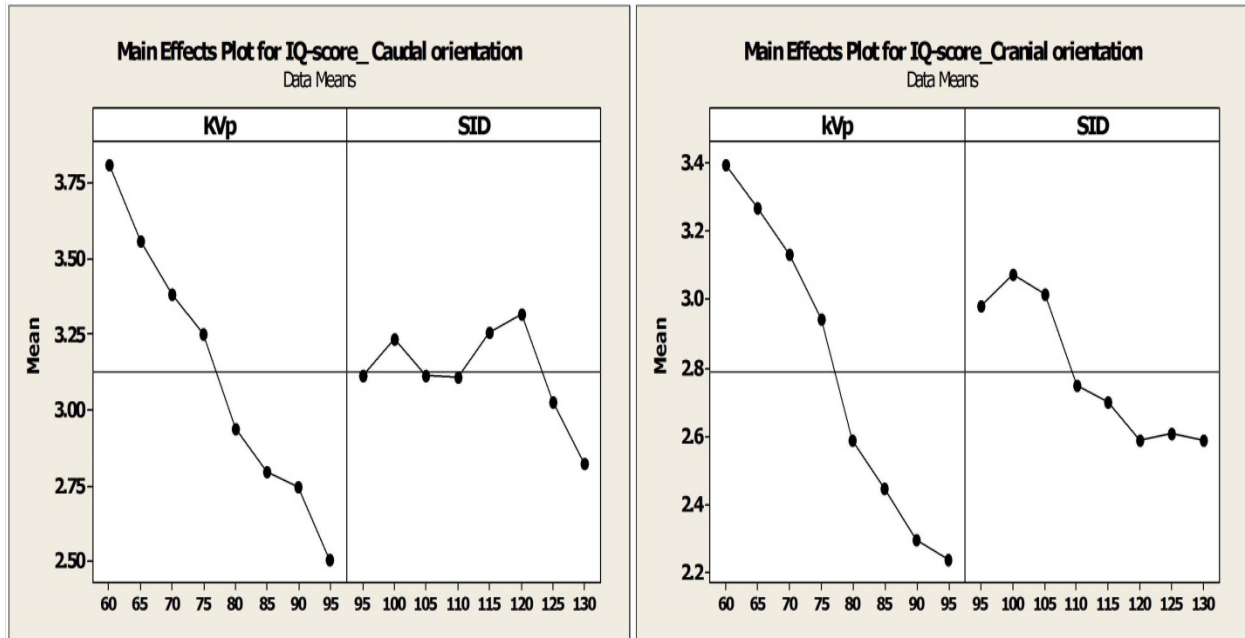
Figure 7-15. This shows the main effect on IQ when the acquisition factors settings changed from lower to higher levels, for both orientations using AEC. The horizontal lines represent the E grand mean (overall).

Figure 7-16 (A and B) illustrates how changing the kVp and SID from lower to higher levels would affect the FOM_{IQ} for both phantom orientations using AEC. From this figure, it can be seen that, for caudal orientation, the effect of kVp and SID on the FOM_{IQ} were nearly comparable, however, the kVp effect on the FOM_{IQ} appeared to be higher than that with cranial orientation (see figure 7-16, A and B) when settings changing from lower to higher levels.
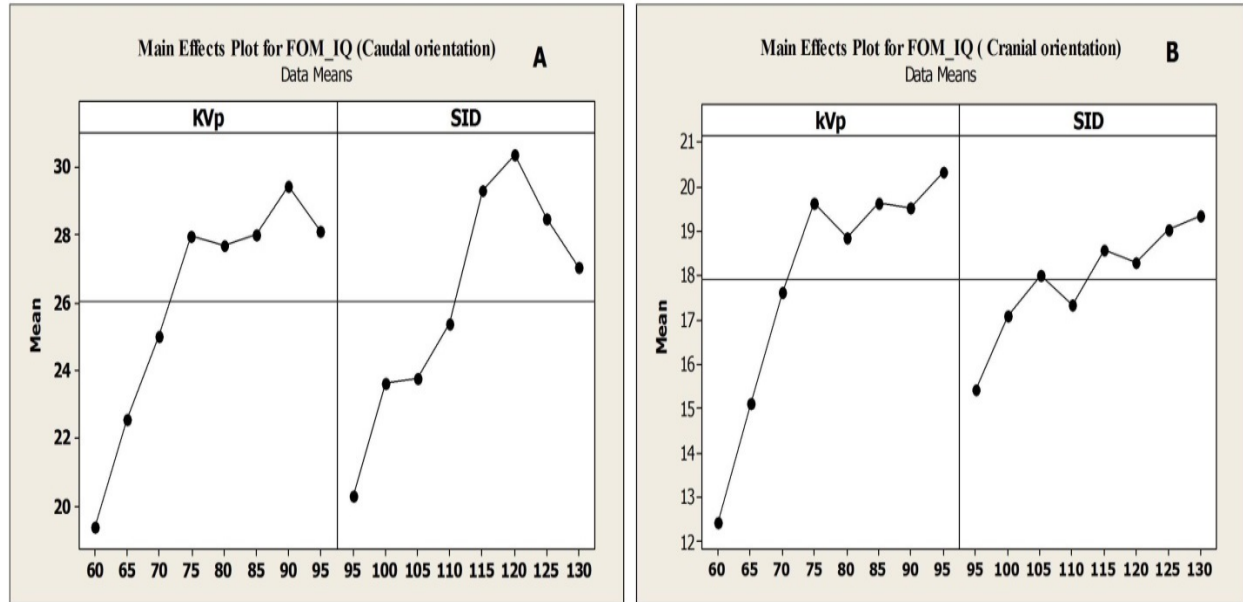
Figure 7-16. This shows the main effect of the kVp and SID on FOM_{IQ} when settings changed from lower to higher levels; A- illustrates the effects on FOM_{IQ} with caudal orientation; B- illustrates the effects on FOM_{IQ} with cranial orientation; the horizontal lines represent the grand mean (overall).

7.3.3. Step 3: Optimising chamber selection configurations (AEC)

7.3.3.1. Optimum technique

The images were acquired at each of the three chamber configurations (i.e. single, 2 outer chambers and all chambers), using the 64 combination settings of kVp and SID while the phantom was set at a feet toward orientation (caudal), as established in Step 2 (sub-section 6.7.3).

With reference to the single chamber, the results demonstrated that the optimised image with the lowest radiation dose (0.129 mSv) had a corresponding SNR of 36.5 SD 2.6. In contrast, the optimised image obtained with the two outer chambers had an effective dose of 0.095 mSv (SNR 32.7 SD 2.6). This meant that the dose reduction difference between using single and two outer chambers was about 27 % (0.126 SD 0.041 vs 0.164 SD 0.058, P<0.001).

With regards to imaging practice, using all three chambers yielded a suitable quality image with an effective dose of 0.104 mSv and 36.9 SD 2.9 SNR. The acquisition factors which led to the above optimised images can be seen in table (7-6).

Table7-6. Acquisitions factors that led to images with suitable image quality but lower E (mSv) when compared to the reference image.

AEC chamber's configuration	Optimum acquisition Factors		E(mSv)	SNR(SD)
	kVp	SID		
Single chamber	80	115	0.129	36.5(2.6)
2 outer chambers	_85_	_115_	_0.095_	_32.7(2.6)_
3 chambers	80	125	0.104	36.9(2.9)
SD, standard deviation, E, effective dose, SNR, signal to noise ratio underline refers to the optimum chamber configuration that will be adapted in the subsequent experiments.				

A wide range of combination settings that were associated with suitable image quality and lower dose, compared with the adult average E for AP pelvis (i.e. 0.7 mSv), especially from the two and all chambers configurations, which are presented in appendices XXV, XXVI and XXVII.

7.3.3.2. Factorial analysis (8^2) - Main effect

The impact of each kVp and SID on the E, IQ and FOM_{IQ} is presented in figures 7-17 (A, B and C), 7-18 (A, B and C) and 7-19 (A, B and C) using AEC mode. All the acquisition factors were found to significantly affect E, IQ and FOM_{IQ}, for all chamber configurations (P<0.01). Data in figure 7-17 demonstrates that the kVp had the highest effect on E, compared with the effect caused by SID when settings changed from lower to higher levels for all chambers' configurations types (A, B and C).
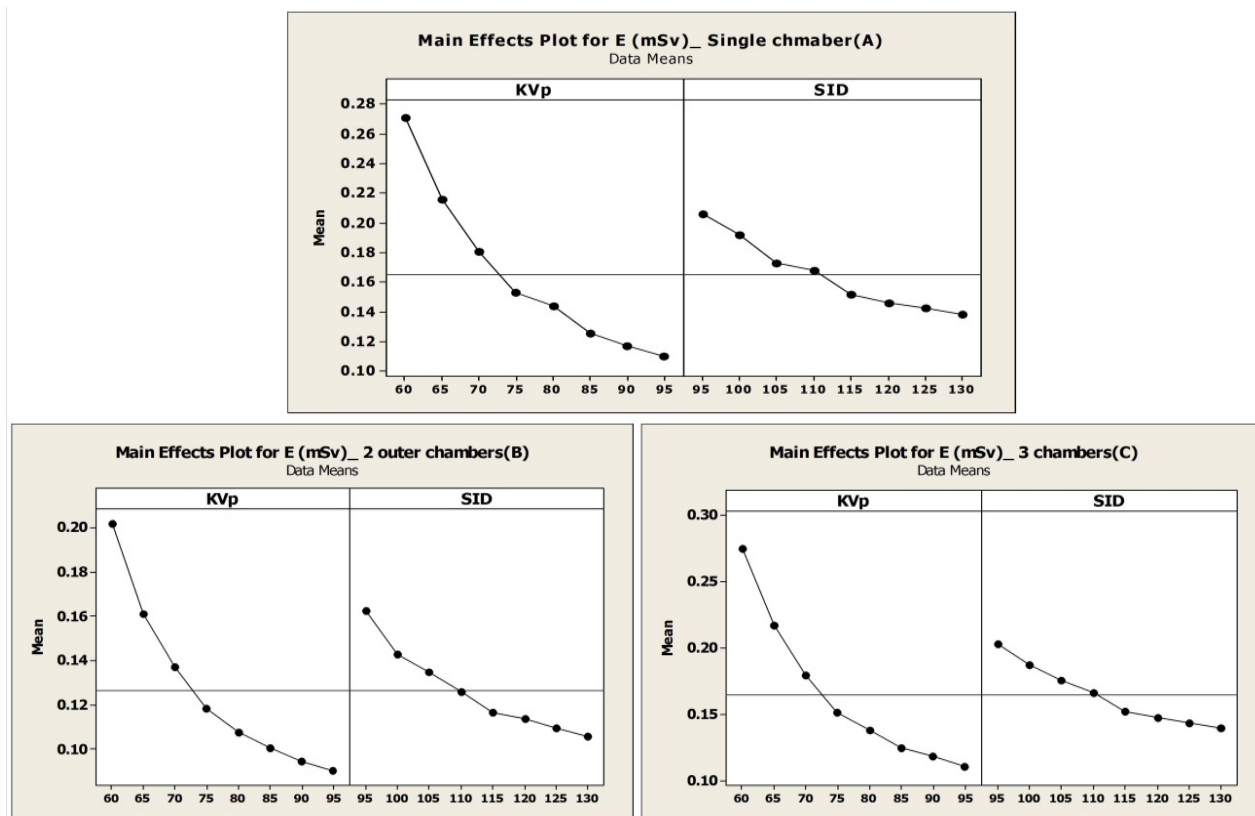
Figure 7-17. This shows the main effect on E when the acquisition factors settings changed from lower to higher levels, for the three different AEC chambers' configurations (A, B and C). The horizontal lines represent the E grand mean (overall).

The main effects of the acquisition factors on the IQ across all different chamber configurations are presented in figure 7-18 (A, B and C). It can be seen that the kVp had the highest impact on the IQ when compared with the corresponding SID effect. To illustrate, the kVp change caused the IQ to decrease by a factor of ~1.5, whereas the SID caused a decrease in the IQ by a factor of ~1.12 when settings changing from lower to higher levels.
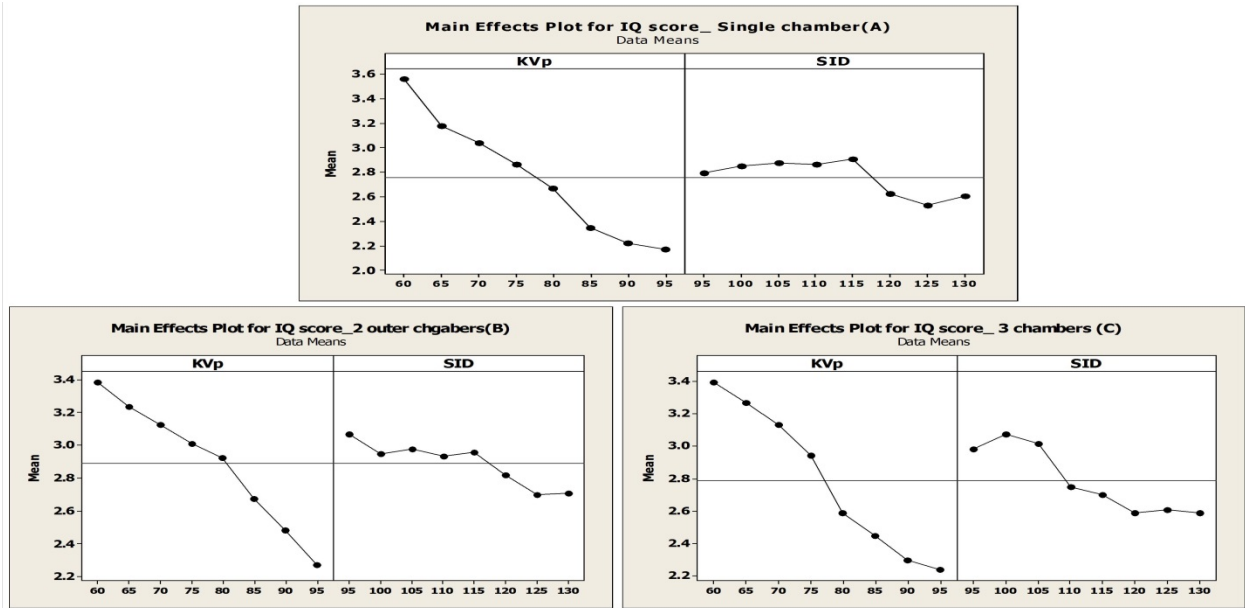
Figure 7-18. This shows the main effect on image quality when the acquisition factors settings changed from lower to higher levels, for the three different AEC chambers' configurations (A, B and C).

The main effects of the kVp and SID on the FOM_{IQ} when their settings changed from lower to higher levels are illustrated in figure 7-19 (A, B and C), for all chamber configurations.
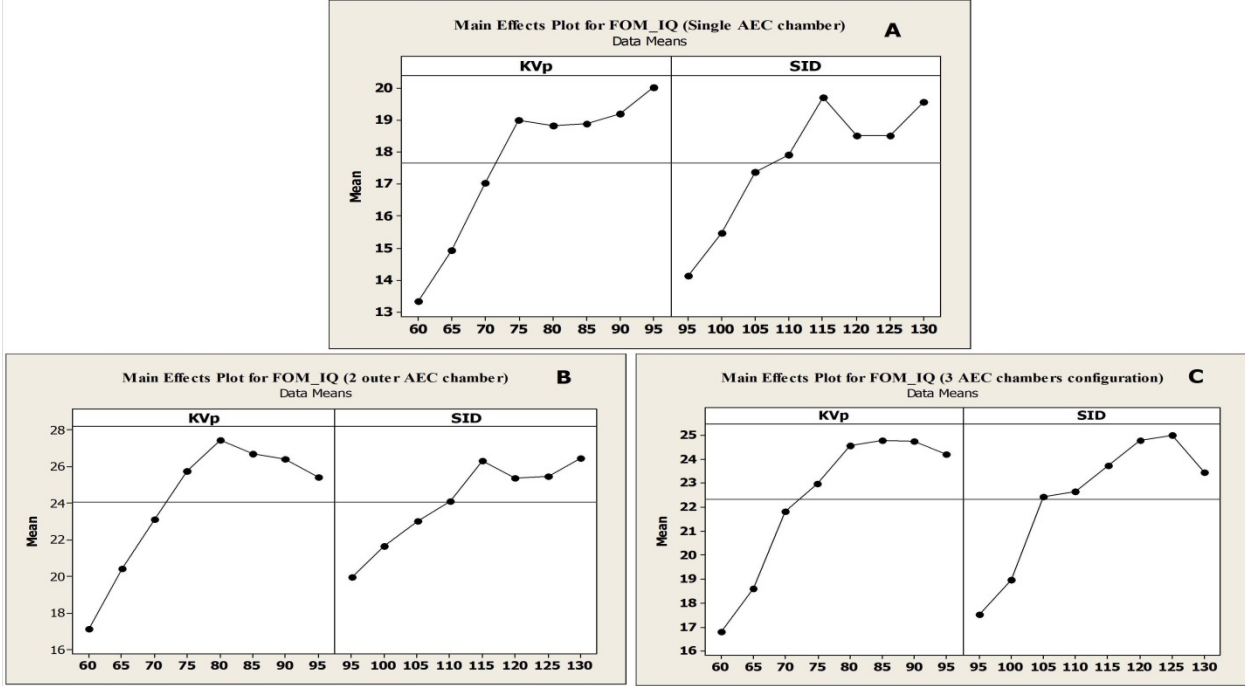
Figure 7-19. This shows the main effect of the kVp and SID on FOM_{IQ} when the acquisition factors settings changed from lower to higher levels. A, B and C illustrate the effects on FOM_{IQ} with a single chamber, 2 chambers and all chamber configurations respectively. The horizontal lines represent the FOM grand mean (overall).

According to figure 7-19, it can be seen that the kVp and SID effects on FOM$_{IQ}$ were comparable with single chamber and all chamber configurations. By contrast, the kVp effect on the FOM$_{IQ}$ appears to be slightly higher than the SID effect, with the two outer chambers' configuration.

7.3.4. Step 4: Optimising of focal spot and filtration using AEC (Phantom orientation and chamber configuration fixed at their optimised settings, step 2 and 3)

7.3.4.1. Focal spot optimisation (AEC)

7.3.4.1.1. Optimum technique

The results demonstrated that the lowest radiation dose with a suitable quality image was obtained using the broad focal spot setting, with an E of 0.093 mSv and an SNR of 31.7 SD. 2.7. On the other hand, the optimised image for fine focus in relation to E was obtained at 0.113 mSv dose. The SNR of this image was 29.8 SD 2.5. Table7-7 presents the acquisition factors that led to these optimised images.

Focal spot type(AEC)	**Optimum acquisition Factors**		**E(mSv)**	**SNR(SD)**
	kVp	**SID**		
Broad focus	_80_	_130_	_0.093_	_31.7(2.7)_
Fine Focus	75	115	0.113	35.9(2.9)

Table7-7. This table presents the acquisitions factors that led to images with suitable image quality but lower E (mSv) when compared to the reference image.

*SD, Standard deviation, E, effective dose, SNR, signal to noise ratio, underline refers to optimum focal spot type that will be adapted with next experiment using AEC

The exposure time associated with a fine focal spot using AEC was significantly higher than that of a broad focal spot (P< 0.001), with a range from 13.6 to 189.4 ms. The higher exposure time resulted from setting a low kVp, which in turn was automatically compensated for by the AEC device, by its giving a very high mAs value. A full range of acquired images for both focal spot types is presented in appendices XXVIII and XXIX.

7.3.4.1.2. Factorial analysis (8²) - Main effect

The data from the investigation into the main effects on E, IQ and FOMs are presented in figures 7-20, 7-21 and 7-22, each with A and B. Regarding the broad focus, the analysis of variance revealed that both the kVp and SID had significant impact on E, IQ and FOM$_{IQ}$ (P<0.001). In contrast, the kVp was found to significantly affect all of the response variables, whereas the SID was found only to significantly affect the E and FOM$_{IQ}$, but not the IQ (P>0.05), when fine focus was in use. Figure 7-20 illustrates how changing the kVp and SID settings from lower to higher levels affected the E for both foci. According to this figure, the kVp had the biggest effect on E (by a factor of ~2.2) and for both foci, compared with the SID effect on the same E.
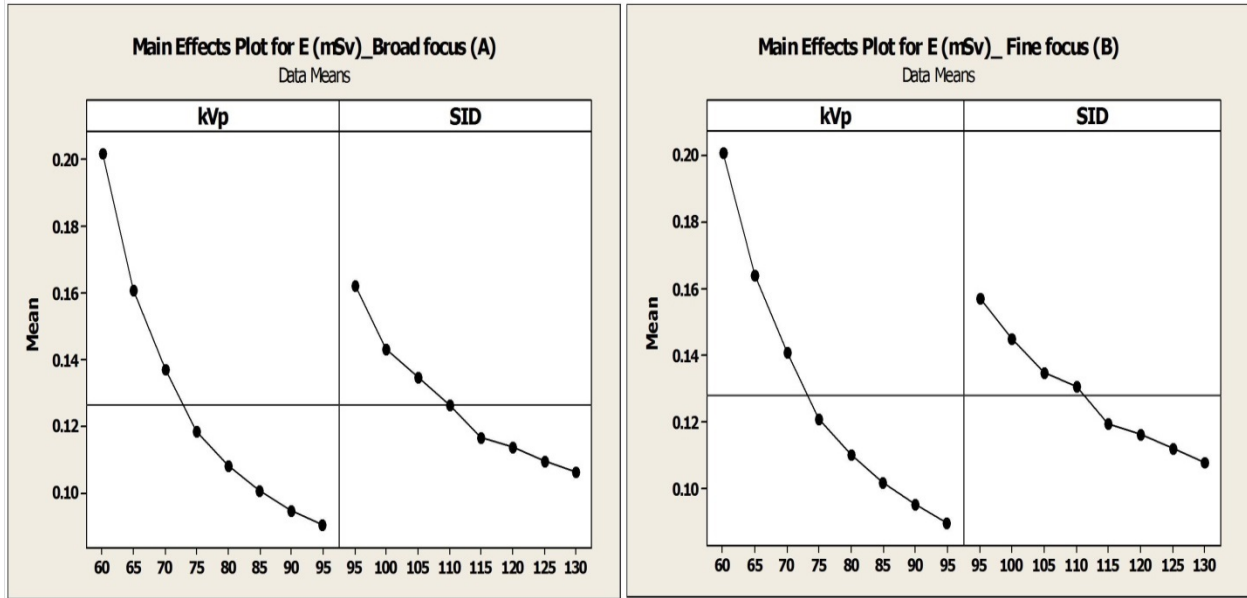
Figure 7-20. This shows the main effect on E (mSv) when the acquisition factors settings changed from lower to higher levels, for the two focal spot types (A-Broad focus; B-Fine focus). The horizontal line represents the grand mean (overall) of E.

The main effect of each of the kVp and SID on IQ, using AEC, with both focal spot types can be seen in figure 7-21 (A and B). It is clear that the kVp affected the IQ more than the SID when their settings changed from low to high levels.
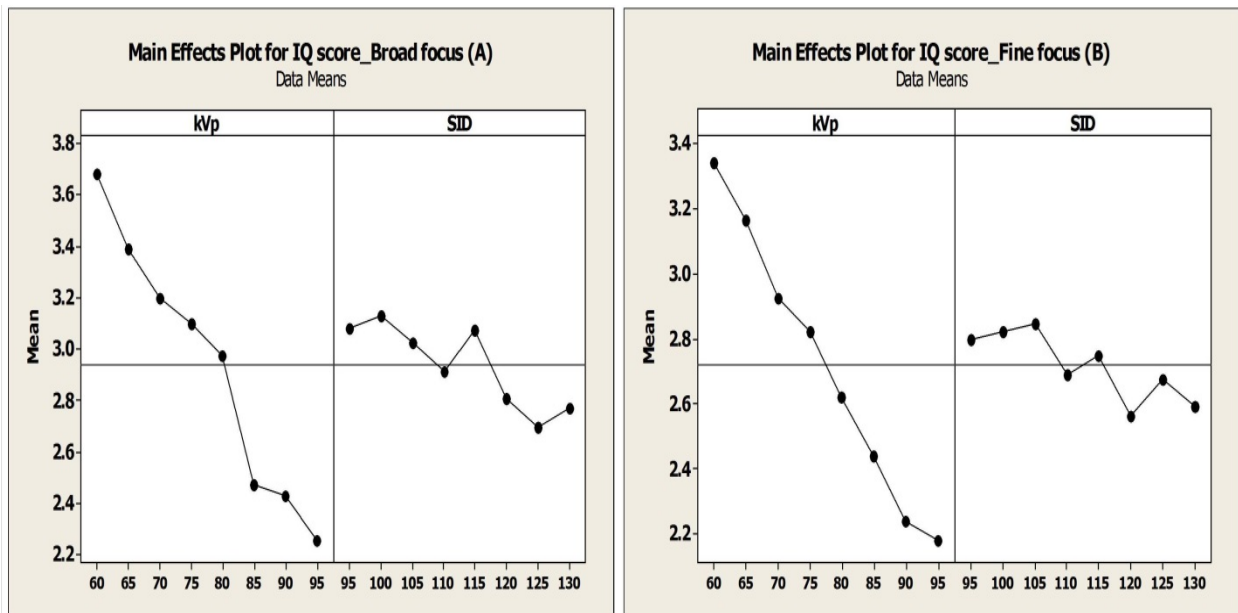
Figure 7-21. This shows the main effect on image quality when the acquisition factors settings changed from lower to higher levels, for the two focal spot types using AEC (A-Broad focus; B-Fine Focus). The horizontal lines represent the IQ grand mean (overall).

Finally, the trends of the FOM_{IQ}, in relation to the kVp and SID individually, for both focal spot types are illustrated in figure 7-22 (A and B).
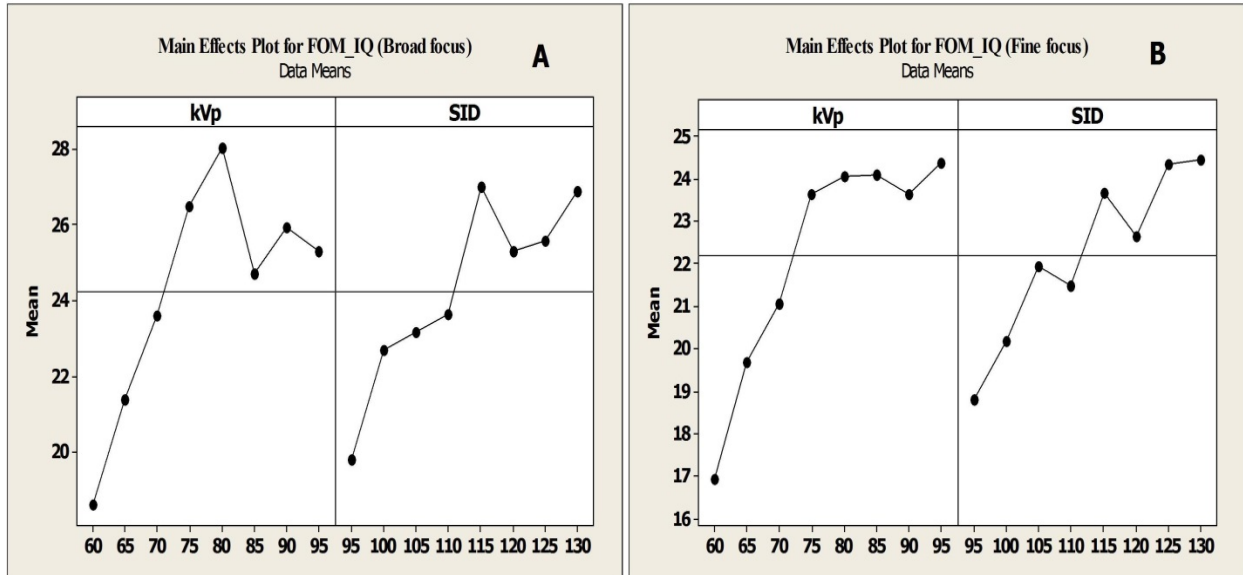
Figure 7-22. This shows the main effect of the kVp and SID on FOM_{IQ} when the acquisition factors settings changed from lower to higher levels. A illustrates the effects on FOM_{IQ} with a broad focus; B illustrates the effects on FOM_{IQ} with a fine focus. The horizontal lines represent the grand mean (overall).

Figure 7-22 shows that the main effect of the kVp on FOM_{IQ} was slightly bigger than the main effect of SID when their settings changed from low to high levels.

7.3.4.2. Filtration thickness optimisation (AEC)

7.3.4.2.1. Optimum technique
The images were acquired at each of the four filtration settings (i.e. inherent, 2 mm Al, 0.1 mm Cu, and 0.2 mm Cu) using the 64 combination settings of kVp, SID created at Stage 2, Step 1; the images were appraised using APPS and the E was estimated for each combination setting. Accordingly, the results demonstrated that the lowest radiation dose, with suitable image quality, when using inherent filtration with AEC resulted in 0.093 mSv with the SNR for the image being 26.6 SD 2.3.

In contrast, when a 2mm Al added filter was used, the optimised acquisition factors were identified according to the suitable image quality with the lowest dose compared with the reference image. The lowest dose image, with a suitable quality, was obtained with an E of 0.9 mSv, the SNR was 36.2 SD 2.9.

The lowest dose with a suitable quality image was produced at 0.095 mSv with an SNR of 35.7 SD 3.4 when using 0.1 mm Cu added filtration. Using 0.2 mm added filtration led to the lowest radiation dose for a suitable quality image when compared with the other filtration options. This optimised image was produced with 0.082 mSv, and gave an 88 % dose reduction compared with the average value (0.7mSv) for adult AP pelvis examination (Sherer, Visconti, Ritenour, &

184

Haynes, 2014; UNSCEAR, 2010). The SNR for this image was 34.5 SD 2.8, meaning that the noise level across the image regions of interest were low, compared with the high number of useful signals, giving such a level of SNR. Table 7-8 presents the acquisition factors which resulted in the optimised images from each filter type optimisation.

| Table7-8. This table presents the acquisitions factors that led to images with suitable image quality but lower E(mSv) when compared to the reference image				
Filter thickness (AEC)	**Optimum acquisition Factors**		**E(mSv)**	**SNR(SD)**
	kVp	**SID**		
Inherent	80	130	0.093	26.6(2.3)
2mm Al	85	120	0.090	36.2(2.9)
0.1mm Cu	80	110	0.960	35.7(3.4)
0.2mm Cu	**_80_**	**_125_**	**_0.082_**	**_34.5(2.8)_**
*SD, standard deviation, E, effective dose, SNR, signal to noise ratio, Al, aluminium, Cu, copper; underline refers to the final optimum technique from optimising the AP pelvis radiography using AEC.				

Appendices XXX to XXXIII present the full range of acquired images with their corresponding response variables (e.g. E) for all filtration types mentioned above using AEC.

7.3.4.2.2. Factorial analysis (8²) - Main effect

The data from studying the main effects of the kVp and SID on E, IQ and FOM_{IQ} across different filtration types are presented in figures 7-23, 7-24 and 7-25 (each with A, B, C and D). The analysis of the variance demonstrated that the kVp and SID had significant effects ($P < 0.001$) on each of the E, IQ and FOM_{IQ} for all filtration types, with the exception that the SID did not have on the IQ when 2mm Al filter was in use.
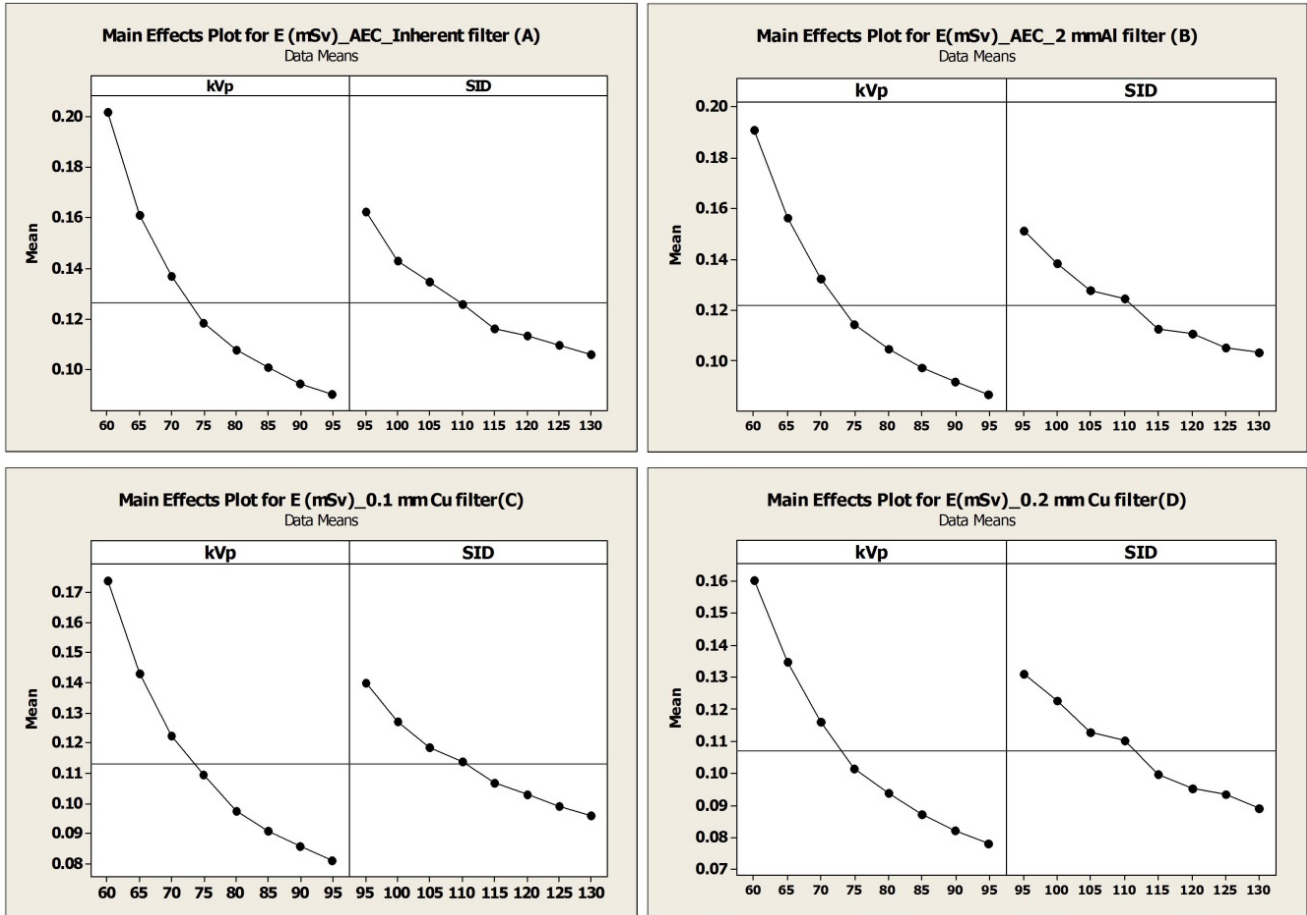
Figure 7-23. This shows the main effect on E (mSv) when the acquisition factors settings changed from lower to higher levels, for the different filter thicknesses using AEC mode. The horizontal lines represent the E grand mean (overall).

From figure 7-23, it can be seen that the kVp had the biggest effect on the E when compared with the SID, for all types of filtration. Figure 7-24 presents the main effect each of the kVp and SID had on the IQ when their settings changing from lower to higher levels, for all filtration types using AEC mode. From figure 7-24, it is clear that the kVp effect on the IQ for all filter types was the biggest compared with SID effect when their settings changed from lower to higher levels. Also, the kVp effect noted a slight increase as filter thickness increased.
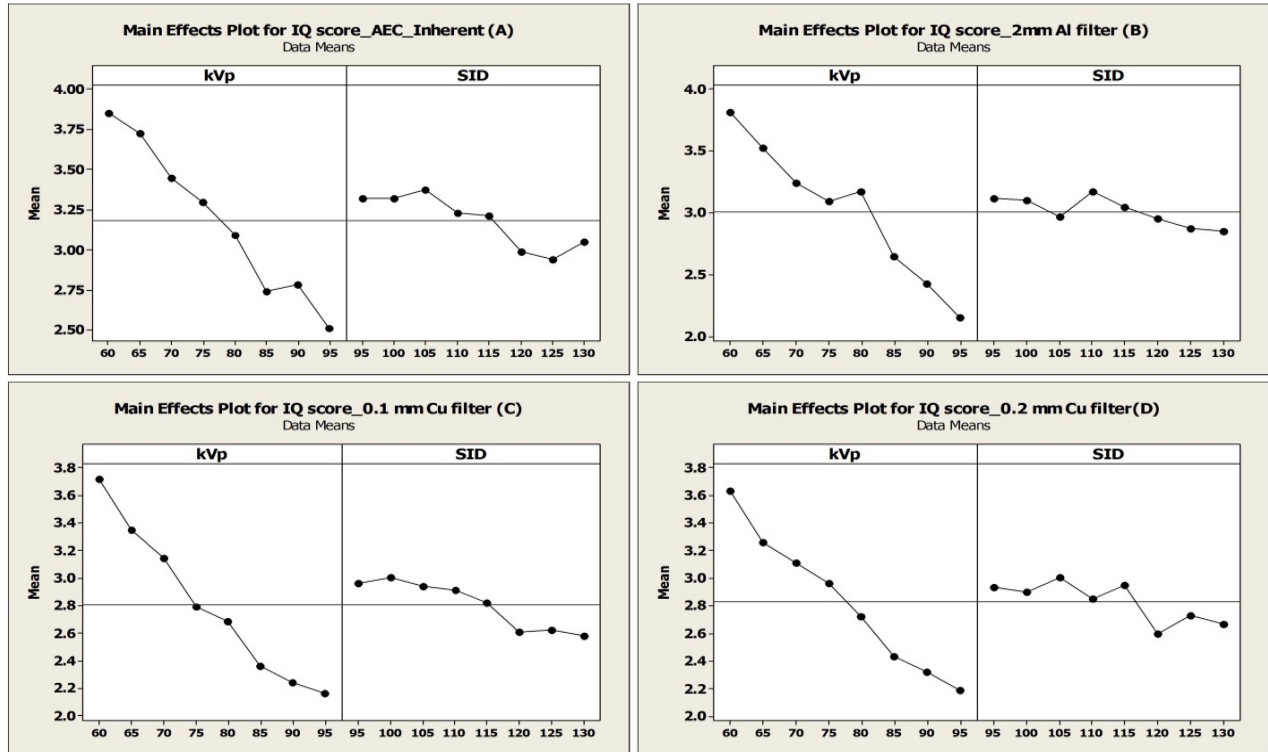
Figure 7-24. This shows the percentage change in image quality when the acquisition factors settings changed from lower to higher levels, for the different filter thicknesses. The horizontal lines represent the FOM_{IQ} grand mean (overall).

Figure 7-25 (A, B, C and D) illustrates how the FOM_{IQ} trends were influenced when the kVp and SID settings changed from low to high levels for all filtration types. From this figure it can be seen that the kVp marginally affected the FOM_{IQ}, compared with the SID effect, when inherent and 2 mm Al filter types were in use. By contrast, the effect of both kVp and SID on the FOM_{IQ} was seen to be closely comparable with 0.1 and 0.2 mm Cu filter types.
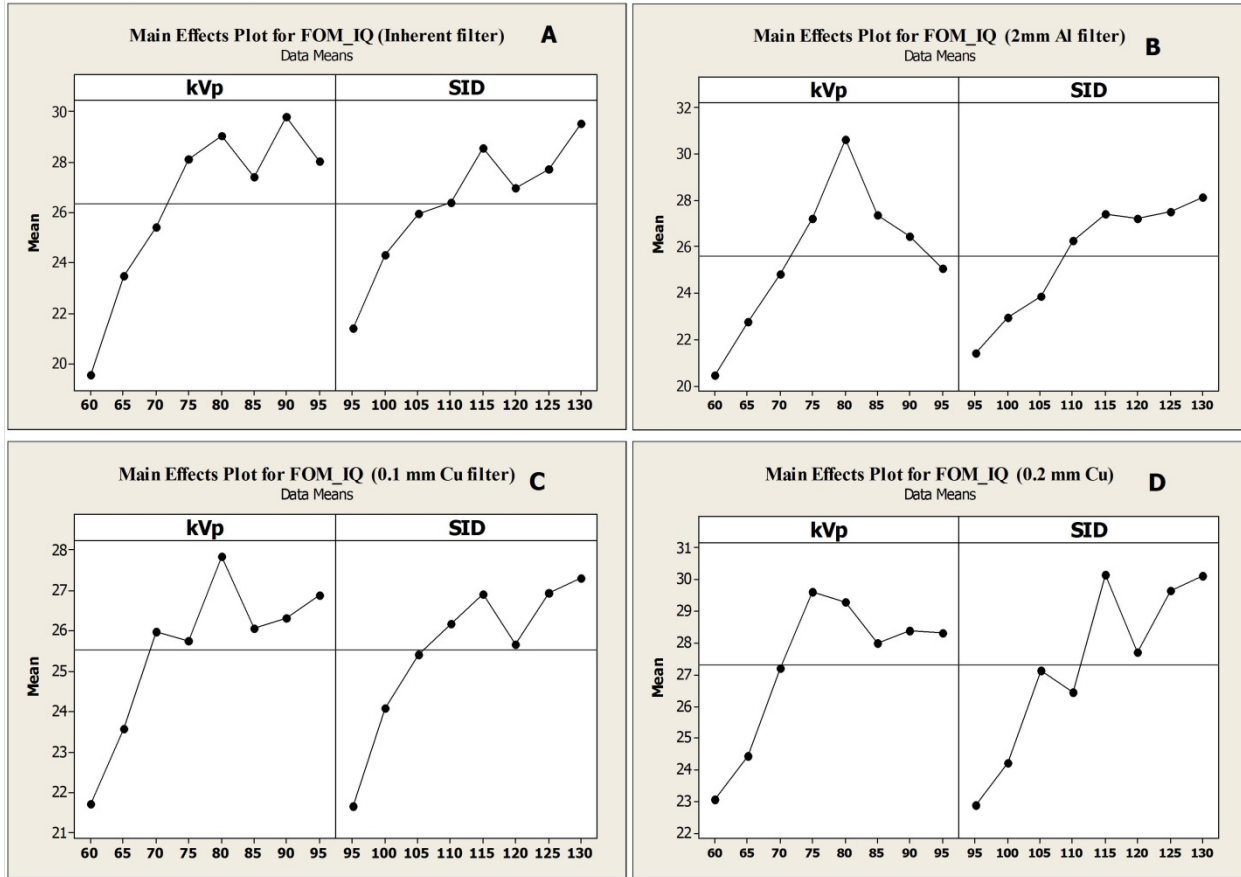
Figure 7-25. This shows the main effect on FOM_{IQ} when the acquisition factors settings changed from lower to higher levels. A, B, C and D illustrate the effects on FOM_{IQ} with inherent filtration, 2mm Al, 0.1 mm Cu and 0.2 mm Cu filter types respectively using AEC mode. The horizontal lines represent the FOM_{IQ} grand mean (overall).

The main effect on the trend of the FOM which based on SNR when the kVp and SID settings changed from lower to higher levels across different filtration types using AEC can be seen in figure 7-26 A, B, C and D (below). This figure shows that, with inherent and 2 mm Al filter types, the SID effects on FOM_{SNR} were slightly higher than the same effects of the kVp when their settings changed from low to high levels using an AEC mode. However, the main effects of the kVp and SID appeared to be similar on the SNR based FOM when settings changed from low to high, with both 0.1 and 0.2 mm Cu filter types. A clear fluctuation was seen in the trends of the FOM_{SNR} for 0.1 and 0.2 mm Cu filter types (heavy filtration).
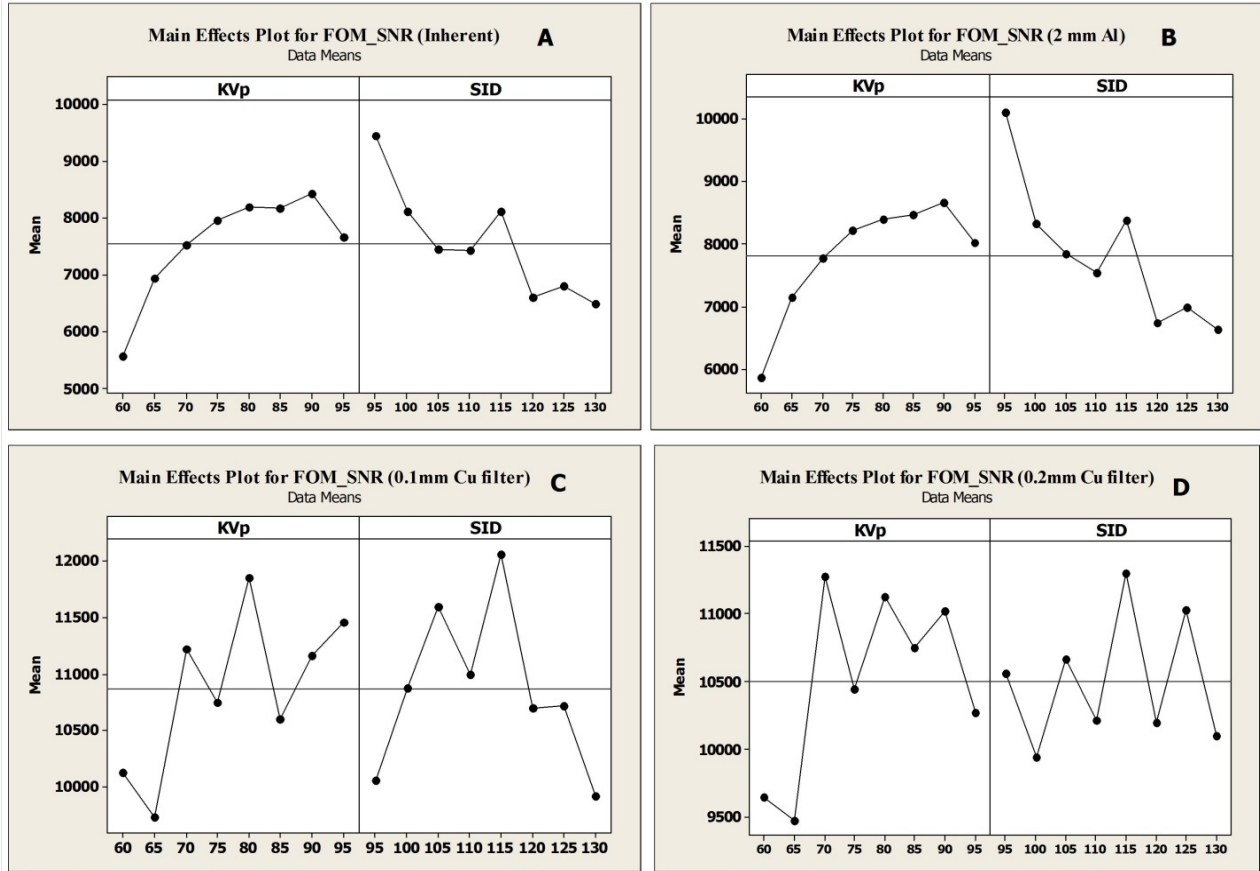
Figure 7-26. This shows the main effect of acquisition factors on FOM$_{SNR}$ when the settings changed from lower to higher levels. A, B, C and D illustrate the effects on FOM$_{SNR}$ across different filter types. The horizontal lines represent the FOM$_{SNR}$ grand mean (overall).

Finally, typical examples for the relationship between the E and IQ scores taken from the optimisation of the inherent and 0.2mm Cu filtration types using AEC mode are illustrated in figure 7-27 (A and B). This figure shows again that the IQ would not be particularly affected, as E increases when using CR detectors. These trends indicate the existence of dose creep with AEC use. Nevertheless, IQs trends appear to be more linear than the same trend, but with manual mode in use when the E increases (see figure 7-13 for comparison).
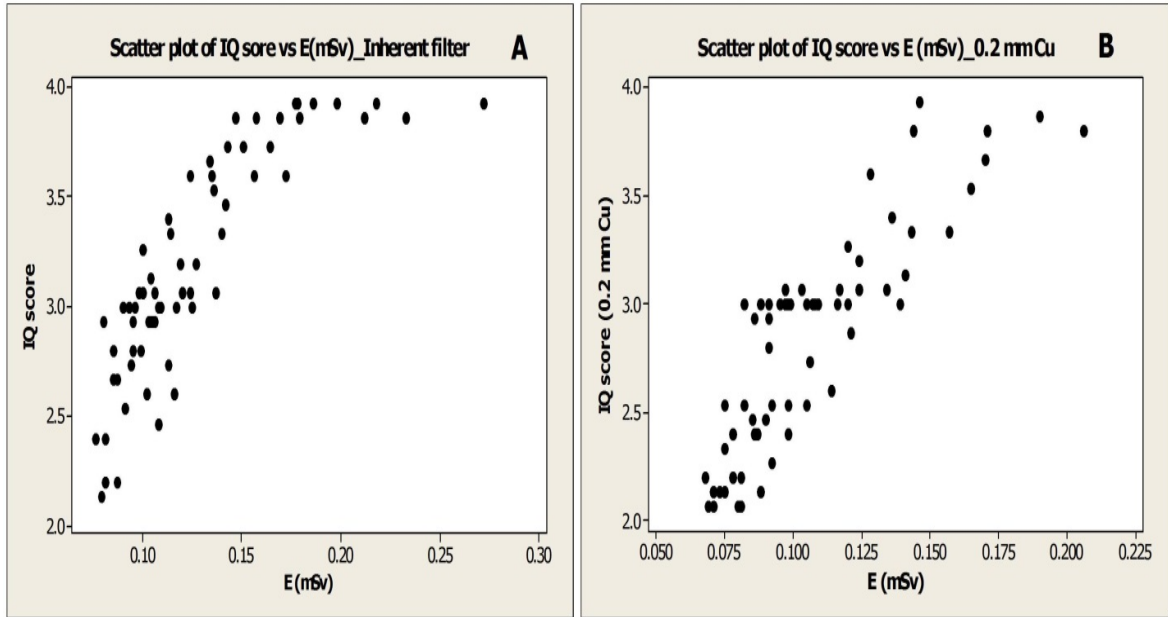
Figure 7-27. This figure illustrates the relationship between the E and IQ score; A was taken from inherent filter optimisation; B was taken from the 0.2 mm Cu filter optimisation.

7.4. Image post-processing testing

Fifty six images were produced using additional post-processing; the six un-suitable images were modified using systematic factorial settings of latitude and windowing (i.e. 56 combinations). The initial results of appraising each set of the 56 images against their original unsuitable quality images demonstrated that there were slight improvements in the IQ of the images across the six images groups. For the APPS IQ, some individual items were improved when compared with the (<3) original image scores, prior to post-processing. However, some of the criteria were scored worse as a result of the post-processing, but these criteria were few in number when compared to the number of improved items. Appendix XXXIV illustrates how post-processing could contribute to enhancing the quality of these images that were scored as unsuitable.

Next, another IQ analysis was performed to see whether the post-processed images had improved in image quality. The post-processed images, which were improved from unsuitable images, were compared against a reference image with suitable quality from their relevant group. This element of analysis was important to further understand the effects of post-processing on improving image quality. Findings demonstrated that few improved images (e.g. 7) were scored as equal to reference image (suitable), and therefore were considered to have been improved by the post-processing manipulation.

7.5. Image quality assessment approaches (Correlation)

This sub-section investigates to what extent the IQ scores obtained from all the images agreed with the relevant SNR measures. For this, Spearman's rank correlation coefficient was used because one of the variables was ordinal data (IQ scores), whereas the second is based on interval data type (SNR). The results of testing the correlation between IQ scores and the relevant SNR measures across all of the experiments using manual and AEC modes can be seen in in table 7-9.

Table7-9. This table presents the level of correlation between the APPS scores and SNR for all of the acquired images.		
System mode	**Correlation range/ Spearman**	**Significance**
Manual	0.851-0.956	0.000
AEC	0.785-0.933	0.000

Regarding the correlation between the two SNR measures which were calculated using the two ROI approaches mentioned in subsection 6.4.2 (methodology) across all of the experiments (manual and AEC modes), table 7-10 shows the relevant correlation ranges of the two approaches.

Table7-10. This table presents the correlation between the SNRs calculated using two different approaches for all images of all experiment.		
System mode	**Correlation range/ Spearman**	**Significance**
Manual	0.777-0.960	0.000
AEC	0.645-0.828	0.000

Chapter 8: Discussion

8.1. Overview

This chapter discusses the results from the optimisation experiments. Similar to chapter 7, the discussion will focus on two main themes. First, an identification of the optimum technique that would produce suitable image quality with the lowest possible radiation dose for each experiment; this includes the primary and secondary acquisition factors. Second, the main effect of the kVp, mAs and SID on different response variables (e.g. IQ and E). Nevertheless, the effect of the secondary acquisition factors on radiation dose and image quality will be considered where appropriate. A general discussion concerning the efficiency of adopting a factorial design to optimise radiation dose and image quality in any radiographic projection will be given in a separate sub-section. The efficiency of the factorial framework will be supported by evidence obtained from this thesis and existing literature. Finally, in order to facilitate navigation through the discussion sub-headings, they have been ordered in the same way as that of the results chapter.

8.2. Stage 1: Optimising the AP pelvis radiography using manual mode

8.2.1. Step 1: Creating the Basic Factorial Set of kVp, mAs and SID Combinations

According to the experimental investigations, some of the 64 combinations of the kVp, mAs and SID led to images with suitable quality. This in turn made it possible to optimise the secondary acquisition factors.

8.2.2. Step 2: Secondary acquisition factors' optimisation

8.2.2.1. Tube anode heel effect

8.2.2.1.1. Optimum technique

Exploiting the anode heel effect provides an opportunity to minimise the dose administered to critical organs. Placing the testes toward the anode is likely to result in dose reduction. The findings in this thesis demonstrate that, when the feet are positioned towards the anode, the testicular dose is significantly lower at 1.1 SD 0.38 mGy, compared to when the feet are positioned towards the cathode (1.6 SD 0.59 mGy, P< 0.001); this orientation results in a 31% dose reduction. Regarding ovarian dose, findings demonstrate that there was no statistical difference (P>0.05) between orientations. An explanation for this could be that the ovaries are situated nearer to the central ray in comparison to the testes (see figure 6-3). Organs situated nearer to the edge of the field are likely to benefit more from the anode heel effect. In addition, the ovaries are located deeper within the pelvic cavity and would therefore naturally benefit from protection against radiation by anterior lying structures; this could reduce the impact of the anode heel effect.

The anode heel effect for the testicular doses was similar to that obtained by Fung and Gilboy (2000), in that the findings in this thesis were similar for the testes, but contradictory in relation to ovarian dose. Fung and Gilboy (2000) found that there were significant differences in ovarian doses caused by anode heel effect. These differences could be explained by the choice of

examination and area examined (lumbar spine) in Fung and Gilboy's work, where both male and female gonads are situated nearer to the X-ray beam edge. They also measured testicular doses by putting the TLDs at appropriate locations on the phantom surface, and not in the predefined testes holes inside the ATOM phantom. These placements could be considered unrealistic and further add to difficulties within comparisons. From the other side, no image quality consideration was seen in this work (Fung and Gilboy, 2000) in relation to the anode heel effect with lateral lumbar spine radiography. This point might be critical when ALARA principle taken into account, which imposes that dose and image quality should be mutually optimised whenever there is an attempt for patients' radiation dose reduction (ICRP, 2007a). This is specifically true when a radiographic projection includes a body part is being imaged with variable thickness along the cranio-caudal line such as lumbar spine.

Regarding image quality, both anode heel orientations were associated with a range of images of suitable quality. However, for the male organ, the optimum orientation that led to the lowest radiation dose image with suitable image quality was when the feet were placed towards the anode. By contrast, both orientations can be adopted for the female organ, since no radiation dose implications were found. This means that switching phantom orientation onto either side could not affect the quality of an image. Therefore, the anode heel effect can provide a good margin for protecting the male patient from unnecessary radiation. In addition, placing the thinner parts of the pelvis toward the anode and thicker parts toward the cathode comply with published recommendations regarding using the heel effect as a wedge filter (Carlton & Adler, 2013; Katz & Nickoloff, 1993).

However, the results of this thesis contradict Al Qaroot *et al* (2014), who investigated the anode heel effect on radiation dose and image quality for lateral lumbar spine. They recommend positioning the feet toward cathode, depending on the number of suitable quality images acquired with a low E in relation to each heel orientation. Optimising the anode heel effect using E would ignore the impact of the X-ray intensity variation on the organs doses, and therefore on the risk estimation (E) (Huda, 2010). This is because estimating E is always based on the measured IAK at the centre of the X-ray beam, where the intensity is 100% compared with either side. This therefore makes comparison difficult in term of radiation dose since no gonads doses measurements were considered when there could be a possibility for gonadal doses reduction, and then the rsik, while still obtaining an acceptable quality radiograph when feet placed toward anode, even with lateral lumbar spine.

Another contradiction was found between the results of this thesis and Mearon & Brennan (2006), who investigated the possibility of image quality improvement during thoracic spine radiography in relation to the heel effect. Overall, they recommended positioning the feet towards the cathode rather than the anode, since this *slightly* improves the quality of the images by exposing the thicker anatomic parts to a higher X-ray intensity, compared with the thinner body parts. However, it is difficult to compare this with the recommendations drawn from this thesis for two reasons: 1) their study was conducted using analogue and not digital systems; and 2) they did not consider the effect of the anode heel on radiation dose, rather they based on variation in the intensity of optical density as an indicator for the variation of the X-ray intensity.

This may explain the difference between the two studies, since this thesis focuses on how to reduce radiation dose without compromising image quality (ICRP, 2007a). By way of comparison, researchers were varied in considering the heel effect in different radiographic examination, where some of them have considered only the effect on the dose; others have tested the heel effect on the image quality only without dose measurement. No similar study has been identified in the literature, focusing on the anode heel effect for AP pelvis radiography in terms of both radiation dose and image quality. Overall, the work in the thesis regarding the heel effect has taken all these issues mentioned above into consideration and clear idea about this effect was obtained in term of IQ and dose (i.e. E and gonads doses)

8.2.2.1.2. Main effect (4^3)
The information provided in Figure 7-1 (A, B, C and D) indicates the strength of the effect for each kVp, mAs and SID on the male and female gonad doses. When the feet were placed towards the cathode, the mAs and SID had the highest effect on testicular dose (~75% increase), when compared with kVp, contributing to a dose increase of ~67 % when their settings changed from low to high levels. This could be explained because of the location of the testes. Increasing the tube potential would increase the penetration and reduce photon absorption compared with that of mAs. When mAs increases, it increases the number of X-ray photons, causing a higher absorbed dose; whereas an SID increase causes the dose to reduce resulting from the reduction in the X-rays intensity (Carroll, 2011; Graham, Cloke, & Vosper, 2011; Martin, 2007).

In contrast, the effect of increasing the kVp on ovarian dose was a higher dose change (~91% increase) when compared with mAs. This could also still be considered higher with an ~82% increase when going from low to high mAs levels. The reason for this could be the depth of ovaries within the body, making increasing the mAs less effective compared with increasing the kVp. Increasing the kVp means increasing the penetrating power and the number of photons which will reach the ovaries, whereas increasing the photon number by doing the same to the mAs would be partially minimised by the overlapping tissues' attenuation (Martin, 2007).

The effects of kVp and mAs on male and female gonad doses when the feet were placed towards the anode (low intensity) were closely comparable to their effects when feet placed toward the cathode (see above). The effect of the SID was nearly comparable on male and female gonad doses and for both feet orientations at around 39.5 SD 0.02% (dose decrement) when the settings changed from low to high. The result of investigating the effect of kVp on male and female gonad doses is supported by Fung and Gilboy, as they obtained similar findings for chest radiography (Fung & Gilboy, 2001). However, the results of this thesis differ slightly with the results from Fauber *et al.,* (Fauber, Cohen, & Dem psey 2011), and the reason may be because they adopted the kVp-mAs 15% rule, meaning that increasing the kVp would reduce testes dose. To illustrate, in Fauber *et al.* (2011) the highest kVp was associated with a very low mAs (e.g. 3.2) and this, of course, drops the dose, even at higher kVp levels.

Regarding the main effect on the IQ, figure 7-2 (A and B) demonstrates that the kVp had the biggest effect on the IQ for both anode heel orientations, compared with the mAs and SID. Nevertheless, the effect trends in relation to both kVp and mAs levels increase proportionally before levelling off at 80 kVp and 27 mAs. IQ improvement as the kVp increases from 70 to 85

is not controversial since, with high kVp more photons reaching the detector, the amount of noise is reduced. Nevertheless, at a very high kVp, subject contrast reduces due to the low attenuation characteristics of the tissues being imaged (Fauber, 2014, Jessen, 2004). The SID had the least effect on the image quality of AP pelvis radiographs. Clearly, the effect of the SID on reducing the dose is higher than the same effect on the IQ, when settings changed from low to high. This would provide the opportunity to use the SID as a good optimising acquisition factor.

Regarding FOM_{IQ} which based on male gonad doses, figure 7-3 (A and C) demonstrates that the SID had the highest effect on the FOM_{IQ} compared with the mAs and kVp effects. This can be explained by the SID change causing the testicular dose to change markedly (reduce) compared with the small IQ change. This then caused the FOM to be influenced, along with the percentage change for both orientations (SID~59% and 49% versus kVp ~19% and 17%) when the settings changed from low to high. In contrast, for female FOM_{IQ}, the kVp had the biggest effect by a factor of ~ 1.5 (decrease), whereas both the mAs and SID had comparable effects on the FOM trends by a factor of ~ 1.4 for both orientations. The explanation for this is related to the ovary location (depth) compared with male gonads, which are exposed. Figure 7-3 (A, B, C and D) provides useful information on how to manipulate/set the kVp, mAs and SID to obtain the highest optimisation index (FOM=IQ/Dose) for males and females, and for both phantom orientations. The FOM_{IQ} trends are consistent with the literature (Williams, Hackney, Hogg, & Szczepura, 2014; Tapiovaara, 1993). Finally, adjusting the feet of the male patient to be towards the anode provides a free-cost strategy for optimising AP pelvis imaging.

8.2.2.2. Focal spot size

8.2.2.2.1. Optimum technique
The results from this experiment demonstrate that there is no statistically significant difference ($p>0.05$) in image quality scores for the images acquired at both focal spot sizes, using the range of kVp, mAs and SID combinations, and fixed secondary acquisitions in accordance to the CEC Guidelines (CEC, 1996). The results agree with similar studies which investigated the effect of using broad and fine focal spots on image quality for lateral lumbar, thoracic, ankle, knee and hand examinations (Al Qaroot, Hogg, Twiste, & Howard, 2014; Gorham & Brennan, 2010; Ma, Hogg, & Norton, 2014). However, the DAP recordings from this thesis appear to contradict Al Qaroot *et al* (2014), who reported a marginal decrease in the DAP values with the broad focus compared with that of the fine (no statistical evidence provided). The results do agree with Gorham & Brennan (2010), who found no implications for radiation dose with either focal spot sizes. It is theoretically proposed that, when using a fine focal spot, anatomical details are better visualised (geometric unsharpness) compared with using a broad focal spot (Bushong, 2013; Carlton & Adler, 2013). Findings from this thesis, however, demonstrated that there is no difference in the visualisation of the anatomical details when a fine focus is used. This could be attributed to the large anatomical structures being imaged with AP pelvis radiography. Therefore, this may support the argument that considers the focal spot as a geometric factor and not necessarily as an image quality factor, since it does not affect image contrast (Katz & Nickoloff, 1993& Carroll, 2007).

Exposure time was found to be significantly lower with broad focal spots when compared with that of fine focus (P<0.05). This finding agreed with Al Qaroot *et al* (2014). Long exposure times with fine focus could generate two issues: 1) shorten the tube life and 2) permit motion blur (Ball & Price, 1995; Gorham & Brennan, 2010). Setting the broad focus for AP pelvis radiography would appear to be the best option.

8.2.2.2.2. Main effect (4³)

From figure 7-4 (A and B), the kVp had the biggest effect on E (~85% increase) when settings changed from low to high levels (for both foci), when compared with the mAs and SID; the mAs is ranked second place in terms of its effect on E (~76% increase). The reason for these high effects for both the kVp and mAs is that, as the kVp increases the amount of photons reaching the internal organs increases, causes the E to increases. Nevertheless, the relationship between kVp and E is not linear, especially for the high kVp values due to the high penetration and lower absorption of the photons by tissues (Bushong, 2013). Increasing the mAs causes an increase in photon absorption by the tissue, and this linearly increased the E. The SID effect was the least influential and was inversely related to E, in accordance with the inverse square law (~26% decrease). The SID effect includes reducing the amount of X-rays reaching the tissues (Dowsett, Kenny, & Johnston, 2006).

Regarding the effect on IQ, the kVp had the biggest effect on the IQ for the broad and fine spot sizes (~29 and ~34%, respectively), whereas the mAs caused a ~ 23 and 30 % change in the IQ for the range of settings. The explanation for this is that increasing the kVp would increase the photons reaching the detector which, in turn, increases the amount of information (signal); increasing the mAs contributes to IQ improvement by increasing photon density and, therefore, reducing the noise. The SID increment reduces the X-ray intensity, which leads to an increase in the noise and a reduction in the IQ, but the magnitude of the SID's effect on the IQ is less than the effects of corresponding kVp and mAs. Similar findings in relation to the effects of mAs and kVp on the IQ were found by Ma, Hogg, & Norton, 2014 using both foci.

Finally, for broad focus, the kVp and mAs had similar effects on FOM_{IQ} as seen in figure 7-6 A; they both caused the FOM_{IQ} to decrease by factor of ~1.4. The SID had the least effect on the FOM_{IQ} when the settings changed from low to high levels. For the fine focus, the effect of the kVp on the FOM_{IQ} appears to be slightly higher than the mAs effect (i.e kVp, by factor of ~1.4; mAs, by factor of ~ 1.3); this could be due to the high exposure time (and low mA) set by the machine itself with the fine focus. The highest FOM_{IQ} at low kVp and mAs (e.g. at 18mAs & 70kVp) and high SID (e.g. at 115 cm) is attributed to the lowest dose alongside acceptable image quality score, reflecting the highest optimisation index at these settings.

8.2.2.3. Tube filtration optimisation

8.2.2.3.1. Optimum technique

The main contribution of added filtration is the elimination of the low energy photons (<50 kev) and an increase in the mean beam energy. This could provide the option of reducing the radiation dose but may potentially reduce image contrast. The results from this thesis demonstrate that the reduction (%) in E when comparing the inherent to 0.2 mm of the added Cu filtration was around

50%. Nevertheless, the reduction percentage reached in E when compared with the E from the inherent to that of the 0.2 mm Cu filtration was ~ 0.44 % (see table 7-3). This would reflect a considerable dose reduction, especially when compared with the average adult AP pelvis E (0.7mSv), giving a ~92% reduction in E. On the other hand, the common concern with added filtration is that it affects the image quality, since hardening the beam could reduce the contrast (Jangland & Axelsso, 1990). Perceptual image quality assessments as based on APPS within this thesis show that, for all filtration types, there were a range of images that were classified as suitable or high quality and were acquired at a wide range of acquisition factors. In this experiment, all acquisitions, other than the filters, were kept the same. Testing the statistical difference of the IQ across all filter types demonstrated that there was no statistical difference in IQ scores (P>0.05). In addition, conducting an ANOVA (with Bonferroni correction) test, assuming the known groups, showed the same results (not statistically significant, P=0.375). Although no previous study has been published to optimise AP pelvis imaging using added filtration, the results from this thesis agreed with previous studies that investigated the significance impact of different filtration types on image quality and dose. These include Lehnert *et al* (2011), who undertook their investigation on cadaveric images using DR, and different filtration, using radiologists to scores the images; Hamer *et al* (2005), who concluded equivalent quality images were acquired before and after adding an 0.3mm Cu filter, but with 45 and 55% dose reduction. Others have identified that with 0.1 mm of added Cu filter using CR, the CNR was the highest across different kVp settings in relation to different anatomical structures (Moore, Beavis, & Saunderson, 2008). Hånsson *et al* (1997) found that using 0.3 mm of added Cu filter did not significantly deteriorate the image quality of paediatric images, but were associated with a 44% dose reduction. Nevertheless, they did note a partially negative effect on the signal to noise ratio.

On the other hand, it is expected that using added filtration could cause a reduction in the photon intensity which would necessitate an increase in the mAs to compensate. This issue could cause an increase in tube loading and reduced the tube life (Jessen, 2004). Observations in this thesis show that photon reduction did not make a difference in the visibility of the anatomical structures within images that scored as suitable or high quality. Nevertheless, in certain images with slightly had higher noise levels the contrast was also high and the images were acceptable for answering the primary clinical question, similar findings have been seen in literature (Kohn, Gooch, & Keller, 1988; Behrmana, 2003). In this thesis, the increase in the noise due to added filtration was noticed through SNR. This was evidenced by the reduction in the SNR (16.5%) when comparing the SNR of the images acquired with an inherent filter to those acquired with a 0.2 mm Cu filter. However, this reduction percentage in the SNR (inherent/0.2 mm Cu filter) could not deteriorate the visibility of the image details, as evidenced by the APPS scores (Hånsson *et al*, 1997).

Regarding the tube loading in this experiment, the same combination settings of the kVp, mAs and SID were used; and the optimised settings that led to suitable quality images (table 7-3) across all filtration options included 18 mAs meaning that the possibility of acquiring optimised images with a low mAs is possible (Behrmana, 2003). Nevertheless, if added filtration reduces patient radiation risk, then the resultant additional tube loading or images obtained with a

marginally higher noise level could be justified. The results of this thesis should encourage using added filtration with special attention given to the 0.2 mm Cu filter for adult AP pelvis radiography considering the existence of the superficial radiosensitive organs within the field of radiation (Brosi *et al*, 2011). Finally, added filtration introduces a considerable strategy for optimising the AP pelvis examination, taking into account the availability of this option in almost every modern imaging system (Martin, 2007).

8.2.2.3.2. Main effect (4^3)

The information provided in figure 7-7 (A, B C and D) reveals that the kVp had the highest effect on the E, whereas the SID had the least for all filtration types when settings changed from low to high levels. It is clear that the effect of kVp on E increases as the filtration thickness increases (from 86% for inherent to 102% for 0.2 mm Cu). The reason for this is that added filtration causes the X-ray beam to harden, increasing its mean energy; this is reflected in the beam's ability to penetrate deeper into the body. This results in an increased organ dose and, therefore, increased E. The mAs had the second highest impact on the E by an average of a ~ 76% ±2 increment for all types of filtration. These findings coincide with previous publications (Norrma & Persliden, 2005).

The main effect of the kVp on IQ with all filtration types was highest compared with the relevant effect of the mAs and SID when setting changed from low to high levels. In this context, the kVp caused an average increase in the IQ of ~40% ± 3 for 2 mm Al, 0.1 mm Cu and 0.2 mm Cu filter types, whereas the kVp caused a ~27 % change in the IQ with inherent filtration. In contrast, the mAs caused an average change in the IQ of a ~25 ± 1.5% increment, when setting changed from low to high levels. The reason for this is that the kVp influences the quality and quantity of the X-ray beam, whereas the mAs only affects the quantity of the beam (Dowsett, Kenny, & Johnston, 2006; Bushong, 2013). The effect of the SID on IQ with 0.2 mm of added Cu filtration was comparable (or slightly higher) at ~24 % to that of the mAs; this could be attributed to the effect of the SID on photon intensity as well as the effect already caused by 0.2 mm Cu filtration which was reflected in the noise level (IQ) of the acquired images as the SID settings changed from lower to higher levels.

Concerning the kVp, mAs and SID effects on the FOM_{IQ}, Figure 7-9 (A, B, C and D) demonstrates that the kVp and mAs had the highest effects on the FOM_{IQ} compared with the effect caused by SID for all filtration types when their settings changed from low to high levels. Nevertheless, the kVp effect on FOM_{IQ} at 0.2 mm Cu was slightly higher compared with other filtration types (caused ~39% decrement). The reason for this could be that the kVp with 0.2 mm Cu filtration had the biggest impact on the E and IQ compared with others factors which, in turn, caused this level of effect. In contrast, the SID had no effect on FOM when using 0.2 mm Cu filtration. The FOM_{IQ} was not numerically different when compared with previous experiments, meaning that the highest FOM_{IQ} set was achieved at the lowest kVp and mAs settings (e.g. 70kVp). This agrees with the existing literature since the contrast is high at lower a kVp against a low E and vice versa (Martin 2007; Geijer, Norrman, & Persliden, 2009).

8.2.3. Step 3: Optimising the AP pelvis using an extended factorial settings of kVp, mAs and SID (Secondary acquisition factors fixed at their optimised settings – stage 1, step 2)

8.2.3.1. Optimum technique

The results of this experiment led to the identification of the optimum (final) technique, associated with suitable image quality and a lower radiation dose image when compared with all optimised images from the experiments using manual mode (see table 4-7). Nevertheless, the number of optimised images acquired with kVp settings lower than the minimum (e.g. <70 kVp) identified in Stage 1, Step 1 was relatively low. This can be attributed to the low penetration power associated with 60 and 65 kVp, limiting the photons' passage through the thick pelvis and onto the image detector. The main characteristic of these images was the high noise level; and this reduces the amount diagnostic information, perhaps leading to the necessity of a repeat examination. The high noise level was also evidenced by low the SNR, measured at around 15. These findings agree with Al Qaroot *et al* (2014), who optimised the lumbar spine using a similar optimisation framework; and Al Khalifah & Brindhaban (2004), who investigated the levels of kVp and mAs and how they limit image quality. Some researchers have recommended administering kVp levels lower than 70kVp, arguing they will result in better image contrast (Geijer, Norrman, & Persliden, 2009); although this contradicts the observations of this thesis, it could be difficult to make a practical comparison due to the 0.2 mm Cu filtration used in the experiments' already contributing to the reduction of photon intensity.

On the other hand, a wide range of optimised images were acquired with the kVp and mAs settings higher than the maximum limits established in Stage 1, Step 1 (>85 kVp). The reason for this is the wide dynamic range of the image detector and the ability of CR to correct for 'exposure errors' (Al Khalifah & Brindhaban, 2004; Bushong, 2013). In this context, the results of this thesis agree with the previous recommendations regarding the use of high kVp, together with added filtration, as an approach for achieving a good optimisation outcome (Lu, *et al*, 2003; Jessen, 2004).

With respect to the low mAs setting (<18 mAs), the results of this thesis demonstrate that few images were acquired with suitable quality at an mAs setting of 10. Nevertheless, these images had a relatively high kVp, agreeing with Brindhaban and Al Khalifah, (2005) who found that imposing a limit of 5 mAs can still create images of acceptable quality, but with a lower dose. In contrast, the images that were acquired with 60 kVp in this thesis, even with a high mAs, were not scored as suitable.

The general impact of SID on image quality and radiation dose was clear. The standard of information acquired from the images with different SIDs suggests that this parameter has little effect on image quality. This is in stark contrast to the effect of SID on the radiation dose. Although the amount of noise in an image increases along with the SID's increase from 95 to 130 cm, this did not have a significant effect on the trabecular details of bone structures, this observation can be supported by the exiting literature (Graham, Cloke, & Vosper, 2011; Tingberg *et al.,* 2002). This could be attributed to the penetration power of the X-ray beam in its being able to reach the image detector, even with a high SID. The radiation dose was significantly reduced by ~56% when the SID increased from 95 cm to 130 cm (p<0.05). By

contrast, no significant difference was found in the perceptual image quality scores across all SIDs (p>0.05). These results agree favourably with Al Qaroot *et al* (2014), who found a marked dose reduction when the SID increased from 100 cm to 130 cm without affecting the image quality. Findings from this thesis also are in agreement with the works of Brennan *et al* (2004), Heath *et al* (2011), Grondin *et al* (2004) and Joyce *et al* (2013) who found dose reductions of 33%, 16.4%, 77.6% and 23.9% when the SID was increased to 150 cm. The differences in dose reduction percentage (i.e. range from 16.4 to 77.6%) seen in previous literature may be attributed to different factors. For example, these include the type of radiographic examination (e.g. skull), study design (using AEC or manual modes) and availability of the space required to set different SID such 140 and 150 cm. Nevertheless, these four studies identified that this dose reduction did not significantly compromise the image quality. A key variation between the mentioned studies and this thesis may be attributed to the framework, dosimetry and imaging system used.

Concerning the issue of grid cutoff, the highest SID used in this thesis (130 cm) was within the focal range of the current Bucky table and, as such, no gridline marks were seen. As such, no deterioration of image quality was apparent due to grid cut-off in this study, which is consistent with the findings of other researchers (Joyce, McEntee, Brennan, & O'Leary, 2013). However, it should be acknowledged that gridlines cutoff testing, when the SID goes beyond the focal range, was conducted subjectively by the researcher (e.g. visualisation). Visual testing in fact may not be as reliable as testing grid cutoff using a physical measurement established for this purpose (BIR, 2001).

Finally, using a high SID (e.g. 130 cm), together with a 0.2 mm added Cu filtration, could provide an effective strategy for radiation dose reduction, whilst maintaining the diagnostic quality of the acquired images (see figure 8-1). Figure 8-1 is the final optimised image produced with suitable quality and had the lowest possible radiation dose amongst all the optimised images from the experiments using the manual mode. Therefore, it can help to describe the optimised practice of the AP pelvis radiography using manual mode. Such a strategy could introduce a reduction of around 90% in radiation dose when compared with the average reported effective dose (0.7 mSv) for adult AP pelvis in the UK (Wall & Hart, 1997). Therefore, it could be stated that the factorial framework used within this thesis is likely to succeed in achieving the ALARA principle for dose and image quality optimisation.
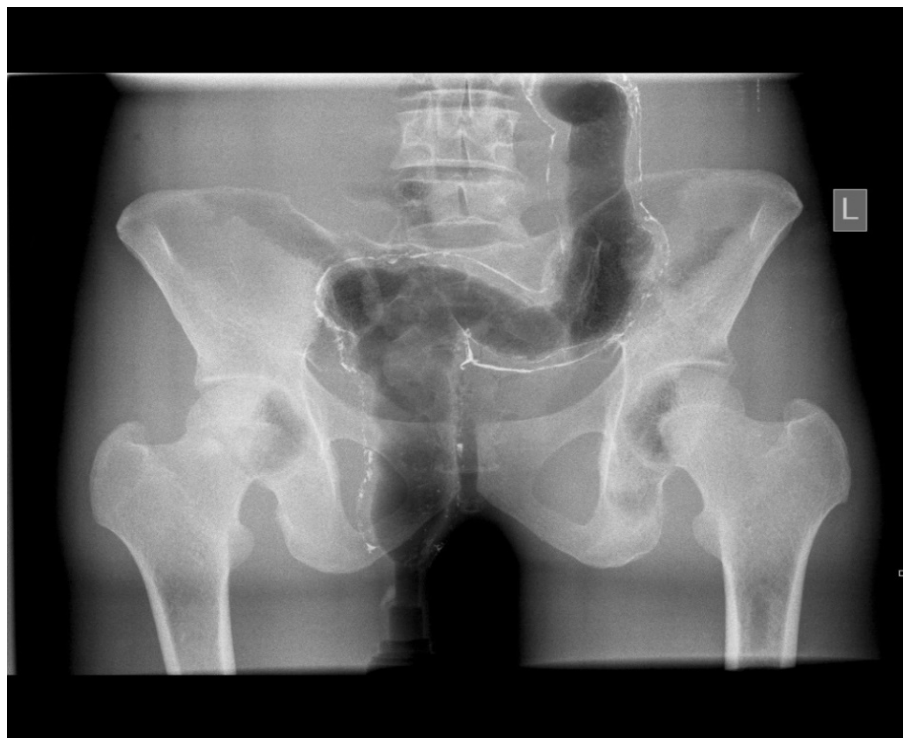
Figure 8-1. This shows the final optimised AP pelvis radiograph acquired using 0.2mm Cu filter, with feet facing toward the anode, 80 kVp, 18mAs and 130 cm SID. This image was acquired with suitable image quality and the lowest radiation dose compared with all the images acquired from the other experiments which used the manual technique. The quality of this image could be reduced due to printing and compression processes made for it to be included in the word document.

8.2.3.2. Main effect (4^3)

The main effect analysis demonstrated that the kVp had the highest effect on the E by factor of ~ 7 when settings changed from 60 to 95 kVp. In contrast, the mAs and SID caused the E trend to alter by factor of ~4 and ~2.25 across the given ranges (figure7-10). These results agree with Norman et al (2005), who identified that the kVp can cause an average increase in E by 8 times its original value. The biggest effect caused by kVp on the E accounted for the photons' high mean energy which increases the organ dose and, in turn, the E. This is especially the case when an added filter is in use (Bushong, 2013). Additionally, kVp increase causes an increase almost proportional to the quantity of X-ray photons, contributing to an increase in radiation dose. However, if the kVp setting increases to a level higher than 95 kVp, a decrease in the E could be seen due to low energy absorption by organs (Carlton & Adler, 2013).

Concerning the main effect on the perceptual IQ, the kVp and mAs had the highest impact on both IQ and SNR (Figure 7-11 A and B); they caused increase in the IQ trend by a factor of ~1.7 and ~1.5 when their settings changed from low to high, whereas their effects on the SNR were by factor of ~1.8 and ~1.5 across the same range. These results agree with Al Khalifah and Brindhaban (2004) who investigated the effect on image quality of varying the kVp and mAs of the AP pelvis radiographs, using CR. The key differences between the results from this this thesis and those of their publication could be attributed to the adapted factorial design, the

phantom orientation and the beam filtration. Positioning the feet toward the anode could result in maintenance of suitable image quality, as, when the kVp and mAs increased, the lower X-ray intensity was directed towards the thinner part of the pelvis as opposed to the thicker abdominal section. Nevertheless, the IQ and SNR trends appear to level off at 90kVp and 36 mAs. This could indicate that, for higher kVps and mAs', the IQ no longer improves alongside an increase in the radiation dose. This is concurrent with the final conclusion made by Al Khalifah and Brindhaban (2004).

On the other hand, the results of this thesis slightly contradict the general understanding that using a high kVp reduces image contrast (McEntee, Brennan, & Connor, 2004). This argument could be true for analogue radiography, but not necessarily digital, because digital systems have a wide dynamic range, and the system automatically corrects exposure error. Thus, the effects of kVp on IQ and SNR described in this thesis contradict Sandborg *et al* (2006), who found that as the kVp increases, both the IQ and SNR decrease for AP pelvis. To illustrate this, in Sandborg *et al* work as the kVp increases from 50 to 110, both the IQ score and the SNR value decrease proportionately from +1.4 to -1.5 (IQ), and from 60 to around 20 (SNR) respectively. By contrast, in this thesis kVp increase from 60 to 95 causes the IQ and SNR to increase proportionately from 2.3 to 3.6 (IQ) and from 18 to 32 (SNR) respectively. The reason behind this difference was that Sandborg *et al* changed the kVp but kept the same E by adjusting the mAs. By contrast, in this thesis, the E was not fixed and the dose varied according to the factorial design. An agreement can be found with Brindhaban, *et al* (2005) regarding the relationship between kVp and IQ, however, the results from this thesis contradict Brindhaban *et al*., (2005) with regard to kVp and the effect on SNR. They found that, as the kVp increases and the mAs decreases (15% kVp rule), the SNR and CNR decrease. This could be attributed to the high kVp already used (e.g. 81 to 105 kVp) which associated with very low mAs, namely 5 and 6.3 (i.e. high noise), compared with the broader kVp range used in this thesis (e.g. 60 to 95).

The SID had the smallest effect on the IQ and SNR compared with that of the kVp and mAs. However, the SID effect on SNR was clearly higher than that on the IQ. This can be explained by the sensitivity of the SNR measure to the variation in noise at a pixel level indeterminable to the human eye (Tugwell *et al.,* 2014).

Figure 7-12 (A and B) demonstrates that the kVp had the biggest impact on both FOM_{IQ} and FOM_{SNR} when its setting was changed from low to high levels. The main effects of each of the mAs and SID on both FOMs were comparable, but with different trends' directions. This suggests that the mAs caused a decrease in the FOMs, whereas the SID led to an increase. A reasonable explanation for this could be that the kVp affects both the quantity and quality of an X-ray beam, therefore, increasing the kVp does result in an IQ increase at a given range, but with a higher radiation dose. The mAs and SID do affect the IQ, but at smaller levels compared with the kVp, since they almost only influence photon intensity (Bushong, 2013 & Carlton & Adler, 2013). Taking this information into account, the optimisation of the X-ray practice in digital imaging necessitates special consideration. To illustrate, one should consider the effects of the acquisition factors in producing images with suitable quality for diagnostic purposes, whilst keeping the dose at the lowest possible level. There was a much agreement in the literature for

setting a low tube voltage, with this leading to good image contrast with a low E. The explanation for this is that, with a low kVp, the penetrating power of the X-rays will be lower, leading to a reduced organ dose and a lesser E (McEntee, Brennan, & Connor, 2004; Geijer, Norrman, & Persliden, 2009). This argument can be supported by the high detector efficiency in digital technology (compared with analogue) which requires a low kVp for photo-electric interaction to occur. Also, the K-absorption edge of a digital detector is 34 keV, compared with 55keV for film materials (Lança & Silva, 2008). The results from this thesis regarding FOMs also reflect this; in all experiments the highest FOM was at the lowest kVp, mAs and highest SID setting, and the reverse is also true. Observations from this thesis on the FOM trend in relation to the kVp agreed with Sandborg *et a*l (2006) who found that, at low kVp settings (e.g. 50), the FOM was highest for AP pelvis. Similarly, both Martin (2007) and Dobbins III *et al* (2003), in their experiments on chest imaging, found that, at low kVp (e.g.60), the FOM_{SNR} was highest, and decreased as the kVp increased.

The systematic investigations from this thesis provided useful information regarding the trends of perceptual and physical measures of image quality in relation to E. They indicate how image quality proportionally increases along with the radiation dose (ICRP, 2004). Accordingly, this would confirm two facts: first, that the dynamic range of the CR detector accommodates high exposure without any detriment to the IQ of the AP pelvis radiographs (Brindhaban & Al Khalifah, 2005); and second, after certain levels of E, image quality ceases to improve. This helps to confirm the phenomenon of *dose creep*, and warrants need for continuous work to the find the best optimisation framework that would reduce the dose whilst keeping the images within a diagnostically acceptable range. The results also coincide with previous studies on dose creep, using CR, by Freedman, *et al* (1993), and, more recently, by Gibson & Davidson (2012) and Ma *et al* (2013), who all identified that patient radiation dose can be inadvertently increased without compromising the IQ.

8.3. Stage 2: Optimising the AP pelvis radiography using AEC mode

8.3.1. Step 1: Creating the Basic Factorial Set of kVp and SID Combinations

As mentioned earlier, the 64 combinations of kVp and SID (mAs was excluded for AEC mode) covered a wide range of settings, making it possible to optimise different technical and procedural conditions for AP pelvis radiography using in an AEC mode.

8.3.2. Step 2: Phantom orientation optimisation (AEC)

4.3.2.1. Optimum technique
The results of this experiment showed that an overall reduction in E by 25% was achieved when the phantom was oriented caudally (P<0.05); and a 35 % dose reduction was seen in relation to the optimised images identified earlier (table 7-5). A reasonable explanation for this dose reduction could be due to the targeted area's anatomy requiring less radiation exposure in order to reach the 2 outer chambers when using the caudal orientation, compared with the cranial. With caudal orientation, the time of the exposure was reduced due to the aforementioned reason, compared with cranial orientation which causes the beams to encounter thick bone structures (Carroll, 2007). Results from this study agree with Manning-Stanley *et al* (2012), who

investigated the phantom orientation impact on the radiation dose and image quality of AP pelvis radiography using AEC mode. However, results from this thesis contradict Manning-Stanley's work in terms of IQ, being that new results displayed a slight increase in the IQ scores and SNR (mean IQ 3.13 SD 0.13 vs. 2.8 SD 0.16, P<0.05; mean SNR 37 SD 4.6 vs. 34.5 SD 4.7, P<0.05) with the caudal orientation. This difference could be attributed to the single combination setting of kVp and SID, *small phantom size* (i.e. around 18 cm thickness compared to 24 cm thickness of current phantom) and visual grading system which was used by Manning-Stanley *et al* (2012) work. Also, the results from this thesis compare favourably with Harding *et al.* (2014) who investigated the effect of patient orientation on radiation dose and IQ. They reported a significant dose reduction of 38 % for CR when the patient was oriented caudally without having any effect on the IQ.

These results relate well to this thesis' previous investigations into the *anode heel effect*, supporting its recommendation. Accordingly, caudally orienting the phantom with AEC would contribute to a reduction in both E and gonadal doses without a compromise in the IQ.

4.3.2.2. Main effect (8^2)

The results demonstrate that the change in kVp from 60 to 95 kVp caused a decrease in E by a factor of ~2.2 (caudal) and 2.4 (cranial). However, the SID effect on E, when the settings changed from 95 to 130, was comparable, and was lower than the kVp effect on E for both orientations by a factor of ~1.53 (caudal) and 1.45 (cranial) (figure 7-14). The reason for the highest effect of the kVp on E is that in the AEC mode, the exposure time and, thus, the mAs are dependent on the kVp and beam centring. Increasing the kVp leads to a reduction in exposure time which, in turn, diminishes the mAs and therefore the E; the opposite is also true (Carrol, 2011). In contrast, the SID affects the intensity of the photons but does not affect the penetrating power of the beam needed to reach the AEC chambers, compared with kVp. These findings agree with Norman and Persliden who investigated the increase of kVp on E and air kerma, using a factorial design. In addition, results from this thesis agree with Lança *et al.* (2014) who found that increasing the kVp (from 60 to 120), using AEC, decreased the E for AP pelvis. Regarding the SID effect, Tugwell *et al.* (2014) demonstrated that, as the SID increased (from 90 to 140 cm) the E decreased accordingly, in the same manner as is seen in this thesis.

The kVp had the biggest effect on the IQ for both orientations; when this setting changed from 60 to 95 kVp it caused a decrease in the IQ by a factor of ~ 1.5 (~34%) for both orientations. The reason for this decrease is that, as the kVp increases, the mAs automatically decreases causing a heightening in the noise level (figure 7-15 A and B). These findings agree with Lança *et al.* (2014) who found that, as kVp increases from 60 to 120, a decrease in the IQ of AP pelvis radiographs occurs. Little effect is caused by the SID change (95 to 130cm) on the IQ (figure 7-15 A and B), when compared with the kVp effect. In this context, Tugwell *et al.* (2014) also found little effect for the SID on the IQ of the AP pelvis radiographs, favourably supporting the results from this thesis.

Finally, the results demonstrate that the main effect trends of the kVp and SID on FOM_{IQ} were opposite to the manual mode, similar trends were found by Norrma & Persliden (2005). For instance, as the kVp and SID settings changed from low to high levels, the FOMs increases. This

is because, with high kVp (low mAs) and SID, the radiation dose is low, which causes FOM_{IQ} to be high with an acceptable IQ. Nevertheless, the SID appears to have a comparable effect to kVp on the FOM_{IQ}, with caudal orientation, whereas the kVp had the highest impact on FOM for the cranial orientations (figure 7-16 A and B). The FOM_{IQ} trends were slightly different for both orientations in relation to the kVp and SID, as illustrated in figure 7-16 (A and B).

8.3.3. Step 3: Optimising chamber selection configurations (AEC)

8.3.3.1. Optimum technique
In general, the results demonstrated that, for all chamber configurations, images with suitable quality in relation to the reference images were generated. However, with the 2 outer chamber configuration, the reduction in E was significantly lower than for single chamber (P<0.05), and slightly lower than for the all chamber (P=0.052). This reduction in E was 23%, 10 % lower than single and all chamber configurations. The lowest radiation dose with the 2 outer chambers could be attributed to the nature of the targeted anatomy, as that the 2 outer chambers are located laterally to the sacrum and inferior to the centring point (off-centred). This would require a lower radiation dose for the AEC to terminate the exposure. By contrast, when all chambers or the single central chamber is in use, the centre chamber will be located over the sacrum, requiring a higher radiation exposure to terminate (Manning-Stanley, Ward, & England, 2012).

The IQ scores for the 2 outer chambers and all chambers configurations were higher than the IQ scores for the single chamber configuration (P<0.05). These results support the findings from Manning-Stanley *et al.*, who, in 2012, found that a two outer chamber configuration could reduce the radiation dose by 44% in relation to other the AEC configurations. The results from this thesis also strongly agree with Hawking and Elmore (2009), who similarly investigated chamber configuration's effect on radiation dose and IQ using a similar pelvis phantom and CR system. They found that, with a 2 outer chamber configuration, the radiation dose reduced significantly without affecting the IQ, compared with the single chamber which had the highest dose and lowest image quality. For this thesis, the overall mean SNR was comparable across all chamber configurations (i.e. single chamber, 34.5 SD 4.9; 2 outer chambers, 33.7 SD 4.8; all chambers, 33.8 SD 4.0 respectively); this could be due to the AEC's automatic compensation.

8.3.3.2. Main effect (8^2)
The main effects of the kVp and SID on E (see figure 7-17 A, B and C) demonstrate that the kVp had the biggest impact on E across all chamber configurations, compared with SID. For example, when kVp settings changed from 60 to 95 kVp, E decreased by a factor of ~2.4, whereas the SID caused a decrease in E by a factor of ~1.5 when it changed from 95 to 130 cm. The effect trends of kVp and SID on E were opposite to the manual mode due to the automatic AEC compensation. This broadly agrees with results obtained by (Norrma & Persliden, 2005).

By contrast, figure 7-18 (A and B) demonstrated that kVp had the biggest effect on IQ compared with that of SID; this was so across all chambers configurations. To illustrate, when the kVp changed from 60 to 95 a decrease in the IQ by factor of ~ 1.5 occurred, whereas, when the SID changed from 95 to 130, cm a decrease in the IQ by factor of ~ 1.12 took place. A decrease in the IQ, as both the kVp and SID increased, is attributed to the high noise level imposed by low mAs,

which is subsequently compensated for by the AEC system (Lança *et al*., 2014). This means that the SNR at high kVp levels could be low, since fewer photons make it to the image receptor. However, the low IQ does not always mean that the quality is not suitable for diagnostic purposes due to CR's dynamic range and system processing (Moore *et al*., 2014).

The trends of the effects of the kVp and SID on FOM_{IQ} appear similar, except at the 2 outer chamber configurations, where the kVp effect seems to be marginally higher than the SID, for same configuration. Nevertheless, the lowest FOM_{IQ} was at the lowest kVp (e.g.60), whereas the highest FOM_{IQ} was varied across different chamber configurations, however it was relatively high with high kVp and SID settings. The fluctuation in the FOM_{IQ} at high kVp and SID values could be attributed to the variations imposed by AEC chambers, when they responded to different beam quality caused by the different combination settings and chamber configurations (Mazzocchi *et al*., 2005).

8.3.4. Step 4: Optimising of focal spot and filtration using AEC (Phantom orientation and chamber configuration fixed at their optimised settings, Step 2 and 3)

8.3.4.1. Focal spot (AEC)

8.3.4.1.1. Optimum technique
The results of this experiment demonstrate the range of optimised images that can be acquired with both focal spot sizes, in relation to the reference image. The image with the lowest radiation dose and suitable image quality was acquired with the broad focal spot (table 7-7). Nevertheless, the results on E for both focal spot sizes demonstrate that there was no statistical difference between the two (*broad*: 0.126 SD 0.041 vs. *fine*: 0.127 SD 0.040, P>0.05). This means that, according to the results of this thesis, choosing either focal spot would have no implications on the radiation dose. These results agree with Gorham and Brennan (2010), who compared the two focal spot sizes in terms of radiation dose and image quality using manual mode. Physical measures of image quality were comparable for both the broad and fine focal spot sizes, indicating that the detector received a similar number of photons across the range of combinations settings (*broad*: 33.5 SD 4.7 *vs. fine:* 33.9 SD 4.6, P>0.05).

However, the exposure time for fine focus was significantly higher than that of the broad focus (i.e. *fine* 123 ms SD 86 versus 66 SD 53 ms for *broad*, P<0.001). These results concur with the aforementioned results on focal spot sizes for the manual mode in this thesis, and also with Al Qaroot *et al*., (2014) who found that the exposure time with fine focus was higher than broad focal spot. Long exposure times, regardless of the radiation dose, may lead to patient movement during imaging and, in turn, a diagnostically inapplicable image (Ball & Price, 1995). Additionally, using a fine focal spot would be appropriate for examining extremities, aiming to visualise the fine anatomical details, and this would necessitate a low mAs value, compared with larger body parts. Using a broad focus for pelvis imaging would also reduce the probability of X-ray tube target damage (Ma, Hogg, & Norton, 2014).

8.3.4.1.2. Main effect (8²)
The main effect analysis demonstrated that kVp had the largest effect on E for both focal spot sizes compared with the SID effect. An increase in kVp from 60 to 95 caused a decrease in E by a factor of ~ 2.2, whereas increasing the SID from 95 to 130 cm caused a decrease in the E by a factor of ~ 1.5 (for both foci; figure 7-20 A & B). Once again, the reduction in the E was due to of the lessening of the mAs, as the kVp increased; the reverse is also true.

The kVp's effect on the IQ was largest when compared with the SID effect for both focal spot sizes. As such, when the kVp increased from 60 to 95, the IQ decreased by a factor of ~ 1.6 for the broad focus and by a factor of ~1.5 for the fine focus. However, when the SID settings changed from 95 to 130 cm, the IQ deceased by a factor of ~ 1.1 (figure 7-21 A & B). The slight effect caused by the SID on the IQ, compared with its effect on the E encourages the use of the SID for reducing the radiation dose without adversely affecting the IQ when using AEC. These results agree with Norrma and Persliden (2005) in relation to the E, but contradict them in regards to the IQ. The reason for this contradiction may be due to their having used a test object (CDRAD) rather than anthropomorphic phantom, and thus a fair comparison of IQ between the two experiments is not possible.

The effect of the kVp on FOM_{IQ} for both focal spot sizes was nearly comparable (see figure 7-22 A and B), and slightly higher than the effect of the SID on the same FOM_{IQ}. Generally speaking, the lowest FOM_{IQ} was still at the lowest kVp (e.g.60), as, with this, the mAs was very high due to the AEC compensation. Similarly, the lowest FOM_{IQ} was at the lowest SID, since the radiation dose, even with AEC, would be high, even at a small SID; whereas, at a high SID, the dose would be lowest and the quality could still be diagnostically acceptable.

8.3.4.2. Tube filtration (AEC)

8.3.4.2.1. Optimum technique
The results demonstrated that, when using 0.2 mm of added Cu filter, a significant reduction in the E (16% less) can be obtained when compared with inherent filtration (P<0.05). However, no significant reduction in E was found between inherent, and the other types of filtration (P>0.05). The perceptual assessment of image quality demonstrated that there was a range of suitable quality images across all filtration types. Nevertheless, the mean IQ scores marginally reduced as the filter thickness increased. However, this did not adversely affect the visualisation of the anatomical structures in the AP pelvis radiographs, as was evidenced by individual item scores on the APPS scale. This makes the 0.2 mm of added Cu filter a viable option for optimising AP pelvis examination when using an AEC (table 7-8). The relevant physical measures of the image quality show that, as the filter thickness increases, the SNR increases slightly, when compared with inherent filtration. This change in SNR may be attributable to the AEC's automatic compensation, to ensure an adequate number of photons reach the image detector, and to the increase in penetration power of the X-ray beam imposed by the added filtration. These results agree favourably with Norman and President (2005), who investigated how added filtration, together with AEC, could affect image quality and radiation dose. However, their investigation was based on a test object (CDRAD), making comparison difficult in regards to IQ. Lehnert *et*

al (2011) also found a similar trend in perceptual image quality scores when compared to the results in this thesis, but used DR.

In summary, using 0.2 mm of added Cu filter during AP pelvis radiography with AEC mode can provide a significant reduction in radiation dose, without adversely affecting image quality. Specifically, this would be most effective, based on this thesis' empirical data, with an 80 to 85 kVp range (table7-8). This method, in turn, led to the optimum image produced, having suitable image quality alongside the lowest radiation dose using AEC mode (see figure 8-2). The radiograph in figure 8-2 shows the result of the optimum practice for AP pelvis radiography when AEC is used.
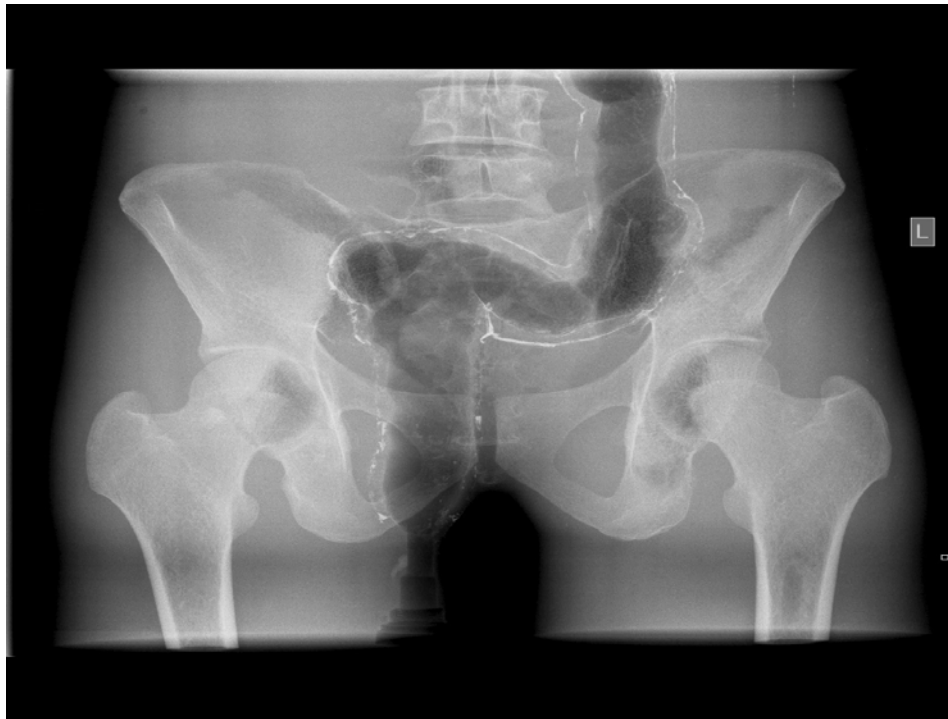
Figure 8-2. This shows the final optimised AP pelvis radiograph acquired using a 0.2mm Cu filter, feet facing caudally with two outer chambers, 80 kVp, and 125cm SID. This image was acquired with the lowest dose for acceptable image quality from all the AEC images. The quality of this image could be reduced due to the printing and compression processes made for it to be included in the word document.

8.3.4.2.2. Main effect (8^2)

Figure 7-23 (A, B, C, and D) demonstrates that kVp had the biggest effect on E, compared with SID, when settings changed from low to high levels, across all filtration types. Increasing the kVp from 60 to 95 caused a decrease in the E by a factor of ~ 2.2, 2.2, 2.1 and 2 in relation to the inherent, 2 mm Cu, 0.1 mm Cu and 0.2 mm Cu filters. This reduction in E is explained by the decrease in mAs as the kVp increased. Nevertheless, the kVp effect for the 0.2mm of added Cu filtration was slightly lower compared with other filter types due to the high penetration power the photons had with a thicker filter suggesting, that, as the penetration power increases, the energy deposition within the organs tissues decreases (Martin, 2007, Brosi *et al*, 2011). The SID

increased from 95 to 130 cm, causing a decrease in the E by a factor of ~ 1.5 for all filtration types.

The trends of the effect of both kVp and SID (figure 7-24 A, B, C and D) on the perceptual IQ demonstrate that kVp had the largest effect, when settings changed from low to high levels. To illustrate, when the kVp settings changed from 60 to 95, a decrease in IQ was seen by factors of ~1.5, 1.8, 1.8 and 1.65 in relation to the inherent, 2 mm Al, 0.1mm Cu and 0.2mm Cu filters, respectively. However, as the SID increased from 95 to 130 cm, it caused a decrease in IQ by a factor of 1.1 across all filtrations. This decrease in IQ can be explained by the increase in noise caused by the low mAs, set to compensate for the high kVp. Once again, the trend of the effect for kVp when using 0.2 mm Cu of added filtration was slightly lower in relation to the other filter types, due to the beam hardening imposed by 0.2 mm Cu. In contrast, the trends of the SID's effect on IQ were very low, especially with added filtration, since beam hardening increases mean energy, enabling the photons to reach the detector irrespective of the SID. Consequently, this again makes SID a practical option for radiation dose image quality optimisation, even with AEC mode.

From figure 7-25 (A, B, C and D) the trends for kVp effct on FOM_{IQ} appear to be marginally larger than that of the SID, in relation to the inherent and 2 mm Al filtration. In contrast, the effects of kVp and SID on FOM_{IQ} were closely comparable with the 0.1 and 0.2 mm Cu filter types; this may be attributed to the subsequent AEC compensation across different settings, and heavy beam hardening. The lowest FOM_{IQ} was at the lowest kVp and SID, due to the higher radiation dose, whereas it was highest at around 75 and 80 kVp when the E was reasonably low with an acceptable IQ. Also, at kVp values above 80, the FOM_{IQ} begins to level off, or decrease, depending on the filter type. In relation to SID, the almost peak in FOM_{IQ} was at higher SID settings across all filtration types.

Figure 7-26 (A, B, C and D) illustrates the effect of kVp and SID on the FOM, based on the SNR. For the inherent and 2 mm Al filter types, the SID appears to have a marginally larger effect on FOM_{SNR} compared with the kVp effect when the AEC is in use. However, their effects on FOM_{SNR} were comparable with fluctuations (peaks and troughs) when the settings changed from low to high levels (Ullman, Sandborg, Dance, Hunt, & Carlsson, 2004). This may be attributable to the sensitivity of the SNR to small variations in the image grey scale levels, which were caused by different beam quality. The FOM_{SNR} gives an idea as to how the system performs in relation to different combination settings, when both the AEC and different added filtrations are in use. Overall, the best system performance appears to coincide with FOM_{IQ} trends for AP pelvis imaging using AEC and added filtration, falling at low kVp settings and peaking at the high ones.

Figure 7-27 (A and B) shows the relationship between the image quality (perceptual and physical) and the radiation dose when AEC is switched on. Similar to manual mode, image quality increases proportionately to the radiation dose, which characterises the wide dynamic range of the CR detector (ICRP, 2004). This, therefore, means that, even with AEC, image quality will not be affected in the same manner as analogue radiography when the radiation dose rises; this feature has been identified previously as dose creep (Willis & Slovis, 2005). To

overcome this, imaging professionals need to be aware of at what level the radiation dose is lowest whilst still being acceptable for diagnosis (Matthews & Brennan, 2009). The suitability of an image for AP pelvis radiography using AEC is of less concern compared with manual mode, because of the automatic compensation imposed by its chambers. Nevertheless, this thesis could provide useful guidelines on how different techniques (kVp and chamber selection) may ensure that the best possible optimisation procedure can be achieved.

8.4. Image post processing testing

The results of image post processing demonstrate that there was a limited improvement in the overall image quality of the images scored as unsuitable. Nevertheless, improvement among individual scale items was seen especially for those representing gross anatomical structures (e.g. iliac crest), or those did not include overlapping anatomy (e.g. lesser trochanters). The latter could be useful when the clinical quisition is focused to a specific region or a body part within the AP pelvis radiograph. However, for the purpose of this thesis, the overall image quality, which means an adequate visualisation of all anatomical structures, is essential. There are two reasons for this specification of overall image quality: 1) no clinical question is specified in this thesis; and 2) its purpose is to systematically investigate the applicability of the proposed framework in reducing the radiation dose whilst maintaining the suitability of the image quality. On the other hand, little improvement in image quality may be attributed to the noise level of the unsuitable images; as a result of which, any further image enhancement is difficult (Decoster, Mol, & Smits, 2015). Moreover, insufficient exposure may cause fewer pixels to be exposed adequately and give it a grey level value, which may therefore limit the post-processing options available to just manipulating the image brightness and contrast (Carrol, 2011; Shephard, 2003). The results in this thesis agree with Al Qaroot *et al.* (2012) who investigated the effect of post processing manipulation on those images that scored as an unacceptable. However, other studies have found that image manipulation using different post processing algorithms can improve the image quality (Freedman & Steller, 1995; Norrman, Geijer, & Persliden, 2007; Wiltz, Petersen, & Axelsson, 2005). The resulted improvement includes either individual anatomical structures or overall image quality. The difference between this thesis finding and others may be attributed to the sufficient exposure the images in those studies had which makes pixels value (i.e. grey level) to be manipulated positively. Overall, the post processing technique can be best utilised to manipulate the quality of images that have sufficient exposure levels; this, therefore, made it less adequate for improving the overall image quality of the lower scoring images in this thesis.

8.5. Image quality assessment approaches (Correlation)

The results demonstrate that there was a positive correlation (P<0.001) between the perceptual (APPS based) and the physical (SNR based) measures of image quality (table 7-9) across the different experiments in this thesis. The strength of this correlation was higher with manual mode than AEC mode, and may be attributed to the AEC's automatic compensation that makes the SNR values across different images (different combination settings) similar to one another (high sensitivity); whereas, the relevant IQ scores varied in relation to the different exposure settings, since the evaluation was based on human vision, which is likely to be less sensitive than mathematical measures (SNR). As a result, less association occurred between the two measures of the image quality compared with manual mode. Such an agreement between these measures

would be interesting for '*evaluating and predicting*' system performance, and its ability to depict clinical images using the physical measure only (Sund, Båth, Kheddache, & Månsson, 2004).

The results in this thesis agree strongly with Sandborg, *et al*. (2006), who compared the physical measures (SNR) and clinical assessment (VGA) of image quality for AP pelvis and PA chest. In their study, they calculated the average SNR from different ROIs in the AP pelvis radiograph. These ROIs were taken from the European Guidelines criteria (CEC, 1996), whereas the VGA scores were obtained from averaging the radiologist scores (from a panel of 6) of the AP pelvis criteria. Ultimately, they found a positive correlation between the clinical and physical assessments (pelvis: r^2=0.94; chest: r^2=0.91). Sandborg *et al*. (2001) also noticed a statistically significant correlation between the clinical assessments (VGAS) obtained from a panel of radiologists using EC criteria, and the physical measure (SNR) in their study on chest and lumbar spine. They finally concluded that the appropriate physical measurement, in some cases, can be used to '*predict'* the clinical image quality.

Others have found a significant correlation between the clinical assessment of the image quality (VGAS) and physical measures (e.g. CNR) (Crop *et al*., 2012; Moore, Wood, Beavis, & Saunderson, 2013). Crop *et al*., (2012) used the CDRAD test object for physical measures and VGA to assess cadaver images of a PA chest; the correlation coefficient(r) ranged between 0.8 and 0.92, P<0.01. Moore *et al* adapted the CNR as a physical measure and VGA for clinical assessment. The correlation coefficient(r) was significant at 0.87, P<0.033. Accordingly, such positive correlations may permit the using of the physical measure, if appropriately conducted, to predict the clinical image quality using an anthropomorphic phantom, but maintained that visual assessment is superior in assessing clinical images for a clinical situation (Månsson, 2000; Båth, 2010).

On the other hand, the results of testing the agreement between the two approaches (in relation to the ROIs) to calculate the SNR demonstrate that there was a positive correlation (table 7-10). However, the approach that is based on the local ROI noise to calculate SNR shows lower SNR values when compared with the SNR-based, background noise approach. The reason for this difference is attributable to the variations in noise values across different ROIs of different anatomical structures (Ullman, Sandborg, Dance, Hunt, & Carlsson, 2004), whereas, with the second approach, the noise value was taken from one uniform region, as recommended by Dobbins (2000), to calculate the average SNR. Practically, the local noise-based SNR could be useful for comparing the quality of different images obtained from the same imaging system. In contrast, an alternative approach may permit the comparison of the results from a given system, with other systems taken into account, to compare the signal from any ROI to its relevant background; this shows the subject contrast of an image and, therefore, a generalisation of the results would be possible (Bryan, 2010). Some researchers adapted the local-based SNR calculation (Brindhaban, Al Khalifah, Al Wathiqi, & Al Ostath, 2005; Luz & Hoff, 2010), whereas others adopted the background noise-based SNR (Chotas, Floyd, Dobbins III, & Ravin, 1993; Tapiovaara, 1993). Overall, to be able to compare the SNR results from any optimisation work with that of others, the SNR based on background noise is most appropriate.

8.6. Implication of the factorial design in radiation protection

This sub-section outlines the implications of the factorial design used in this thesis, for the optimisation of the radiation protection in digital radiography. The results of this thesis demonstrate that this experimental design is robust enough to optimise X-ray practice. Factorial design is an efficient approach when an experiment includes multiple factors, and one or more response variables. As such, this design would allow for the studying of the effect of each factor, or a combination of factors, on the response variable(s) systematically. Also, it states whether the effect of any factor on the response variable is statistically significant, or not, using an ANOVA analysis (Montgomery, 2013). Reflecting on the methods used within this thesis, there are many acquisition factors which need consideration for their ability to optimise the radiation dose and image quality systematically. The focus was on the kVp, mAs and SID, since they were included in the factorial design. To illustrate, the factorial design served this thesis in two ways:

First, it provided the experiments with the combinations of settings, generated systematically from the acquisition factors and their relevant levels. Doing this ensured that the possibility of obtaining suitable quality image(s) with the lowest possible radiation dose was increased, since a wide range of diagnostic combination settings were used to generate the X-ray images. These combinations were balanced between the levels of the factors. Through this process, a clear idea of the effect of these interactions between acquisition factors on image quality and radiation dose was obtained. The practical evidence of the factorial interaction was most noticeable in the optimum techniques that resulted in suitable quality images with a considerable reduction in E, compared with the adult average value of E for AP pelvis (Sherer, Visconti, Ritenour, & Haynes, 2014). This outcome could be expected, since the experiments were conducted in a structured manner, taking into account the effect of all acquisition factors on the response variable(s). In addition, the experiments were conducted using a full factorial design, meaning there were 3 factors set at 4 and 8 different levels individually. This yielded statistically powerful numbers of combination of settings between the kVp, mAs and SID, allowing rigorous statistical analyses to take place (Wise, Sandborg, Persliden, & Carlsson, 1999). This option, overall, overcame the drawbacks attributed to using one factor at a time when optimising (Matthews & Brennan, 2009).

Secondly, the factorial design permits the exploration of the main effect of each individual factor on the response variable(s), using a systematic approach. Our results demonstrate that the main effect analysis was an efficient approach to providing a trend that works both ways in medical imaging; these ways include its representing a normal trend through which one can see how varying a single factor influences the response variable, and, most interestingly, its being able to explore the strength of each factor on the outcome measure. The factor strength can be measured by comparing the drawn points on the Y-axis (means) to the reference line (grand mean). As such, for the radiation dose and image quality graphs, the steeper the trend's gradient is the stronger the effect of the given factor on a given response variable (Norrma & Persliden, 2005; Lesik, 2010). By contrast, the closer the trend (or drawn points) is/are to the reference line, the lesser the effect of the factor on the response variable. The main effect analysis is systematically conducted via the following process: a factor is varied from one level to another (e.g. 70 to 85 kVp) causing the settings (levels) of the others to change accordingly; this allows a systematic evaluation of the effect of each factor. This therefore provides an efficient way to study the main

effect without ignoring the relevant impact of the corresponding factors (e.g. mAs and SID). To illustrate, varying one factor, whilst fixing others, results in incomplete idea on the actual effect of that factor; this argument could be evidenced by the fact that, in medical imaging, the kVp, mAs and SID play a reciprocal role on radiation dose and image quality (Jessen, 2004 & Carlton & Adler, 2013). Apart from investigating the main effect of the kVp, mAs and SID individually, this thesis provides an opportunity to broadly studying the effect of different sets of secondary acquisition factors (e.g. phantom orientations). Finally, it should be noted that the main effect was, for the first time in medical imaging (digital), studied using multiple factors, and more than two levels for each of these factors (e.g. 4 and 8 levels).

The results from the factorial experiment, on the other hand, are supportive of the current body of knowledge found within the literature. This, in turn, provides another scientific recommendation for the factorial design's value as an efficient framework for radiation protection and image optimisation. To illustrate, the trends of the effect of the kVp and mAs on E, when their settings change from low levels to high, show that the E increased proportionally when both the kVp and mAs do too, in manual mode. This is a well-known fact, which characterises the kVp and mAs' impact on radiation dose (Martin, Sutton, & Sharp, 1999 & Bushong, 2013). As such, increasing the kVp increases the penetration power and, therefore, the organ doses; whereas, increasing the mAs would increase the number of photons absorbed by body tissue. Both of these ultimately increase the E (Tingberg & Sjöström, 2005). In contrast, their effect on image quality scores were in broad agreement with what has already been established in existing literature, in relation to the range of settings, particularly in digital imaging. For instance, kVp and mAs increase cause a rise in IQ, since both of these factors clearly influence the noise level of the images, and therefore the contrast (Brindhaban, Al Khalifah, Al Wathiqi, & Al Ostath, 2005; Tingberg & Sjöström, 2005; Martin, 2007). The amount of noise is inversely proportional to image contrast; by contrast, the effects of the acquisition factors on the SNR were similar to that on the IQ, but with some exceptions which are attributable to the high sensitivity of the SNR to radiation exposure. However, the trend of the SID effect on radiation dose and IQ was inverse when compared with the effect of the kVp and mAs, since the SID variation influences the X-ray intensity.

Interestingly, the effects of the kVp, mA and SID on both FOMs (which based on IQ and SNR) are also in agreement with what has been mentioned in the literature. For instance, the highest FOM was at the lowest kVp and mAs settings, and the highest SID settings. As was mentioned earlier, this indicates the best optimisation index since, at these settings, the dose is lowest alongside a high image quality score (Williams, Hackney, Hogg, & Szczepura, 2014). On the other hand, with the AEC mode, the effect trends of the acquisition factors (kVp and SID) were the reverse, compared with manual mode. The reasons for the opposite trends can be attributed to the automatic compensation sets done by the AEC chambers (Norrma & Persliden, 2005). Consequently, the information provided by the main effect analysis would help professionals in manipulating the acquisition factors in a manner that could optimise the X-ray practice, taking into account their impacts on dose and image quality.

ICRP publications concerning the optimisation of protection recommend the need to search for a framework that can produce images with suitable quality and the lowest possible radiation dose (ICRP, 1991; 2007a). This recommendation has been translated into a considerable body of research to optimise different radiologic examinations. However, a common feature of the previously used frameworks was to manipulate one factor at time. Adopting this approach overlooks the *combined effect* of the acquisition factors on radiation dose and image quality (Wise, Sandborg, Persliden & Carlsson, 1999; Lesik, 2010). Therefore, the difference in the percentages of dose reduction achieved in this thesis compared with that of others was high, yet image quality was still maintained. For example, a radiation dose of up to 80 to 90 % less than the average E of the adult AP pelvis was reached in the identified optimum technique. By contrast, the average dose reduction reached by other researchers was up to 50 % (Matthews & Brennan, 2009; Seeram, Davidson, Bushong, & Swan, 2013). The percent of dose reduction reached in this thesis can be attributed to the *combined effects* of the prime acquisition factors, together with the possible effect of secondary acquisition factors. The immediate manipulation of multiple factors could not have been achieved systematically without the factorial design (Mathews, 2005). Overall, this factorial manipulation introduces an efficient and systematic framework to optimise any X-ray practice.

Chapter 9: Conclusion

This chapter presents the final conclusions that were obtained from section I, and then an overall conclusion regarding the optimisation of the AP pelvis practice for both the manual and AEC modes, using the novel visual image quality assessment scale (APPS). A statement of novelty, and recommendations for future work, will also be presented.

From section I of this thesis, it was established that a dearth of validated visual grading scales for image quality assessment exists within the literature. Many researchers rely on the EC criteria; however, even at the time of publication, these criteria had deficiencies. Almost no validation data exists within the literature about image visual quality criteria performance. In section I of this thesis, the psychometric theory was identified to be a robust, theoretical foundation on which to begin the procedure of scale development and validation. Accordingly, a theoretical framework was created to successfully develop and validate a visual grading scale for assessing the perception of image quality. The created scale was reduced using factor and item analysis (Appendix V).

The 24-item scale displays a high level of internal reliability and validity. The findings suggest that the scale is almost entirely focused on how clearly the anatomical structures can be visualised; this was because a large proportion of variance was explained by those that include anatomical related items. In addition, evidence was found to support the scale's ability to assess quality in relation to technical parameters (i.e. other than anatomical). According to this analysis, and significant agreement between subjective and objective measures for the two phases of scale validation, the scale could be utilised to assess the perception of the quality of AP pelvis using both a phantom, and in a clinical situation. As a result, the scale was used to visually assess the quality of the acquired images for the purpose of optimising AP pelvis radiographic practice in this thesis. Also, the novel approach used here to develop the AP pelvis visual image quality assessment scale could be used to develop another scale for other radiographic examinations. Further work on this scale is necessary to further assess its validity.

Section II of this thesis was conducted using a factorial, experimental design to optimise AP pelvis imaging, according to the ALARA, and using CR and an anthropomorphic phantom. The major objectives of this research were to investigate whether adopting this kind of experimental design would be efficient to systematically optimise radiation dose and image quality, taking into account the combined effect of all the primary acquisition factors. One way that was used to do this was through identifying the optimum combined settings that could produce suitable quality images with the lowest possible radiation dose (E or organ dose). In this context, the suitability of image quality was determined visually in relation to the visualisation of the scale items (as weighted by the reference images), and physically so through SNR (threshold SNR value >5). The second essential investigation using the factorial approach was to identify the strength of each of the primary acquisition factors (the main effect) on dose, image quality and FOM, since this would help discover how to manipulate the acquisition factors systematically to optimise the X-ray practice.

For manual, AP pelvis radiographic examinations, the optimised radiographic practice was with 80 kVp, 18 mAs, 130 cm SID, 0.2 mm Cu added filter, with feet positioned toward anode, and a broad focal spot. From this thesis, the associated E was 0.04 mSv; by this level of E, a 94 % dose reduction was achieved when compared with the UK and International reference value for the average adult AP pelvis E, which is 0.7 mSv (Wall & Hart, 1997; Sherer, Visconti, Ritenour, & Haynes, 2014 & UNSCEAR, 2010). By comparing this value of E (0.04 mSv) with the optimised radiographic image's E (0.088 mSv), acquired using inherent filtration, there was a 54% dose reduction. Further to the percentage reduction in the E, the optimised radiographic practice lead to a testicular dose reduction, which came from positioning the feet towards the anode, compared with positioning the feet toward the cathode. Having recognised earlier that there was no significant difference between the ovarian doses, in regards to the anode heel effect, it may simply be appropriate to adopt the optimised practice for both genders.

From this study, the kVp appeared to have the biggest impact on the E, image quality and FOMs when its settings change from low to high levels across different technical and procedural conditions when using the manual mode. The mAs was found to be the second most influential acquisition factor, and SID, the least effective factor on the image quality. However, it should be noted that mAs had the biggest effect on the testicular dose when compared with the kVp. By contrast, kVp had the largest effect on the ovarian dose. Overall, these effects were almost significant (P<0.001) in regards to the response variables, except for some situations wherein the SID effect on image quality scores was not notable (P>0.001).

For the AEC mode, the recommended optimised radiographic practice from this thesis is 80 kVp, 125 cm SID, two outer chambers, phantom oriented caudally, a broad focal spot and a 0.2mm Cu added filter. The associated E was 0.08 mSv, giving a 88 % dose reduction, compared with the average adult AP pelvis E of 0.7 mSv used in the UK and internationally as a reference value (Wall & Hart, 1997; Sherer, Visconti, Ritenour, & Haynes, 2014 & UNSCEAR, 2010). Comparing this value of E (0.08 mSv) with the optimised radiographic image E acquired using inherent filtration in this thesis (0.093 mSv), there was a 14% dose reduction.

In this section, the kVp appeared to have the biggest effect on the E, image quality and FOMs when its settings change from low to high levels, compared with the SID. Thus, the factorial method was successful in considerably reducing the radiation dose, whilst maintaining suitable image quality. Also, it was efficient in exploring the main effects of the primary acquisition factors on IQ, E and FOMs, especially when more than 2 levels for each of the acquisition factors were used (manual mode: 4^3, 8^3 & AEC mode: 8^2). The factorial method proved effective for AP pelvis radiography, and therefore should also be considered for the systematic optimisation of other radiographic examinations. Finally, in order to confirm the results obtained from this study regarding dose reduction and image quality level, the identified optimum techniques (final) for both manual and AEC modes should be further investigated by the conducting of a clinical study involving cadavers before being directly applied into the patients. For this to be achieved, taking into account a range of the optimised combination settings (i.e. those that their corresponding dose up to 75% less that 0.7 mSv), further to those identified in the final optimum techniques, would be recommended in order to cover the numerous variations

imposed by patient body size and other factors that have not been taken into consideration in this phantom-based study.

9.1. Statement of novelty

The main novel contributions of this PhD thesis are summarised below:

1. Creating a method to develop and validate an image quality visual grading scale.

2. Developing and validating an AP pelvis image quality visual grading scale.

3. Using the validated visual grading scale to visually assess image quality.

3. Developing a factorial method to systematically optimise image quality and radiation dose for AP pelvis practice, taking into account all the primary and secondary acquisition factors.

4. The multifactorial optimisation procedure producing images with suitable image quality and significantly reducing the dose (i.e. 88% for AEC mode and 94% for manual mode), compared to average adult AP pelvis examinations (0.7 mSv).

5. The full reporting of a wide range of acquisition factor combination settings that can be considered as standards for determining future imaging protocols.

6. Exploring the main effect (strength) of the primary acquisition factors on the radiation dose, image quality (physical and clinical) and figure of merit for the first time, using 4 and 8 levels and a human-simulated, anthropomorphic phantom.

9.2. Summary of study limitations

This thesis includes several limitations, as outlined below:

9.2.1. Limitations associated with section I of this thesis:

The image acquisition for the some of the validation work involved a single phantom. The phantom was of a fixed size and did not have any anatomical or pathological variants. As such, this could limit some of the validation work. However, to compensate, there was a section of the validation which used images produced from human cadavers. Even so, human cadavers introduce some limitations, such as their fixed positions and radiographic appearances which may have resulted from their being dead, as such things are not typically seen on images from live participants.

The sample size of participants could be regarded as an issue for limitation. Increasing the sample size would provide results which are more representative of the intended population. However, there was a relatively large sample size used within the validation experiments. Similar studies have used comparable sample sizes, and within this work numerous attempts were made to increase the number of participants, such as the recruitment of volunteers from overseas. However, critics could comment on the use of undergraduate radiography students, though it is likely that this aspect of the study would have produced little variation in the results;

the reason for this is that all participants received detailed training and participant information literature. Students, as well as qualified radiographers, routinely undertake image appraisal and thus were both adequate for the tasks required of them in this study. Also, it should be acknowledged that for those volunteers recruited from other EU institutions, different Radiography programmes may cause some variation when compared with the student's radiographer studying at the UOS.

9.2.2. Limitations associated with section II of this thesis

Being that there were many limitations within this section, it would be most helpful to indicate them in a numbered list:

1. Using a phantom (containing barium) to acquire the images for the optimisation procedure did raise some issues. As previously stated, the phantom lacks anatomical and pathological variation, and is at a set size. Using cadavers or live patients/participants could have provided a more valid result, however, there would numerous ethical and logistical challenges with such an approach.

2. The optimisation procedure was conducted using only computed radiography (CR). It is likely that this study would be more valuable if direct digital radiography (DR) was also used, since this is the current dominant system within the clinical environment. At the start of this thesis, CR was the only acquisition modality available at the local institution. Many sites still have only CR systems, and thus these results will be highly useful for such places.

3. All the primary acquisition factors were optimised in this study; however, several other factors, such as exposure index and system speed, were not optimised, as there was not enough time.

4. The optimisation procedures for AP pelvis projection made use of an antiscatter radiation grid throughout the study; however, no attempt was made to consider using non-grid techniques. Supporting this decision is that the current literature supports the widespread use of grids for AP pelvis examinations and reflects current clinical practice.

5. The organs doses measured in this study were only for gonads using TLDs; it may have been more practical for other organs doses to be measured directly (e.g. colon, liver….etc.), instead of relying solely on the effective dose. It may also be possible that certain acquisition factor combinations may deliver lower organ doses, and this may have clinical utility.

6. The main dosimetry method was based on effective dose (mSv). However, more recent evidence has suggested that effective risk is a more useful indication of the radiation exposure from an examination. Data from this study could be used as a model for assessing the effective risk, and thus provides a pillar for future work.

7. The physical assessment of image quality was based on SNR values only. SNR is highly useful as a measure of image quality, however, it would have been useful to consider including

other metrics, such as CNR. CNR values, if calculated, may be more difficult to interpret, because there are no formal baseline values which suggest suitable image quality.

9.3. Future work

1. Conduct the same optimisation procedure using direct digital radiography (DR) and single phantom or different phantoms of different sizes.

2. Study the effect of optimisation on the detection of pathology using a ROC approach (including pathologies, e.g. subtle hip fractures). This can be done by inserting a simulating lesion(s) in the phantom or in the images and then applying the same protocols of optimisation to see how could this affect the image quality and therefore detection performance.

3. Use the methodology for scale development and validation to create other image quality visual grading scales, such as a generic radiographic image scale. However, in this case it is best to recruit qualified radiographers for better sample representation and to lessen the variation that might rise from sample with different groups' levels.

5. Consider the secondary acquisition factors (anode heel effect) within the factorial design to clearly investigate the combined effect of the primary and secondary acquisitions on image quality and radiation dose.

6. It is highly recommended that data from this thesis (i.e. optimum techniques) whether those which were identified as final optimum techniques or those which were identified through different experiments to be tested/verified first by conducting cadaver based experiments before being directly applied into the patients. This can be done by taking a range of optimised techniques which their dose reduction % reached upto 75 % compared with 0.7 mSv (*italicised within appendices*) average adult effective dose for AP pelvis radiography. The justification for latter recommendation is because the experiments in this thesis were conducted using a single phantom and this may not necessarily reflect the real situation in term of anatomical variations and clinical questions.

Appendices

Appendix I: University of Salford ethical approval

5 February 2013

Dear Hussien,

RE: ETHICS APPLICATION HSCR12/83 – Optimisation of image quality and radiation dose for AP pelvis radiographic examinations

Following your responses to the Panel's queries, based on the information you provided, I am pleased to inform you that application HSCR12/83 has now been approved.

If there are any changes to the project and/ or its methodology, please inform the Panel as soon as possible.

Yours sincerely,

Rachel Shuttleworth

Rachel Shuttleworth
College Support Officer (R&I)

6 November 2013

Dear Hussien,

RE: ETHICS APPLICATION HSCR13/44 – Optimisation of image quality and radiation dose for AP pelvis radiographic examinations

Based on the information you provided, I am pleased to inform you that application HSCR13/44 has now been approved.

If there are any changes to the project and/ or its methodology, please inform the Panel as soon as possible.

Yours sincerely,

Rachel Shuttleworth

Rachel Shuttleworth
College Support Officer (R&I)

Appendix II: Ethical approval provided by Human Ethics Committee of the Canton de Vaud (Switzerland)

Arbeitsgemeinschaft der Schweizerischen Forschungs-Ethikkommissionen für klinische Versuche
Communauté de travail des Commissions d'éthique de la recherche en Suisse

**Commission cantonale d'éthique
de la recherche sur l'être humain**
Av. de Chailly 23, 1012 Lausanne

Prof. P. Francioli, Président
Prof. R. Darioli, Past-President

Secrétariat central
Tél. 021 316 18 30/31/32/33
Fax 021 316 18 37
E-mail: secretariat.cer@vd.ch

Sous-Commission I
Sous-Commission II
Sous-Commission III

Prof. Alexandre Dominguez
Prof. HES/S2
HESAV/filière TRM
Bugnon 19/03/333
1011 Lausanne

Lausanne, September 5th, 2013
PF/ns

Protocol 263/13: Optimization of image quality and radiation dose for AP pelvis radiographic examinations

Dear Mr Dominguez,

We confirm that the protocol mentioned above and the documents submitted to the Human Research Ethics Committee of the Canton de Vaud (Switzerland) on June 12th, 2013 have been approved after review by the Board on June 21st, 2013.

Sincerely yours,

Prof. Patrick Francioli
Président

Appendix III: Research participant's consent form

University of
Salford
MANCHESTER

Research Participant (Volunteer) Consent Form

Title of the project: **Optimization of image quality and radiation dose for AP pelvis radiographic examinations.**

RGEC Ref. NO:

Name of Researcher: Hussien Mraity

Please initial box

I confirm that I have read and understand the information sheet for the above study and understand what my contribution will be.

☐

I have the opportunity to ask questions in person (face to face).

☐

I agree to take part in the survey.

☐

I understand that my participation is voluntary and that I am free to withdraw at **any time without giving any reason.**

☐

I agree to take part in the above study.

Name of participant ....

Signature ....

Date ....

Name Of Researcher Taking Consent............................... Hussien Mraity

Appendix IV: AP pelvis image quality assessment draft scale (29 items)

Name: _____

Year (1, 2, or 3): _____

IMAGE SET NO (ie 1-7): _____

Please indicate your level of agreement with each statement by **circling** a response between **1**(strongly disagree) and **5** (strongly agree).

1. The left hip joint is adequately visualised.

1. Strongly disagree   **2. Disagree**   **3. Neither agree or disagree**   **4. Agree**   **5. Strongly agree**

2. The right lesser trochanter is visualized adequately.

1. Strongly disagree   **2. Disagree**   **3. Neither agree or disagree**   **4. Agree**   **5. Strongly agree**

3. The right hip joint is adequately visualised.

1. Strongly disagree   **2. Disagree**   **3. Neither agree or disagree**   **4. Agree**   **5. Strongly agree**

4. The left greater trochanter is visualized adequately.

1. Strongly disagree   **2. Disagree**   **3. Neither agree or disagree**   **4. Agree**   **5. Strongly agree**

5. The left sacro-iliac joint is adequately visualized.

1. Strongly disagree   **2. Disagree**   **3. Neither agree or disagree**   **4. Agree**   **5. Strongly agree**

6. The right sacro-iliac joint is adequately visualized.

1. Strongly disagree   **2. Disagree**   **3. Neither agree or disagree**   **4. Agree**   **5. Strongly agree**

7. The exposure factors used for this image are correct.

1. Strongly disagree   **2. Disagree**   **3. Neither agree or disagree**   **4. Agree**   **5. Strongly agree.**

8. Fine bony detail is insufficiently demonstrated.

1. Strongly disagree   **2. Disagree**   **3. Neither agree or disagree**   **4. Agree**   **5. Strongly agree**

9. The right iliac crest is visualized adequately.

1. Strongly disagree   **2. Disagree**   **3. Neither agree or disagree**   **4. Agree**   **5. Strongly agree**

10. The right greater trochanter is visualized adequately.

1. Strongly disagree   **2. Disagree**   **3. Neither agree or disagree**   **4. Agree**   **5. Strongly agree.**

11. There is appropriate differentiation between soft tissues.

1. Strongly disagree   **2. Disagree**   **3. Neither agree or disagree**   **4. Agree**   **5. Strongly agree**

12. The left iliac crest is visualized adequately.

1. Strongly disagree   **2. Disagree**   **3. Neither agree or disagree**   **4. Agree**   **5. Strongly agree**

13. The left lesser trochanter is visualized adequately.

1. Strongly disagree   **2. Disagree**   **3. Neither agree or disagree**   **4. Agree**   **5. Strongly agree**

14. Both acetabula are visualised clearly

1. Strongly disagree   **2. Disagree**   **3. Neither agree or disagree**   **4. Agree**   **5. Strongly agree**

15. The pubic and ischial rami are not adequately visualized.

1. Strongly disagree   2. Disagree   3. Neither agree or disagree   4. Agree   5. Strongly agree

16. The obturator foramina are symmetrical.

1. Strongly disagree   2. Disagree   3. Neither agree or disagree   4. Agree   5. Strongly agree

17. There is no movement artefact on this image.

1. Strongly disagree   2. Disagree   3. Neither agree or disagree   4. Agree   5. Strongly agree

18. The presence of artefact prevents image quality evaluation.

1. Strongly disagree   2. Disagree   3. Neither agree or disagree   4. Agree   5. Strongly agree

19. The Medial Sagittal Plane of sacrum and coccyx is aligned through the symphysis pubis.

1. Strongly disagree   2. Disagree   3. Neither agree or disagree   4. Agree   5. Strongly agree

20. The levels of rotation and axial tilting are within acceptable limits.

1. Strongly disagree   2. Disagree   3. Neither agree or disagree   4. Agree   5. Strongly agree

21. The body of L5 is adequately demonstrated.

1. Strongly disagree   2. Disagree   3. Neither agree or disagree   4. Agree   5. Strongly agree

22. The medulla and cortex of the pelvis are adequately demonstrated.

1. Strongly disagree   2. Disagree   3. Neither agree or disagree   4. Agree   5. Strongly agree

23. The proximal femora are demonstrated adequately.

1. Strongly disagree   2. Disagree   3. Neither agree or disagree   4. Agree   5. Strongly agree

24. The left femoral neck is visualized adequately.

1. Strongly disagree   2. Disagree   3. Neither agree or disagree   4. Agree   5. Strongly agree

25. There is a significant amount of noise in this image.

1. Strongly disagree   2. Disagree   3. Neither agree or disagree   4. Agree   5. Strongly agree

26. This image is sufficient for diagnostic purposes.

1. Strongly disagree   **2. Disagree**   **3. Neither agree or disagree**   **4. Agree**   **5. Strongly agree**

---

27. The sacrum and its intervertebral foramina are visualized adequately.

1. Strongly disagree   **2. Disagree**   **3. Neither agree or disagree**   **4. Agree**   **5. Strongly agree**

---

28. The right femoral neck is visualized adequately.

1. Strongly disagree   **2. Disagree**   **3. Neither agree or disagree**   **4. Agree**   **5. Strongly agree**

---

29. Bony pelvis and soft tissues cannot be differentiated.

1. Strongly disagree   **2. Disagree**   **3. Neither agree or disagree**   **4. Agree**   **5. Strongly agree**

Appendix V: **AP pelvis scale (APPS)- First 15 items used for 2AFC**

1- The left hip joint is adequately visualised.

2- The right hip joint is adequately visualised.

3- The right lesser trochanter is adequately visualised.

4- The left lesser trochanter is adequately visualised.

5- The left greater trochanter is adequately visualised.

6- The right greater trochanter is adequately visualised.

7-The left iliac crest is adequately visualised.

8- The right iliac crest is adequately visualised.

9- The pubic and ischial rami are adequately visualised.

10- The proximal femora are demonstrated.

11- The left femoral neck is adequately visualised.

12- The right femoral neck is adequately visualised.

13- The left sacro-iliac joint is adequately visualised.

14- The right sacro-iliac joint is adequately visualised.

15- The sacrum and its intervertebral foramina are adequately visualised.

..===.

16-There is appropriate differentiation between soft tissues.

17- The exposure factors used for this image are correct.

18- This image is sufficient for diagnostic purposes.

19- The medulla and cortex of the pelvis are adequately demonstrated.

20- The body of L5 is adequately demonstrated.

21- The obturator foramina are symmetrical.

22- Both acetabula are visualised clearly

23-The levels of rotation and axial tilting are within acceptable limits.

24- Fine bony detail is sufficiently demonstrated.

Appendix VI: QC sheet

	TASKS FOR USING QC DATA AND CALCULATING QC PARAMETERS [FOR RADIOGRAPHY]									
DATA:					X-RAY GENERATOR AND TUBE MEASUREMENTS					
								FDD(cm) =	100	
Focus	Set kV	Set mA	Set Time	Set mAs	Meas kV	Meas T	Meas exp	Air kerma		
	(kV)	(mA)	(ms)	(mAs)	(kV)	(ms)	(mR)	(mGy)		
B	60	200	100	20						
B	80	200	100	20						
B	100	200	100	20						
B	120	200	100	20						
F	50	100	200	20						
F	70	100	200	20						
F	90	100	200	20						
F	110	100	200	20						
B	80	200	100	20						
B	80	200	100	20						
B	80	200	100	20						
B	80	25	100	2.5						
B	80	300	100	30						
B	80	500	100	50						
B	80	200	20	4						
B	80	200	400	80						

	B	80	200	800	160					
	Half Value Layer Measurements are shown below									
	B+0mm Al	80	200	100	20					
	B+0mm Al	80	200	100	20					
	B+1mm Al	80	200	100	20					
	B+2mm Al	80	200	100	20					
	B+3mm Al	80	200	100	20					
	B+4mm Al	80	200	100	20					
	CALCULATE THE FOLLOWING PARAMETRES USING THE DATA FROM THE TABLE									
1	X-ray beam filtration (HVL) - plot the graph									
2	Dose Output Consistency % [100*(st.dev)/(average)] for BF									
3	kVp Consistency % [100*(st.dev)/(average)] for BF									
4	Timer Consistency % [100*(st.dev)/(average)] for BF									
5	kVp accuracy [100*(mean error)/(real value)] for BF and FF									
6	kVp Linearity [plot the graph mGy/mAs against kVp2] for BF and FF									
7	Timer accuracy [100*(mean error)/(real value)] for BF									
8	Dose Output variation with mA [100*st.dev/average] for BF									
9	kVp variation with mA [100*st.dev/average] for BF									

Appendix VII: Quality control (QC) test procedure

Dose

1. Raise the table to a comfortable height and remove the mattress
2. Set source image distance to 100cm using the tape measure.
3. Place detector two in the primary beam and collimate to an area slightly larger than the detector.
4. Switch on the dosemeter and press parameter until "Gy" is displayed on the screen. Press and hold parameter and the dosimeter display should flash.
5. On the control panel select table top and kV and mAs
6. Record the dose for the following exposures.
   a. 60kV 2mAs Fine Focus
   b. 70kV 6.3mAs Fine Focus
   c. 80kV 25mAs Broad Focus
   d. 90kV 50mAs Broad Focus
7. Record the results on the attached sheet and update the Excel spreadsheet
8. Report any results that are outside the indicated tolerances to the RPS.

kV

1. Raise the table to a comfortable height and remove the mattress
2. set source image distance to 100cm
3. Place detector one in the primary beam and collimate to an area slightly larger than the detector.
4. Switch on the dosemeter and press parameter until "kV" is displayed in the screen. Press and hold parameter and the dosimeter display should flash.

5. On the control panel select table top and kV and mAs
6. Set 10mAs
7. Record the kV for the following exposures on broad and fine focus
   a. 60kV
   b. 81kV
   c. 102kV
8. Record the results on the attached sheet and update the Excel spreadsheet
9. Report any results that are outside the indicated tolerances to the RPS.

Time

1. Raise the table to a comfortable height and remove the mattress
2. Set source image distance to 100cm
3. Place detector one in the primary beam and collimate to an area slightly larger than the detector.
4. Switch on the dosemeter and press parameter until "s" is displayed in the screen. Press and hold parameter and the dosimeter display should flash.
5. On the control panel select table top and kV and mA and s
6. Set 70kV, 100mA and broad focus
7. Record the time for the following exposures
   a. 20ms
   b. 50ms
   c. 160ms
   d. 400ms
   e. 1000ms*
   f. 2500ms*
9. Record the results on the attached sheet and update the Excel spreadsheet
10. Report any results that are outside the indicated tolerances to the RPS.

* These are long exposures. Keep the button pressed until exposure terminates.

Light beam diaphragm alignment

1. Raise the table to a comfortable height and remove the mattress.
2. Place a 24x30 cassette on the table in the landscape orientation with the smooth "name area" to the bottom.
3. Set a source to image distance of 100cm.
4. Place the copper collimator test tool centrally over the cassette with the blue dot to your left.
5. Under dimmed lighting, centre and collimate to the 10cm border.
6. Place the Tube alignment test tool over the centre of the copper plate.
7. On the control panel set 50kV, 2mAs and fine focus and make an exposure.
8. WITHOUT MOVING ANY EQUIPMENT… open the collimation fully.
9. Make a second exposure using the same exposure factors.
10. Process the cassette.
11. Repeat the method using broad focus and broad and fine foci on the vertical chest stand.

12. Record the results on the attached sheet and update the Excel spreadsheet
13. Report any results that are +/- 1cm or the ball bearing is outside the centre circles to the RPS.

AEC sensitivity

1. Open the collimators.
2. *Carefully* place the copper filter in the primary beam.
3. Place a 18x24 CR cassette into the Bucky in the portrait orientation and fully close the draw.
4. Centre the X-ray tube and set a source to image distance of 110cm.
5. Select all chambers and make an exposure using 70kV and 80mA.
6. Record the post mAs
7. Record the results on the attached sheet and update the Excel spreadsheet
8. Report any results that are outside the indicated tolerances to the RPS.

AEC Cassette interlocks

1. Select the table bucky
2. Set 70kV, 80mA and all chambers.
3. Without a cassette in the bucky make an exposure
4. The system should not expose and should display an error on the control panel.
5. Report any failure to the RPS.

AEC system feedback

1. Open the collimators.
2. Place the lead filter in the primary beam.
3. Select the chamber 1 and make an exposure using 40kV and 50mA.
4. The generator should terminate the exposure and an error should be indicated on the control panel.
5. Report any failure to the RPS.

AEC Guard timer

1. Open the collimators.
2. Place the lead filter in the primary beam.
3. Select the lateral chambers and make an exposure using 60kV and 50mA Broad focus
4. The guard timer should terminate the exposure and an error should be indicated on the control panel.
5. Repeat for each chamber in the table and vertical bucky.
6. Report any failure of the guard timer to the RPS.

Appendix VIII : **The APPS IQ score, SNR and the associated testicular doses and ovarian doses(mGy) with optimising the anode heel effect** (Feet placed toward cathode)

kVp	mAs	SID	IQ score(SD)	Testes dose (mGy)	Ovaries dose (mGy)	SNR(SD)
70	18	105	2.47(0.52)	1.19	0.21	31.99(1.64)
70	18	110	2.27(0.46)	1.08	0.22	27.58(0.99)
70	18	115	2.40(0.51)	0.79	0.16	29.44(1.33)
70	18	120	2.47(0.52)	0.66	0.13	30.64(1. 58)
70	22	105	2.87(0.35)	1.30	0.24	31.59(1.93)
70	22	110	2.87(0.35)	1.18	0.27	33.26(1.53)
70	22	115	2.53(0.52)	0.95	0.17	26.63(1.22)
70	22	120	2.53(0.52)	0.83	0.15	27.62(1.67)
70	28	105	3.47(0.52)	1.76	0.31	41.28(2.03)
70	28	110	3.00(0.38)	1.61	0.32	33.27(1.55)
70	*28*	*115*	*3.07(0.26)*	*1.27*	0.25	30.36(1.37)
70	28	120	2.73(0.46)	1.09	0.22	30.60(2.04)
70	32	105	3.53(0.64)	1.85	0.37	45.58(1.86)
70	32	110	3.33(0.49)	1.73	0.36	38.11(1.50)
70	*32*	*115*	*3.07(0.26)*	*1.45*	0.24	32.94(1.53)
70	*32*	*120*	*3.07(0.26)*	*1.09*	0.23	34.78(2.02)
75	18	105	3.00(0.00)	1.29	0.28	31.78(1.78)
75	*18*	*110*	*3.07(0.46)*	*1.26*	0.24	31.33(1.16)
75	18	115	2.60(0.51)	0.87	0.21	28.53(1.28)
75	18	120	2.33(0.49)	0.81	0.15	27.03(1.76)
75	22	105	3.60(0.51)	1.65	0.31	37.54(1.66)
75	22	110	3.20(0.56)	1.64	0.32	35.68(1.20)
75	*22*	*115*	*3.40(0.63)*	*1.12*	0.22	34.05(1.12)
75	22	120	2.73(0.46)	0.97	0.19	30.65(1.65)
75	28	105	3.47(0.52)	1.97	0.45	38.16(1.65)
75	28	110	3.87(0.35)	1.74	0.43	40.34(1.57)
75	28	115	3.27(0.46)	1.61	0.30	32.791.55)
75	28	120	2.87(0.35)	1.24	0.24	33.21(2.01)
75	32	105	3.13(0.35)	2.37	0.49	34.27(1.49)
75	32	110	3.67(0.62)	2.01	0.50	36.32(1.26)
75	32	115	3.47(0.52)	1.64	0.36	35.16(1.53)
75	32	120	3.33(0.62)	1.27	0.32	34.80(2.25)
80	18	105	3.40(0.51)	1.57	0.31	33.91(1.62)
80	*18*	*110*	*3.27(0.59)*	*1.22*	0.30	36.81(1.18)
80	*18*	*115*	*3.13(0.52)*	*1.16*	0.26	34.80(1.37)
80	18	120	2.93(0.26)	0.83	0.20	31.74(1.63)

80	22	105	3.80(0.41)	1.93	0.39	43.19(1.64)
80	22	110	3.60(0.51)	1.74	0.39	37.87(1.02)
80	*22*	*115*	*3.40(0.51)*	*1.47*	0.29	32.62(1.41)
80	*22*	*120*	*3.13(0.52)*	*0.99*	0.28	*33.96(1.99)*
80	28	105	3.67(0.49)	2.47	0.47	47.21(1.29)
80	28	110	3.60(0.51)	2.17	0.51	41.90(1.08)
80	28	115	3.27(0.46)	1.70	0.35	35.49(1.46)
80	28	120	3.73(0.46)	1.47	0.32	41.12(1.94)
80	32	105	3.73(0.46)	2.56	0.63	38.48(1.49)
80	32	110	3.40(0.51)	2.38	0.61	36.72(1.06)
80	32	115	3.60(0.51)	1.97	0.43	37.54(1.58)
80	32	120	3.80(0.41)	1.54	0.35	40.00(2.27)
85	18	105	3.33(0.49)	1.77	0.37	36.98(1.26)
85	18	110	3.40(0.51)	1.52	0.42	33.14(0.99)
85	*18*	*115*	*3.13(0.35)*	*1.28*	0.30	31.89(1.36)
85	*18*	*120*	*3.33(0.49)*	*1.01*	0.25	36.46(1.85)
85	22	105	3.33(0.49)	2.43	0.48	39.07(1.50)
85	22	110	3.60(0.51)	2.21	0.47	36.35(1.27)
85	22	115	3.33(0.49)	1.48	0.36	32.63(1.47)
85	*22*	*120*	*3.67(0.49)*	*1.15*	0.30	38.36(1.59)
85	28	105	3.60(0.51)	2.82	0.62	39.48(1.10)
85	28	110	3.87(0.35)	2.70	0.55	39.96(0.97)
85	28	115	3.80(0.41)	2.05	0.45	37.60(1.34
85	28	120	3.87(0.35)	1.52	0.39	39.82(2.11)
85	32	105	3.53(0.74)	3.22	0.74	55.42(0.75)
85	32	110	3.67(0.49)	3.00	0.69	39.19(1.32)
85	32	115	3.87(0.35)	2.22	0.57	42.34(1.78)
85	32	120	3.47(0.52)	1.80	0.38	36.65(2.25)
IQ, image quality score, SD, standard deviation, SNR, signal to noise ratio						

kVp	mAs	SID	IQ score(SD)	Testes dose(mGy)	Ovaries dose(mGy)	SNR(SD)
			Appendix IX : The APPS IQ score, SNR and the associated testicular doses and ovarian doses(mGy) with optimising the anode heel effect (Feet placed toward anode)			
70	18	105	2.27(0.46)	0.78	0.21	33.26(3.91)
70	18	110	2.73(0.46)	0.64	0.15	34.56(3.00)
70	18	115	2.13(0.35)	0.63	0.16	28.62(1.99)
70	18	120	2.33(0.49)	0.48	0.13	29.84(2.32)
70	22	105	2.87(0.35)	0.93	0.26	31.76(3.58)
70	22	110	2.73(0.46)	0.77	0.20	36.45(3.26)
70	22	115	2.27(0.46)	0.73	0.18	31.59(2.45)
70	22	120	2.47(0.52)	0.57	0.15	32.70(1.95)
70	28	105	3.07(0.26)	1.14	0.35	39.50(4.05)
70	28	110	3.40(0.51)	0.93	0.24	40.61(3.33)
70	28	115	3.07(0.26)	0.99	0.24	34.64(2.57)
70	28	120	2.53(0.52)	0.79	0.22	33.93(2.28)
70	32	105	3.13(0.35)	1.30	0.40	39.18(4.08)
70	32	110	3.07(0.46)	1.16	0.31	39.99(3.39)
70	32	115	2.47(0.52)	1.17	0.27	30.62(2.66)
70	32	120	2.80(0.56)	0.83	0.22	34.09(2.20)
75	18	105	3.07(0.26)	1.01	0.25	31.38(3.33)
75	18	110	2.47(0.52)	0.82	0.22	33.35(2.99)
75	18	115	2.53(0.52)	0.78	0.19	34.41(2.54)
75	18	120	2.53(0.52)	0.58	0.15	31.98(2.24)
75	22	105	3.07(0.52)	1.29	0.30	34.67(3.75)
75	22	110	3.20(0.56)	0.95	0.28	37.79(3.36)
75	22	115	3.00(0.56)	0.89	0.24	37.95(2.77)
75	22	120	3.00(0.00)	0.67	0.19	37.77(2.18)
75	28	105	3.40(0.51)	1.52	0.41	41.19(3.98)
75	28	110	3.27(0.46)	1.15	0.32	43.71(3.60)
75	28	115	3.20(0.41)	1.14	0.32	37.00(2.52
75	28	120	2.87(0.35)	0.88	0.25	36.45(2.47)
75	32	105	3.60(0.51)	1.82	0.50	40.96(4.26)
75	32	110	3.20(0.41)	1.27	0.40	41.46(3.44)
75	32	115	3.40(0.51)	1.33	0.34	43.08(2.93)
75	32	120	3.20(0.41)	0.95	0.31	35.24(2.08)
80	18	105	3.27(0.46)	1.10	0.32	38.88(3.92)
80	18	110	3.13(0.35)	0.80	0.26	37.97(2.97)
80	18	115	2.67(0.49)	0.73	0.27	30.01(2.10)
80	18	120	3.00(0.38)	0.65	0.20	35.32(2.34)

80	22	105	3.53(0.52)	1.46	0.38	41.82(4.33)
80	22	110	3.00(0.53)	1.14	0.36	33.59(2.81)
80	*22*	*115*	*3.27(0.46)*	*1.01*	0.32	*42.39(2.78)*
80	*22*	*120*	*3.13(0.35)*	*0.89*	0.27	37.82(2.34)
80	28	105	3.67(0.49)	1.81	0.52	40.71(4.04)
80	28	110	3.53(0.52)	1.34	0.42	40.85(3.86)
80	28	115	3.27(0.46)	1.31	0.42	36.42(2.54)
80	28	120	3.47(0.52)	1.12	0.33	41.48(1.71)
80	32	105	3.53(0.52)	2.12	0.56	38.63(3.95)
80	32	110	3.87(0.35)	1.58	0.44	48.78(3.69)
80	32	115	3.80(0.41)	1.36	0.43	44.39(2.75)
80	32	120	3.13(0.52)	1.23	0.39	42.42(2.25)
85	18	105	3.27(0.46)	1.29	0.41	35.38(3.88)
85	*18*	*110*	*3.27(0.46)*	*0.99*	0.32	*34.17(2.96)*
85	18	115	3.00(0.00)	0.99	0.32	35.96(2.75)
85	18	120	2.93(0.26)	0.79	0.26	36.38(2.89)
85	22	105	3.80(0.41)	1.47	0.51	39.23(4.08)
85	22	110	3.47(0.52)	1.26	0.39	37.98(3.36)
85	22	115	3.13(0.35)	1.20	0.46	38.09(2.58)
85	*22*	*120*	*3.40(0.51)*	*0.99*	0.30	*38.53(2.46)*
85	28	105	3.87(0.35)	1.90	0.63	43.16(4.04)
85	28	110	3.93(0.26)	1.44	0.52	47.74(3.85)
85	28	115	3.73(0.46)	1.77	0.51	43.93(2.88)
85	28	120	3.67(0.49)	1.16	0.40	46.17(2.82)
85	32	105	3.93(0.26)	1.94	0.79	43.06(4.06)
85	32	110	3.80(0.26)	1.73	0.58	37.80(3.08)
85	32	115	3.80(0.41)	1.74	0.56	41.71(3.02)
85	32	120	3.93(0.26)	1.30	0.43	45.69(2.54)
IQ, image quality score, SD, standard deviation, SNR, signal to noise ratio						

Appendix X : APPS IQ score, SNR, time of exposure(s), the associated DAP(mGy.cm^2) and E(mSv) with optimising Broad focal spot

kVp	mAs	SID	IQ score (SD)	E(mSv)	SNR (SD)	Time (ms)	DAP (mGy.cm^2)
70	18	105	2.60(0.51)	0.09	29.82(1.45)	40.00	589.67
70	18	110	2.47(0.52)	0.08	30.16(0.97)	40.00	541.00
70	18	115	2.20(0.41)	0.07	24.98(0.97)	40.00	497.67
70	18	120	2.07(0.26)	0.07	22.88(1.55)	40.00	769.00
70	22	105	3.00(0.00)	0.10	31.48(1.31)	48.89	717.00
70	22	110	3.07(0.26)	0.10	32.15(0.93)	48.89	654.33
70	22	115	2.13(0.35)	0.09	26.01(1.10)	48.89	605.00
70	22	120	2.07(0.26)	0.08	23.39(1.53)	48.89	978.67
70	28	105	3.00(0.00)	0.13	33.39(1.15)	62.22	912.00
70	28	110	3.07(0.46)	0.12	31.30(0.81)	62.22	834.00
70	28	115	3.07(0.46)	0.11	36.471.45)	62.22	765.67
70	28	120	2.27(0.46)	0.10	28.86(1.79)	62.22	1116.33
70	32	105	3.07(0.26)	0.15	37.41(0.78)	71.11	1038.33
70	32	110	3.00(0.00)	0.14	33.04(1.06)	71.11	953.67
70	32	115	2.87(0.35)	0.12	33.36(1.25)	71.11	868.00
70	32	120	2.33(0.49)	0.11	28.91(1.74)	71.11	737.33
75	18	105	3.00(0.00)	0.11	32.31(1.35)	40.00	686.67
75	18	110	2.87(0.35)	0.10	35.15(0.89)	40.00	630.00
75	18	115	3.00(0.00)	0.09	33.08(1.15)	40.00	578.67
75	18	120	2.27(0.46)	0.08	25.70(1.51)	40.00	898.00
75	22	105	3.00(0.00)	0.13	32.37(0.74)	48.89	834.00
75	22	110	3.00(0.00)	0.12	34.24(0.85)	48.89	765.67
75	22	115	2.73(0.46)	0.11	29.71(1.32)	48.89	702.67
75	22	120	2.13(0.35)	0.10	28.01(1.67)	48.89	1142.33
75	28	105	3.07(0.26)	0.17	30.65(0.50)	62.22	1060.00
75	28	110	3.20(0.41)	0.15	33.95(0.88)	62.22	972.67
75	28	115	3.00(0.38)	0.14	31.14(1.47)	62.22	891.33
75	28	120	2.67(0.49)	0.12	33.74(2.00)	62.22	1304.33
75	32	105	3.53(0.52)	0.19	38.58(0.58)	71.11	1209.33
75	32	110	3.47(0.52)	0.18	41.90(0.97)	71.11	1110.00
75	32	115	3.53(0.52)	0.16	37.51(1.40)	71.11	1015.33
75	32	120	3.00(0.53)	0.14	32.57(1.82)	71.11	845.67
80	18	105	3.33(0.49)	0.13	38.04(0.50)	40.00	784.67
80	18	110	3.00(0.38)	0.12	30.89(0.59)	40.00	717.33
80	18	115	2.80(0.41)	0.11	30.66(1.12)	40.00	659.00
80	18	120	2.40(0.51)	0.10	32.05(1.79)	40.00	1029.67

80	**22**	**105**	3.13(0.35)	0.16	36.43(0.42)	48.89	954.67
80	*22*	*110*	*3.13(0.35)*	*0.15*	*33.90(0.80)*	*48.89*	*874.00*
80	*22*	*115*	*3.20(0.41)*	*0.13*	*35.50(1.26)*	*48.89*	*801.33*
80	**22**	**120**	2.67(0.49)	0.12	31.96(1.71)	48.89	1307.67
80	**28**	**105**	3.27(0.46)	0.21	36.89(0.27)	62.22	1212.67
80	**28**	**110**	3.33(0.49)	0.19	36.88(0.79)	62.22	1112.00
80	**28**	**115**	3.60(0.51)	0.17	43.47(1.49)	62.22	1017.67
80	**28**	**120**	2.80(0.41)	0.15	32.43(1.71)	62.22	1492.00
80	**32**	**105**	3.47(0.52)	0.24	40.75(0.38)	71.11	1382.67
80	**32**	**110**	3.60(0.51)	0.22	37.60(0.78)	71.11	1267.33
80	**32**	**115**	3.60(0.51)	0.19	42.39(1.36)	71.11	1160.33
80	**32**	**120**	3.07(0.26)	0.17	34.99(2.00)	71.11	959.00
85	**18**	**105**	3.00(0.38)	0.16	29.88(0.15)	40.00	889.00
85	*18*	*110*	*3.40(0.51)*	*0.15*	*35.06(0.81)*	*40.00*	*812.33*
85	**18**	**115**	2.87(0.35)	0.13	32.08(1.41)	40.00	745.33
85	**18**	**120**	2.53(0.52)	0.12	30.64(1.81)	40.00	1164.33
85	**22**	**105**	3.47(0.52)	0.20	35.46(0.09)	48.89	1081.00
85	**22**	**110**	3.73(0.46)	0.18	36.54(0.74)	48.89	992.33
85	**22**	**115**	3.40(0.63)	0.16	34.75(1.24)	48.89	906.33
85	**22**	**120**	2.67(0.49)	0.14	32.94(1.99)	48.89	1480.00
85	**28**	**105**	3.73(0.46)	0.25	39.11(0.31)	62.22	1374.00
85	**28**	**110**	3.27(0.46)	0.23	36.75(0.59)	62.22	1256.33
85	**28**	**115**	3.73(0.59)	0.20	47.83(1.24)	62.22	1151.33
85	**28**	**120**	3.40(0.51)	0.18	36.25(2.06)	62.22	1688.33
85	**32**	**105**	3.80(0.41)	0.29	41.84(0.30)	71.11	1567.67
85	**32**	**110**	3.80(0.41)	0.26	46.48(0.64)	71.11	1435.67
85	**32**	**115**	3.87(0.35)	0.23	41.82(1.56)	71.11	1313.33
85	**32**	**120**	3.73(0.46)	0.21	38.26(1.96)	71.11	589.67

IQ, image quality score, SD, standard deviation, E, effective dose, SNR, signal to noise ratio, ms, millisecond, DAP, dose area product

Appendix XI : APPS IQ score, SNR, time of exposure(s), the associated DAP(mGy.cm²) and E(mSv) with optimising Fine focal spot

kVp	mAs	SID	IQ score (SD)	E (mSv)	SNR(SD)	Time (ms)	DAP (mGy.cm²)
70	18	105	2.33(0.49)	0.09	32.18(1.50)	64.29	623.00
70	18	110	2.47(0.52)	0.08	30.77(0.94)	64.29	571.67
70	18	115	2.07(0.26)	0.07	25.10(1.15)	64.29	524.00
70	18	120	2.07(0.26)	0.07	24.06(1.76)	64.29	563.33
70	22	105	2.67(0.49)	0.10	31.78(1.49)	78.57	758.67
70	22	110	2.27(0.46)	0.09	29.79(0.92)	78.57	696.67
70	22	115	2.47(0.52)	0.08	28.80(1.38)	78.57	639.33
70	22	120	2.27(0.46)	0.08	28.12(1.69)	78.57	575.67
70	28	105	2.87(0.35)	0.13	35.11(1.29)	112.00	959.67
70	28	*110*	*3.00(0.00)*	*0.12*	*33.59(1.12)*	*112.00*	*884.00*
70	28	115	2.93(0.26)	0.10	34.15(1.48)	112.00	806.67
70	28	120	2.13(0.35)	0.10	26.91(1.98)	112.00	728.00
70	32	105	3.07(0.26)	0.15	37.19(0.93)	128.00	1094.67
70	32	*110*	*3.07(0.26)*	*0.14*	*37.90(0.98)*	*128.00*	*1004.67*
70	32	115	2.93(0.26)	0.12	31.55(1.36)	128.00	921.33
70	32	120	2.93(0.46)	0.11	32.18(2.09)	128.00	833.00
75	18	105	2.87(0.35)	0.11	33.37(1.10)	72.00	720.00
75	18	110	2.73(0.46)	0.10	34.92(0.73)	72.00	661.00
75	18	115	2.27(0.46)	0.08	26.60(1.17)	72.00	606.33
75	18	120	2.07(0.26)	0.08	27.53(1.57)	72.00	547.67
75	*22*	*105*	*3.00(0.00)*	*0.13*	*33.33(0.53)*	*88.00*	*879.33*
75	22	110	2.93(0.26)	0.12	30.25(0.88)	88.00	806.67
75	*22*	*115*	*3.00(0.00)*	*0.10*	*32.10(1.24)*	*88.00*	*741.00*
75	22	120	2.80(0.41)	0.09	30.18(1.70)	88.00	668.00
75	28	105	3.13(0.52)	0.16	39.22(0.54)	112.00	1117.33
75	28	110	2.93(0.26)	0.15	36.34(0.94)	112.00	1023.67
75	*28*	*115*	*3.00(0.00)*	*0.13*	*32.34(1.45)*	*112.00*	*941.33*
75	28	120	2.40(0.51)	0.12	29.59(2.03)	112.00	849.00
75	32	105	2.73(0.46)	0.19	31.50(0.48)	145.45	1285.00
75	32	110	3.13(0.35)	0.17	33.97(0.97)	145.45	1179.00
75	32	115	3.07(0.26)	0.15	34.50(1.56)	145.45	1072.33
75	*32*	*120*	*3.07(0.26)*	*0.14*	*33.40(1.84)*	*145.45*	*3919.33*
80	*18*	*105*	*3.00(0.00)*	*0.13*	*32.91(0.44)*	*81.82*	*831.00*
80	18	110	3.00(0.00)	0.12	35.16(0.78)	81.82	760.67
80	18	115	2.60(0.51)	0.10	29.29(1.06)	81.82	699.67
80	18	120	2.33(0.49)	0.10	28.22(1.68)	81.82	632.33
80	22	105	3.33(0.62)	0.16	36.61(0.26)	100.00	1015.67

80	*22*	*110*	*3.00(0.00)*	*0.14*	*39.59(1.04)*	*100.00*	*929.33*
80	*22*	*115*	*3.53(0.52)*	*0.13*	*38.66(1.42)*	*100.00*	*853.67*
80	**22**	**120**	2.73(0.46)	0.12	31.01(1.83)	100.00	771.67
80	**28**	**105**	3.80(0.41)	0.20	43.31(0.36)	127.27	1288.67
80	*28*	*110*	*3.87(0.35)*	*0.18*	*45.44(0.95)*	*127.27*	*1182.33*
80	**28**	**115**	3.47(0.52)	0.16	36.10(1.49)	127.27	1086.67
80	**28**	**120**	3.00(0.00)	0.15	32.69(1.96)	127.27	981.67
80	**32**	**105**	3.73(0.46)	0.23	45.58(0.41)	145.45	1475.00
80	**32**	**110**	3.73(0.46)	0.21	40.05(1.01)	145.45	1349.67
80	**32**	**115**	3.80(0.41)	0.18	41.97(1.40)	145.45	1241.33
80	**32**	**120**	3.60(0.51)	0.17	37.86(2.10)	145.45	1122.33
85	**18**	**105**	2.87(0.35)	0.16	29.38(0.31)	81.82	941.67
85	*18*	*110*	*3.00(0.00)*	*0.14*	*32.23(0.82)*	*81.82*	*862.00*
85	**18**	**115**	2.80(0.41)	0.13	30.98(1.20)	81.82	791.67
85	*18*	*120*	*3.00(0.00)*	*0.11*	*30.40(1.57)*	*81.82*	*716.33*
85	**22**	**105**	3.40(0.63)	0.19	40.67(0.30)	100.00	1149.67
85	**22**	**110**	3.80(0.41)	0.15	36.87(0.86)	100.00	1052.33
85	**22**	**115**	3.87(0.35)	0.15	41.13(1.32)	100.00	967.67
85	*22*	*120*	*3.00(0.00)*	*0.14*	*33.09(1.71)*	*100.00*	*873.33*
85	**28**	**105**	3.93(0.26)	0.25	45.21(0.30)	127.27	1460.67
85	**28**	**110**	3.80(0.41)	0.22	42.88(0.99)	127.27	1340.33
85	**28**	**115**	3.07(0.46)	0.20	37.84(1.23)	127.27	1231.33
85	**28**	**120**	3.73(0.46)	0.18	36.02(1.83)	127.27	1111.67
85	**32**	**105**	3.93(0.26)	0.28	46.36(0.29)	145.45	1671.67
85	**32**	**110**	3.73(0.46)	0.25	37.35(0.86)	145.45	1527.67
85	**32**	**115**	3.87(0.35)	0.22	40.23(1.33)	145.45	1407.67
85	**32**	**120**	3.80(0.41)	0.20	40.05(2.00)	145.45	1271.33

IQ, image quality score, SD, standard deviation, E, effective dose, SNR, signal to noise ratio, ms, millisecond, DAP, dose area product

Appendix XII: APPS IQ score, SNR, and the associated E(mSv) with optimising inherent filter type					
kVp	mAs	SID	IQ score (SD)	E (mSv)	SNR (SD)
70	18	105	2.47(0.52)	0.09	29.25(1.42)
70	18	110	2.47(0.52)	0.08	30.21(0.97)
70	18	115	2.07(0.26)	0.07	25.48(0.99)
70	18	120	2.27(0.46)	0.07	23.28(1.58)
70	22	105	2.60(0.51)	0.10	31.02(1.30)
70	22	110	2.93(0.26)	0.10	32.27(0.93)
70	22	115	2.13(0.35)	0.09	26.01(1.10)
70	22	120	2.33(0.49)	0.08	23.09(1.51)
70	*28*	*105*	*3.00(0.00)*	*0.13*	*32.80(1.13)*
70	*28*	*110*	*3.00(0.00)*	*0.12*	*31.74(0.82)*
70	*28*	*115*	*3.00(0.00)*	*0.11*	*35.63(1.41)*
70	28	120	2.80(0.41)	0.10	28.55(1.77)
70	*32*	*105*	*3.00(0.38)*	*0.15*	*36.23(0.75)*
70	32	110	2.93(0.26)	0.14	33.04(1.06)
70	*32*	*115*	*3.00(0.00)*	*0.12*	*33.15(1.24)*
70	32	120	2.33(0.49)	0.11	29.25(1.76)
75	18	105	2.60(0.51)	0.11	31.01(1.30)
75	18	110	2.80(0.41)	0.10	34.45(0.87)
75	*18*	*115*	*3.00(0.00)*	*0.09*	*33.08(1.15)*
75	18	120	2.13(0.35)	0.08	25.79(1.52)
75	22	105	2.80(0.41)	0.13	31.68(0.73)
75	22	110	2.93(0.46)	0.12	35.74(0.89)
75	22	115	2.33(0.49)	0.11	29.71(1.32)
75	22	120	2.20(0.41)	0.10	27.95(1.67)
75	28	105	3.00(0.00)	0.17	29.49(0.48)
75	*28*	*110*	*3.07(0.26)*	*0.15*	*36.32(0.94)*
75	28	115	2.67(0.49)	0.14	31.14(1.47)
75	28	120	2.87(0.35)	0.12	33.52(1.98)
75	32	105	3.00(0.00)	0.19	37.62(0.56)
75	32	110	3.33(0.49)	0.18	40.89(0.95)
75	32	115	3.40(0.51)	0.16	37.43(1.40)
75	32	120	2.93(0.26)	0.14	33.36(1.87)
80	*18*	*105*	*3.13(0.35)*	*0.13*	*36.60(0.48)*
80	18	110	2.80(0.41)	0.12	31.39(0.60)
80	18	115	2.73(0.46)	0.11	30.66(1.12)
80	18	120	2.80(0.41)	0.10	31.92(1.78)
80	22	105	3.13(0.35)	0.16	37.58(0.43)

80	*22*	*110*	*3.00(0.00)*	*0.15*	*34.11(0.81)*
80	*22*	*115*	*3.07(0.26)*	*0.13*	*36.69(1.31)*
80	**22**	**120**	2.67(0.49)	0.12	32.64(1.74)
80	**28**	**105**	3.13(0.35)	0.21	36.64(0.27)
80	**28**	**110**	3.33(0.49)	0.19	36.30(0.78)
80	**28**	**115**	3.67(0.49)	0.17	42.69(1.47)
80	**28**	**120**	2.93(0.26)	0.15	31.47(1.66)
80	**32**	**105**	3.73(0.46)	0.24	38.03(0.35)
80	**32**	**110**	3.60(0.51)	0.22	37.51(0.78)
80	**32**	**115**	3.87(0.35)	0.19	43.25(1.39)
80	**32**	**120**	2.93(0.26)	0.17	34.28(1.96)
85	**18**	**105**	3.00(0.00)	0.16	28.48(0.14)
85	**18**	**110**	3.40(0.51)	0.15	35.21(0.81)
85	*18*	*115*	*3.00(0.00)*	*0.13*	*31.35(1.38)*
85	**18**	**120**	2.60(0.51)	0.12	31.02(1.83)
85	**22**	**105**	3.53(0.52)	0.20	35.54(0.09)
85	**22**	**110**	3.33(0.49)	0.18	36.63(0.74)
85	**22**	**115**	3.00(0.00)	0.16	34.98(1.25)
85	**22**	**120**	2.80(0.41)	0.14	33.16(2.00)
85	**28**	**105**	3.87(0.35)	0.25	39.89(0.32)
85	**28**	**110**	3.40(0.51	0.23	37.35(0.60)
85	**28**	**115**	3.73(0.59)	0.20	50.93(1.32)
85	**28**	**120**	3.20(0.41)	0.18	37.39(2.13)
85	**32**	**105**	3.87(0.35)	0.29	39.69(0.31)
85	**32**	**110**	3.93(0.26)	0.26	46.48(0.64)
85	**32**	**115**	3.87(0.35)	0.23	41.30(1.54)
85	**32**	**120**	3.47(0.52)	0.21	38.55(1.97)
IQ, image quality score, SD, standard deviation, effective dose, SNR, signal to noise ratio.					

Appendix XIII: APPS IQ score, SNR, and the associated E (mSv) with optimising 2 mm Al filter type					
kVp	mAs	SID	IQ score (SD)	E (mSv)	SNR(SD)
70	18	105	2.33(0.49)	0.07	29.70(1.46)
70	18	110	2.53(0.52)	0.06	28.51(1.29)
70	18	115	2.07(0.26)	0.05	21.55(0.81)
70	18	120	2.07(0.26)	0.05	20.34(1.23)
70	22	105	2.80(0.41)	0.08	29.44(1.75)
70	22	110	2.20(0.41)	0.07	26.36(0.90)
70	22	115	2.07(0.26)	0.06	22.39(1.03)
70	22	120	2.07(0.26)	0.06	23.84(1.27)
70	28	105	3.00(0.00)	0.10	34.75(1.64)
70	28	110	2.87(0.35)	0.09	28.68(0.95)
70	28	115	2.33(0.49)	0.08	27.17(1.18)
70	28	120	2.40(0.51)	0.08	27.44(1.48)
70	32	105	3.33(0.62)	0.12	35.96(1.35)
70	32	110	3.00(0.00)	0.11	31.73(0.96)
70	32	115	2.40(0.51)	0.09	27.95(1.29)
70	32	120	2.60(0.51)	0.09	30.16(1.59)
75	18	105	3.00(0.00)	0.09	31.78(1.59)
75	18	110	2.33(0.49)	0.08	26.36(0.82)
75	18	115	2.13(0.35)	0.07	25.07(0.89)
75	18	120	2.13(0.35)	0.06	23.94(1.48)
75	22	105	3.13(0.35)	0.10	33.70(1.48)
75	22	110	3.00(0.00)	0.09	31.03(0.89)
75	22	115	2.33(0.49)	0.08	25.21(1.11)
75	22	120	2.07(0.26)	0.08	27.02(1.39)
75	28	105	3.20(0.41)	0.13	34.86(1.01)
75	28	110	3.00(0.00)	0.12	31.51(0.90)
75	28	115	3.00(0.00	0.11	30.57(1.28)
75	28	120	2.73(0.46)	0.10	30.49(1.59)
75	32	105	3.73(0.46)	0.15	37.49(0.87)
75	32	110	3.00(0.00)	0.14	31.62(0.96)
75	32	115	3.73(0.46)	0.12	36.30(1.36)
75	32	120	2.87(0.35)	0.11	29.13(1.90)
80	18	105	3.40(0.51)	0.11	34.89(0.97)
80	18	110	3.00(0.00)	0.10	31.74(0.74)
80	18	115	2.20(0.41)	0.08	26.53(1.00)
80	18	120	2.33(0.49)	0.08	26.83(1.30)

80	*22*	*105*	*3.13(0.35)*	*0.13*	*32.30(0.68)*
80	**22**	**110**	2.93(0.26)	0.12	29.31(0.76)
80	*22*	*115*	*3.00(0.00)*	*0.10*	*30.63(1.13)*
80	**22**	**120**	2.87(0.35)	0.09	30.01(1.41)
80	**28**	**105**	3.80(0.41)	0.17	34.50(0.54)
80	*28*	*110*	*3.80(0.41)*	*0.15*	*31.83(0.91)*
80	*28*	*115*	*3.27(0.46)*	*0.13*	*32.88(1.09)*
80	*28*	*120*	*3.13(0.35)*	*0.12*	*32.54(1.36)*
80	**32**	**105**	3.73(0.46)	0.19	35.48(0.53)
80	**32**	**110**	3.80(0.41)	0.17	37.22(1.02)
80	**32**	**115**	3.60(0.51)	0.15	36.83(1.07)
80	*32*	*120*	*3.07(0.26)*	*0.14*	*34.16(1.74)*
85	**18**	**105**	3.60(0.51)	0.13	35.84(0.33)
85	*18*	*110*	*3.27(0.59)*	*0.12*	*33.17(0.69)*
85	*18*	*115*	*3.60(0.51)*	*0.10*	*36.89(1.26)*
85	**18**	**120**	2.60(0.51)	0.09	29.02(1.47)
85	*22*	*105*	*3.73(0.46)*	*0.16*	*35.70(0.42)*
85	*22*	*110*	*3.33(0.49)*	*0.14*	*31.18(0.54)*
85	*22*	*115*	*3.00(0.00)*	*0.13*	*30.10(0.95)*
85	**22**	**120**	2.67(0.49)	0.12	30.99(1.54)
85	**28**	**105**	3.80(0.41)	0.20	40.30(0.46)
85	**28**	**110**	3.93(0.26)	0.18	33.93(0.83)
85	**28**	**115**	3.80(0.41)	0.16	45.97(1.26)
85	*28*	*120*	*3.40(0.51)*	*0.15*	*34.74(1.76)*
85	**32**	**105**	3.80(0.41)	0.23	35.86(0.29)
85	**32**	**110**	3.93(0.26)	0.21	36.53(0.99)
85	**32**	**115**	3.87(0.35)	0.18	37.10(1.16)
85	**32**	**120**	3.67(0.49)	0.16	35.98(1.87)
IQ, image quality score, SD, standard deviation, effective dose, SNR, signal to noise ratio.					

Appendix XIV: APPS IQ score, SNR, and the associated E (mSv) with optimising 0.1 mm Cu filter type					
kVp	mAs	SID	IQ score (SD)	E(mSv)	SNR(SD)
70	**18**	**105**	2.13(0.35)	0.05	24.93(0.70)
70	**18**	**110**	2.13(0.35)	0.05	25.68(1.24)
70	**18**	**115**	2.07(0.26)	0.04	20.80(0.91)
70	**18**	**120**	2.07(0.26)	0.04	17.85(1.03)
70	**22**	**105**	2.73(0.46)	0.06	28.34(0.89)
70	**22**	**110**	2.73(0.46)	0.06	25.95(0.98)
70	**22**	**115**	2.07(0.26)	0.05	21.96(1.06)
70	**22**	**120**	2.20(0.41)	0.05	22.98(1.32)
70	*28*	*105*	*3.00(0.53)*	*0.08*	*32.55(1.09)*
70	*28*	*110*	*3.07(0.26)*	*0.07*	*29.56(1.16)*
70	**28**	**115**	2.20(0.41)	0.07	23.88(1.09)
70	**28**	**120**	2.27(0.46)	0.06	24.73(1.60)
70	**32**	**105**	3.13(0.35)	0.09	31.89(1.30)
70	*32*	*110*	*3.20(0.41)*	*0.08*	*31.34(0.85)*
70	**32**	**115**	2.93(0.26)	0.08	29.22(1.03)
70	*32*	*120*	*3.00(0.00)*	*0.07*	*29.73(1.45)*
75	**18**	**105**	2.73(0.46)	0.07	27.03(1.00)
75	*18*	*110*	*3.00(0.00)*	*0.06*	*28.05(0.92)*
75	**18**	**115**	2.67(0.49)	0.06	25.98(1.03)
75	**18**	**120**	2.13(0.35)	0.05	22.74(1.13)
75	*22*	*105*	*3.00(0.00)*	*0.08*	*30.74(1.17)*
75	*22*	*110*	*3.00(0.00)*	*0.08*	*30.00(0.94)*
75	*22*	*115*	*3.20(0.41)*	*0.07*	*28.99(1.04)*
75	**22**	**120**	2.47(0.52)	0.06	25.23(1.38)
75	**28**	**105**	3.20(0.41)	0.11	32.44(0.68)
75	*28*	*110*	*3.33(0.49)*	*0.10*	*31.81(0.87)*
75	*28*	*115*	*3.00(0.00)*	*0.09*	*29.74(1.14)*
75	**28**	**120**	2.73(0.46)	0.08	27.53(1.67)
75	*32*	*105*	*3.20(0.410*	*0.12*	*37.07(0.70)*
75	*32*	*110*	*3.07(0.26)*	*0.11*	*33.86(0.94)*
75	*32*	*115*	*3.07(0.26)*	*0.10*	*28.74(1.11)*
75	*32*	*120*	*3.00(0.38)*	*0.09*	*28.18(1.55)*
80	*18*	*105*	*3.00(0.00)*	*0.09*	*32.69(0.64)*
80	*18*	*110*	*3.00(0.00)*	*0.08*	*32.28(0.73)*
80	**18**	**115**	2.80(0.41)	0.08	27.29(0.96)
80	**18**	**120**	2.47(0.52)	0.06	25.31(1.40)
80	*22*	*105*	*3.47(0.52)*	*0.11*	*33.51(0.51)*

80	*22*	*110*	*3.13(0.35)*	*0.10*	*32.25(0.83)*
80	*22*	*115*	*3.00(0.00)*	*0.09*	*30.08(1.10)*
80	**22**	**120**	2.53(0.52)	0.08	26.53(1.68)
80	*28*	*105*	*3.47(0.52)*	*0.14*	*33.65(0.47)*
80	*28*	*110*	*3.60(0.51)*	*0.12*	*38.27(0.96)*
80	*28*	*115*	*3.53(0.52)*	*0.11*	*33.05(1.12)*
80	**28**	**120**	*3.00(0.00)*	*0.10*	*31.66(1.54)*
80	**32**	**105**	3.80(0.41)	0.17	37.03(0.43)
80	**32**	**110**	*3.93(0.26)*	*0.14*	*35.43(0.79)*
80	**32**	**115**	*3.33(0.49)*	*0.12*	*32.92(1.13)*
80	**32**	**120**	*3.27(0.59)*	*0.11*	*32.39(1.65)*
85	*18*	*105*	*3.60(0.51)*	*0.11*	*33.54(0.44)*
85	*18*	*110*	*3.47(0.64)*	*0.10*	*35.98(0.86)*
85	*18*	*115*	*3.00(0.00)*	*0.09*	*31.09(0.98)*
85	*18*	*120*	*3.33(0.49)*	*0.08*	*32.70(1.40)*
85	*22*	*105*	*3.93(0.26)*	*0.13*	*37.02(0.38)*
85	*22*	*110*	*3.53(0.52)*	*0.12*	*32.36(0.62)*
85	*22*	*115*	*3.60(0.51)*	*0.11*	*32.43(1.11)*
85	*22*	*120*	*3.00(0.00)*	*0.10*	*28.82(1.54)*
85	**28**	**105**	3.73(0.59)	0.17	40.80(0.38)
85	**28**	**110**	*3.93(0.26)*	*0.15*	*40.25(0.90)*
85	**28**	**115**	*3.93(0.26)*	*0.14*	*43.37(1.15)*
85	**28**	**120**	*3.73(0.46)*	*0.12*	*38.37(1.53)*
85	**32**	**105**	3.93(0.26)	0.19	39.50(0.67)
85	**32**	**110**	3.87(0.35)	0.17	37.42(0.88)
85	**32**	**115**	3.80(0.41)	0.15	36.29(1.20)
85	**32**	**120**	*3.93(0.26)*	*0.14*	*39.56(1.52)*
IQ, image quality score, SD, standard deviation, effective dose, SNR, signal to noise ratio.					

Appendix XV: APPS IQ score, SNR, and the associated E (mSv) with optimising 0.2 mm Cu filter type					
kVp	mAs	SID	IQ Score (SD)	E(mSv)	SNR(SD)
70	18	105	2.60(0.51)	0.04	26.55(0.91)
70	18	110	2.53(0.52)	0.04	24.27(0.73)
70	18	115	2.07(0.26)	0.03	18.98(0.99)
70	18	120	2.07(0.26)	0.03	17.90(1.04)
70	22	105	2.87(0.35)	0.05	28.71(1.04)
70	22	110	2.80(0.41)	0.04	22.34(1.38)
70	22	115	2.07(0.26)	0.04	18.92(0.95)
70	22	120	2.07(0.26)	0.04	18.66(1.18)
70	28	105	3.73(0.46)	0.06	33.31(1.03)
70	28	110	3.00(0.00)	0.06	28.57(0.72)
70	28	115	2.13(0.35)	0.05	22.72(1.02)
70	28	120	2.93(0.26)	0.04	23.88(1.22)
70	32	105	3.80(0.41)	0.07	34.01(1.02)
70	32	110	3.13(0.35)	0.06	28.96(1.08)
70	32	115	2.67(0.49)	0.06	24.53(1.07)
70	32	120	2.20(0.41)	0.05	21.44(1.31)
75	18	105	3.00(0.00)	0.05	27.97(0.67)
75	18	110	2.93(0.26)	0.05	25.95(0.67)
75	18	115	2.13(0.35)	0.04	20.95(0.87)
75	18	120	2.07(0.26)	0.04	18.85(1.10)
75	22	105	3.20(0.41)	0.06	29.27(0.83)
75	22	110	3.20(0.41)	0.06	28.66(0.68)
75	22	115	2.40(0.51)	0.05	23.63(0.97)
75	22	120	2.33(0.49)	0.05	21.43(1.11)
75	28	105	3.80(0.41)	0.08	32.88(0.96)
75	28	110	3.67(0.49)	0.07	32.90(0.76)
75	28	115	2.60(0.51)	0.07	25.75(0.99)
75	28	120	2.27(0.46)	0.06	21.80(1.29)
75	32	105	3.93(0.26)	0.09	32.54(0.67)
75	32	110	3.73(0.46)	0.08	34.41(1.14)
75	32	115	3.00(0.00)	0.07	26.25(1.13)
75	32	120	2.60(0.51)	0.07	23.33(1.40)
80	18	105	3.60(0.51)	0.07	30.80(0.76)
80	18	110	3.33(0.49)	0.06	26.44(0.71)
80	18	115	3.00(0.00)	0.05	24.58(0.98)
80	18	120	2.13(0.35)	0.05	21.64(1.15)

80	*22*	*105*	*3.87(0.35)*	*0.08*	*32.90(0.98)*
80	*22*	*110*	*3.60(0.51)*	*0.08*	*28.06(0.61)*
80	*22*	*115*	*3.00(0.00)*	*0.07*	*24.95(1.02)*
80	*22*	*120*	*3.07(0.46)*	*0.06*	*25.39(1.14)*
80	**28**	**105**	3.80(0.56)	0.11	36.06(0.41)
80	*28*	*110*	*3.13(0.35)*	*0.10*	*28.01(1.43)*
80	**28**	**115**	3.60(0.51)	0.08	30.50(1.15)
80	*28*	*120*	*3.27(0.46)*	*0.08*	*27.78(1.43)*
80	*32*	*105*	*3.87(0.35)*	*0.12*	*39.58(0.27)*
80	*32*	*110*	*3.80(0.41)*	*0.11*	*35.06(0.73)*
80	*32*	*115*	*3.80(0.41)*	*0.10*	*32.26(1.24)*
80	*32*	*120*	*3.47(0.64)*	*0.09*	*26.61(1.53)*
85	**18**	**105**	*3.80(0.41)*	*0.09*	*32.84(0.44)*
85	**18**	**110**	*3.80(0.41)*	*0.08*	*32.71(0.63)*
85	**18**	**115**	3.00(0.00)	0.07	24.67(1.00)
85	**18**	**120**	*2.40(0.51)*	*0.06*	*25.10(1.25)*
85	**22**	**105**	*3.87(0.35)*	*0.11*	*36.81(0.30)*
85	**22**	**110**	*3.80(0.41)*	*0.09*	*35.56(0.72)*
85	**22**	**115**	3.40(0.51)	0.08	30.76(1.20)
85	**22**	**120**	2.93(0.46)	0.08	25.98(1.53)
85	**28**	**105**	3.93(0.26)	0.14	38.18(0.17)
85	**28**	**110**	3.80(0.41)	0.12	37.44(0.83)
85	**28**	**115**	*3.73(0.46)*	*0.11*	*31.63(1.19)*
85	**28**	**120**	*3.67(0.49)*	*0.10*	*31.05(1.42)*
85	**32**	**105**	3.93(0.26)	0.15	37.69(0.30)
85	**32**	**110**	*3.93(0.26)*	*0.14*	*41.32(0.77)*
85	**32**	**115**	*3.93(0.26)*	*0.12*	*33.87(0.94)*
85	**32**	**120**	3.93(0.26)	0.11	32.33(1.57)
IQ, image quality score, SD, standard deviation, E, effective dose, SNR, signal to noise ratio.					

Appendix XVI: APPS IQ score, SNR, and the associated E (mSv) with optimising 95 cm SID **(Extended factorial)**

kVp	mAs	SID	IQ Score (SD)	E(mSv)	SNR(SD)
60	**10**	**95**	2.00(0.00)	0.01	15.59(2.47)
60	**14**	**95**	2.07(0.26)	0.02	17.46(2.76)
60	**18**	**95**	2.07(0.26)	0.03	18.17(2.90)
60	**22**	**95**	2.07(0.26)	0.03	20.52(3.30)

60	28	95	2.07(0.26)	0.04	21.60(3.76)
60	32	95	2.20(0.41)	0.05	24.02(3.71)
60	36	95	2.27(0.46)	0.05	23.62(4.05)
60	40	95	2.13(0.35)	0.06	24.95(4.36)
65	10	95	2.07(0.26)	0.02	19.39(2.89)
65	14	95	2.13(0.35)	0.03	19.69(3.21)
65	18	95	2.07(0.26)	0.04	24.30(3.76)
65	22	95	2.07 0.26)	0.05	23.02(3.66)
65	28	95	2.33(0.49)	0.06	25.67(4.12)
65	32	95	2.67(0.49)	0.07	27.30(4.43)
65	36	95	2.87(0.35)	0.08	29.54(4.49)
65	*40*	*95*	*3.00(0.00)*	*0.08*	*29.70(4.47)*
70	10	95	2.13(0.35)	0.03	21.12(3.15)
70	14	95	2.07(0.26)	0.04	23.01(3.67)
70	18	95	2.33(0.49)	0.05	26.24(4.19)
70	22	95	2.47(0.52)	0.06	28.12(4.45)
70	28	95	2.73(0.46)	0.08	30.68(5.10)
70	*32*	*95*	*3.00(0.00)*	*0.09*	*29.98(4.95)*
70	*36*	*95*	*3.33(0.49)*	*0.10*	*32.17(5.06)*
70	*40*	*95*	*3.20(0.56)*	*0.11*	*31.17(4.86)*
75	10	95	2.20(0.41)	0.04	23.76(3.55)
75	14	95	2.20(0.41)	0.05	27.36(4.12)
75	18	95	2.93(0.46)	0.07	27.74(4.42)
75	*22*	*95*	*3.00(0.00)*	*0.08*	*29.63(4.72)*
75	*28*	*95*	*3.07(0.26)*	*0.11*	*30.63(4.68)*
75	*32*	*95*	*3.53(0.52)*	*0.12*	*31.92(4.93)*
75	*36*	*95*	*3.87(0.35)*	*0.14*	*33.37(5.31)*
75	*40*	*95*	*3.87(0.35)*	*0.15*	*34.64(5.34)*
80	10	95	2.53(0.52)	0.05	25.35(3.97)
80	*14*	*95*	*3.00(0.00)*	*0.07*	*29.08(4.48)*
80	*18*	*95*	*3.00(0.00)*	*0.09*	*30.77(4.78)*
80	*22*	*95*	*3.00(0.00)*	*0.11*	*31.93(5.10)*
80	*28*	*95*	*3.87(0.35)*	*0.14*	*34.81(5.13)*
80	32	95	3.73(0.46)	0.16	34.74(5.44)
80	36	95	3.87(0.35)	0.18	35.15(5.30)
80	40	95	3.87(0.35)	0.20	34.69(5.72)
85	10	95	2.67(0.49)	0.06	28.58(4.35)
85	*14*	*95*	*3.07(0.26)*	*0.09*	*31.29(4.93)*
85	*18*	*95*	*3.67(0.49)*	*0.10*	*33.45(5.34)*
85	*22*	*95*	*3.40(0.51)*	*0.14*	*28.83(4.88)*
85	28	95	3.73(0.46)	0.18	35.17(5.14)

kVp	mAs	SID	IQ score (SD)	E(mSv)	SNR(SD)
85	**32**	**95**	3.67(0.49)	0.20	33.05(5.68)
85	**36**	**95**	3.80(0.41)	0.23	38.10(5.64)
85	**40**	**95**	3.87(0.35)	0.25	37.30(5.84)
90	*10*	*95*	*2.60(0.51)*	*0.08*	*29.28(4.43)*
90	*14*	*95*	*3.13(0.35)*	*0.11*	*33.52(5.28)*
90	*18*	*95*	*3.27(0.46)*	*0.14*	*34.37(5.22)*
90	**22**	**95**	3.73(0.46)	0.17	34.80(5.32)
90	**28**	**95**	3.80(0.41)	0.17	37.78(5.44)
90	**32**	**95**	3.87(0.35)	0.25	30.81(5.14)
90	**36**	**95**	3.93(0.26)	0.28	38.12(5.90)
90	**40**	**95**	3.93(0.26)	0.31	36.04(5.75)
95	*10*	*95*	*3.13(0.35)*	*0.10*	*31.10(4.67)*
95	*14*	*95*	*3.40(0.51)*	*0.13*	*31.06(5.19)*
95	**18**	**95**	3.87(0.35)	0.17	34.67(5.22)
95	**22**	**95**	3.60(0.51)	0.21	34.68(5.24)
95	**28**	**95**	3.93(0.26)	0.27	34.62(5.33)
95	**32**	**95**	3.80(0.56)	0.30	34.25(5.50)
95	**36**	**95**	3.93(0.26)	0.34	33.12(5.02)
95	**40**	**95**	3.80(0.41)	0.36	32.56(5.40)

IQ, image quality score, SD, standard deviation, E, effective dose, SNR, signal to noise ratio

---

Appendix XVII: APPS IQ score, SNR, and the associated E (mSv) with optimising 100 cm SID (Extended factorial)

kVp	mAs	SID	IQ score (SD)	E(mSv)	SNR(SD)
60	**10**	**100**	2.07(0.26)	0.01	15.74(2.12)
60	**14**	**100**	2.07(0.26)	0.02	18.51(2.65)
60	**18**	**100**	2.07(0.26)	0.02	19.11(2.82)
60	**22**	**100**	2.07(0.26)	0.03	20.22(2.99)
60	**28**	**100**	2.13(0.35)	0.04	23.53(3.48)
60	**32**	**100**	2.33(0.49)	0.04	21.92(3.44)
60	**36**	**100**	2.27(0.46)	0.04	23.69(3.58)
60	**40**	**100**	2.93(0.46)	0.05	24.66(3.59)
65	**10**	**100**	2.07(0.26)	0.02	18.70(2.57)
65	**14**	**100**	2.20(0.41)	0.03	21.59(2.85)
65	**18**	**100**	2.33(0.62)	0.03	22.72(3.41)
65	**22**	**100**	2.60(0.51)	0.04	23.46(3.33)
65	**28**	**100**	2.53(0.52)	0.05	26.70(3.96)

65	32	100	3.00(0.00)	0.06	29.20(4.08)
65	36	100	3.00(0.38)	0.07	27.73(3.69)
65	40	100	3.07(0.26)	0.07	30.11(4.08)
70	10	100	2.13(0.35)	0.03	21.02(3.02)
70	14	100	2.20(0.41)	0.04	23.18(3.36)
70	18	100	2.60(0.51)	0.05	25.10(3.39)
70	22	100	3.00(0.38)	0.06	26.64(3.66)
70	28	100	3.00(0.00)	0.07	28.12(3.54)
70	32	100	3.20(0.41)	0.08	30.68(3.90)
70	36	100	3.47(0.52)	0.09	30.22(4.05)
70	40	100	3.53(0.52)	0.10	31.62(4.04)
75	10	100	2.13(0.35)	0.03	22.45(3.22)
75	14	100	2.47(0.52)	0.05	24.29(3.51)
75	18	100	2.93(0.26)	0.06	28.09(3.45)
75	22	100	3.13(0.35)	0.08	29.54(3.84)
75	28	100	3.07(0.26)	0.10	31.81(4.19)
75	32	100	3.20(0.41)	0.11	33.38(4.39)
75	36	100	3.73(0.46)	0.12	33.31(4.18)
75	40	100	3.73(0.46)	0.14	32.30(4.00)
80	10	100	2.13(0.35)	0.04	25.13(3.83)
80	14	100	2.60(0.51)	0.06	27.00(4.07)
80	18	100	3.00(0.00)	0.08	31.42(4.08)
80	22	100	3.67(0.49)	0.10	31.73(3.74)
80	28	100	3.80(0.41)	0.12	31.87(4.03)
80	32	100	3.60(0.51)	0.14	32.73(4.72)
80	36	100	3.87(0.35)	0.16	34.70(4.15)
80	40	100	3.87(0.35)	0.18	34.17(4.42)
85	10	100	3.00(0.00)	0.06	27.74(3.73)
85	14	100	2.93(0.26)	0.08	30.21(4.04)
85	18	100	3.40(0.51)	0.10	33.05(4.62)
85	22	100	3.33(0.49)	0.013	33.48(3.98)
85	28	100	3.87(0.35)	0.16	33.09(4.79)
85	32	100	3.87(0.35)	0.18	33.23(3.96)
85	36	100	3.80(0.41)	0.20	33.66(4.33)
85	40	100	3.93(0.26)	0.23	36.31(4.41)
90	10	100	2.93(0.26)	0.07	29.22(4.41)
90	14	100	3.13(0.35)	0.10	31.40(4.30)
90	18	100	3.67(0.49)	0.13	34.01(4.24)
90	22	100	3.53(0.52)	0.16	33.94(5.00)
90	28	100	3.87(0.35)	0.20	35.82(4.63)
90	32	100	3.80(0.41)	0.22	34.80(5.08)

90	**36**	**100**	3.93(0.26)	0.25	35.92(4.84)
90	**40**	**100**	4.00(0.00)	0.28	35.36(5.18)
95	*10*	*100*	*3.00(0.00)*	*0.09*	*30.16(4.16)*
95	*14*	*100*	*3.60(0.51)*	*0.12*	*32.44(4.20)*
95	**18**	**100**	3.73(0.46)	0.16	33.24(4.69)
95	**22**	**100**	3.87(0.35)	0.19	35.26(4.32)
95	**28**	**100**	3.80(0.41)	0.24	34.99(4.75)
95	**32**	**100**	3.87(0.35)	0.28	36.10(4.50)
95	**36**	**100**	3.87(0.35)	0.31	33.83(3.39)
95	**40**	**100**	3.93(0.26)	0.34	34.93(4.48)

IQ, image quality score, SD, standard deviation, E, effective dose, SNR, signal to noise ratio

---

Appendix XVIII: APPS IQ score, SNR, and the associated E (mSv) with optimising 105 cm SID **(Extended factorial)**

kVp	mAs	SID	IQ score (SD)	E(mSv)	SNR(SD)
60	**10**	**105**	2.07(0.26)	0.01	15.14(2.03)
60	**14**	**105**	2.07(0.26)	0.02	16.60(2.13)
60	**18**	**105**	2.13(0.35)	0.02	18.27(2.26)
60	**22**	**105**	2.13(0.35)	0.02	18.93(2.37)
60	**28**	**105**	2.27(0.46)	0.03	20.88(2.51)
60	**32**	**105**	2.33(0.49)	0.03	22.20(2.93)
60	**36**	**105**	2.27(0.46)	0.04	23.46(3.12)
60	**40**	**105**	2.60(0.51)	0.04	24.81(2.99)
65	**10**	**105**	2.00(0.00)	0.02	15.44(2.14)
65	**14**	**105**	2.07(0.26)	0.02	21.95(2.45)
65	**18**	**105**	2.07(0.26)	0.03	21.00(2.73)
65	**22**	**105**	2.20(0.41)	0.04	23.61(2.86)
65	**28**	**105**	2.73(0.46)	0.04	26.61(3.18)
65	**32**	**105**	2.80(0.41)	0.05	25.73(3.18)
65	**36**	**105**	2.87(0.35)	0.06	25.08(3.02)
65	**40**	**105**	2.87(0.35)	0.06	25.18(2.71)
70	**10**	**105**	2.13(0.35)	0.02	19.78(2.24)
70	**14**	**105**	2.13(0.35)	0.03	24.01(2.85)
70	**18**	**105**	2.27(0.46)	0.04	20.38(2.77)
70	*22*	*105*	*3.00(0.00)*	*0.05*	*26.30(2.79)*
70	**28**	**105**	2.93(0.46)	0.06	26.43(2.68)
70	*32*	*105*	*3.00(0.00)*	*0.07*	*28.54(3.21)*
70	*36*	*105*	*3.00(0.00)*	*0.08*	*27.81(3.15)*

70	*40*	*105*	*3.33(0.49)*	*0.09*	*29.65(3.07)*
75	**10**	**105**	2.13(0.35)	0.03	20.28(2.50)
75	**14**	**105**	2.33(0.49)	0.04	23.97(2.74)
75	**18**	**105**	2.80(0.41)	0.05	26.23(2.95)
75	*22*	*105*	*3.00(0.00)*	*0.07*	*25.93(2.71)*
75	*28*	*105*	*3.07(0.26)*	*0.08*	*30.32(3.51)*
75	*32*	*105*	*3.07(0.26)*	*0.09*	*27.66(2.90)*
75	*36*	*105*	*3.27(0.46)*	*0.11*	*27.76(2.67)*
75	*40*	*105*	*3.87(0.35)*	*0.12*	*31.84(3.09)*
80	**10**	**105**	2.13(0.35)	0.04	21.73(2.91)
80	**14**	**105**	2.80(0.41)	0.05	25.70(2.86)
80	*18*	*105*	*3.00(0.00)*	*0.07*	*29.10(3.38)*
80	*22*	*105*	*3.13(0.35)*	*0.08*	*28.57(3.27)*
80	*28*	*105*	*3.47(0.52)*	*0.11*	*29.83(2.95)*
80	*32*	*105*	*3.87(0.35)*	*0.12*	*30.29(2.85)*
80	*36*	*105*	*3.60(0.51)*	*0.14*	*30.61(3.11)*
80	*40*	*105*	*3.87(0.35)*	*0.15*	*36.27(3.70)*
85	**10**	**105**	2.87(0.35)	0.05	26.62(3.24)
85	**14**	**105**	2.93(0.26)	0.07	26.23(2.87)
85	*18*	*105*	*3.00(0.00)*	*0.09*	*27.10(3.35)*
85	*22*	*105*	*3.60(0.51)*	*0.11*	*31.09(3.57)*
85	*28*	*105*	*3.87(0.35)*	*0.14*	*31.68(3.03)*
85	**32**	**105**	3.80(0.41)	0.16	30.31(3.31)
85	**36**	**105**	3.80(0.41)	0.18	31.74(3.12)
85	**40**	**105**	3.93(0.26)	0.19	34.25(3.31)
90	**10**	**105**	2.67(0.49)	0.06	26.56(3.25)
90	*14*	*105*	*3.47(0.52)*	*0.08*	28.22(2.85)
90	*18*	*105*	*3.60(0.51)*	*0.11*	32.09(3.48)
90	*22*	*105*	*3.93(0.26)*	*0.13*	33.06(3.31)
90	**28**	**105**	3.60(0.63)	0.17	33.20(3.36)
90	**32**	**105**	4.00(0.00)	0.20	35.33(3.66)
90	**36**	**105**	3.93(0.26)	0.22	36.47(3.12)
90	**40**	**105**	3.87(0.35)	0.24	34.55(3.44)
95	*10*	*105*	*3.00(0.00)*	*0.07*	*26.48(3.31)*
95	*14*	*105*	*3.67(0.49)*	*0.10*	28.80(2.86)
95	*18*	*105*	*3.67(0.49)*	*0.13*	28.67(3.32)
95	**22**	**105**	3.80(0.41)	0.16	32.36(3.28)
95	**28**	**105**	3.87(0.35)	0.21	33.70(3.80)
95	**32**	**105**	3.93(0.26)	0.23	34.28(3.69)
95	**36**	**105**	3.87(0.35)	0.26	32.50(3.74)
95	**40**	**105**	4.00(0.00)	0.29	31.58(3.46)

IQ, image quality score, SD, standard deviation, E,
effective dose, SNR, signal to noise ratio.

Appendix XIX: **APPS IQ score, SNR, and the associated E (mSv) with optimising** 110 cm SID **(Extended factorial)**

kVp	mAs	SID	IQ score (SD)	E(mSv)	SNR(SD)
60	10	110	2.00(0.00)	0.01	14.08(1.49)
60	14	110	2.07(0.26)	0.01	16.80(1.74)
60	18	110	2.07(0.26)	0.02	17.50(1.82)
60	22	110	2.13(0.35)	0.02	16.26(2.00)
60	28	110	2.27(0.46)	0.03	20.73(2.19)
60	32	110	2.20(0.41)	0.03	21.37(2.36)
60	36	110	2.67(0.49)	0.03	23.25(2.23)
60	40	110	2.27(0.46)	0.04	22.26(2.53)
65	10	110	2.07(0.26)	0.01	16.64(1.65)
65	14	110	2.13(0.35)	0.02	20.13(1.95)
65	18	110	2.20(0.41)	0.03	19.91(2.10)
65	22	110	2.07(0.26)	0.03	19.09(2.25)
65	28	110	2.33(0.49)	0.04	23.02(2.44)
65	32	110	2.87(0.35)	0.05	24.75(2.52)
65	36	110	2.53(0.52)	0.05	21.60(2.71)
65	*40*	*110*	*3.00(0.00)*	*0.06*	*25.69(2.57)*
70	10	110	2.07(0.26)	0.02	16.75(1.84)
70	14	110	2.33(0.49)	0.03	21.47(2.17)
70	18	110	2.73(0.46)	0.04	21.66(2.19)
70	*22*	*110*	*3.00(0.00)*	*0.05*	*24.41(2.57)*
70	*28*	*110*	*3.00(0.00)*	*0.06*	*26.18(2.50)*
70	*32*	*110*	*3.07(0.26)*	*0.06*	*28.06(2.57)*
70	*36*	*110*	*3.13(0.35)*	*0.07*	*27.91(2.79)*
70	*40*	*110*	*3.20(0.41)*	*0.08*	*28.19(2.79)*
75	10	110	2.33(0.49)	0.03	20.69(2.07)
75	14	110	2.40(0.51)	0.04	22.77(2.33)
75	*18*	*110*	*3.00(0.00)*	*0.05*	*23.65(2.48)*
75	*22*	*110*	*3.00(0.00)*	*0.06*	*27.14(2.81)*
75	*28*	*110*	*3.33(0.49)*	*0.08*	*28.06(2.61)*
75	*32*	*110*	*3.13(0.35)*	*0.09*	*30.06(2.89)*
75	*36*	*110*	*3.67(0.49)*	*0.10*	*30.92(2.95)*
75	*40*	*110*	*3.80(0.41)*	*0.11*	*34.86(3.09)*

80	10	110	2.33(0.49)	0.04	22.92(2.40)
80	14	110	2.60(0.51)	0.05	23.27(2.46)
80	*18*	*110*	*3.00(0.00)*	*0.06*	*26.58(2.64)*
80	*22*	*110*	*3.33(0.49)*	*0.08*	*28.81(2.83)*
80	*28*	*110*	*3.67(0.49)*	*0.10*	*29.99(2.96)*
80	*32*	*110*	*3.73(0.46)*	*0.11*	*31.59(3.33)*
80	*36*	*110*	*3.80(0.41)*	*0.13*	*36.27(3.25)*
80	*40*	*110*	*4.00(0.00)*	*0.14*	*37.54(3.65)*
85	10	110	2.53(0.52	0.04	25.02(2.58)
85	*14*	*110*	*3.00(0.00)*	*0.06*	*27.57(2.85)*
85	*18*	*110*	*3.40(0.51)*	*0.08*	*30.16(2.99)*
85	*22*	*110*	*3.87(0.35)*	*0.10*	*32.01(3.04)*
85	*28*	*110*	*4.00(0.00)*	*0.12*	*30.86(2.91)*
85	*32*	*110*	*3.80(0.41)*	*0.14*	*32.52(3.23)*
85	36	110	3.93(0.26)	0.16	33.25(3.58)
85	40	110	3.93(0.26)	0.18	38.79(3.48)
90	*10*	*110*	*2.80(0.41)*	*0.06*	*25.70(2.66)*
90	14	110	2.93(0.26)	0.08	27.34(2.77)
90	*18*	*110*	*3.73(0.46)*	*0.10*	*33.61(3.13)*
90	*22*	*110*	*3.80(0.41)*	*0.12*	*32.22(3.38)*
90	28	110	3.87(0.35)	0.16	34.22(3.42)
90	32	110	3.93(0.26)	0.18	33.52(3.30)
90	36	110	3.93(0.26)	0.20	37.98(3.49)
90	40	110	3.93(0.26)	0.22	39.47(3.86)
95	10	110	2.67(0.49)	0.07	27.43(3.15)
95	*14*	*110*	*3.67(0.49)*	*0.10*	*30.03(3.06)*
95	*18*	*110*	*3.80(0.41)*	*0.12*	*31.65(3.44)*
95	*22*	*110*	*3.73(0.46)*	*0.15*	*38.53(3.55)*
95	28	110	3.87(0.35)	0.19	35.69(3.31)
95	32	110	3.93(0.26)	0.21	36.34(3.64)
95	36	110	3.87(0.35)	0.24	36.49(3.63)
95	40	110	4.00(0.00)	0.27	38.05(4.14)

IQ, image quality score, SD, standard deviation, E, effective dose, SNR, signal to noise ratio.

Appendix XX: APPS IQ score, SNR, and the associated E (mSv) with optimising 115 cm SID (Extended factorial)					
kVp	mAs	SID	IQ score (SD)	ED(mSv)	SNR(SD)
60	**10**	**115**	2.00(0.00)	0.01	13.71(1.10)
60	**14**	**115**	2.07(0.26)	0.01	12.39(1.26)
60	**18**	**115**	2.07(0.26)	0.01	16.54(1.64)
60	**22**	**115**	2.07(0.26)	0.02	17.48(1.67)
60	**28**	**115**	2.07(0.26)	0.02	17.36(1.84)
60	**32**	**115**	2.20(0.41)	0.03	21.48(1.91)
60	**36**	**115**	2.13(0.35)	0.03	19.50(1.79)
60	**40**	**115**	2.13(0.35)	0.03	21.21(1.94)
65	**10**	**115**	2.07(0.26)	0.01	13.42(1.40)
65	**14**	**115**	2.07(0.26)	0.02	17.89(1.62)
65	**18**	**115**	2.13(0.35)	0.02	17.38(1.72)
65	**22**	**115**	2.20(0.41)	0.03	21.20(1.70)
65	**28**	**115**	2.27(0.46)	0.03	21.38(2.06)
65	**32**	**115**	2.60(0.51)	0.04	22.82(2.09)
65	**36**	**115**	2.73(0.46)	0.04	22.98(2.21)
65	**40**	**115**	2.80(0.41)	0.05	24.82(2.46)
70	**10**	**115**	2.07(0.26)	0.02	15.70(1.53)
70	**14**	**115**	2.13(0.35)	0.02	20.81(1.76)
70	**18**	**115**	2.20(0.41)	0.03	21.64(1.89)
70	**22**	**115**	2.33(0.49)	0.04	21.05(2.14)
70	**28**	**115**	2.80(0.41)	0.05	25.46(2.29)
70	**32**	**115**	2.93(0.26)	0.05	27.38(2.15)
70	*36*	*115*	*3.00(0.00)*	*0.06*	*27.07(2.38)*
70	*40*	*115*	*3.00(0.00)*	*0.07*	*27.42(2.58)*
75	**10**	**115**	2.13(0.35)	0.02	16.70(1.65)
75	**14**	**115**	2.13(0.35)	0.03	22.02(1.91)
75	**18**	**115**	2.47(0.52)	0.04	24.23(1.95)
75	*22*	*115*	*3.00(0.00)*	*0.05*	*26.49(2.25)*
75	*28*	*115*	*3.07(0.26)*	*0.06*	*27.97(2.23)*
75	*32*	*115*	*3.00(0.00)*	*0.07*	*28.81(2.58)*
75	*36*	*115*	*3.60(0.51)*	*0.08*	*31.23(2.70)*
75	*40*	*115*	*3.80(0.41)*	*0.09*	*33.77(2.92)*
80	**10**	**115**	2.13(0.35)	0.03	21.10(1.64)
80	**14**	**115**	2.53(0.52)	0.04	23.59(2.03)
80	*18*	*115*	*3.00(0.00)*	*0.05*	*26.93(2.32)*
80	*22*	*115*	*3.00(0.00)*	*0.07*	*25.20(2.13)*

80	28	115	3.07(0.26)	0.09	28.66(2.75)
80	32	115	3.60(0.51)	0.10	32.69(2.60)
80	36	115	3.47(0.52)	0.11	31.76(3.03)
80	40	115	3.73(0.59)	0.12	35.32(3.04)
85	10	115	2.20(0.41)	0.04	20.83(2.00)
85	14	115	2.80(0.41)	0.06	26.49(2.48)
85	18	115	2.87(0.35)	0.07	27.71(2.65)
85	22	115	3.40(0.51)	0.08	31.99(2.74)
85	28	115	3.27(0.46)	0.11	29.39(2.94)
85	32	115	3.73(0.46)	0.12	37.61(3.05)
85	36	115	3.73(0.59)	0.14	35.67(3.36)
85	40	115	3.80(0.41)	0.15	35.38(3.24)
90	10	115	2.67(0.49)	0.05	23.44(2.17)
90	14	115	3.00(0.00)	0.07	25.22(2.56)
90	18	115	3.53(0.52)	0.09	32.64(2.82)
90	22	115	3.53(0.52)	0.11	31.48(3.06)
90	28	115	3.93(0.26)	0.13	37.46(3.42)
90	32	115	3.73(0.46)	0.15	32.78(3.22)
90	36	115	3.80(0.41)	0.17	31.48(3.35)
90	40	115	3.87(0.35)	0.19	42.27(3.80)
95	10	115	2.67(0.49)	0.06	26.30(2.47)
95	14	115	3.33(0.49)	0.08	30.30(2.79)
95	18	115	3.07(0.46)	0.11	29.70(3.08)
95	22	115	3.67(0.62)	0.13	34.15(3.40)
95	28	115	3.73(0.46)	0.16	34.80(3.48)
95	32	115	3.67(0.62)	0.19	35.44(3.71)
95	36	115	3.93(0.26)	0.21	36.40(3.84)
95	40	115	4.00(0.00)	0.23	41.52(4.20)

IQ, image quality score, SD, standard deviation, E, effective dose, SNR, signal to noise ratio.

Appendix XXI: APPS IQ score, SNR, and the associated E (mSv) with optimising 120 cm SID **(Extended factorial)**

kVp	mAs	SID	IQ score (SD)	ED(mSv)	SNR(SD)
60	10	120	2.00(0.00)	0.01	12.19(0.77)
60	14	120	2.07(0.26)	0.01	14.38(0.99)
60	18	120	2.13(0.35)	0.01	13.52(1.15)
60	22	120	2.20(0.41)	0.02	17.65(1.12)

60	28	120	2.07(0.26)	0.02	17.93(1.37)
60	32	120	2.20(0.41)	0.02	20.18(1.37)
60	36	120	2.13(0.35)	0.03	20.96(1.42)
60	40	120	2.27(0.46)	0.03	20.68(1.48)
65	10	120	2.07(0.26)	0.01	14.42(0.99)
65	14	120	2.00(0.00)	0.02	14.62(1.05)
65	18	120	2.07(0.26)	0.02	15.96(1.33)
65	22	120	2.13(0.35)	0.02	20.02(1.36)
65	28	120	2.40(0.51)	0.03	21.15(1.47)
65	32	120	2.60(0.51)	0.04	22.37(1.66)
65	36	120	2.47(0.52)	0.04	22.40(1.60)
65	40	120	2.93(0.26)	0.04	24.66(1.93)
70	10	120	2.13(0.35)	0.02	17.15(1.20)
70	14	120	2.07(0.26)	0.02	18.41(1.39)
70	18	120	2.33(0.49)	0.03	20.72(1.36)
70	22	120	2.73(0.46)	0.03	22.28(1.69)
70	28	120	2.40(0.51)	0.04	22.68(1.66)
70	*32*	*120*	*3.00(0.00)*	*0.05*	*25.40(1.97)*
70	*36*	*120*	*3.13(0.35)*	*0.06*	*27.33(2.15)*
70	*40*	*120*	*3.00(0.00)*	*0.06*	*27.05(2.49)*
75	10	120	2.07(0.26)	0.02	18.11(1.38)
75	14	120	2.40(0.51)	0.03	19.92(1.36)
75	18	120	2.73(0.46)	0.04	22.19(1.56)
75	*22*	*120*	*3.00(0.00)*	*0.05*	*25.00(1.89)*
75	*28*	*120*	*3.07(0.26)*	*0.06*	*28.32 2.14)*
75	*32*	*120*	*3.00(0.00)*	*0.07*	*25.52(2.25)*
75	*36*	*120*	*3.67(0.49)*	*0.08*	*34.33(2.49)*
75	*40*	*120*	*3.47(0.52)*	*0.08*	*31.85(2.52*
80	10	120	2.27(0.46)	0.03	20.37(1.41)
80	14	120	2.40(0.51)	0.04	21.66(1.59)
80	*18*	*120*	*3.00(0.00)*	*0.05*	*25.51(1.97)*
80	*22*	*120*	*3.00(0.00)*	*0.06*	*24.28(2.00)*
80	*28*	*120*	*3.20(0.41)*	*0.08*	*29.18(2.52)*
80	*32*	*120*	*3.80(0.41)*	*0.09*	*33.79(2.78)*
80	*36*	*120*	*3.67(0.49)*	*0.10*	*32.80(2.94)*
80	*40*	*120*	*3.67(0.49)*	*0.11*	*34.22(3.16)*
85	10	120	2.27(0.46)	0.04	21.32(1.57)
85	*14*	*120*	*3.00(0.00)*	*0.05*	*26.27(1.82)*
85	*18*	*120*	*3.00(0.00)*	*0.06*	*27.87(2.35)*
85	*22*	*120*	*3.40(0.51)*	*0.08*	*31.77(2.70)*
85	*28*	*120*	*3.53(0.52)*	*0.10*	*31.16(2.80)*

kVp	mAs	SID	IQ score (SD)	E(mSv)	SNR(SD)
85	*32*	**120**	*3.87(0.35)*	*0.11*	*31.67(2.95)*
85	*36*	**120**	*3.73(0.59)*	*0.13*	*33.20(3.17)*
85	*40*	**120**	*3.87(0.35)*	*0.14*	*39.90(3.64)*
90	**10**	**120**	2.13(0.35)	0.04	21.06(1.58)
90	*14*	**120**	*3.00(0.00)*	*0.06*	*27.68(2.24)*
90	*18*	**120**	*3.60(0.51)*	*0.08*	*30.84(2.55)*
90	*22*	**120**	*3.53(0.52)*	*0.10*	*31.69(3.02)*
90	*28*	**120**	*3.87(0.35)*	*0.12*	*32.59(3.01)*
90	*32*	**120**	*3.87(0.35)*	*0.14*	*38.81(3.29)*
90	*36*	**120**	*3.80(0.41)*	*0.15*	*34.68(3.40)*
90	**40**	**120**	3.93(0.26)	0.17	40.54(3.86)
95	**10**	**120**	2.80(0.41)	0.05	22.20(1.81)
95	*14*	**120**	*3.27(0.46)*	*0.07*	*29.24(2.42)*
95	*18*	**120**	*3.60(0.51)*	*0.09*	*31.52(2.63)*
95	*22*	**120**	*3.73(0.46)*	*0.11*	*33.98(3.20)*
95	*28*	**120**	*3.93(0.26)*	*0.15*	*34.46(3.24)*
95	**32**	**120**	3.93(0.26)	0.17	34.42(3.48)
95	**36**	**120**	4.00(0.00)	0.19	33.85(3.47)
95	**40**	**120**	3.93(0.26)	0.21	35.80(3.51)

IQ, image quality score, SD, standard deviation, E, effective dose, SNR, signal to noise ratio.

Appendix XXII: APPS IQ score, SNR, and the associated E (mSv) with optimising 125 cm SID **(Extended factorial)**

kVp	mAs	SID	IQ score (SD)	E(mSv)	SNR(SD)
60	**10**	**125**	2.00(0.00)	0.01	12.25(0.71)
60	**14**	**125**	2.07(0.26)	0.01	12.82(1.09)
60	**18**	**125**	2.07(0.26)	0.01	11.94(1.17)
60	**22**	**125**	2.07(0.26)	0.01	14.16(1.14)
60	**28**	**125**	2.00(0.00)	0.02	16.45(1.30)
60	**32**	**125**	2.07(0.26)	0.02	15.88(1.39)
60	**36**	**125**	2.20(0.41)	0.02	19.04(1.41)
60	**40**	**125**	2.13(0.35)	0.03	17.15(1.64)
65	**10**	**125**	2.07(0.26)	0.01	13.15(1.06)
65	**14**	**125**	2.07(0.26)	0.01	13.04(1.08)
65	**18**	**125**	2.13(0.35)	0.02	17.62(1.39)
65	**22**	**125**	2.07(0.26)	0.02	19.08(1.37)
65	**28**	**125**	2.13(0.35)	0.03	17.90(1.43)

65	32	125	2.87(0.35)	0.03	22.38(1.71)
65	36	125	2.47(0.52)	0.04	18.90(1.63)
65	40	125	2.60(0.51)	0.04	21.83(1.56)
70	10	125	2.07(0.26)	0.01	15.18(1.05)
70	14	125	2.07(0.26)	0.02	16.81(1.33)
70	18	125	2.07(0.26)	0.03	18.24(1.36)
70	22	125	2.13(0.35)	0.03	19.07(1.46)
70	28	125	2.80(0.41)	0.04	21.78(1.57)
70	32	125	3.00(0.00)	0.04	23.33(1.90)
70	*36*	*125*	*3.00(0.00)*	*0.05*	*21.94(2.00)*
70	*40*	*125*	*3.27(0.46)*	*0.06*	*27.09(2.03)*
75	10	125	2.07(0.26)	0.02	11.56(7.40)
75	14	125	2.47(0.52)	0.03	21.36(1.46)
75	18	125	2.40(0.51)	0.03	21.57(1.63)
75	22	125	2.80(0.41)	0.04	21.09(1.76)
75	*28*	*125*	*3.00(0.00)*	*0.05*	*24.37(2.12)*
75	*32*	*125*	*3.80(0.41)*	*0.06*	*28.78(2.35)*
75	*36*	*125*	*3.80(0.41)*	*0.07*	*30.23(2.42)*
75	*40*	*125*	*3.67(0.49)*	*0.07*	*28.37(2.40)*
80	10	125	2.07(0.26)	0.02	15.90(1.34)
80	14	125	2.80(0.41)	0.03	21.89(1.54)
80	*18*	*125*	*3.00(0.00)*	*0.04*	*24.00(1.87)*
80	*22*	*125*	*3.07(0.26)*	*0.05*	*27.98(2.10)*
80	*28*	*125*	*3.00(0.00)*	*0.07*	*25.59(2.43)*
80	*32*	*125*	*3.73(0.46)*	*0.08*	*31.41(2.69)*
80	*36*	*125*	*3.80(0.41)*	*0.09*	*35.34(2.72)*
80	*40*	*125*	*3.80(0.41)*	*0.10*	*32.24(2.95)*
85	10	125	2.20(0.41)	0.03	20.81(1.56)
85	*14*	*125*	*3.00(0.00)*	*0.04*	*22.40(1.65)*
85	*18*	*125*	*3.13(0.35)*	*0.06*	*21.62(1.87)*
85	*22*	*125*	*3.73(0.46)*	*0.07*	*30.41(2.47)*
85	*28*	*125*	*3.67(0.49)*	*0.09*	*27.28(2.73)*
85	*32*	*125*	*3.87(0.35)*	*0.10*	*28.99(2.86)*
85	*36*	*125*	*3.73(0.46)*	*0.11*	*37.05(3.29)*
85	*40*	*125*	*3.87(0.35)*	*0.12*	*36.48(3.37)*
90	10	125	2.27(0.46)	0.04	19.35(1.65)
90	14	125	2.67(0.49)	0.05	20.69(1.91)
90	*18*	*125*	*3.40(0.51)*	*0.07*	*30.17(2.28)*
90	*22*	*125*	*3.87(0.35)*	*0.08*	*29.97(2.67)*
90	*28*	*125*	*3.87(0.35)*	*0.11*	*35.89(3.29)*
90	*32*	*125*	*3.87(0.35)*	*0.12*	*34.35(3.42)*

kVp	mAs	SID	IQ score(SD)	E	SNR(SD)
90	*36*	*125*	*3.87(0.35)*	*0.14*	*32.34(3.46)*
90	*40*	*125*	*3.87(0.35)*	*0.15*	*37.13(3.83)*
95	*10*	*125*	*2.47(0.52)*	*0.05*	*21.99(1.76)*
95	*14*	*125*	*3.47(0.52)*	*0.07*	*25.23(2.22)*
95	*18*	*125*	*3.87(0.35)*	*0.08*	*31.60(2.67)*
95	*22*	*125*	*3.93(0.26)*	*0.10*	*29.29(2.94)*
95	*28*	*125*	*3.80(0.41)*	*0.13*	*31.49(3.36)*
95	*32*	*125*	*3.87(0.35)*	*0.15*	*32.98(3.46)*
95	**36**	**125**	3.87(0.35)	0.17	42.04(4.05)
95	**40**	**125**	3.93(0.26)	0.18	37.58(3.98)

IQ, image quality score, SD, standard deviation, E, effective dose, SNR, signal to noise ratio.

Appendix XXIII: APPS IQ score, SNR, and the associated E (mSv) with optimising 130 cm SID (Extended factorial)

kVp	mAs	SID	IQ score(SD)	E(mSv)	SNR(SD)
60	**10**	**130**	2.00(0.00)	0.01	12.22(0.84)
60	**14**	**130**	2.00(0.00)	0.01	10.96(0.91)
60	**18**	**130**	2.20(0.41)	0.01	12.07(1.04)
60	**22**	**130**	2.07(0.26)	0.01	12.53(1.09)
60	**28**	**130**	2.07(0.26)	0.02	13.66(1.27)
60	**32**	**130**	2.07(0.26)	0.02	14.49(1.34)
60	**36**	**130**	2.80(0.41)	0.02	19.28(1.41)
60	**40**	**130**	2.20(0.41)	0.02	16.20(1.45)
65	**10**	**130**	2.20(0.41)	0.01	13.74(0.98)
65	**14**	**130**	2.07(0.26)	0.01	12.64(1.05)
65	**18**	**130**	2.07(0.26)	0.02	15.68(1.20)
65	**22**	**130**	2.27(0.46)	0.02	17.36(1.33)
65	**28**	**130**	2.53(0.52)	0.02	18.53(1.45)
65	**32**	**130**	2.93(0.26)	0.03	20.34(1.47)
65	**36**	**130**	3.00(0.00)	0.03	20.51(1.58)
65	**40**	**130**	2.93(0.26)	0.04	20.50(1.72)
70	**10**	**130**	2.13(0.35)	0.01	15.05(1.10)
70	**14**	**130**	2.07(0.26)	0.02	16.37(1.25)
70	**18**	**130**	2.07(0.26)	0.02	16.55(1.31)
70	**22**	**130**	2.73(0.46)	0.03	18.85(1.49)
70	**28**	**130**	2.93(0.26)	0.03	21.12(1.53)
70	**32**	**130**	2.93(0.26)	0.04	22.62(1.80)

70	36	130	3.13(0.35)	0.04	22.93(1.90)
70	40	130	3.27(0.46)	0.05	23.00(2.08)
75	10	130	2.07(0.26)	0.02	14.80(1.15)
75	14	130	2.20(0.41)	0.02	18.05(1.31)
75	18	130	2.60(0.63)	0.03	17.61(1.48)
75	22	130	3.00(0.00)	0.04	21.30(1.68)
75	28	130	3.47(0.52)	0.05	22.48(1.84)
75	32	130	3.73(0.46)	0.05	23.52(2.31)
75	36	130	3.67(0.49)	0.06	24.01(2.22)
75	40	130	3.60(0.63)	0.07	25.96(2.64)
80	10	130	2.13(0.35)	0.02	15.99(1.27)
80	14	130	2.47(0.52)	0.03	19.10(1.56)
80	18	130	3.07(0.26)	0.04	23.53(1.73)
80	22	130	3.33(0.49)	0.05	24.60(1.97)
80	28	130	3.60(0.51)	0.06	24.53(2.28)
80	32	130	3.73(0.46)	0.07	30.05(2.52)
80	36	130	3.73(0.46)	0.08	27.18(2.77)
80	40	130	3.87(0.35)	0.09	29.98(2.94)
85	10	130	2.80(0.41)	0.03	19.90(1.49)
85	14	130	2.93(0.26)	0.04	21.99(1.62)
85	18	130	3.60(0.51)	0.05	25.87(1.96)
85	22	130	3.60(0.51)	0.06	23.42(2.24)
85	28	130	3.87(0.35)	0.08	29.55(2.80)
85	32	130	3.87(0.35)	0.09	28.06(2.88)
85	36	130	3.93(0.26)	0.10	30.67(3.16)
85	40	130	3.93(0.26)	0.11	28.03(3.17)
90	10	130	2.40(0.51)	0.04	17.39(1.55)
8	14	130	2.93(0.26)	0.05	20.98(1.90)
90	18	130	3.53(0.52)	0.06	22.67(2.24)
90	22	130	3.87(0.35)	0.08	28.37(2.68)
90	28	130	3.80(0.41)	0.10	27.11(2.82)
90	32	130	3.93(0.26	0.11	30.87(3.25)
90	36	130	3.80(0.41)	0.12	35.05(3.65)
90	40	130	3.80(0.41)	0.14	36.80(3.85)
95	10	130	2.93(0.26)	0.04	23.96(1.70)
95	14	130	3.40(0.51)	0.06	22.28(2.04)
95	18	130	3.73(0.46)	0.08	24.53(2.57)
95	22	130	3.87(0.35)	0.09	32.77(2.74)
95	28	130	3.93(0.26)	0.12	30.29(3.36)
95	32	130	3.93(0.26)	0.13	33.08(3.60)
95	36	130	3.80(0.41)	0.15	33.99(3.88)

| 95 | 40 | 130 | 3.87(0.35) | 0.17 | 36.71(4.37) |

IQ, image quality score, SD, standard deviation, E, effective dose, SNR, signal to noise ratio.

Appendix XXIV: **APPS IQ score, SNR, and the associated E (mSv) with optimising** Caudal Orientation**-AEC**

kVp	SID	IQ score (SD)	E (mSv)	SNR(SD)
60	95	3.73(0.46)	0.26	42.06(6.49)
60	100	3.87(0.35)	0.23	45.54(6.24)
60	105	3.80(0.41)	0.22	43.32(6.21)
60	110	3.93(0.26)	0.21	44.64(5.64)
60	115	3.73(0.46)	0.18	43.34(5.51)
60	120	3.93(0.26)	0.18	40.68(5.52)
60	125	3.67(0.49)	0.17	41.45(5.57)
60	130	3.80(0.41)	0.16	43.65(5.20)
65	95	3.40(0.51)	0.21	40.99(6.20)
65	100	3.67(0.49)	0.19	36.95(5.44)
65	105	3.80(0.41)	0.18	45.34(6.11)
65	110	3.60(0.51)	0.16	39.62(5.66)
65	115	3.20(0.41)	0.15	40.11(5.50)
65	120	3.80(0.41)	0.14	41.87(5.20)
65	125	3.60(0.51)	0.14	41.09(4.96)
65	130	3.40(0.51)	0.14	33.21(5.10)
70	95	3.60(0.51)	0.18	45.56(5.60)
70	100	3.73(0.46)	0.16	42.93(5.36)
70	105	3.47(0.52)	0.14	37.19(4.91)
70	110	3.07(0.26)	0.14	40.31(4.99)
70	43	3.33(0.49)	0.13	38.43(4.57)
70	120	3.60(0.51)	0.12	35.06(4.43)
70	125	3.07(0.26)	0.12	37.23(4.35)
70	130	3.20(0.41)	0.11	33.40(4.44)
75	95	3.07(0.26)	0.15	38.79(5.43)
75	100	3.27(0.46)	0.13	42.29(4.88)
75	105	3.47(0.52)	0.12	39.87(4.39)
75	110	3.00(0.00)	0.12	38.72(4.13)
75	115	3.73(0.46)	0.11	39.11(4.02)
75	120	3.00(0.00)	0.11	34.98(4.25)
75	125	3.40(0.51)	0.10	38.61(4.29)

75	130	3.07(0.26)	0.10	35.70(4.00)
80	95	2.80(0.41)	0.14	37.82(5.07)
80	100	3.00(0.00)	0.12	37.71(4.86)
80	105	3.00(0.00)	0.11	34.73(4.44)
80	110	3.00(0.00)	0.11	32.24(4.35)
80	115	3.07(0.26)	0.10	36.48(4.13)
80	120	3.13(0.35)	0.10	32.83(4.08)
80	125	3.00(0.00)	0.10	34.72(4.31)
80	130	2.53(0.52)	0.09	28.10(4.17)
85	95	3.00(0.00)	0.13	34.90(4.77)
85	100	3.00(0.00)	0.11	38.65(4.80)
85	105	2.53(0.52)	0.10	32.70(3.18)
85	110	3.07(0.26)	0.11	36.72(3.43)
85	115	2.93(0.26)	0.10	34.25(4.10)
85	120	3.00(0.00)	0.09	36.52(4.21)
85	125	2.73(0.46)	0.09	36.27(3.62)
85	130	2.13(0.35)	0.09	27.61(3.55)
90	95	2.73(0.46)	0.12	37.46(5.14)
90	100	2.60(0.51)	0.10	34.94(4.70)
90	105	2.67(0.49)	0.11	33.52(4.04)
90	110	3.00(0.00)	0.10	36.01(3.34)
90	115	3.07(0.26)	0.09	35.44(4.11)
90	120	3.07(0.26)	0.09	34.99(3.6)
90	125	2.47(0.52)	0.08	27.70(2.69)
90	130	2.40(0.51)	0.08	28.46(3.27)
95	95	2.60(0.51)	0.11	35.24(4.89)
95	100	2.73(0.46)	0.10	36.68(3.56)
95	105	2.20(0.41)	0.10	28.91(3.54)
95	110	2.20(0.41)	0.09	31.61(3.75)
95	115	3.00(0.00)	0.09	35.74(3.04)
95	120	3.00(0.00)	0.08	34.77(3.25)
95	125	2.27(0.46)	0.08	30.20(2.83)
95	130	2.07(0.26)	0.08	26.16(2.88)

IQ, image quality score, SD, standard deviation, E, effective dose, SNR, signal to noise ratio.

Appendix XXV: APPS IQ score, SNR, and the associated E (mSv) with optimising Cranial Orientation-AEC				
kVp	SID	IQ score (SD)	E(mSv)	SNR(SD)
60	95	3.73(0.46)	0.35	44.06(2.79)
60	100	3.87(0.35)	0.32	50.49(1.54)
60	105	3.67(0.49)	0.30	37.45(1.14)
60	110	3.33(0.49)	0.28	41.96(1.52)
60	115	3.20(0.41)	0.25	33.72(1.67)
60	120	3.13(0.35)	0.24	36.39(2.12)
60	125	3.00(0.00)	0.24	38.46(2.80)
60	130	3.20(0.41)	0.23	43.53(3.54)
65	95	3.67(0.62)	0.27	42.54(2.38)
65	100	3.73(0.46)	0.25	43.78(1.17)
65	105	3.67(0.49)	0.23	42.57(1.02)
65	110	3.00(0.00)	0.22	37.46(1.31)
65	115	3.07(0.26)	0.20	36.11(1.70)
65	120	3.00(0.00)	0.19	37.11(1.96)
65	125	3.00(0.00)	0.19	35.18(2.42)
65	130	3.00(0.00)	0.18	33.62(2.66)
70	95	3.27(0.59)	0.23	34.90(2.20)
70	100	3.47(0.52)	0.20	40.28(1.31)
70	105	3.40(0.74)	0.19	38.56(0.63)
70	110	3.00(0.00)	0.18	35.25(1.08)
70	43	3.00(0.00)	0.17	33.00(1.33)
70	120	2.93(0.26)	0.16	34.61(1.88)
70	125	3.07(0.26)	0.16	36.81(2.48)
70	*130*	*2.93(0.26)*	*0.15*	*34.75(2.62)*
75	95	3.13(0.52)	0.18	33.86(1.93)
75	100	3.07(0.46)	0.18	37.61(1.46)
75	105	2.87(0.35)	0.16	35.68(0.56)
75	110	2.87(0.35)	0.15	32.19(0.80)
75	115	2.87(0.350	0.14	30.14(1.18)
75	*120*	*3.00(0.00)*	*0.14*	*33.67(1.83)*
75	*125*	*3.00(0.38)*	*0.13*	*30.45(2.07)*
75	130	2.73(0.46)	0.13	32.24(2.35)
80	95	2.80(0.56)	0.17	33.85(1.52)
80	100	2.93(0.46)	0.16	37.23(0.88)
80	105	2.73(0.46)	0.15	35.91(0.50)
80	110	2.60(0.51)	0.14	35.79(0.83)

80	115	2.60(0.51)	0.13	29.19(1.15)
80	120	2.27(0.46)	0.12	30.03(1.54)
80	125	2.33(0.49)	0.12	31.46(2.16)
80	130	2.47(0.52)	0.12	32.12(2.41)
85	95	2.73(0.46)	0.15	33.10(1.75)
85	100	2.93(0.70)	0.14	38.88(1.16)
85	105	2.53(0.52)	0.14	35.73(0.19)
85	110	2.53(0.52)	0.13	29.19(0.70)
85	115	2.20(0.41)	0.12	31.14(1.19)
85	120	2.13(0.35)	0.11	30.95(1.62)
85	125	2.33(0.49)	0.11	32.48(1.88)
85	130	2.20(0.41)	0.11	27.84(2.11)
90	95	2.33(0.49)	0.14	33.19(1.53)
90	100	2.20(0.41)	0.14	34.62(0.97)
90	105	2.73(0.46)	0.13	34.12(0.32)
90	110	2.40(0.51)	0.12	28.53(0.620
90	115	2.33(0.49)	0.12	27.30(1.11)
90	120	2.20(0.41)	0.11	30.29(1.52)
90	125	2.07(0.26)	0.10	29.95(1.86)
90	130	2.13(0.35)	0.10	29.61(2.19)
95	95	2.20(0.41)	0.13	32.74(1.26)
95	100	2.40(0.51)	0.13	35.81(1.08)
95	105	2.53(0.52)	0.12	37.49(0.00)
95	110	2.27(0.46)	0.12	27.66(0.74)
95	115	2.33(0.49)	0.11	28.33(1.11)
95	120	2.07(0.26)	0.11	29.00(1.50)
95	125	2.07(0.26)	0.10	30.42(1.65)
95	130	2.07(0.26)	0.09	27.32(1.95)
IQ, image quality score, SD, standard deviation, E, effective dose, SNR, signal to noise ratio.				

Appendix XXVI: APPS IQ score, SNR, and the associated E (mSv) with optimising Single chamber **configuration-AEC**

kVp	SID	IQ score (SD)	E(mSv)	SNR(SD)
60	95	3.67(0.49)	0.35	42.77(5.81)
60	100	3.67(0.49)	0.33	41.54(5.56)
60	105	3.93(0.26)	0.29	41.77(4.74)
60	110	3.67(0.49)	0.27	39.60(3.26)

60	115	3.87(0.35)	0.24	42.35(3.54)
60	120	3.27(0.46)	0.24	41.19(3.57)
60	125	3.20(0.41)	0.23	40.58(3.91)
60	130	3.20(0.41)	0.22	43.47(4.06)
65	95	3.27(0.46)	0.28	40.96(5.57)
65	100	3.47(0.52)	0.26	37.68(4.93)
65	105	3.20(0.41)	0.23	40.75(4.42)
65	110	3.07(0.26)	0.22	37.15(3.53)
65	115	3.47(0.52)	0.20	43.86(3.18)
65	120	3.07(0.26)	0.19	38.07(3.53)
65	125	3.00(0.00)	0.19	36.58(3.55)
65	130	2.87(0.35)	0.18	33.89(3.81)
70	95	3.33(0.49)	0.23	40.25(5.47)
70	100	3.00(0.38)	0.21	38.12(4.91)
70	105	3.00(0.00)	0.19	38.45(3.89)
70	110	3.07(0.26)	0.18	37.16(3.40)
70	43	3.13(0.35)	0.17	38.61(2.90)
70	120	3.00(0.00)	0.16	38.70(3.05)
70	125	2.80(0.41)	0.16	34.09(3.20)
70	*130*	*3.00(0.00)*	*0.15*	*37.15(3.52)*
75	95	2.87(0.64)	0.19	38.18(5.70)
75	100	2.87(0.35)	0.18	35.09(4.64)
75	105	2.80(0.41)	0.16	34.98(3.63)
75	*110*	*3.00(0.00)*	*0.15*	*35.96(2.82)*
75	*115*	*3.00(0.00)*	*0.14*	*36.55(2.81)*
75	120	2.80(0.41)	0.14	29.50(2.65)
75	125	2.60(0.51)	0.14	33.26(2.88)
75	*130*	*3.00(0.00)*	*0.13*	*33.55(3.14)*
80	95	2.67(0.49)	0.18	34.35(4.86)
80	100	2.80(0.56)	0.16	32.42(4.25)
80	*105*	*3.07(0.26)*	*0.15*	*37.79(3.91)*
80	110	2.73(0.46)	0.18	35.61(2.92)
80	*115*	*3.00(0.00)*	*0.13*	*36.51(2.61)*
80	120	2.53(0.52)	0.13	31.17(2.48)
80	125	2.27(0.46)	0.12	28.09(2.77)
80	130	2.27(0.46)	0.12	29.91(2.68)
85	95	2.20(0.41)	0.15	32.10(4.91)
85	100	2.60(0.51)	0.14	32.62(3.95)
85	105	2.40(0.51)	0.13	30.97(3.81)
85	110	2.73(0.46)	0.13	34.96(3.14)
85	115	2.33(0.49)	0.12	30.34(2.61)

kVp	SID			
85	120	2.20(0.41)	0.12	28.44(2.25)
85	125	2.13(0.35)	0.11	27.50(2.57)
85	130	2.20(0.41)	0.11	30.60(2.65)
90	95	2.13(0.35)	0.14	29.58(4.53)
90	100	2.27(0.46)	0.14	30.49(3.89)
90	105	2.33(0.49)	0.13	34.15(3.73)
90	110	2.47(0.52)	0.12	32.77(2.96)
90	115	2.20(0.41)	0.11	30.80(2.63)
90	120	2.07(0.26)	0.11	25.15(2.25)
90	125	2.20(0.41)	0.10	28.07(2.52)
90	130	2.13(0.35)	0.10	25.97(2.45)
95	95	2.20(0.41)	0.13	30.48(4.20)
95	100	2.13(0.35)	0.13	27.51(3.71)
95	105	2.27(0.46)	0.11	31.93(3.42)
95	110	2.20(0.41)	0.11	33.34(3.08)
95	115	2.27(0.46)	0.11	31.16(2.490
95	120	2.07(0.26)	0.10	29.69(2.23)
95	125	2.07(0.26)	0.10	27.40(2.39)
95	130	2.20(0.41)	0.10	25.82(2.30)

IQ, image quality score, SD, standard deviation, E, effective dose, SNR, signal to noise ratio.

Appendix XXVII: APPS IQ score, SNR, and the associated E (mSv) with optimising 2 outer chambers configuration**-AEC**

kVp	SID	IQ score (SD)	E (mSv)	SNR(SD)
60	95	3.67(0.49)	0.27	45.66(6.02)
60	100	3.20(0.41)	0.23	39.71(5.10)
60	105	3.47(0.52)	0.22	42.20(4.86)
60	110	3.53(0.52)	0.20	39.96(3.36)
60	115	3.40(0.51)	0.18	40.21(3.30)
60	120	3.73(0.46)	0.18	42.90(3.53)
60	125	3.07(0.26)	0.17	32.06(3.55)
60	130	3.00(0.00)	0.16	39.34(3.93)
65	95	3.20(0.41)	0.21	40.05(5.33)
65	100	3.60(0.51)	0.19	41.94 (4.86)
65	105	3.27(0.59)	0.17	38.30(4.11)
65	110	3.13(0.35)	0.16	36.46(2.95)
65	*115*	*3.47(0.52)*	*0.15*	*41.01(2.89)*

65	*120*	*3.07(0.26)*	*0.14*	*31.48(2.95)*
65	*125*	*3.07(0.26)*	*0.14*	*34.31(3.41)*
65	*130*	*3.07(0.26)*	*0.14*	*30.15(3.47)*
70	**95**	3.40(0.51)	0.18	37.23(4.88)
70	**100**	3.13(0.52)	0.16	39.55(4.86)
70	**105**	*3.33(0.49)*	*0.14*	*37.64(3.75)*
70	**110**	*3.00(0.00)*	*0.14*	*35.09(2.56)*
70	**43**	*3.00(0.00)*	*0.13*	*34.27(2.43)*
70	**120**	*3.07(0.26)*	*0.12*	*32.67(3.08)*
70	**125**	*3.07(0.26)*	*0.12*	*32.90(3.05)*
70	**130**	*3.00(0.00)*	*0.11*	*35.52(3.12)*
75	**95**	*3.27(0.59)*	*0.15*	*35.25(4.56)*
75	**100**	*3.13(0.52)*	*0.13*	*38.38(4.58)*
75	**105**	2.87(0.35)	0.12	37.23(4.00)
75	**110**	*3.00(0.00)*	*0.12*	*31.88(2.60)*
75	**115**	2.93(0.26)	0.11	29.53(2.52)
75	**120**	2.93(0.26)	0.11	31.04(2.42)
75	**125**	2.93(0.26)	0.10	34.32(2.87)
75	**130**	*3.00(0.00)*	*0.10*	*31.42(2.70)*
80	*95*	*3.00(0.53)*	*0.14*	*33.18(5.07)*
80	*100*	*3.07(0.46)*	*0.12*	*36.36(4.35)*
80	**105**	2.73(0.46)	0.11	34.10(3.34)
80	*110*	*3.07(0.26)*	*0.11*	*31.75(2.21)*
80	*115*	*3.00(0.00)*	*0.10*	*34.33(2.42)*
80	**120**	2.80(0.41)	0.10	32.55(2.38)
80	*125*	*3.00(0.00)*	*0.10*	*34.40(2.88)*
80	**130**	2.73(0.46)	0.09	31.54(2.73)
85	*95*	*3.07(0.46)*	*0.13*	*36.15(4.33)*
85	**100**	2.53(0.52)	0.11	35.27(4.37)
85	**105**	2.93(0.46)	0.10	32.47(3.39)
85	**110**	2.87(0.35)	0.11	29.27(2.52)
85	*115*	*3.00(0.00)*	*0.10*	*32.74(2.59)*
85	**120**	2.40(0.51)	0.09	26.73(2.27)
85	**125**	2.20(0.41)	0.09	26.44(2.55)
85	**130**	2.40(0.51)	0.09	26.38(2.48)
90	**95**	2.53(0.52)	0.12	32.88(4.46)
90	**100**	2.67(0.49)	0.10	33.73(4.28)
90	**105**	2.93(0.26)	0.11	31.53(3.42)
90	**110**	2.47(0.52)	0.10	32.66(2.94)
90	**115**	2.40(0.51)	0.09	30.79(2.32)
90	**120**	2.40(0.51)	0.09	27.15(2.20)

kVp	SID	IQ	E	SNR
90	125	2.20(0.41)	0.08	27.71(2.22)
90	130	2.27(0.46)	0.08	23.75(2.22)
95	95	2.40(0.51)	0.11	36.79(4.870
95	100	2.27(0.46)	0.10	28.31(4.02)
95	105	2.27(0.46)	0.10	31.94(3.60)
95	110	2.40(0.51)	0.09	31.11(2.88)
95	115	2.47(0.52)	0.09	28.57(2.28)
95	120	2.13(0.35)	0.08	25.62(2.11
95	125	2.07(0.26)	0.08	23.76(2.24)
95	130	2.20(0.41)	0.08	24.96(2.22)

IQ, image quality score, SD, standard deviation, E, effective dose, SNR, signal to noise ratio.

Appendix XXVIII: APPS IQ score, SNR, and the associated E (mSv) with optimising all chambers configuration-**AEC**

kVp	SID	IQ score (SD)	E(mSv)	SNR(SD)
60	95	3.73(0.46)	0.29	38.25(3.84)
60	100	3.87(0.35)	0.26	39.98(4.81)
60	105	3.73(0.46)	0.25	39.03(3.95)
60	110	3.60(0.51)	0.22	38.51(3.62)
60	115	3.93(0.26)	0.20	43.19(3.47)
60	120	3.87(0.35)	0.20	41.46(3.30)
60	125	3.47(0.52)	0.19	37.85(3.89)
60	130	3.20(0.56)	0.18	37.52(4.30)
65	95	3.27(0.46)	0.23	39.29(3.55)
65	100	3.27(0.46)	0.21	33.28(4.47)
65	105	3.80(0.41)	0.20	36.13(3.62)
65	110	3.80(0.41)	0.18	38.33(3.54)
65	115	3.00(0.38)	0.16	31.16(3.23)
65	120	3.27(0.46)	0.16	40.21(3.20)
65	125	3.07(0.26)	0.16	34.92(3.42)
65	130	3.07(0.46)	0.15	32.69(3.54)
70	95	3.47(0.52)	0.20	36.91(3.11)
70	100	3.53(0.52)	0.18	36.01(4.25)
70	105	3.67(0.49)	0.17	37.40(3.78)
70	110	3.00(0.00)	0.15	32.85(2.92)
70	43	3.60(0.51)	0.14	34.28(2.72)
70	120	3.07(0.26)	0.14	33.87(3.00)

70	*125*	*3.00(0.00)*	*0.13*	*31.27(3.31)*
70	*130*	*3.13(0.35)*	*0.13*	*34.42(3.07)*
75	**95**	3.070.46)	0.17	35.63(2.84)
75	**100**	2.93(0.26)	0.16	32.77(3.94)
75	*105*	*3.93(0.26)*	*0.15*	*35.51(3.40)*
75	*110*	*3.00(0.00)*	*0.13*	*33.36(2.81)*
75	*115*	*3.00(0.00)*	*0.12*	*34.12(2.59)*
75	**120**	2.87(0.35)	0.12	32.21(2.65)
75	**125**	2.60(0.51)	0.11	29.20(2.70)
75	**130**	2.7390.46)	0.11	31.52(3.20)
80	**95**	2.87(0.35)	0.15	32.43(2.46)
80	*100*	*3.00(0.38)*	*0.14*	*30.95(3.81)*
80	*105*	*3.27(0.46)*	*0.14*	*35.76(3.61)*
80	*110*	*3.00(0.00)*	*0.12*	*31.40(2.82)*
80	**115**	2.93(0.26)	0.11	30.17(2.67)
80	*120*	*3.00(0.00)*	*0.11*	*33.84(2.74)*
80	*125*	*3.13(0.35)*	*0.10*	*36.89(2.86)*
80	**130**	2.40(0.51)	0.10	29.48(3.00)
85	**95**	2.67(0.49)	0.14	33.63(2.71)
85	*100*	*3.00(0.00)*	*0.13*	*33.56(3.89)*
85	*105*	*3.00(0.00)*	*0.13*	*31.82(3.390)*
85	**110**	2.93(0.26)	0.12	31.18(2.810)
85	**115**	2.67(0.49)	0.11	30.17(2.43)
85	**120**	2.80(0.41)	0.10	29.87(2.51)
85	**125**	2.80(0.41)	0.10	29.78(2.64)
85	**130**	2.40(0.51)	0.09	28.86(2.76)
90	**95**	2.47(0.52)	0.13	34.27(2.94)
90	**100**	2.47(0.52)	0.12	33.78(3.88)
90	**105**	2.87(0.52)	0.12	33.28(3.19)
90	**110**	2.80(0.41)	0.11	32.15(2.79)
90	**115**	2.67(0.49)	0.10	28.35(2.21)
90	**120**	2.80(0.41)	0.09	31.24(2.33)
90	**125**	2.60(0.51)	0.09	33.13(2.53)
90	**130**	2.07(0.26)	0.09	26.16(2.76)
95	**95**	2.33(0.49)	0.12	32.41(2.96)
95	**100**	2.33(0.49)	0.12	32.30(3.90)
95	**105**	2.53(0.52)	0.11	28.66(2.99)
95	**110**	2.73(0.46)	0.11	27.98(2.59)
95	**115**	2.20(0.41)	0.10	27.50(2.52)
95	**120**	2.20(0.41)	0.09	25.36(2.31)
95	**125**	2.40(0.51)	0.08	25.57(2.52)

| 95 | 130 | 2.20(0.41) | 0.08 | 27.38(2.34) |

IQ, image quality score, SD, standard deviation, E, effective dose, SNR, signal to noise ratio.

Appendix XXIX: APPS IQ score, SNR, and the associated E (mSv) with optimising
Broad focal spot**-AEC**

kVp	SID	IQ score (SD)	E(mSv)	SNR(SD)
60	95	3.80(0.41)	0.28	45.31(5.97)
60	100	3.93(0.26)	0.24	40.47(5.20)
60	105	3.80(0.41)	0.22	41.06(4.73)
60	110	3.80(0.41)	0.21	39.20(3.30)
60	115	3.87(0.35)	0.17	39.92(3.28)
60	120	3.73(0.46)	0.17	40.88(3.37)
60	125	3.07(0.46)	0.18	31.77(3.52)
60	130	3.47(0.52)	0.16	39.04(3.90)
65	95	3.67(0.49)	0.22	39.39(5.24)
65	100	3.53(0.64)	0.17	42.25(4.89)
65	105	3.33(0.49)	0.15	36.38(3.90)
65	110	3.53(0.52)	0.17	37.06(3.00)
65	115	3.93(0.26)	0.16	41.31(2.92)
65	120	3.07(0.26)	0.14	32.79(3.07)
65	125	3.00(0.00)	0.15	34.23(3.40)
65	130	3.07(0.26)	0.16	30.34(3.49)
70	95	3.40(0.51)	0.17	37.99(4.98)
70	100	3.53(0.52)	0.15	39.74(4.88)
70	105	3.53(0.52)	0.14	37.72(3.75)
70	110	3.00(0.00)	0.14	34.06(2.49)
70	115	3.07(0.26)	0.14	34.13(2.42)
70	120	3.00(0.00)	0.13	32.46(3.06)
70	125	3.00(0.00)	0.13	32.98(3.05)
70	130	3.07(0.26)	0.12	35.52(3.12)
75	95	3.33(0.62)	0.13	37.53(4.85)
75	100	3.53(0.52)	0.13	38.29(4.57)
75	105	3.00(0.00)	0.13	36.57(3.93)
75	110	2.93(0.26)	0.12	30.91(2.52)
75	115	3.00(0.00)	0.12	29.83(2.55)

75	*120*	*3.00(0.00)*	*0.12*	*30.97(2.41)*
75	*125*	*3.00(0.00)*	*0.13*	*34.40(2.88)*
75	*130*	*3.00(0.00)*	*0.11*	*31.81(2.74)*
80	*95*	*3.00(0.38)*	*0.14*	*32.77(5.01)*
80	**100**	2.93(0.26)	0.12	35.97(4.31)
80	**105**	2.93(0.26)	0.11	32.82(3.21)
80	**110**	2.93(0.26)	0.12	31.57(2.20)
80	*115*	*3.00(0.00)*	*0.13*	*34.33(2.42)*
80	*120*	*3.00(0.00)*	*0.10*	*32.42(2.37)*
80	*125*	*3.00(0.00)*	*0.10*	*34.63(9.90)*
80	*130*	*3.00(0.00)*	*0.09*	*31.67(2.74)*
85	**95**	2.60(0.63)	0.14	35.85(4.29)
85	**100**	2.80(0.56)	0.11	35.87(4.44)
85	**105**	2.67(0.49)	0.10	31.58(3.30)
85	**110**	2.40(0.51)	0.12	28.61(2.46)
85	**115**	2.87(0.35)	0.10	32.34(2.56)
85	**120**	2.20(0.41)	0.09	27.56(2.34)
85	**125**	2.07(0.26)	0.09	26.44(2.55)
85	**130**	2.20(0.41)	0.09	26.33(2.48)
90	**95**	2.47(0.52)	0.13	32.55(4.42)
90	**100**	2.67(0.49)	0.10	33.45(4.25)
90	**105**	2.47(0.52)	0.13	30.80(3.34)
90	**110**	2.60(0.51)	0.10	31.45(2.83)
90	**115**	2.67(0.49)	0.09	30.91(2.33)
90	**120**	2.40(0.51)	0.09	27.87(2.26)
90	**125**	2.13(0.35)	0.07	27.98(2.25)
90	**130**	2.07(0.26)	0.07	24.09(2.26)
95	**95**	2.40(0.51)	0.11	36.96(4.89)
95	**100**	2.13(0.35)	0.10	27.80(3.95)
95	**105**	2.47(0.52)	0.10	32.13(3.62)
95	**110**	2.13(0.35)	0.08	30.69(2.84)
95	**115**	2.20(0.41)	0.09	28.57(2.28)
95	**120**	2.07(0.26)	0.08	25.67(2.11)
95	**125**	2.33(0.62)	0.06	23.76(2.24
95	**130**	2.33(0.49)	0.07	25.23(2.25)
IQ, image quality score, SD, standard deviation, E, effective dose, SNR,signal to noise ratio.				

Appendix XXX: APPS IQ score, SNR, and the associated E (mSv) with optimising Fine focal spot-AEC				
kVp	**SID**	IQ score (SD)	E(mSv)	SNR(SD)
60	**95**	3.60(0.51)	0.26	39.27(5.76)
60	**100**	3.53(0.52)	0.23	32.44(4.77)
60	**105**	3.40(0.51)	0.21	40.95(4.31)
60	**110**	3.00(000)	0.20	40.95(4.10)
60	**115**	3.55(0.52)	0.18	42.67(3.81)
60	**120**	3.13(0.35)	0.18	41.36(3.86)
60	**125**	3.36(0.56)	0.17	38.87(3.94)
60	**130**	3.33(0.58)	0.16	43.55(4.48)
65	**95**	3.00(0.00)	0.21	38.93(5.12)
65	**100**	3.33(0.58)	0.19	39.97(4.90)
65	**105**	3.33(0.49)	0.17	39.79(3.77)
65	*110*	3.00(0.00)	0.17	38.10(3.64)
65	*115*	*3.07(0.26)*	*0.15*	*40.64(3.25)*
65	*120*	*3.00(0.00)*	*0.15*	*34.78(3.60)*
65	*125*	*3.60(0.51)*	*0.14*	*40.41(3.76)*
65	*130*	*3.00(0.00)*	*0.14*	*34.39(4.17)*
70	**95**	2.93(0.46)	0.17	39.69(5.30)
70	*100*	3.07(0.26)	0.16	38.36(4.56)
70	*105*	*3.00(0.00)*	*0.15*	*34.24(3.34)*
70	**110**	*3.00(0.00)*	*0.14*	*36.25(3.42)*
70	**115**	2.670.49)	0.13	36.11(3.05)
70	**120**	2.87(0.35)	0.13	29.11(3.01)
70	**125**	2.93(0.26)	0.12	35.37(3.39)
70	**130**	2.93(0.26)	0.12	34.77(3.84)
75	*95*	2.80(0.41)	0.15	38.31(5.02)
75	**100**	*3.00(0.00)*	*0.14*	*36.00(4.50)*
75	**105**	2.93(0.26)	0.13	35.51(3.71)
75	*110*	2.67(0.49)	0.12	31.47(2.75)
75	**115**	*3.00(0.00)*	*0.11*	*35.92(2.93)*
75	**120**	2.87(0.35)	0.11	32.28(2.92)
75	**125**	2.47(0.52)	0.11	29.44(3.33)
75	**130**	2.87(0.35)	0.10	34.61(3.58)
80	**95**	2.67(0.49)	0.13	34.81(4.14)
80	*100*	2.33(0.49)	0.12	29.89(4.28)
80	**105**	*3.00(0.00)*	*0.12*	*35.22(3.79)*

80	**110**	2.80(0.41)	0.11	34.66(3.40)
80	**115**	2.87(0.35)	0.10	31.94(2.85)
80	**120**	2.40(0.51)	0.10	30.08(2.92)
80	**125**	2.73(0.46)	0.10	31.42(3.45)
80	**130**	2.20(0.41)	0.10	27.65(3.33)
85	**95**	2.27(0.46)	0.12	33.67(4.28)
85	**100**	2.73(0.46)	0.11	37.95(4.39)
85	**105**	2.87(0.52)	0.11	34.58(3.76)
85	**110**	2.73(0.46)	0.10	33.05(3.07)
85	**115**	2.47(0.52)	0.10	31.73(2.75)
85	**120**	2.07(0.26)	0.09	27.49(2.86)
85	**125**	2.13(0.35)	0.09	27.15(3.01)
85	**130**	2.27(0.46)	0.09	32.14(3.71)
90	**95**	2.47(0.52)	0.11	34.03(4.40)
90	**100**	2.40(0.51)	0.11	32.14(4.22)
90	**105**	2.13(0.35)	0.10	33.18(3.64)
90	**110**	2.20(0.41)	0.10	31.35(3.06)
90	**115**	2.33(0.49)	0.09	28.66(2.75)
90	**120**	2.13(0.35)	0.09	27.60(2.64)
90	**125**	2.20(0.41)	0.08	28.84(3.31)
90	**130**	2.07(0.26)	0.08	28.50(3.04)
95	**95**	2.67(0.49)	0.11	34.48(4.37)
95	**100**	2.20(0.41)	0.10	32.31(4.08)
95	**105**	2.13(0.35)	0.09	25.55(3.06)
95	**110**	2.13(0.35)	0.09	28.95(2.72)
95	**115**	2.13(0.35)	0.09	34.04(2.69)
95	**120**	2.07(0.26)	0.08	23.48(2.68)
95	**125**	2.07(0.26)	0.08	26.09(2.81)
95	**130**	2.07(0.26)	0.08	28.06(3.32)

IQ, image quality score, SD, standard deviation, E, effective dose, SNR, signal to noise ratio.

Appendix XXXI: APPS IQ score, SNR, and the associated E (mSv) with optimising inherent filter type**-AEC**

kVp	**SID**	IQ score (SD)	E(mSv)	SNR(SD)
60	**95**	3.93(0.26)	0.26	49.43(6.52)
60	**100**	3.87(0.35)	0.24	38.19(4.91)
60	**105**	3.93(0.26)	0.23	29.91(3.44)

60	**110**	3.93(0.26)	0.21	30.48(2.57)
60	**115**	3.87(0.35)	0.18	33.36(2.74)
60	**120**	3.93(0.26)	0.19	30.99(2.55)
60	**125**	3.60(0.51)	0.16	25.81(2.86)
60	**130**	3.73(0.46)	0.17	28.44(2.84)
65	**95**	3.87(0.35)	0.21	41.75(5.56)
65	**100**	3.93(0.26)	0.18	35.50(4.11)
65	**105**	3.87(0.35)	0.18	34.79(3.73)
65	**110**	3.87(0.35)	0.16	28.88(2.34)
65	*115*	*3.87(0.35)*	*0.15*	*39.30(2.77)*
65	*120*	*3.47(0.52)*	*0.14*	*29.10(2.73)*
65	*125*	*3.33(0.49)*	*0.14*	*29.87(2.97)*
65	*130*	*3.60(0.51)*	*0.14*	*26.55(3.06)*
70	**95**	3.93(0.26)	0.18	40.75(5.35)
70	**100**	3.60(0.51)	0.16	35.57(4.37)
70	*105*	*3.73(0.46)*	*0.14*	*31.64(3.15)*
70	*110*	*3.53(0.52)*	*0.14*	*34.35(2.51)*
70	*115*	*3.20(0.41)*	*0.13*	*29.09(2.06)*
70	*120*	*3.07(0.26)*	*0.12*	*25.75(2.43)*
70	*125*	*3.20(0.41)*	*0.12*	*29.35(2.72)*
70	*130*	*3.33(0.49)*	*0.11*	*29.86(2.62)*
75	*95*	*3.73(0.46)*	*0.15*	*39.10(5.06)*
75	*100*	*3.67(0.49)*	*0.13*	*33.82(4.03)*
75	*105*	*3.60(0.51)*	*0.12*	*30.20(3.24)*
75	*110*	*3.00(0.00)*	*0.12*	*30.12(2.45)*
75	*115*	*3.00(0.00)*	*0.11*	*27.34(2.34)*
75	*120*	*3.00(0.00)*	*0.11*	*27.18(2.12)*
75	*125*	*3.13(0.35)*	*0.10*	*28.66(2.40)*
75	*130*	*3.27(0.46)*	*0.10*	*28.78(2.48)*
80	*95*	*3.07(0.46)*	*0.14*	*31.60(4.83)*
80	*100*	*3.07(0.26)*	*0.13*	*34.28(4.10)*
80	*105*	*3.40(0.51)*	*0.11*	*29.87(2.92)*
80	*110*	*3.07(0.26)*	*0.12*	*29.20(2.04)*
80	*115*	*3.07(0.26)*	*0.10*	*29.47(2.08)*
80	*120*	*3.07(0.26)*	*0.11*	*28.32(2.07)*
80	*125*	*3.00(0.00)*	*0.10*	*27.77(2.33)*
80	*130*	*3.00(0.00)*	*0.09*	*26.57(2.30)*
85	*95*	*3.00(0.53)*	*0.13*	*37.16(4.45)*
85	**100**	2.73(0.46)	0.11	31.38(3.88)
85	**105**	2.93(0.46)	0.12	32.60(3.40)
85	**110**	2.93(0.26)	0.11	26.90(2.32)

273

85	115	2.93(0.26)	0.10	29.38(2.32)
85	120	2.53(0.52)	0.09	26.73(2.27)
85	125	2.20(0.41)	0.08	22.72(2.19)
85	130	2.67(0.49)	0.09	22.18(2.09)
90	95	2.60(0.51)	0.12	32.42(4.40)
90	100	2.93(0.59)	0.10	30.19(3.83)
90	105	2.93(0.26)	0.11	29.28(3.17)
90	110	2.80(0.41)	0.10	29.71(2.67)
90	*115*	*3.00(0.00)*	*0.09*	*29.70(2.23)*
90	120	2.67(0.49)	0.09	25.49(2.07)
90	125	2.93(0.26)	0.08	26.58(2.13)
90	130	2.40(0.51)	0.08	22.06(2.07)
95	95	2.47(0.52)	0.11	35.31(4.67)
95	100	2.80(0.41)	0.10	27.90(3.96)
95	105	2.60(0.51)	0.12	27.98(3.15)
95	110	2.73(0.46)	0.09	28.81(2.66)
95	115	2.80(0.41)	0.09	24.54(1.95)
95	120	2.20(0.41	0.08	21.66(1.78)
95	125	2.13(0.35)	0.07	22.19(2.10)
95	130	2.40(0.51)	0.06	21.95(1.96)

IQ, image quality, SD, standard deviation, E, effective dose, SNR, signal to noise ratio.

Appendix XXXII: APPS IQ score, SNR, and the associated E (mSv) with optimising 2 mm Alt filter type**-AEC**

kVp	SID	IQ score (SD)	E(mSv)	SNR(SD)
60	95	3.93(0.26)	0.25	33.45(4.53)
60	100	3.87(0.35)	0.22	38.01(5.13)
60	105	3.73(0.46)	0.20	42.96(4.65)
60	110	3.93(0.26)	0.19	45.49(4.25)
60	115	3.93(0.26)	0.17	43.94(3.64)
60	120	3.60(0.51)	0.17	36.54(3.67)
60	125	3.93(0.26)	0.16	45.37(4.22)
60	130	3.60(0.51)	0.16	38.10(4.04)
65	95	3.67(0.49)	0.20	40.51(5.60)
65	100	3.87(0.35)	0.18	38.08(4.63)

65	105	3.67(0.49)	0.17	36.52(4.10)
65	110	3.60(0.51)	0.16	40.14(3.87)
65	115	3.47(0.52)	0.14	39.80(3.50)
65	120	3.53(0.52)	0.14	39.08(3.62)
65	125	3.40(0.51)	0.14	39.59(3.66)
65	130	3.00(0.00)	0.13	31.73(3.52)
70	95	3.07(0.46)	0.17	33.40(5.32)
70	100	3.60(0.51)	0.15	38.14(4.92)
70	105	3.07(0.26)	0.14	33.60(3.67)
70	110	3.20(0.41)	0.14	37.11(3.63)
70	115	3.80(0.41)	0.12	39.87(3.03)
70	120	3.07(0.26)	0.12	29.60(3.16)
70	125	3.13(0.35)	0.12	35.38(3.56)
70	130	3.00(0.00)	0.11	29.70(3.19)
75	95	3.27(0.46)	0.14	39.60(5.16)
75	100	3.13(0.64)	0.13	35.68(4.12)
75	105	3.00(0.00)	0.12	34.04(3.61)
75	110	3.40(0.51)	0.12	37.97(3.55)
75	115	3.07(0.26)	0.11	35.74(2.95)
75	120	3.00(0.00)	0.11	34.46(3.38)
75	125	2.87(0.35)	0.10	28.41(3.14)
75	130	3.00(0.00)	0.10	34.10(2.96)
80	95	3.47(0.52)	0.13	33.93(4.30)
80	100	3.07(0.46)	0.12	31.99(4.08)
80	105	2.87(0.35)	0.11	32.76(3.58)
80	110	3.13(0.35)	0.11	36.32(2.66)
80	115	3.00(0.00)	0.10	33.59(2.79)
80	120	3.00(0.00)	0.10	34.92(3.00)
80	125	3.13(0.35)	0.09	32.90(3.08)
80	130	3.73(0.46)	0.09	34.15(2.91)
85	95	2.73(0.46)	0.12	36.52(4.80)
85	100	2.40(0.51)	0.11	33.67(4.41)
85	105	2.80(0.41)	0.10	32.67(3.57)
85	110	2.93(0.26)	0.10	34.89(3.35)
85	115	2.93(0.26)	0.09	33.82(2.74)
85	120	3.00(0.00)	0.09	36.25(2.92)
85	125	2.33(0.49)	0.09	28.20(2.71)
85	130	2.07(0.26)	0.08	25.67(2.69)
90	95	2.67(0.62)	0.11	34.25(4.75)
90	100	2.47(0.52)	0.10	33.42(4.12)
90	105	2.33(0.49)	0.10	30.43(3.22)

90	*110*	*3.00(0.00)*	*0.09*	*32.57(3.46)*
90	**115**	2.13(0.35)	0.09	27.28(2.61)
90	**120**	2.33(0.49)	0.09	30.96(2.87)
90	**125**	2.13(0.35)	0.08	26.19(2.75)
90	**130**	2.33(0.49)	0.08	31.20(2.68)
95	**95**	2.13(0.35)	0.10	33.90(4.46)
95	**100**	2.40(0.51)	0.10	32.09(4.10)
95	**105**	2.27(0.46)	0.09	28.91(3.33)
95	**110**	2.20(0.41)	0.09	30.18(3.32)
95	**115**	2.07(0.26)	0.08	30.64(2.75)
95	**120**	2.07(0.26)	0.08	27.58(2.63)
95	**125**	2.07(0.26)	0.08	28.95(2.81)
95	**130**	2.07(0.26)	0.08	25.13(2.36)
IQ, image quality, SD, standard deviation, E, effective dose, SNR, signal to noise ratio.				

Appendix XXXIII: APPS IQ score, SNR, and the associated E (mSv) with optimising 0.1 mm Cu filter type-AEC

kVp	SID	IQ score (SD)	E(mSv)	SNR(SD)
60	**95**	3.93(0.26)	0.23	41.23(5.65)
60	**100**	3.87(0.35)	0.20	42.06(5.76)
60	**105**	3.93(0.26)	0.19	43.51(4.99)
60	**110**	3.87(0.35)	0.18	41.48(4.25)
60	**115**	3.80(0.41)	0.16	42.65(3.74)
60	**120**	3.47(0.52)	0.16	43.03(3.73)
60	*125*	*3.47(0.52)*	*0.15*	*40.84(3.71)*
60	*130*	*3.40(0.51)*	*0.14*	*37.48(3.82)*
65	**95**	3.80(0.41)	0.18	41.11(5.47)
65	**100**	3.87(0.35)	0.16	39.12(4.85)
65	*105*	*3.53(0.52)*	*0.15*	*38.96(4.41)*
65	*110*	*3.20(0.41)*	*0.14*	*34.86(3.60)*
65	*115*	*3.47(0.52)*	*0.13*	*39.48(3.30)*
65	**120**	3.00(0.38)	0.13	35.24(3.45)
65	**125**	2.87(0.35)	0.12	34.00(3.47)
65	*130*	*3.07(0.26)*	*0.12*	*34.33(3.74)*
70	*95*	*3.40(0.51)*	*0.15*	*42.89(5.28)*
70	*100*	*3.47(0.52)*	*0.14*	*37.58(4.61)*
70	*105*	*3.07(0.26)*	*0.13*	*37.54(4.10)*

70	*110*	*3.13(0.35)*	*0.12*	*37.67(3.51)*
70	*115*	*3.40(0.51)*	*0.11*	*38.91(2.96)*
70	*120*	*3.00(0.00)*	*0.11*	*37.00(3.01)*
70	*125*	*3.00(0.38)*	*0.11*	*34.18(2.97)*
70	**130**	2.73(0.46)	0.11	29.63(3.08)
75	**95**	2.93(0.46)	0.13	34.61(4.65)
75	*100*	*3.00(0.00)*	*0.12*	*35.62(4.39)*
75	*105*	*3.00(0.00)*	*0.11*	*35.35(3.78)*
75	*110*	*3.00(0.000*	*0.11*	*37.06(3.16)*
75	**115**	2.33(0.49)	0.12	31.18(2.66)
75	**120**	2.87(0.35)	0.10	34.40(2.68)
75	**125**	2.73(0.46)	0.10	35.34(3.10)
75	**130**	2.47(0.52)	0.09	29.06(2.99)
80	**95**	2.67(0.62)	0.12	34.70(4.65)
80	**100**	2.60(0.51)	0.11	36.43(4.55)
80	*105*	*3.00(0.00)*	*0.10*	*36.61(4.08)*
80	*110*	*3.00(0.00)*	*0.10*	*35.68(3.40)*
80	**115**	2.73(0.46)	0.09	34.29(2.49)
80	**120**	2.13(0.35)	0.09	29.82(2.57)
80	**125**	2.67(0.49)	0.09	34.28(2.73)
80	**130**	2.73(0.46)	0.09	29.36(2.79)
85	**95**	2.47(0.52)	0.11	32.51(4.44)
85	**100**	2.67(0.49)	0.10	32.43(4.15)
85	**105**	2.47(0.52)	0.09	35.71(3.95)
85	**110**	2.93(0.26)	0.09	34.68(3.26)
85	**115**	2.13(0.35)	0.09	30.30(2.57)
85	**120**	2.07(0.26)	0.08	28.82(2.33)
85	**125**	2.07(0.26)	0.08	25.39(2.46)
85	**130**	2.13(0.35)	0.08	27.83(2.66)
90	**95**	2.33(0.49)	0.10	31.98(4.53)
90	**100**	2.40(0.51)	0.10	33.23(4.28)
90	**105**	2.20(0.41)	0.09	31.75(3.77)
90	**110**	2.13(0.35)	0.09	28.79(3.01)
90	**115**	2.47(0.52)	0.08	34.82(2.80)
90	**120**	2.20(0.41)	0.08	27.02(2.51)
90	**125**	2.13(0.35)	0.08	27.51(2.46)
90	**130**	2.07 0.26)	0.07	31.17(2.54)
95	**95**	2.20(0.41)	0.10	35.11(4.71)
95	**100**	2.20(0.41)	0.09	35.43(4.61)
95	**105**	2.33(0.49)	0.08	32.35(3.79)
95	**110**	2.07(0.26)	0.08	28.64(3.27)

95	115	2.27(0.46)	0.08	31.38(2.62)
95	120	2.13(0.35)	0.08	28.77(2.20)
95	125	2.07(0.26)	0.07	26.87(2.32)
95	130	2.07(0.26)	0.07	25.27(2.28)
IQ, image quality, SD, standard deviation, E, effective dose, SNR, signal to noise ratio.				

Appendix XXXIV: APPS IQ score, SNR, and the associated E (mSv) with optimising 0.2 mm Cu filter type-AEC

kVp	SID	IQ score (SD)	E(mSv)	SNR(SD)
60	95	3.80(0.41)	0.21	40.25(6.03)
60	100	3.87(0.35)	0.19	40.91(5.28)
60	105	3.80(0.41)	0.17	39.86(4.27)
60	110	3.53(0.52)	0.17	38.39(3.62)
60	115	3.93(0.26)	0.15	39.44(3.18)
60	120	3.13(0.35)	0.14	34.54(3.29)
60	125	3.40(0.51)	0.14	39.31(3.80)
60	130	3.60(0.51)	0.13	38.83(3.89)
65	95	3.67(0.49)	0.17	41.67(5.75)
65	100	3.33(0.49)	0.16	32.27(4.93)
65	105	3.80(0.41)	0.14	37.24(4.30)
65	110	3.00(0.00)	0.14	32.92(3.40)
65	115	3.20(0.41)	0.12	37.63(3.12)
65	120	3.00(0.00)	0.12	37.50(3.14)
65	125	3.07(0.26)	0.12	33.80(3.26)
65	130	3.00(0.00)	0.11	30.56(3.31)
70	95	3.33(0.49)	0.14	37.17(5.05)
70	100	3.07(0.26)	0.13	36.00(4.65)
70	105	3.07(0.26)	0.12	35.99(3.99)
70	110	3.27(0.59)	0.12	35.98(3.07)
70	115	3.00(0.00)	0.11	35.44(2.65)
70	120	3.00(0.00)	0.10	36.02(2.70)
70	125	3.07(0.26)	0.10	36.50(2.84)
70	130	3.07(0.26)	0.10	34.07(3.21)
75	95	2.87(0.52)	0.12	37.57(5.01)
75	100	3.00(0.00)	0.12	34.10(3.94)
75	105	3.00(0.38)	0.11	32.17(3.77)
75	110	3.00(0.00)	0.11	33.25(2.83)

75	*115*	*3.00(0.00)*	*0.10*	*30.80(2.65)*
75	*120*	*3.00(0.00)*	*0.09*	*28.45(2.66)*
75	**125**	2.93(0.26)	0.09	34.46(2.79)
75	**130**	2.93(0.26)	0.09	28.92(2.82)
80	**95**	2.60(0.51)	0.11	34.90(4.66)
80	**100**	2.73(0.46)	0.11	35.31(4.27)
80	*105*	*3.00(0.00)*	*0.10*	*32.90(3.25)*
80	*110*	*3.00(0.00)*	*0.10*	*35.31(3.14)*
80	*115*	*3.00(0.00)*	*0.09*	*30.85(2.29)*
80	**120**	2.40(0.51)	0.09	28.33(2.36)
80	*125*	*3.00(0.00)*	*0.08*	*34.51(2.84)*
80	**130**	2.07(0.26)	0.08	25.52(2.67)
85	**95**	2.53(0.52)	0.11	35.13(4.73)
85	**100**	2.53(0.52)	0.10	34.03(4.11)
85	**105**	2.80(0.41)	0.09	32.90(3.40)
85	**110**	2.47(0.52)	0.09	29.89(3.13)
85	**115**	2.53(0.52)	0.08	29.47(2.59)
85	**120**	2.07(0.26)	0.08	26.98(2.24)
85	**125**	2.20(0.41)	0.08	27.19(2.62)
85	**130**	2.33(0.49)	0.08	29.45(2.760
90	**95**	2.40(0.51)	0.10	33.83(4.56)
90	**100**	2.53(0.52)	0.09	33.94(4.22)
90	**105**	2.40(0.51)	0.09	31.44(3.43)
90	**110**	2.47(0.52)	0.09	30.56(3.32)
90	**115**	2.40(0.51)	0.08	30.72(2.21)
90	**120**	2.13(0.35)	0.08	29.27(2.20)
90	**125**	2.13(0.35)	0.07	25.21(2.31)
90	**130**	2.13(0.35)	0.07	25.76(2.26)
95	**95**	2.27(0.46)	0.09	31.74(4.41)
95	**100**	2.13(0.35)	0.09	27.08(3.88)
95	**105**	2.20(0.41)	0.08	31.33(3.35)
95	**110**	2.07(0.26)	0.08	28.35(3.10)
95	**115**	2.53(0.52)	0.08	31.58(2.29)
95	**120**	2.07(0.26)	0.07	26.00(2.42)
95	**125**	2.07(0.26)	0.07	24.09(2.34)
95	**130**	2.20(0.41)	0.07	25.54(2.21)

IQ, image quality, SD, standard deviation, E, effective dose, SNR, signal to noise ratio.

Appendix XXXV: APPS IQ score associated with image post-processing testing

Post-processing factors		Image 1		Image 2		Image 3		Image 4		Image 5		Image 6	
Latitude	Windowing	IQ	SD	IQ	SD	IQ	SD	IQ	SD	IQ	SD	IQ	SD
0	-0.05	2.93	0.26	2.93	0.26	3.27	0.46	3.00	0.38	3.00	0.38	2.80	0.56
0	0	2.60	.51	3.13	0.52	2.93	0.26	3.20	0.41	2.87	0.74	2.27	0.46
0	0.05	2.73	0.46	3.00	0.53	2.93	0.59	3.07	0.70	2.87	0.52	2.07	0.26
0	0.1	2.60	0.51	2.73	0.59	2.80	0.56	3.07	0.59	2.40	0.51	2.33	0.49
0	0.15	2.53	0.52	2.40	0.51	2.60	0.51	2.40	0.51	2.20	0.41	2.13	0.35
0	0.2	2.33	0.49	2.27	0.59	2.53	0.64	2.73	0.59	2.13	0.35	2.07	0.26
0	0.25	2.47	0.64	2.20	0.41	2.27	0.46	2.27	0.46	2.07	0.26	2.07	0.26
0.5	-0.05	3.07	0.26	2.93	0.26	2.93	0.26	3.00	0.00	3.00	0.00	3.00	0.00
0.5	0	3.00	0.00	3.13	0.35	3.07	0.26	3.07	0.26	2.87	0.35	3.13	0.52
0.5	0.05	2.93	0.46	3.27	0.46	2.80	0.41	3.13	0.35	3.20	0.56	3.13	0.35
0.5	0.1	2.60	0.51	2.80	0.56	2.53	0.52	2.87	0.64	2.93	0.46	2.93	0.70
0.5	0.15	2.60	0.51	2.80	0.68	2.40	0.51	2.93	0.59	2.60	0.63	2.47	0.64
0.5	0.2	3.00	0.65	2.47	0.52	2.27	0.46	2.53	0.52	2.07	0.26	2.13	0.35
0.5	0.25	2.20	0.41	2.20	0.41	2.13	0.35	2.27	0.46	2.27	0.46	2.07	0.26
1	-0.05	3.00	0.00	3.07	0.26	3.13	0.35	3.00	0.00	2.93	0.26	3.00	0.00
1	0	3.07	0.26	3.13	0.35	3.07	0.26	3.07	0.26	3.07	0.26	3.13	0.35
1	0.05	3.00	0.38	3.27	0.59	3.13	0.35	3.20	0.56	3.20	0.41	2.80	0.56
1	0.1	2.73	0.59	3.07	0.46	2.87	0.35	3.13	0.64	2.80	0.56	2.93	0.59
1	0.15	2.80	0.41	3.00	0.65	2.67	0.62	3.00	0.38	2.80	0.68	2.80	0.77
1	0.2	2.67	0.49	2.53	0.64	2.47	0.52	2.47	0.64	2.60	0.63	2.13	0.35
1	0.25	2.60	0.51	2.20	0.41	2.13	0.35	2.73	0.46	2.40	0.51	2.20	0.41
1.5	-0.05	3.00	0.00	3.00	0.00	3.00	0.00	3.00	0.00	3.00	0.00	3.00	0.00
1.5	0	3.00	0.00	3.13	0.35	3.00	0.00	3.00	0.00	3.00	0.00	3.00	0.00
1.5	0.05	3.20	0.41	3.13	0.35	3.00	0.00	3.13	0.35	3.00	0.00	3.00	0.00
1.5	0.1	2.93	0.26	3.00	0.38	3.07	0.26	3.07	0.26	3.00	0.00	3.07	0.46
1.5	0.15	2.67	0.62	2.80	0.41	2.80	0.41	2.87	0.35	3.00	0.53	3.07	0.46
1.5	0.2	3.00	0.65	2.67	0.49	2.40	0.51	2.73	0.46	2.73	0.59	2.73	0.59
1.5	0.25	2.80	0.68	2.47	0.52	2.53	0.64	2.33	0.49	2.47	0.64	2.93	0.59
2	-0.05	3.00	0.00	3.00	0.00	2.93	0.26	3.00	0.00	2.93	0.26	3.00	0.00
2	0	3.00	0.00	3.07	0.26	3.00	0.00	3.00	0.00	3.00	0.00	3.00	0.00
2	0.05	3.00	0.00	3.00	0.00	3.00	0.00	3.00	0.00	3.00	0.00	3.00	0.00
2	0.1	3.00	0.00	3.07	0.26	3.00	0.00	3.00	0.00	3.07	0.26	3.07	0.26
2	0.15	2.80	0.41	2.93	0.26	2.80	0.41	2.87	0.35	3.00	0.53	2.87	0.35
2	0.2	3.00	0.38	2.40	0.51	2.60	0.63	2.67	0.49	2.73	0.59	2.93	0.26
2	0.25	2.67	0.49	2.53	0.52	2.33	0.49	2.33	0.49	2.80	0.56	2.80	0.56
2.5	-0.05	3.00	0.00	2.20	0.41	3.00	0.00	2.07	0.26	2.13	0.35	3.00	0.00
2.5	0	3.00	0.00	2.80	0.41	3.00	0.00	2.27	0.46	2.27	0.46	3.00	0.00

2.5	0.05	3.00	0.00	3.00	0.00	3.00	0.00	2.87	0.35	2.73	0.46	3.00	0.00
2.5	0.1	2.93	0.26	3.00	0.00	3.00	0.00	3.00	0.00	2.53	0.52	2.93	0.26
2.5	0.15	3.13	0.35	3.00	0.00	3.07	.26	3.00	.00	3.00	0.00	3.00	0.00
2.5	0.2	2.73	0.46	3.00	0.00	2.80	.41	3.00	.00	2.93	0.26	3.07	0.26
2.5	0.25	3.07	0.46	2.93	0.26	2.33	.49	2.93	.26	2.93	0.26	2.73	0.46
3	-0.05	2.20	0.41	2.33	0.49	2.13	.35	2.13	.35	2.07	0.26	2.07	0.26
3	0	2.87	0.35	2.93	0.26	2.20	.41	2.07	.26	2.07	0.26	2.13	0.35
3	0.05	3.00	0.00	3.00	0.00	2.40	.51	2.47	.52	2.07	0.26	2.73	0.46
3	0.1	3.00	0.00	3.00	0.00	2.93	.26	2.80	.41	3.00	0.00	2.87	0.35
3	0.15	3.00	0.00	2.93	0.26	3.13	.35	3.00	.00	2.80	0.41	3.00	0.00
3	0.2	3.07	0.46	2.87	0.35	3.00	.00	3.00	.00	3.00	0.00	3.00	0.00
3	0.25	3.00	0.38	2.87	0.35	2.80	.56	3.07	.26	2.87	0.35	3.00	0.00
3.5	-0.05	2.20	0.41	2.13	0.35	2.27	.46	2.13	.35	2.07	0.26	2.07	0.26
3.5	0	3.00	0.00	2.60	0.51	2.33	.49	2.13	.35	2.07	0.26	2.07	0.26
3.5	0.05	3.00	0.00	2.87	0.35	2.87	.35	2.07	.26	2.47	0.52	2.13	0.35
3.5	0.1	3.00	0.00	3.00	0.00	3.00	.00	2.13	.35	2.67	0.49	2.07	0.26
3.5	0.15	3.00	0.53	3.07	0.26	2.93	.26	2.53	.52	3.00	0.00	3.00	0.00
3.5	0.2	3.07	0.26	3.00	0.00	2.87	.35	2.80	.41	3.00	0.00	3.00	0.00
3.5	0.25	3.13	0.35	2.93	0.46	2.80	.56	3.00	.00	3.07	0.26	3.00	0.00
IQ, image quality score, SD, Standard deviation													

References

American Association of Physicists and Medicine (AAPM). (2006). Acceptance testing and quality control of photostimulable storage phosphor imaging systems:AAPM REPORT NO. 93 Report of AAPM Task Group 10. California: AAPM.

Abdelhalim, M. A. K. (2010). Patient dose levels for seven different radiographic examination types. *Saudi Journal of Biological Sciences, 17*(2), 115–118.

Abell, N., Springer, D.W., & Kamata, A. (2009). *Developing and validating rapid assessment instruments.* Oxford: Oxford University Press.

Al Khalifah, A., & Brindhaban, A. (2004). Comparison between conventional radiography and digital radiography for various kVp and mAs settings using a pelvic phantom. *Radiography, 10*(2), 119–123.

Al Qaroot, B., Hogg, P., Twiste, M., & Howard, D. (2014). A systematic procedure to optimise dose and image quality for the measurement ofinter-vertebral angles from lateral spinal projections using Cobb and superimposition methods. *Journal of X-Ray Science and Technology, 22*(5), 613–625.

Aldrich, J., Duran, E., Dunlop, P., & Mayo, J. (2006). Optimization of dose and image quality for computed radiography and digital radiography. *Journal of Digital Imaging, 19*(2), 126-131.

Allen, E., Hogg, P., Ma, W. K., & Szczepura, K. (2013). Fact or fiction: An analysis of the 10 kVp 'rule' in computed radiography. *Radiography, 19*, 223-227.

Almén, A., Tingberg, A., Mattson, S., Besjakov, J., Kheddache, S., & Lanhede, B. (2000). The influence of different technique factors on image quality of lumbar spine radiographs as evaluated by established CEC image criteria. *British journal of radiology, 73*(875), 1192-1199.

Alsleem, H. , & Davidson, R. (2012). Quality parameters and assessment methods of digital radiography images. *The radiographer, 59*(2), 46-55.

Arakawa, S., Itoh, W., Kohda, K., & Suzuki, T. (1999, February 20, 1999). *Novel computed radiography system with improved image quality bydetection of emissions from both sides of an imaging plate*, San Diego, CA.

Ashford, J. B., & LeCroy, C. W. (2010). *Human behavior in the social environment: A multidimensional perspective* (4 ed.). Belmont, CA: Wadsworth, Cengage Learning.

Båth, M. (2010). Evaluating imaging systems: Practical applications. *Radiation protection dosimetry, 139*(1-4), 26–36.

Båth, M., Sund, P., & Månsson, L. G. (2002). Evaluation of image quality of a new CCD-based system for chest imaging. *Medical physics, 29*(10), 2297.

Ball, J. , & Price, T. (1995). *Chesneys' radiographic imaging* (6 ed.). Germany: Wiley-Blackwell.

Balnaves, M. , & Caputi, P. (2001). *Introduction to quantitative research methods : An investigative approach*. London Sage Publishing.

Bandura, A. (1986). *Social foundations of thought and action: A social cognitive theory*. New Jersey: Prentice Hall.

Bandura, A. (1995). *Self-efficacy in changing societies* (A. Bandura Ed.). New York: Cambridge University Press.

Bandura, A. (1977). Self-efficacy: Toward a unifying theory of behavioral change. *Psychological Review, 84*(2), 191-215.

Bandura, A. (1997). *Self-efficacy: The exercise of control*. New York: Worth Publishers.

Bandura, A. (2006). *Self-efficacy beliefs of adolescents*. New York: Information Age.

Båth, M., Håkansson, M., Hånsson, J., & Månsson, L. G. (2005). A conceptual optimisation strategy for radiography in a digital environment. *Radiation protection dosimetry, 114*(1-3), 230–235.

Båth, M., & L.G., Månsson. (2007). Visual grading characteristics (VGC) analysis: a non-parametric rank-invariant statistical method for image quality evaluation. *British journal of radiology, 80*(951), 169-176.

Behrmana, R. H. (2003). The impact of increased Al filtration on x-ray tube loading and image quality in diagnostic radiology. *Medical physics, 30*(1), 69-78.

British Institute of Radiology (BIR). (1989a). Technical and physical parameters for quality assurance in medical diagnostic radiology: (BIR report 18). In B. Moores, F. Stieve, H. Eriskat & H. Schibilla (Eds.). London: the British institue of radiology.

British Institute of Radiology (BIR). (1989b). Optimization of image quality and patient exposure in diagnostic radiology (BIR Report 20). In B. Moores, F. Stieve, H. Eriskat & H. Schibilla (Eds.). London: BIR.

British Institute of Radiology (BIR). (2001). Assurance of the quality in the diagnostic imaging depratment (2 ed.). London.

Bjorner, J., Damsgaard, M., Watt, T., & Groenvold, M. (1998). Tests of data quality, scaling assumptions, and reliability of the Danish SF-36. *Journal of clinical epidemiology, 51*(1), 1001–1011.

Bochud, O., Valley, J-F., & Verdun, F. R. (1999). Estimation of the noisy component of anatomical backgrounds. *Medical physics, 26*(7), 1365-1370.

Bontrager, K. L., & Lampignano, J. P. (2014). *Textbook of radiographic positioning and related anatomy* (8 ed.). Missouri: Mosby.

Borasi, G., Samei, E., Bertolini, M., Nitrosi, A., & Tassoni, D. (2006). Contrast-detail analysis of three flat panel detectors for digital radiography. *Medical physics, 33*(6), 1707-1719.

Bouzarjomehri, F. . (2004). Patient dose in routine X-ray examinations in Yazd state. *International journal of radiation research, 1*(4), 199-204.

Bragg, D., Murray, K., & Tripp, D. (1997). Experiences with computed radiography: Can we afford the cost ? . *American journal of roentgenology, 169*(4), 935-941.

Brennan, P., McDonnell, S., & O'Leary, D. (2004). Increasing film-focus distance (ffd) reduces radiation dose for x-ray examinations. *Radiation protection dosimetry, 108*(3), 263-268.

Brennan, P., & Nash, M. (1998). Increasing FFD: an effective dose-reducing tool for lateral lumbar spine investigations. *Radiography, 4*, 251-259.

Brenner, D. J., Doll, R., Goodhead, D. T., Hall, E. J., Land, C. E., Little, J. B., . . . Zaider, M. (2003). Cancer risks attributable to low doses of ionizing radiation: Assessing what we really know. *The National Academy of Sciences of the USA, 100*(24), 13761–13766. doi: 10.1073pnas.2235592100.

Brenowitz, N., & Tutle, C. (2003). Development and testing of a nutrition-teaching selfefficacy scale for elementary school teachers. *Journal of nutrition education and behavior, 35*(6), 308-311.

Brindhaban, A., & Al Khalifah, A. (2005). Radiation dose in pelvic imaging. *Radiologic technology, 77*(1), 32-40.

Brindhaban, A., Al Khalifah, A., Al Wathiqi, G, & Al Ostath, H. (2005). *Effect of x-ray tube potential on image quality and patient dose for lumbar spine computed radiography examinations, 28*(4), 216-222.

Brosi, P., Stuessi, A., Verdun, F. R., Vock, P., & Wolf, R. (2011). Copper filtration in pediatric digital X-ray imaging: its impact on image quality and dose. *Radiological Physics and Technology, 4*(3), 148–155.

Brusin, J. H. (2007). Radiation protection. *Radiologic technology, 87*(5), 378-392.

Bryan, R. N. (2010). *Introduction to the Science of Medical Imaging*. Cambridge Cambridge University Press.

Burgess, A. E. (1995). Image quality, the ideal observer, and human performance of radiologic decision tasks. *Academic radiology, 2*(6), 522-526.

Burgess, A. E. (2011). Visual perception studies and observer models in medical imaging. *Seminars in nuclear medicine., 4*(16), 419-436. doi: 10.1053/j.semnuclmed.2011.06.005

Busch, H. P. (1997). Digital radiography for clinical applications. *Euorpean radiology, 7*(Suppl. 3), 66–72.

Busch, H. P. (2004). Image quality and dose management for digital radiography: DIMOND III Report.

Busch, H. P., Faulkner, K., & Malone, J. F. (1995). Image quality criteria applied to digital radiography. *Radiation protection dosimetry*, 57(1-4), 139-140.

Busch, H. P., & Jaschke, W. (1998). Adaptation of the quality criteria concept to digital radiology. *Radiation protection dosimetry*, 80(1-3), 61-63.

Bushberg, J. T., Seibert, J. A., Leidholdt JR, E. M., & Boone, J. M. (2012). *The essential Physics of medical imaging* (3 ed.). Philadelphia: Lippincott Williams & Wilkins.

Bushong, S. C. (2013). *Radiologic science for technologists physics, biology, and protection* (3 ed.). Missouri: Mosby.

Butler, M. L., Rainford, L., Last, J., & Brennan, P. (2009, (13 March 2009)). *Optimization of Exposure Index values for the antero--posterior pelvis and antero-posterior knee examination.* Paper presented at the Image Perception, Observer Performance, and Technology Assessment, Lake Buena Vista, FL.

Butler, M. L., Rainford, L., Last, J., & Brennan, P. (2010). Are exposure index values consistent in clinical practice? A multi-manufacturer investigation. *Radiation protection dosimetry*, 139(1-3), 371–374.

Cappelleri, j. C., Gerber, R. A., Kourides, I. A., & Gelfand, R. A. (2000). Development and Factor Analysis of a Questionnaire to Measure Patient Satisfaction With Injected and Inhaled Insulin for Type 1 Diabetes. *Diabetes care,, 23*(12), 1799-1803.

Carlton, R. R., & Adler, A. M. (2013). *Principles of Radiographic Imaging: An Art and A Science* (5 ed.). Australia: Cengage Learning.

Carmichael, J. H. (1989). Measures to achieve the optimization of image quality and patient exposure in diagnostic radiology. In B. M. Moores, B. F. Wall, H. Eriskat & H. Schibilla (Eds.), *Optimization of image quality and patient exposure in diagnostic radiology: (BIR report 20)* (pp. 4-6). London: the British institue of radiology.

Carroll, Q. B. (2007). *Practical radiographic imaging* (8 ed.). USA: Charles C Thomas.

Carter, C. E., & Vealé, B. L. (2014). *Digital radiography and PACS* (2 ed.). Missouri: Mosby.

Carver, B., & Carver, B. (2012). *Medical imaging techniques, reflection & evaluation* (2 ed.). Edinburgh: Churchill Livingstone.

Cassidy, S., & Eachus, P. (2002). Developing the computer user self-efficacy (cuse) scale: Investigating the relationship between computer self-efficacy, gender and experience with computers. *Journal of educational computing research, 26*(2), 133-153.

Champion, V., Skinner, C. S., & Menon, U. (2005). Development of a self-efficacy scale for mammography. *Research in Nursing & Health, 28*(4), 329–336

Chan, C. T. P., & Fung, K. L. L. (2015). Dose optimization in pelvic radiography by air gap method on CR and DR systems e A phantom study. Radiography, 21(3), 214–223.

Chotas, H. G., Floyd, C. E., Dobbins III, J. T., & Ravin, C. E. (1993). Digital chest radiography with photostimulable storage phosphors: Signal-to-noise ratio as a function of kilovoltage with matched exposure risk. *Radiology, 186*(2), 395-398.

Christodoulou, E., Goodsitt, M., & Chan, H. (2000). Phototimer setup for CR imaging. *Medical physics, 27*(12), 2652-2658.

CIRS. (2013a). ATOM dosimetry phantom :Adult male phantom model number 701-D appendix 5. Virginia, USA: CIRS, Inc.

CIRS. (2013b). Tissue simulation and phantom technology:Dosimetry verification phantoms model 701-706 data sheet.

Clarke, R. (1999). Control of low-level radiation exposure: time for a change? *Journal of radiological protection, 19*(12), 107–115.

Commission of the European Communitie (CEC). (1996). European guidelines on quality criteria for diagnostic radiographic images: (EUR 16260 EN). Brussels: CEC.

Coakes , S. (2005). *SPSS version 12.0 for windows analysis without anguish*. Australia: John Wiley & Sons.

Coaley, K. (2010). *An introduction to psychological assessment and psychometrics*. Los Angels: Sage Publications.

Cohen, B. L. (2008). The linear no-threshold theory of radiation carcinogenesis should be rejected. *Journal of American Physicians and Surgeons*, 13(3), 70-76.

Compagnone, G. (2008). Radiation doses to patients using computed radiography, direct digital radiography, and screen-film radiography general methods and overviews, lung carcinoma and prostate carcinoma. In M. A. Hayat (Series Ed.) (Vol. 2, pp. 109-128). Netherlands: Springer.

Compagnone, G., Baleni, M., Pagan, L., Calzolaio, F., Barozzi, L., & Bergamin, C. (2006). Comparison of radiation doses to patients undergoing standard radiographic examinations with conventional screen–film radiography, computed radiography and direct digital radiography. *British journal of radiology, 79*(947), 899-904.

Cowen, A.R., Davies, A.G., & Kengyelics, S.M. (2007). Advances in computed radiography systems and their physical imaging characteristics. *Clincal radiology, 62*(12), 1132-1141.

Cronbach, L. (1951). Coefficient alpha and the internal structure of tests. *Sychometrika, 16*(1), 297-334.

Crop, A. D., Bacher, K., Hoof, T. V., Smeets, P. V., Smet, B. S., Vergauwen, M., . . . Thierens, H. (2012). Correlation of contrast-detail analysis and clinical image quality assessment in chest radiography with a human cadaver study. *Radiology, 262*(1), 298-304.

Cuthill, F. M., Espie, C. A., & Cooper, S. A. (2003). Development and psychometric properties of the Glasgow depression scale for people with a learning disability. *British journal of p sychiatry, 182*, 3 4 7 - 3 5 3.

DeCoster, J. (1998). Overview of Factor Analysis. Retrieved 24 October, 2014, from www.stat-help.com/notes.html

Decoster, R., Mol, H., & Smits, D. (2015). Post-processing, is it a burden or a blessing? Part 2 CNR saturation as a new hypothesis. *Radiography, 21*(1), 5-8.

Dennis, C. L. (2003). The breastfeeding self-efficacy scale: Psychometric assessment of the short form. *Journal of Obstetric, Gynecologic, & Neonatal Nursing, 32*, 734–744. doi: 0.1177/0884217503258459

Dennis, C. L., & Faux, S. (1999). Development and psychometric testing of the breastfeeding self-efficacy scale. *Research in Nursing & Health, 22*(5), 399–409.

DeVellis, R. F. (2012). *Scale development: Theory and applications (applied social research methods)* (3 ed.). London: SAGE Publications.

Dhawan, A. P. (2011). Medical image analysis (2 ed.). New Jersey: Wiley-IEEE Press.

Dobbins III, J. T., Samei, E., Chotas, H. G., Warp, R. J., Baydush, A. H., Floyd, C. E., & Ravin, C. E. (2003). Chest Radiography:Optimization of X-ray spectrum for cesium iodide– amorphous silicon flat-panel detector. *Radiology, 226*(1), 221-230.

Dobbins, J.T. (2000). Metrics for measuring image quality. In L. V. Metter, J. Beutel & H. L. Kundel (Eds.), *Handbook of medical imaging, physics and psychophysics, Vol 1*. Canadian: SPIE Press.

Don, S. (2004). Radiosensitivity of children: potential for overexposure in CR and DR and magnitude of doses in ordinary radiographic examinations. *Paediatric radiology, 34*(Suppl 3), 167–172.

Dowsett, D. J., Kenny, P. A., & Johnston, D. A. (2006). *The Physics of Diagnostic Imaging.* (2 ed.). Boca Raton: CRC Press.

European Commision (EC). (1990). CEC Quality Criteria for Diagnostic Radiographic Images and Patient Exposure Trial:, (Report EUR 12952), . Brussels:CEC.

European Commision (EC). (1996). Council Directive 96/29/Euratom of 13 May 1996 laying down basic safety standards for the protection of the health of workers and the general public against the danger arising from ionising radiation. (Vol. 39: L159).

European Commision (EC). (1997). Council Directive 97/43/Euratom of June 30 1997 on health protection of individuals against the dangers of ionising radiation in relation to medical exposures (Vol. L180/22).

European Commision (EC). (2009). European commission guidelines on clinical audit for medical radiological practices (diagnostic radiology, nuclear medicine and radiotherapy):Radiation protection NO. 59 Luxembourg: Publications Office of the European Union.

Eisenhuber, E., Stadler, A., Prokop, M., Fuchsjäger, M., Weber, M., & Schaefer-Prokop, C. (2003). Detection of monitoring materials on bedside chest radiographs with the most recent generation of storage phosphor plates: Dose increase does not improve detection performance. *Radiation protection dosimetry, 227*(1), 216-221.

Ekpo, E. U., Hoban, A. C., & McEntee, M. (2014). Optimisation of direct digital chest radiography using Cu filtration. *Radiography, 20*(4), 346–350.

Elmore, J. G., Wells, C. K., Lee, C. H., Howard, D. H. , & Feinstein, A. R. (1994). Variability in radiologists' interpretation of mammograms. The new england journal of medicine, 331, 1493-1499.

European Medical Radiation Learning Development (EMERALD). (2001). Physics of diagnostic radiology: Student training workbook module 1.

Engeldrum, P.G. (1999, April 25-28 1999). *Image quality modeling: Where are we.* Paper presented at the image processing, image quality and image capture systems (PICS-99), Savannah, Georgia, USA.

England, A., Evans, P., Harding, L., Taylor, E. M., Charnock, P., & Williams, G. (2015). Increasing source-to-image distance to reduce radiation dose from digital radiography pelvic examinations. *Radiologic technology, 86*(3), 246-256.

Fauber, T. L. (2014). *Radiographic imaging & exposure* (4 ed.). Missouri: Mosby.

Fauber, T. L., Cohen, T., & Dem psey , M. C. (2011). High kilovoltage digital exposure techniques and patient dosimetry. *Radiologic technology, 82*(6), 501-510.

Fetterly, K., & Schueler, B. . (2007). Experimental evaluation of fiber-interspaced antiscatter grids for large patient imaging with digital x-ray systems. *phyiscs in biology and medicine, 52*(16), 4863-4880.

Field, A. (2013). *Discovering Statistics using IBM SPSS Statistics* (4 ed.). London: Sage publications.

Field, A. (2000). *Discovering statistics using SPSS for windows*. London: Sage Publications.

Field, A. (2005). Research methods II: project 2, questionnaire design [Lecture note]

Filliben, J. (2012). *Exploratory data analysis. C., Croarkin &W., Guthrie, NIST/SEMATECH e-Handbook of statistical methods (Web-based book) . Retrieved from http://www.itl.nist.gov/div898/handbook/eda/section3/eda35h1.htm.*

Flemming, D. J., & Walker,E. A. (2010). Imaging of hip and pelvis injuries. In P. H. Seidenberg. & J. D. Bowen (Eds.), *The hip and pelvis in sports medicine and primary care*. New York: Springer.

Frank, E. D., Long, B. W., & Smith, B. J. (2012). *Merri l l's at las of radiographic positioning & procedures* (12 ed. Vol. 1). Missouri: Mossby.

Freedman, M., & Osicka, T. (2006). Reader variability: What we can learn from computer-aided detection experiments. *Journal of American college of radiology*, 3(6), 446-455.

Freedman, M., Pe, E., Mun, S. K., Lo, S., & Nelson, M. (1993). *The potential for unnecessary patient exposure from the use of storage phosphor imaging systems.* Paper presented at the the image capture, formatting, and display, Newport Beach, CA.

Freedman, M., & Steller, D. (1995). Digital radiography of the musculoskeletal system: The optimal image. *Journal of Digital Imaging*, 8(1), 37-42.

Fung, K. L. L., & Gilboy, W. B. (2000). Anode heel effect" on patient dose in lumbar spine radiography. *British journal of radiology, 73*(2000), 531-536.

Garland, L. H. (1949). On the scientific evaluation of diagnostic procedures. Radiology, 52(3), 309-328.

Geijer, H., Norrman, E., & Persliden, J. (2009). Optimizing the tube potential for lumbar spine radiography with a flat-panel digital detector. *British journal of radiology, 82*(973), 62–68.

Gibson, D. J., & Davidson, R. A. (2012). Exposure creep in computed radiography: A longitudinal study. *Academic Radiology, 19*(4), 458-462.

Gkanatsios, N., Huda, Walter., & Peters, K. R. (2002). Effect of radiographic techniques ''kVp and mAs'' on image quality and patient doses in digital subtraction angiography. *Medical physics, 29*(8), 1643-1650.

Goodman, L. R., Wilson, C. R., & Foley, W. D. (1988). Digital radiography of the chest: Promises and problems. *American Journal of Roentgenology, 150*(6), 1241-1252.

Gorham, S., & Brennan, P. (2010). Impact of focal spot size on radiologic image quality: A visual grading analysis. *Radiography, 16*(4), 304-313.

Graham, D. T., & Cloke, P. (2003). *Principles of radiological physics* (4 ed.). Edinburgh: Churchill livingstone.

Graham, D. T., Cloke, P., & Vosper, M. (2011). *Principles and applications of radiological physics* (6 ed.). Livingstone: Churchill.

Grupen, c. (2010). *Introduction to radiation protection practical knowledge for handling radioactive sources*. Heidelberg: Springer Publishing Company.

Guy, C., & ffytche, D. . (2005). *An introduction to the principles of medical imaging* (Revised ed.). London: Imperial College Press.

Guyatt, G., Feeny, D., & Patrick, D. (1993). Measuring health-related quality of life. *Annals of Internal Medicine, 118*(8), 622-629.

Håkansson, M., Båth, M., Börjesson, S., Kheddache, S., Flinck, A., Ullman, G., & Månsson, L. G. (2005). Nodule detection in digital chest radiography: Effect of nodule location. *Radiation protection dosimetry, 114*(1-3), 92–96.

Hair, J. F., Black, W. C., Babin, B. J., & Andersson, R. E. (2009). *Multivariate data analysis* (7 ed.): Prentice Hall.

Hamer, O., Völk, M., Zorger, N., Borisch, I., Büttner, R., Feuerbach, S., & Strotzer, M. (2004). Contrast-detail phantom study for X-ray spectrum optimization regarding chest radiography using a cesium iodide–amorphous silicon flat-panel detector. *Acta Radiologica, 39*(10), 610-618.

Hamer, O. W., Sirlin, C. B., Strotzer, M., Borisch, L., Zorger, N., Feuerbach, S., & Völk, M. (2005). Chest radiography with a flat-panel detector: Image quality with dose reduction after copper filtration. *Radiology, 237*(2), 691–700.

Hånsson, B., Finnbogason, Th., Schuwert, P., & Persliden, J. (1997). Added copper filtration in digital paediatric double-contrast colon examinations: Eeffects on radiation dose and image quality. *European Radiology 7*(7), 1117–1122.

Harding, L., Manning-Stanley, A.S., Evans, P., Taylor, E. M., Charnock, P., & England, A. (2014). Optimum patient orientation for pelvic and hip radiography: A randomised trial. *radiography, 20*(1), 22–32

Hart, D., Wall, B.F., Hillier, M.C., & Shrimpton, P.C. (2010). Frequency and collective dose for medical and dental X-ray examinations in the UK (pp. 1-50). Chilton: Health Protection Agency

Hawking, N., & Elmore, A. (2009). Effects of AEC chamber selection on patient dose and image quality. *Radiologic technology, 80*(5), 411-419.

Department of Health. (2007). Ionising radiation (medical exposure) regulations 2000. Statutory instrument No. 1059. London: HMSO.

HealthCare, AGFA. (2009). CR 35-X digitizer specifications sheet. In A. HealthCare (Ed.).

Heath, R., England, A., Ward, A., Charnock, P., Ward, M., Evans, P., & Harding, L. (2011). Digital pelvic radiography: Increasing distance to reduce dose. *Raediologic technology, 83*(1), 20-28.

Hemdal, B., Andersson, I., Grahn, A., Håkansson, M., Ruschin, M., Thilander-Klang, A., . . . Mattsson, S. (2005). Can the average glandular dose in routine digital mammography screening be reduced? A pilot study using revised image quality criteria. *Radiation protection dosimetry*, 114(383-388).

Hendee, W. R., & O'Connor, M. K. (2012). Radiation risks of medical imaging: Separating fact from fantasy. *Radiology, 264*(2), 312-321. doi: 10.1148/radiol.12112678

Hiles, P., Mackenzie, A., Scally, A., & Wall, B. (2005). Recommended standards for the routine performance testing of diagnostic X-ray imaging systems: Institute of physics and engineering in medicine; Report No. 91.

Ho, R. . (2006). *Handbook of univariate and multivariate analysis and interpretation with SPSS*. Boac Raton: Taylor & Francis Group.

Hogg, P., & Blindell, P. (2012). *Software for image quality evaluation using a forced choice method*. Paper presented at the UKRC, Manchster, UK.

Hogg, P., & Lança, L. (2015). *Radiation dose and image quality optimisation in medical imaging* Erasmus Intensive Programme OPTIMAX#2014: Lisbon, Portugal.

Holmes, K., Elkington, M., & Harris, P. (2014). *Clark's essential physics in imaging for radiographers*. Boca Raton: CRC Press.

Honey, I., & Hogg, P. (2012). Balancing radiation dose and image quality in diagnostic imaging. *Radiography, 18*(1), 1-2.

Huang, H. K. . (2010). *PACS and imaging informatics basic principles and applications*. Canada: John Wiley & Sons, Inc.

Huda, Walter. (2010). *Review of radiologic physics* (3 ed.). Philadelphia,: Lippincott Williams & Wilkins.

International Atomic Energy Agency (IAEA). (1997). International basic safety standards for protection against ionizing radiation and for the safety of radiation sources.IAEA safety series -ISBN 92-0-104295-7. Vienna,Austria.

International Atomic Energy Agency (IAEA). (2002). Radiological protection for medical exposure to ionizing radiation : IAEA safety standards series.Safety guides. Vienna, Austria: IAEA.

International Atomic Energy Agency (IAEA). (2007). Dosimetry in diagnostic radiology: an international code of. IAEA- Technical report series No.457; Vienna: IAEA.

International Commission on Radiological Protection (ICRP). (1977). PUBLICATION 26: Recommendations of the international commission on radiological protection. *Annals of ICRP, 1*(3), 1-50.

International Commission on Radiological Protection (ICRP). (1991). 1990 Recommendations of the international commission on radiological protection: ICRP Publication 60. *Annals of ICRP, 21*(1-3).

International Commission on Radiological Protection (ICRP). (1996). Publication73: Radiological protection and safety in medicine. *Annals of ICRP, 26*(2), 1-31.

International Commission on Radiological Protection (ICRP). (2001a). Radiation and your patients: A guide for medical practionaers:ICRP supporting guidance 2. *Annals of ICRP, 31*(4), 5-52.

International Commission on Radiological Protection (ICRP). (2001b). A report on progress towards new recommendations: A communication from the international commission on radiological protection. *Journal of radiological protection, 21*(2), 113-125.

International Commission on Radiological Protection (ICRP). (2003). The evolution of the system of radiological protection: the justification for new ICRP recommendations. *Journal of radiological protection, 23*(1), 129–142.

International Commission on Radiological Protection (ICRP). (2004). Managing patient dose in digital radiology. A report of the international commission on radiological protection. *Annals of ICRP, 34*(1), 1-73.

International Commission on Radiological Protection (ICRP). (2006). The optimisation of radiological protection: Broadening the process, ICRP 101. *Annals of ICRP, 36*(3), 69-87.

International Commission on Radiological Protection (ICRP). (2007a). The 2007 recommendations of the international commission on radiological protection.ICRP Publication 103. *Annals of ICRP, 37*(2-4), 1-332.

International Commission on Radiological Protection (ICRP). (2007b). Draft recommendations of the international commission on radiological protection.

International Labour Office (ILO). (2002). Guidelines for the use of the ILO international classification of radiographs of pneumoconioses. Revised Edition 2000. In: Occupational safety and health series, No. 22. Geneva: International Labour Office.

ImageJ. (2014). Image processing and analysis in Java (*Version 1.47*). Retrieved from http://rsb.info.nih.gov/ij/.

Inoue, K., Sato, T., Kitamura, H., Hirayama, A., Kurosawa, H., Tanaka, T., . . . Fujii, H. (2009). An anthropomorphic pelvis phantom for optimizationof the diagnosis of lymph node metastases in the pelvis. *Annals of Nuclear Medicine, 23*(3), 245-255.

Ionising Radiation((IR)[ME](MedicalExposure)). (2000). The ionising radiation (medical exposure) regulations 2000.Statutory instrument.Available from:http://www.legislation.gov.uk/uksi/2000/1059/ contents/made. No. 1059. London:HMSO.

Jangland, L., & Axelsso, B. (1990). Niobium filters for dose reduction in pediatric Radiology. *Acta Radiologica 31*(5), 540-541.

Jessen, K. A. . (2001). The quality criteria concepts: An introduction and overview. *Radiation protection dosimetry, 94*(1-2), 29–32

Jessen, K.A. (2004). Balancing image quality and dose in diagnostic radiology. *European Radiology Supplements, 14*(1), 9-18.

Joët, G., & Usher, E. (2011). Sources of self-efficacy: An investigation of elementary school students in france. *Journal of Educational Psychology, 103*(3), 649–663

Johnston, D. A., & Brennan, P. C. (2000). Reference dose levels for patients undergoing common diagnostic x-ray examinations in Irish hospitals. *British journal of radiology, 73*(868), 396-402.

Johnston, J. N., & Fauber, T. L. (2012). *Essentials of radiographic physics and imaging*. Missouri: Mossby.

Jones, C. G. . (2005). Review of the history of U.S radiation protection regulation, recommendations, and standards. *Health physics, 88*(2), 105-124. doi: 10.1097/01.HP.0000146629.45823.da

Joyce, M., McEntee, M., Brennan, P., & O'Leary, D. (2013). Reducing dose for digital cranial radiography: The Increased sourceto the image-receptor distance approach. *Journal of Medical imaging and radiation sciences, 44*(4), 180–187.

Kaiser, S. F. (1974). An index of factorial simplicity. *Sychometrika 39*(1), 31-36.

Katz, M.C., & Nickoloff, E.L. (1993). Radiographic detail and variation of the nominal focal spot size: the "focal effect". *radiographics, 12*(4), 753-761.

Khattak, Y., Sajjad, Z., & Alam, T. (2010). Digital radiography, a paradigm shift. *Pakistan journal of radiology, 20*(1), 34-40.

King, S., Pitcher, E., & Smail, M. (2002). Optimizing medical radiation exposures for uroradiological procedures, with special emphasis on paediatric imaging. *BJU international, 89*(6), 510–516.

Kitching, J., Cassidy, S., & Hogg, P. (2011). Creating and validating self-efficacy scales for students. *Radiologic technology, 43*(1), 10-19.

Kohn, M. L., Gooch, A. W., & Keller, W. S. (1988). Filters for radiation reduction: A comparison. *Radiology, 167*(1), 255-257.

Kotre, C. J., & Marshall, N. W. . (2001). A review of image quality and dose issues in digital fluorography and digital subtraction angiography. *Radiation protection dosimetry, 94*(1-2), 73-76.

Kottamasu, S., Kuhns, L., & Stringer, D. (1997). Pediatric musculoskeletal computed radiography. *Pediatric radiology, 27*(7), 563–575.

Kottamasu, S. R., & Kuhns, L. R. (1997). Musculoskeletal computed radiography in children: scatter reduction and improvement in bony trabecular sharpness using air gap placement of the imaging plate. *Pediatric radiology, 27*(2), 119-123.

Koutra, K., Orfanos, P., Roumeliotaki, T., Kritsotakis, G., Kokkevi, A., & Philalithis, A. (2012). Psychometric validation of the youth social capital scale in greece. *Research on social work practice, 22*(3), 333-343.

Krupinski, E. A. (2011). The role of perception in imaging: past and future. *Seminars in nuclear medicine., 41*(6), 392-400.

Krupinski, E. A., Kundel, H.L., Judy, P. F., & Nodine, C. F. (1998). Key Issues for Image Perception Research. Radiology, 209(3), 611-612.

Krupinski, E.A., & Jiang, Y. (2008). Anniversary paper: Evaluation of medical imaging systems. *Medical physics, 35*(2), 645-659.

Kumar, G. A., Kumar, Ch. R. P., & Malleswararao, V. (2011). Evaluation on X-ray exposure parameters considering tube voltage and exposure time. *International journal of engineering science and technology, 3*(4), 3210- 3215.

Kundel, H.L. (1979). Images, image quality and observer performance: New horizons in radiology lecture. *Radiology, 132*(2), 265-271

Kundel, H.L. (1993, September). *Perception and representation of medical images.* Paper presented at the medical imaging : Image processing.

Kundel, H.L. (2006). History of research in medical image perception. *Journal of the American college of radiology, 3*(6), 402–408

Lança, L. , & Silva, A. (2009). Digital radiography detectors e A technical overview: Part 1. *radiography, 15*(1), 1-5.

Lança, L., & Silva, A. (2008). Digital radiography detectors – A technical overview: Part 2. *Radiography, 15*(2), 134–138.

Lança, L., Franco, L., Ahmed, A., Harderwijk, M., Marti, C., Nasir, S., . . . Hogg, P. (2014). 10 kVp rule: An anthropomorphic pelvis phantom imaging study using a CR system: Impact on image quality and effective dose using AEC and manual mode. *Radiography, 20*(4), 333–338.

Laney, A., Petsonk, E., Wolfe, A., & Attfield, M. (2010). Comparison of storage phosphor computed radiography with conventional film-screen radiography in the recognition of pneumoconiosis. *European respiratory journal, 36*(1), 122–127.

Leblans, P., Struye, L., & Willems, P. . (2000). A New needle-crystailine computed Radiography detector. *Joumal of digital imaging, 13*(2), 117-120.

Leblans, P., Vandenbroucke, D., & Willems, P. (2011). Storage phosphors for medical imaging. *materials, 4*(6), 1034-1086.

Lehnert, T., Naguib, N., Korkusuz, H., Bauer, R., Kerl, J., Mack, M., & Vogl, T. J. (2011). Image-quality perception as a function of dose in digital radiography. *American journal of roentgenology, 197*(6), 1399-1403

Lemoigne, Y., Caner, A., & Rahal, G. (2007). *Physics for medical imaging applications*. Amsterdam: IOS Press & Springer.

Lesik, S. A. (2010). *Applied statistical inference with MINITAB®* (N. Balakrishnan & W. R. Schucany Eds.). Boca Raton: Taylor & Francis Group, LLC.

Li, Y., Poulos, A., McLean, D., & Rickard, M. (2010). A review of methods of clinical image quality evaluation in mammography. *European journal of radiology*, 74(3), 122-131.

Lin, Y., Luo, H., Dobbins III, J. T., McAdams, H. P., Wang, X., Sehnert, W. J., . . . Samei, E. (2012). An image-based technique to assess the perceptual quality of clinical chest radiographs. *Medical physics, 39*(11), 7019-7031.

Little, M. P., Wakeford, R., Tawn, E. J., Bouffler, S. D., & Gonzalez, A. B. (2009). Risks associated with low doses and low dose rates of ionizing radiation: Why linearity may be (almost) the best we can do. *Radiology, 251*(1), 6-12.

Lu, Z. F., Nickoloff, E.L., So, J. C., & Dutta, A. K. (2003). Comparison of computed radiography and film/screen combination using a contrast-detail phantom. *Journal of applied clinical medical physics, 4*(1), 91-98.

Ludewig, E., Richter, A., & Frame, M. (2010). Diagnostic imaging – evaluating image quality using visual grading characteristic (VGC) analysis *Veterinary research communications, 34*(5), 473–479. doi: 10.1007/s11259-010-9413-2.

Lunenburg, F. C. (2011). Self-efficacy in the workplace: Implications for motivation and performance. *International journal of management, business and administration, 14*(1), 1-6.

Luz, R., & Hoff, G. (2010). Comparative study of image quality and entrance and exit air kerma measurements on chest phantom utilizing analog and CR digital imaging systems. *Radiologia brasileira, 34*(1), 39–45.

Ma, W. K., Hogg, P., & Norton, S. (2014). Effects of kilovoltage, milliampere seconds, and focal Spot size on image quality. *Radiologic technology, 85*(5), 479-485.

Ma, W. K., Hogg, P., Tootell, A., Manning, D. J., Thomas, N., Kane, T., . . . Kitching , J. (2013). Anthropomorphic chest phantom imaging e The potential for dose creep in computed radiography. *Radiography, 19*(3), 207-211.

Maccia, C., Ariche-Cohen, M. , Nadeau, X., & Severo, C. (1995). The 1991 CEC trial on quality criteria for diagnostic radiographic images. *Radiation protection dosimetry, 57*(1-4), 111-117.

Maccia, C., Moores, B.M., & Wall, B.F. (1997). The 1991 CEC trial on quality criteria for diagnostic radiographic images: detailed results and findings: EUR 16635 EN. Commision of European Communities (CEC).

Mamisch, N., Brumann, M., Hodler, J., Held, U., Brunner, F., & Steurer, J. (2012). Radiologic criteria for the diagnosis of spinal stenosis: Results of a delphi survey. *Radiology, 264*(1), 174-179.

Manning-Stanley, A.S., Ward, A.J., & England, A. (2012). Options for radiation dose optimisation in pelvic digital radiography: A phantom study. *Radiography, 18*(4), 256-263.

Manning, D.J., Gale, A. , & Krupinski, E. (2005). Perception research in medical imaging. *British journal of radiology, 78*(932), 683–685

Månsson, L.G. (2000). Methods for the evaluation of image quality. *Radiation protection dosimetry, 90*(1-2), 89–99.

Martin, C.J. (2007). The importance of radiation quality for optimisation in radiology. *Biomedical imaging and intervention journal COMMENTARY, 3*(2), 1-38.

Martin, C.J., Sutton, D.G., & Sharp, F.P. (1999). Balancing patient dose and image quality. *Applied radiation and isotopes, 50*(1), 1-19.

Mathews, P. G. (2005). *Design of experiments with MINITAB*. USA: William A. Tony.

Matthews, k., & Brennan, P. (2008). Justification of x-ray examinations: General principles and an Irish perspective. *Radiography, 14*(4), 349-355.

Matthews, K., & Brennan, P. (2009). Optimisation of X-ray examinations:General and an Irish perspective. *radiography, 15*(3), 262-268.

Mazzocchi, S., Belli, G., Busoni, S., Gori, C., Menchi, I., Salucci, P., . . . Zatelli, G. (2005). AEC set-up optimisation with computed radiography imaging. *Radiation protection dosimetry, 117*(1-3), 169–173.

McCollough, C. H., Bruesewitz, M. R., & Kofler, F. M. (2006). CT dose reduction and dose management tools: Overview of available options. *Radiographics, 26*(2), 503-512.

McDowell, I. (2006). *Measuring health : A Guide to rating scales and questionnaires* (3 ed.). Oxford: Oxford university press.

McEntee, M., Brennan, P., & Connor, G. O. (2004). The effect of X-ray tube potential on the image quality of PA chest radiographs when using digital image acquisition devices. *Radiography, 10*(4), 287–292.

Mearon, T. , & Brennan, P.C. (2006). *Anode heel affect in thoracic radiology: a visual grading analysis.* Paper presented at the medical imaging 2006: Physics of medical imaging, San Diego, CA.

Montgomery, D. C. (2013). *Design and analysis of experiments* (Vol. 8). USA: John Wiley & Sons.

Moore, C. S., Beavis, A. W., & Saunderson, J. R. (2008). Investigation of optimum X-ray beam tube voltage and filtrationfor chest radiography with a computed radiography system. *The British Journal of Radiology, 81*(970), 771-777.

Moore, C. S., Liney, G. P., Beavis, A. W., & Saunderson, J. R. (2007). A method to optimize the processing algorithm of a computed radiography system for chest radiography. *British journal of radiology, 80*(957), 724-730.

Moore, C. S., Wood, T. J., Avery, G., Balcam, S., Needler, L., Beavis, A. W., & Saunderson, J. R. (2014). An investigation of automatic exposure control calibration for chest imaging with a computed radiography system. *Phyiscs in biology and medicine, 59*(9), 2307–2324.

Moore, C.S., Wood, T.J., Beavis, A.W., & Saunderson, J.R. (2013). Correlation of the clinical and physical image quality in chest radiography for average adults with a computed radiography imaging system. *The British journal of radiology, 86*(1027), 1-12.

Moores, B. M., Mattsson, S., Månsson, L. G., & Panzer, W. (2000). Quality criteria development within the fourth framework research programme. *Radiation protection dosimetry, 90*(1-2), 63–71.

Moran, B. (2012). *The Development and validation of a psychometric scale to measure mammographic image quality (MSc. Dissertation).* University of Salford; UK.

Morán, L.M., Rodríguez, R, Calzado. A, Turrero, A, Arenas, A., Cuevas, A., . . . Morán, P. (2004). Image quality and dose evaluation in spiral chest CT examinations of patients with lung carcinoma. *British journal of radiology, 77* (922), 839-846.

Mot z, J. W., & Danos, M. (1978). Image information content and patient exposure. *Medical physics, 5*(1), 8-22.

Mraity, H., England, A., & Hogg, P. (2014). Developing and validating a psychometric scale for image quality assessment. *radiography, 20*(4), 306–311.

Murphey, M., Quale, L., Martin, N., Bramble, J., Cook, L., & Dwyer, J. (1992). Computed radiography in musculoskeletal imaging: State of the art. *American journal of roentgenology, 158*(1), 19-27.

National Research Council. (1990). Commission of life sciences, committee on biological effects on ionizing radiation (BEIR V), board on radiation effects research: Health effects of exposure to low levels of ionizing radiations. Washington,: National Academies Press.

National Council on Radiation Protection & Measurements (NCRP). (1968). Medical x-ray and gamma-ray protection for energies up to 10 MeV(Equipment design and use): NCRP Report No. 33: NCRP.

National Council on Radiation Protection & Measurements (NCRP). (1989). Radiation protection for medical and allied health personnel: Report NO. 105 recommendations of the national council on radiation protection and measurements. Maryland.

National Council on Radiation Protection & Measurements (NCRP). (1994). Radiation protection in pediatric radiology: NCRP Report NO.68 recommendations of the national council on radiation protection and measurements. Maryland.

Neitzel, U. . (2004). Management of pediatric radiation dose using Philips digital radiography. *Paediatric radiology, 34*(Suppl 3), S227–S233.

Niroomand-Rad, A. (2003). Radiological protection of patients. *Iranian Journal for radiation researches, 1*(3), 125-131.

Noel, A (2007). Patient dose in diagnostic radiology. In Y. Lemoigne, A.Caner & G. Rahal (Eds.), *Physics for medical imaging applications* (pp. 397–404). France Springer.

Norrma, E., & Persliden, J. (2005). A factorial experiment on image quality and radiation dose. *Radiation protection dosimetry, 114*(1-3), 246–252.

Norrman, E., Geijer, H., & Persliden, J. (2007). Optimization of image process parameters through factorial experiments using a flat panel detector. *Phyiscs in biology and medicine*, 52(17), 5263–5276.

Norweck, J. T., Seibert, J. A., Andriole, K. P., Clunie, D. A., Curran, B. H., Flynn, M. J., . . . Mian, T. A. (2013). A,erican college of radiology (ACR)–AAPM–SIIM technical standard for electronic practice of medical imaging. *Journal of digital imaging, 26*(1), 38-52.

Nunnally, J., & Bernstein, I. (1994). *Psychometric theory* (3 ed.). New York: McGRAW-HILL.

Oliveira, A. C., Martins, A. P., Avelãs, R. T., Santos, M. S., Martins, P. M., Francesco, S. D., . . . Coimbra, P. (2013). Visual grading analysis of image quality in pediatric abdominal images acquired by direct digital radiography and computer radiography systems. Paper presented at the European conference of radiology, Vienna.

Pajares, F. (2008). Information on self-efficacy – a community of scholars. Retrieved 5 July, 2013, from http://des.emory.edu/mfp/self-efficacy.html#search.

Pajares, F. (1996). Self-efficacy beliefs in academic settings. *Review of educational research, 66*(4), 543-578.

Panagiotakos, D. (2009). Health measurement scales: methodological issues. *Open cardiovascular medicine journal, 23*(3), 160-165.

Parsian, N., & Dunning, T. (2009). Developing and validating a auestionnaire to measure spirituality:A psychometric process. *Global journal of health science, 1*(1), 2-11.

Pelli, D. G., & Farell, B. (1995). Psychophysical methods. In M. Bass, E. W. Stryland, D. R. Williams & W. L. Wolfe (Eds.), *Handbook of optics:Fundamentals , techniques , and design* (2 ed., Vol. 1). New York: McGRAW-HILL , INC.

Persliden, J., Beckman, K., Geijer, H., & Andersson, T. (2002). Dose-image optimisation in digital radiology with a direct digital detector: an example applied to pelvic examinations. *European radiology supplements, 12*(1), 1584-1588.

Pettersson, H., Aspelin, P., Boijsen, E., Herrlin, K., & Egund, N. (1988). Digital radiography of the spine, large bones and joints using stimulable phosphor Early clinical experience. *Acta Radiologica, 29*(3), 267-271.

Phantoms, sectional. (2014). The Phantom laboratory. Sectional lower Torso SK250.   Retrieved May, 1st, 2014, from http://www.phantomlab.com/library/pdf/sectional_ SK250DS.pdf

Pina, D. R., Duarte, S. B., Netto, T. G., Trad, C. S., Brochi, M. A. A., & Oliverira, S. C. . (2004). Optimization of standard patient radiographic images for chest, skull and pelvis exams in conventional x-ray equipment. *Phyiscs in biology and medicine, 49*(41), 215-226.

Polit, D. , & Beck, C. (2003). *Nursing research: principles and methods* (7 ed.): Lippincott Williams & Wilkins

Presser, S., Rothgeb, J., Couper, M., Lessler, J., Martin, E., Martin, J., & Singer, E. (2004). *Methods for testing and evaluating survey questionnaires*. Canada: John Wiley & Sons.

Prokop, M., Neitzel, U., & Schaefer-Prokop, C. . (2003). Principles of Image Processing in Digital chest radiography. *Journal of thoracic imaging, 18*(3), 148–164.

Puchta, C., & Potter, J. (2004). Focus group practice. Sage publishing: London.

Rainford, L. A., Al-Qattan, E., McFadden, S. , & Brennan, P. C. (2007). CEC analysis of radiological images produced inEurope and Asia. *Radiography, 13*(3), 202-209.

Ramanandraibe, M. J., Andriambololona, R., Rakotoson, E. C., Tsapaki, V., & Gfirtner, H. (2009). *Survey of image quality and patient dose in simple radiographic examinations in Madagascar: Initial results*. Paper presented at the HEP-MAD 09, Antananarivo (Madagascar).

Raykov, T., & Marcoulides, G. A. (2011). *Introduction to psychometric theory*. New York: Routledge.

Rivera, T. (2012). Thermoluminescence in medical dosimetry. *Applied radiation and isotopes, 71*(Supplement), 30–34.

Robinson, I. (2002). Optimisation and common sense. *Journal of radiological protection, 22*(1), 57-61.

Rose, A. (1973). The visual process: *Vision: human and electronic*. New York: NY: Plenum Press.

Rose, A., Peters, N., Shea, J., & Armstrong, K. (2004). Development and testing of the health care system distrust scale. *Journal of general internal medicine, 19*(1), 57-63.

Rosner, B. (2010). *Fundamentals of biostatistics* (7 ed.). Boston: Cengage Learning.

Rossmann, K., & Wiley, B. (1970). The central problem in the study of radiographic image quality. *Radiology, 96*(1), 113-118.

RSNA. (2010). RadLex: a lexicon for uniform indexing and retrieval of radiology information resources. Retrieved January 10, 2013, from http://www.rsna.org/ radlex/

Samei, E. (2003). Performance of digital radiographic detectors:Quantification and assessment methods advances in digital radiography: RSNA categorical course in diagnostic radiology physics (pp. 37–47).

Sandborg, M., Carlsson, C. A., & Carlsson, G. A. (1994). Shaping X-ray spectra with filters in X-ray diagnostics. *Medical & Biological Engineering & Computing*, 32(4), 384-390.

Sandborg, M., Tingberg, A., Dance, D. R., Lanhede, B., Almén, A., Mcvey, G., . . . Carlsson, G. A. (2001). Demonstration of correlations between clinical and physical image quality measures in chest and lumbar spine screen–film radiography. *The British journal of radiology, 74*(882), 520–528.

Sandborg, M., Tingberg, A., Ullman, G., Dance, D. R. , & Alm Carlson, G. (2006). Comparison of clinical and physical measures of image quality in chest and pelvis computed radiography at different tube voltages. *Medical physics, 33*(11), 4169–4175.

Sandmayr, H, & Wallentin, D. (1997). Computer integrated radiology system: analogue goes digital. *Euorpean radiology, 7*(Suppl. 3), 90-93.

Sanfridsson, J., Holje, G., Svahn, G., Ryd, L., & Jonsson, K. (2000). Radiation dose and image information in computed radiography. *Academic radiology, 41*(4), 310-316.

Schaefer-Prokop, C., & Neitzel, U. (2006). Computed radiography/digital radiography: Radiologist perspective on controlling dose and study quality In D. P. Frush. & W. Huda (Eds.), *RSNA Categorical Course in Diagnostic Radiology Physics: From Invisible to Visible—The Science and practice of X-ray imaging and radiation dose optimization* (pp. RSNA). USA: RSNA.

Schaefer-Prokop, C., Neitzel, U., Venema, H., Uffmanna, M., & Prokop, M. (2008). Digital chest radiography: an update on modern technology, dose containment and control of image quality. *Paediatric radiology, 18*(9), 1818–1830.

Schaefer-Prokop, C., De Boo, D. W., Uffmanna, M., & Prokop, M. (2009). DR and CR: recent advances in technology. *Euorpean journal radiology*, 72(2), 194-201..

Schibilla, H., & Moores, B.M. (1995). Diagnostic radiology better images - lower dose. Compromise or correlation? A European strategy with historical overview. *Journal belge de radiologie, 78*(6), 382-387.

Schreiner-Karoussou , A. (2005). Review of image quality standards to control digital X-ray systems. *Radiation protection dosimetry, 117*(1-3), 23-25.

Schueler, B. A. (1998). Clinical applications of basic X-ray physics principles. *Radiographics, 18*(3), 725-730.

Seeram, E. (2001). *Rad tech's guide to radiation protection*. Boston: Mass: Blackwell Science.

Seeram, E., & Brennan, P. (2006). Diagnostic reference levels in radiology. *Radiologic technology, 77*(5), 373-384.

Seeram, E., Bushong, S., Davidson, R., & Swan, H. (2014). Image quality assessment tools for radiation dose optimization in digital radiography: An overview. *Radiologic technology, 85*(5), 555-562.

Seeram, E., Davidson, R., Bushong, S., & Swan, H. (2013). Radiation dose optimization research: exposure technique approaches in CR imaging e a literature review. *Radiography, 19*(4), 331-338.

Seggern, H. . (1999). Photostimulable X-ray storage phosphors:a review of present understanding. *Brazilian journal of physics, 29*(2), 254-268.

Seibert, J. A. (2004). Computed radiography technology 2004 AAMP summer school (pp. 153-175). California: AAMP.

Seo, D., Jang, S., Kim, Y., Sung, D., Kim, H., & Yoon, Y. (2014). Acomparative assessment of entrance surface doses in analogue and digital radiography during common radiographic examinations. *Radiation protection dosimetry*, 158(1), 22–27

Servomaa, A. , & Tapiovaara, M. (1998). Organ dose calculation in medical x ray examinations by the programme PCXMC. *Radiation protection dosimetry, 80*(1-3), 213-219.

Sezdi, M. (2011). Dose optimization for the quality control tests of X-ray equipment. In A. B. Eldin (Ed.), *Modern approaches to quality control: InTech*.

Sharp, F.P. (1990). Quantifying image quality. *Clinical physics and physiological measurement, 11*(Suppl. A), 21-26.

Shaughnessy, J., Zechmeister, E., & Zechmeister, J. (2012). *Research methods in psychology* (9 ed.). New York: McGraw-Hil.

Shephard, C. T. (2003). *Radiographic image production and manipulation*. New York: McGraw-Hill Medical.

Sherer, M. A. S., Visconti, P. J., Ritenour, E. R., & Haynes, K. W. (2014). *Radiation protection seventh edition in medical radiography* (7 ed.). Phalidelphia: Mosby.

Shet, N., Chen, J. , & Siegel, E.L. (2011). Continuing challenges in defining image quality. *Paediatric radiology, 41*(5), 582-587.

Sim, J., & Wright, C. (2000). *Research in health care: Concepts, designs and methods*. Hampshire Lucy Millis: Cengage Learning.

Sjöström, D. (2002). Optimisation of an image plate system with respect of tube voltage: An observer performance study based on chest and pelvis images. Malmö: University of Lund:Department of Radiation Physics.

Smedby, O., & Fredrikson, M. (2010). Visual grading regression: analysing data from visual grading experiments with regression models. *British journal of radiology, 83*(993), 767-775.

Smith, N. B., & Webb, A. (2011). *Introduction to Medical Imaging Physics, Engineering and Clinical Applications*. Cambridge: cambridge university press.

Soares, J. F. D. S., Dores, R. E. S., Sousa, P., Rodrigues, S., Ribeiro, L. P. V., Abrantes, A. F., & Almeida , R. P. P. A. (2013). *Attenuation of anode heel effect with an aluminum filter and their influence on patient dose in lumbar spine radiography*. Paper presented at the ECR 2013, Vienna.

Spector, P. (1992). *Summated rating scale construction e an introduction*. California: Sage Publications.

Stajkovic, A. D., & Luthans, F. (1998). Social cognitive theory and self-efficacy: Goin beyond traditional motivational and behavioral approaches. *Organizational Dynamics, 26*(4), 62–74.

Staniszewska, M. A., Biegan´sk, T., Midel, A., & Barańska, D. (2000). Filters for dose reduction in conventional x ray examinations of children. *Radiation protection dosimetry*, 90(1-2), 127–133.

Streiner, D. L., & Norman, G. R. (2008). *Health measurement scales : A practical guide to their development and use* (4 ed.). USA Oxford University Press.

Strickland, O., & Dilorio, C. . (2003). *Measurement of Nursing Outcomes* (2 ed.). New York: Springer Publishing Company.

Suhr, D. D. (2006). *Exploratory or confirmatory factor analysis?* Paper presented at the SUGI 31 Proceedings, San Francisco, California.

Suliman, I. I., & Mohammedzein, T. S. (2014). Estimation of adult patient doses for common diagnostic X-ray examinations in Wad-madani, Sudan: derivation of local diagnostic reference levels. *Australasian Physical and Engineering Science in Medicine, 37*(2), 425-429.

Sund, P., Båth, M., Kheddaché, S., Tylén, U., & Månsson, L. G. (2000). *Evaluation of image quality of a new CCD-based system for chestimaging.* Paper presented at the Medical Imaging 2000: Physics of medical imaging; San Diego, CA.

Sund, P., Båth, M., Kheddache, S. , & Månsson, L.G. (2004). Comparison of visual grading analysis and determination of detective quantum efficiency for evaluating system performance in digital chest radiography. *Euorpean radiology, 14*(1), 48-58.

Sund, P., Herrrnannb, C., Tingberg, A., Kheddached, S., Månsson, L. G., Almén, A., & Mattsson, S. (2000, February 12, 2000). *Comparison of two methods for evaluating image quality of chest radiographs.* Paper presented at the Image Perception and Performance, San Diego, CA.

Tabachnick, B., & Fidell, L. . (2013). *Using multivariate statistics* (5 ed.). Boston: Pearson Education.

Tapiovaara, M. (1993). SNR and noise measurements for medical imaging: LT. Application to fluoroscopic x-ray equipment. *Phyiscs in biology and medicine, 38*(12), 1761-1788.

Tapiovaara, M. (2006). Relationships between physical measurements and user evaluation of image quality in medical radiology - a review. *STUK-A219*, 1-62.

Theocharopoulos, N., Perisinakis, K., Damilakis, J., Varveris, H., & Gourtsoyiannis, N. (2002). Comparison of four methods for assessing patient effective dose from radiological examinations. . *Medical physics, 29*(9), 2070-2079.

Thornbury, J. R., Fryback, D. G., Patterson, F. E., & Chiavarini, R. L. (1977). Effect of screen/film combinations on diagnostic certainty: Hi-Plus/RPL versus Lanex/Ortho G in excretory urography. *American journal of roentgenology, 130*(1), 83-87.

Tingberg, A., Herrmann, C., Besjakov, J., Almén, A., Sund, P., Adliene, D., . . . Panzer, W. (2002, February 23, 2002). *What is worse: Decreased spatial resolution or increased noise?* Paper presented at the medical imaging 2002: Image perception, observer performance, and technology assessment, San Diego, CA.

Tingberg, A., Herrmann, C., Besjakov, J., Rodenacker, K., Almén, A., Sund, P., . . . Månsson, L. G. (2000, 34 (April 14, 2000)). Evaluation of lumbar spine images with added pathology. Paper presented at the Medical Imaging 2000: Image Perception and Performance, San Diego, CA

Tingberg, A., & Sjöström, D. (2005). Optimisation of image plate radiography with respect to tube voltage. *Radiation protection dosimetry, 114*(1-3), 286–293.

Tingberg, T., Herrmann, C., Lanhede, B., Almén, A., Sandborg, M., Mcvey, G., . . . Zankl, M. (2004). Influence of the characteristic curve on the clinical image quality of lumbar spine and chest radiographs. *British journal of radiology, 77*, 204–215.

Tootell, A. K., Szczepura, K. R., & Hogg, P. (2013). Optimising the number of thermoluminescent dosimeters required for the measurement of effective dose for computed tomography attenuation correction data in SPECT/CT myocardial perfusion imaging. *Radiography, 19*(1), 42–47.

Tootell, A., Lundie, M., Szczepura, K., & Hogg, P. (2013). *Reducing error in TLD dose radiation measurments* Paper presented at the UKRC, UK.

Tucker, D. M., Souto, M., & Barnes, G. T. (1993). Scatter in computed radiography. *Radiology, 188*(1), 271-274.

Tudor, G. R., Finlay, D., & Taub, N. (1997). An Assessment of inter-observer agreement and accuracy when reporting plain radiographs. *Clincal radiology*, 52(3), 235-238.

Tugwell, J., Everton, C., Kingma, A., Oomkens, D. M., Pereira, G. A., Pimentinha, D. B., . . . Hogg, P. (2014). Increasing source to image distance for AP pelvis imaging e Impact onradiation dose and image quality. *radiography, 20*(4), 351–355.

Tylén, U. (1997). Stimulable phosphor plates in chest radiology. *Euorpean radiology, 7*(Suppl.3), 83–86.

Uffmann, M., & Schaefer-Prokop, C. (2009). Digital radiography: The balance between image quality and required radiation dose. *European Journal of Radiology, 72*(2), 202–208.

Ullman, G., Sandborg, M., Dance, D. R., Hunt, R., & Carlsson, G. A. (2004). Optimisation of chest radiology by computer modelling of image quality measures and patient effective dose. Department of Medicine and Care Radio Physics: Universiteteti Linköping.

United Nations Scientific Committee on the Effects of Atomic Radiation (UNSCEAR). (2000). Sources and effects of ionizing radiation: Report to the general assembly with scientific annex - dose assessment methodologies. New York : United Nations.

United Nations Scientific Committee on the Effects of Atomic Radiation (UNSCEAR). (2010). Medical radiation exposure: Annex A sources and effects of ionizing radiation:UNSCEAR 2008 (Vol. 1). New York: United Nations.

Vaňo, E., Fernãndez, J., Ignacio, J., Prieto, C., Gonzãlez, L., Rodríguez, R., & Heras, D. (2007). Transition from screen-film to digital radiography: Evolution of patient radiation doses at pojection radiography. *Radiology, 246*(2), 461-466.

Vaňo, E. . (2005). ICRP Recommendations on 'managing patient dose in digital radiology. *Radiation protection dosimetry, 114*(1-3), 126–130.

Vaňo, E., Fernandez, J. M., Ten, J., Guibelalde, E., Gonzalez, L., & Pedrosa, c. (2002). Real-time measurement and audit of radiation dose to patients undergoing computed radiography. *Radiology, 225*(1), 283-288.

Vaňo, E., Guibelalde, E., Morillo, A., Alvarez-Pedrosa, C.S., & Fernandez, J.M. (1995). Evaluation of the European image quality criteria for chest examinations. *British journal of radiology, 68*(816), 1349-1355.

Vassileva, J. (2002). A phantom for dose-image quality optimization in chest radiography. *british journal of radiology, 75*(898), 837-842.

Völk, M., Paetzel, C., Angele, P., Seitz, J., Füchtmeier, B., Hente, R., . . . Strotzer, M. (2003). Routine skeleton radiography using a flat-panel detector: Image quality and clinical acceptance at 50% dose reduction. *Inestigative radiology*, 38(4), 230-235.

Walker, S., Allen, D., Burnside, C. , & Small, I. (2011, October 2011). Determining the relationship between exposure factors, dose and exposure index value in digital radiography. *Synergy imaging & therapy practice*, 7-14.

Wall, B., & Hart, D. (1997). Revised radiation doses for typical X-ray examinations. Report on a recent review of doses to patients from medical X-ray examinations in the UK by NRPB.National radiological protection board. *British journal of radiology, 70*(833), 437-439.

Wang, Z., Bovik, A. C., & Lu, L. (2002). Why is image quality assessment so difficult? *IEEE, 4*, 3313 -3316.

Ware, J., & Gandek, B. (1998). Methods for testing data quality, scaling assumptions, and reliability: The IQOLA project approach. *Journal of clinical epidemiology, 51*(11), 945–952.

Weatherburn, G., & Bryan, S. (1999). The effect of a picture archiving and communication system (PACS) on patient radiation doses for examination of the lateral lumbar spine. *British journal of radiology, 217*(3), 707-715.

Weatherburn, G., Bryan, S., & Davies, J.G. (2000). Comparison of doses for bedside examinations of the chest with conventional screen-film and computed radiography: results of a randomized controlled trial. *Radiology, 217*(3), 707-715.

Weiser, J. (1997). Digital radiography using storage phosphor technology: How computed radiography acquires data. *Seminars in roentgenology, 32*(1), 7-11.

Whitley, A. S., Sloane, C. , Hoadley, G., Moore, A. D., & Alsop, C. W. (2005). *Clark's positioning in radiography* (12 ed.). London:: Hodder Arnold.

Williams, G., Zankl, m., Abmayr, W., Veit, R., & Drexler, G. . (1986). The calculations of dose from external photon exposures using reference and realistic human phantoms and Monte Carlo methods. *Phyiscs in biology and medicine, 31*(4), 449-452.

Williams, S., Hackney, L., Hogg, P., & Szczepura, K. (2014). Breast tissue bulge and lesion visibility during stereotactic biopsy: A phantom study. *Radiography, 20*(3), 271-276.

Willis, C. E. (2009). Optimizing digital radiography of children. *European journal of radiology, 72*(2), 266-273.

Willis, C. E. . (2002). Computed radiography: a higher dose? *Pediatric radiology, 32*(10), 745-750.

Willis, C. E., & Slovis, T. L. (2004). The ALARA concept in pediatric CR and DR: dose reduction in pediatric radiographic exams – A white paper conference Executive Summary. *Paediatric radiology, 34*(Suppl 3), S162–S164.

Willis, C. E., & Slovis, T. L. (2005). The ALARA concept in pediatric CR and DR: Dose reduction in pediatric radiographic exams—a white paper conference executive summary1. *Radiology, 234*(2), 343–344.

Wiltz, H. J., Petersen, U., & Axelsson, B. (2005). Reduction of absorbed dose in storage phosphor urography by significant lowering of tube voltage and adjustment of image display parameters. *Acta Radiologica*, 46(4), 391-395.

Wise, K. N., Sandborg, M., Persliden, J., & Carlsson, G. A. (1999). Sensitivity of coefficients for converting entrance surface dose and kerma–area product to effective dose and energy imparted to the patient. *Phyiscs in biology and medicine, 44*(8), 1937-1954.

Wolf, M. , Chang. C, Davis, T. , & Makoul, M. . (2005). Development and validation of the communication and attitudinal self-efficacy scale for cancer (CASE-cancer). *Patient education and counselling, 57*(3), 333-341.

Wu, S. V., Courtney, M., Edwards, H., McDowell, J., Shortridge-Baggett, L. M., & Chang, P. . (2007). Self-efficacy, outcome expectations and self-care behaviour in people with type 2 diabetes in Taiwan. *Journal of clinical nursing, 16*(11), 250–257.

Yoshiura, K. (2012). Image quality assessment of digital intraoral radiography — perception to caries diagnosis. *Japanese dental science review, 48*(1), 42–47.

Zarb, F., Rainford, L. , & McEntee, M. (2010). Image quality assessment tools for optimization of CT images. *Radiography, 16*(2), 147e153.

Zetterberg, L. G., & Espeland, A. (2011). Lumbar spine radiography — poor collimation
practices after implementation of digital technology. *British journal of radiology,
84*(1002), 566–569.

Zoetelief, J., Julius, H.W., & Christensen, P. (2000). Recommendations for patient dosimetry in
diagnosticradiology using TLD. Rep. EUR 19604. Luxembourg: European Commission.

Zoetelief, J., Soldt, R. T. M., Suliman, I. I., Jansen, J. T. M., & Bosmans, H. (2005). Quality
control of equipment used in digital and interventional radiology. *Radiation protection
dosimetry*, 117(1-3), 277–282.